Vol. 298, No. 3, December 10, 1994
Completing Volume 298

ISSN 0003-2670

ANALYTICA CHIMICA ACTA

An international journal devoted to all branches of analytical chemistry

ELSEVIER

ANALYTICA CHIMICA ACTA

Scope. *Analytica Chimica Acta* publishes original papers, rapid publication letters and reviews dealing with every aspect of modern analytical chemistry. Reviews are normally written by invitation of the editors, who welcome suggestions for subjects. Letters can be published within **four months** of submission. For information on the Letters section, see inside back cover.

Submission of Papers

Americas

Prof. Harry L. Pardue
Department of Chemistry
1393 BRWN Bldg, Purdue University
West Lafayette, IN 47907–1393
USA

Tel:(+1-317) 494 5320
Fax:(+1-317) 496 1200

Computer Techniques

Prof. J.T. Clerc
Universität Bern
Pharmazeutisches Institut
Baltzerstrasse 5, CH-3012 Bern
Switzerland

Tel:(+41-31) 6314191
Fax:(+41-31) 6314198

Prof. Sarah C. Rutan
Department of Chemistry
Virginia Commonwealth University
P.O. Box 2006
Richmond, VA 23284-2006
USA
Tel:(+1-804) 367 7517
Fax:(+1-804) 367 8599

Other Papers

Prof. Alan Townshend
Department of Chemistry
The University
Hull HU6 7RX
Great Britain

Tel:(+44-482) 465027
Fax:(+44-482) 466410

Prof. Willem E. van der Linden
Laboratory for Chemical Analysis
Department of Chemical Technology
Twente University of Technology
P.O. Box 217, 7500 AE Enschede
The Netherlands
Tel:(+31-53) 892629
Fax:(+31-53) 356024

Prof. Paul Worsfold
Dept. of Environmental Sciences
University of Plymouth
Plymouth PL4 8AA
Great Britain

Tel:(+44-752) 233006
Fax:(+44-752) 233009

Submission of an article is understood to imply that the article is original and unpublished and is not being considered for publication elsewhere. *Anal. Chim. Acta* accepts papers in English only. There are no page charges. Manuscripts should conform in layout and style to the papers published in this issue. See inside back cover for "Information for Authors".

Publication. *Analytica Chimica Acta* appears in 18 volumes in 1995 (Vols. 297–314). *Vibrational Spectroscopy* appears in 2 volumes in 1995 (Vols. 8 and 9). Subscriptions are accepted on a prepaid basis only, unless different terms have been previously agreed upon. It is possible to order a combined subscription (*Anal. Chim. Acta* **and** *Vib. Spectrosc.*).
Our p.p.h. (postage, packing and handling) charge includes surface delivery of all issues, except to subscribers in the U.S.A., Canada, Australia, New Zealand, China, India, Israel, South Africa, Malaysia, Thailand, Singapore, South Korea, Taiwan, Pakistan, Hong Kong, Brazil, Argentina and Mexico, who receive all issues by air delivery (S.A.L.–Surface Air Lifted) at no extra cost. For Japan, air delivery requires 25% additional charge of the normal postage and handling charge; for all other countries airmail and S.A.L. charges are available upon request.

Subscription orders. Subscription prices are available upon request from the publisher. Subscription orders can be entered only by calendar year and should be sent to: Elsevier Science B.V., Journals Department, P.O. Box 211, 1000 AE Amsterdam, The Netherlands. Tel: (+31-20) 4853 642, Telex: 18582, Telefax: (+31-20) 4853 598, to which requests for sample copies can also be sent. Claims for issues not received should be made within six months of publication of the issues. If not they cannot be honoured free of charge. Readers in the U.S.A. and Canada can contact the following address: Elsevier Science Inc., Journal Information Center, 655 Avenue of the Americas, New York, NY 10010, U.S.A. Tel: (+1-212) 633 3750, Telefax: (+1-212) 633 3990, for further information, or a free sample copy of this or any other Elsevier Science journal.
Advertisements. Advertisement rates are available from the publisher on request.

US mailing notice – Analytica Chimica Acta (ISSN 0003-2670) is published 3 times a month (total 54 issues) by Elsevier Science B.V. (Molenwerf 1, Postbus 211, 1000 AE Amsterdam). Annual subscription price in the USA US$ 3677.75 (valid in North, Central and South America), including air speed delivery. Second class postage paid at Jamaica, NY 11431. *USA Postmasters*: Send address changes to Anal. Chim. Acta, Publications Expediting, Inc., 200 Meacham Av., Elmont, NY 11003. Airfreight and mailing in the USA by Publication Expediting.

ANALYTICA CHIMICA ACTA

An international journal devoted to all branches of analytical chemistry

(Full texts are incorporated in CJELSEVIER, a file in the Chemical Journals Online database available on STN International; Abstracted, indexed in: Aluminum Abstracts; Anal. Abstr.; Biol. Abstr.; BIOSIS; Chem. Abstr.; Curr. Contents Phys. Chem. Earth Sci.; Engineered Materials Abstracts; Excerpta Medica; Index Med.; Life Sci.; Mass Spectrom. Bull.; Material Business Alerts; Metals Abstracts; Sci. Citation Index)

VOL. 298 NO. 3 CONTENTS DECEMBER 10, 1994

(Continued overleaf)

Contents (continued)

ELSEVIER

Analytica Chimica Acta 298 (1994) 285–302

ANALYTICA CHIMICA ACTA

Development and experimental evaluation of a simple system for scanning electrochemical microscopy

Gunther Wittstock [a], Hendrik Emons [b,*], Thomas H. Ridgway [c], Elmo A. Blubaugh [c], William R. Heineman [c]

[a] *University of Leipzig, Department of Chemistry, Linnéstrasse 3, D-04103 Leipzig, Germany*
[b] *Research Center of Jülich, Institute of Applied Physical Chemistry, D-52425 Jülich, Germany*
[c] *University of Cincinnati, Department of Chemistry, Cincinnati, OH 45221-0172, USA*

Received 19 April 1994

Abstract

The development of a scanning electrochemical microscope (SECM) is described. The device was assembled from a commercially available open-loop piezoelectric micropositioning system and a digitally addressable bipotentiostat system. Software development had to be adapted to the special features of the micropositioning system and, along with minor hardware modifications, could eventually provide a partial closed-loop control. The user interface offers convenient access to the core routines, which are tightly time controlled by the clock of the analog–digital converter in order to achieve highly reproducible positioning and significant enhancement of the signal-to-noise ratio. The capabilities and limitations of the system are discussed using measurements of modified analytical electrodes and ultramicroelectrode arrays. A new approach is introduced for quantifying the spatial resolution, which simplifies its experimental determination. A general expression for the proposed resolution limit as a function of the tip radius and the tip-substrate distance was derived, which is based on experiments with different tip electrodes, substrates and mediator solutions. After investigating a set of microelectrodes with decreasing size, the parameter "smallest imageable object" was found to be less useful for comparing the ability of the instrument and the tip for high spatial resolution.

Keywords: Scanning electrochemical microscopy (SECM); Open-loop piezoelectric micropositioning system; Spatial resolution; Ultramicroelectrode arrays; Modified electrodes

1. Introduction

The characterization of electrode/solution interfaces is of major importance for their analytical application in electroanalytical procedures, for sensor development, electrochemical technology as well as for fundamental electrochemistry. During the last years topographic in situ investigations of such electrochemical systems with local resolution became possible because of advances in modern microscopic techniques such as scanning tunnelling microscopy (STM) and atomic force microscopy (AFM) [1–4].

Recently, Engstrom et al. [5] have described a microelectrode/macroelectrode system, in which the microelectrode acted as probe to detect electroactive species generated at the specimen macroelectrode. Liu et al. [6] exploited the feedback effect (see below) and have introduced in combination with substantial

* Corresponding author.

SSDI 0003-2670(94)00290-8

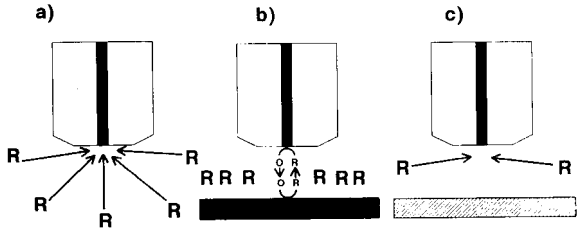

Fig. 1. Principle of the SECM feedback mode; (a) UME in batch experiment under diffusion-controlled conditions; (b) UME in vicinity of a conducting surface where the reactant of the UME is regenerated by heterogeneous electrochemical reaction at the substrate ("positive feedback"); (c) UME close to an insulating surface, diffusion of the reactant to the UME is hindered.

instrumental improvements a new scanning technique suitable for in situ measurements of the electrochemical reactivity of various interfaces with spatial resolution. This so-called scanning electrochemical microscopy is based on the measurement of faradaic currents at an ultramicroelectrode (UME) that is moved over a substrate of interest. The solution has to contain electroactive species that are oxidized (or reduced) at the UME, transported to the substrate surface under certain conditions by diffusion and reduced (or oxidized) there. An enhanced current can be observed with respect to common batch experiments (Fig. 1a) at the UME if the tip electrode (UME) is close to a conducting surface (positive feedback effect, Fig. 1b). On the other hand, the current is reduced in the vicinity of insulating areas because of shielding effects affecting the diffusion field of the UME (Fig. 1c) [7–9].

Bard and co-workers [10,11] have developed a computer-controlled SECM system where the UME can be moved in horizontal (x, y) and vertical (z) directions above a substrate by piezoelectric motors and the potential control as well as the measurement of currents is performed by a bipotentiostat. For that purpose they modified micropositioning devices consisting of piezoelectric motors and a motor controller equipped with closed-loop capability, i.e., the controller is not only receiving an electronic signal from the computer to initiate a motor action but is also sending a signal after performance of the movement back to the computer.

Unfortunately, the commercial components for this original design of the micropositioning system are not available anymore. In addition, it seemed to be advantageous to develop a less expensive open-loop SECM configuration, which is capable of lateral movements of the UME with extremely high resolution. Such a system is described in this paper together with experiments aimed to characterize its performance in terms of image distortion, reproducibility and spatial resolution.

2. Experimental

2.1. Instrumentation

The schematic hardware configuration of the SECM system is shown in Fig. 2. The micropositioning system consists of three Burleigh Inchworm™ motors IW-701-00, mounted on Burleigh TS-100 and TS-300 translation stages and a Burleigh motor controller 6000-3-0-1-1 (Burleigh Instruments, Fishers, NY). The motor controller is connected to a 486 personal computer (33 MHz, 4 MB RAM) via a Burleigh model 660-2 interface card. Some modifications, described in the section below, allow for partial closed-loop control.

Calibration of the motors was carried out by performing 2,000,000 single incremental motions with each of the three Inchworm™ motors resulting in a translocation of about 11 mm. This distance was measured with a dial caliper (Mitutoyo, Japan) which has 0.02 mm graduations. Measurements were assumed to be accurate to ± 0.04 mm.

The electrochemical four-electrode system is controlled by a locally constructed bipotentiostat which was designed for a different purpose [12], but some of its characteristics seemed to be appropriate for this application. For this work the most important features are a low end current gain of 1 V nA^{-1} and the ability

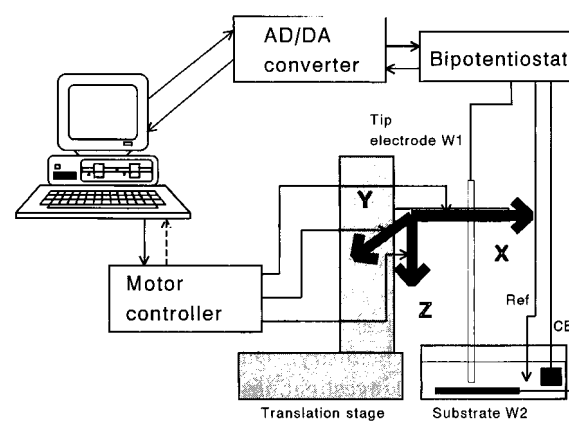

Fig. 2. Schematic view of the SECM system.

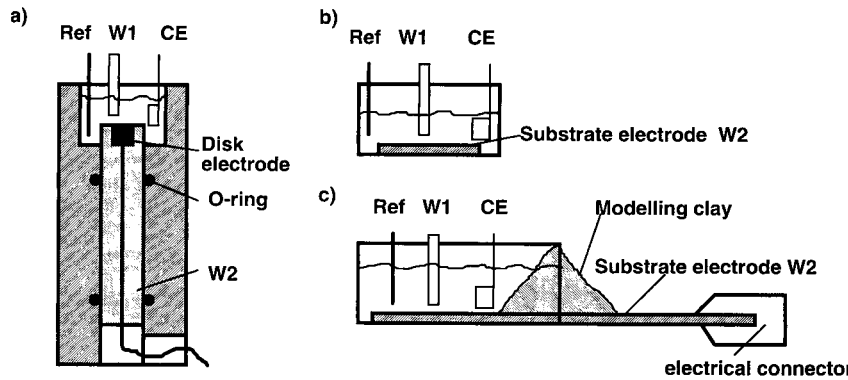

Fig. 3. Different cells for introducing (a) pen-shaped disk electrodes; (b) flat substrates; (c) large flat samples.

to suppress background or steady state currents of up to 10 μA on both working electrodes. The overall time constant for the potentiostat is about 10 μs and no further hardware signal filtering is employed. The bipotentiostat was constructed using surface mount technology fitting the instrument onto a single printed circuit board of 7.7 cm by 10.2 cm which allowed it to be located very close to the electrochemical cell and to minimize lead lengths.

The bipotentiostat is interfaced to the computer via a previously described analog-to-digital (ADC) and digital-to-analog (DAC) converter board [13]. This assembly has four 12-bit DACs, of which two are used for potential control and two are used for current compensation. The 12-bit 8 μs ADC is connected to the bipotentiostat via an 8-channel analog multiplexer and individual sample and hold (S and H) amplifiers. The interface has 32 kB words (16 bit) of local memory and conversions can be carried out independently of the host computer by control via its six 16-bit clocks driven by a 4 MHz crystal oscillator. The interface also has 16 bits of digital input and 16 bits of digital output which are available for control of the bipotentiostat transducer gain and other functions.

The electrochemical cell includes the tip electrode (UME) as working electrode W1. Home-made microdisk electrodes were used for which platinum wires had been sealed directly into glass [14] or carbon fibers had been embedded into PTFE [15]. A normal-sized platinum wire and a silver wire immersed in a 0.1 M chloride solution served as counter and quasi-reference electrode (AgQRE), respectively. All potentials are reported with respect to the AgQRE. The substrate of interest was either connected as working electrode W2 to the bipotentiostat or it was operated at open circuit.

A special cell was constructed for investigating surfaces of disk electrodes (Fig. 3a). It allows an upwards orientation of commercial disk electrodes in solution. Flat substrates were investigated in a normal glass cell with flat bottom (Fig. 3b). Larger substrates were accommodated by an open plastic box (Fig. 3c). After sealing the open side with modelling clay (van Aken, Rancho Cucamonga, CA), this cell as well as the alternative cells were fixed on an optical table (Oriel, Stratford, CT), which permits a fine adjustment of the vertical position of the substrate. The micropositioning system as well as the bipotentiostat were placed on aluminum plates separated by rubber sheets to minimize any mechanical vibrations of the system.

2.2. Software

The software was developed as a combination of compiled Basic and Assembly Language. Assembly Language (Turbo Assembler, Borland, Scotts Valley, CA) was used for the time-critical operations while Power Basic Vers. 2.0 (Spectra, Sunnyvale, CA) was employed for all other parts. Table 1 outlines the features of the home-made software package. Special attention was paid to achieve a high signal to noise ratio and accurate positioning which are discussed below. Furthermore, data safety and protection of the system from maloperations by users were considered.

The potentiostat allows separate background current suppression for each working electrode. This is accomplished by applying a potential from a 12 bit digital-to-analog converter (DAC) via a resistor. The resistor is

Table 1
Functions of the SECM control software

Feature group	Description
Input and output control	Pictogram assisted parameter input by user
	Saving and retrieval of experimental parameters
	Display of progressing experiments outside time-critical routines
	Automated storage, compression and export of data
Bipotentiostat operation at fixed tip position	Automated background current suppression
	Cyclic voltammetry of tip and substrate
	Tip chronoamperometry during potential scan or potential step at the substrate
Motor control	Horizontal and vertical approach to surface
Imaging	Supporting routines for searching a surface for the spot of interest
	Comb-like arranged line scans

one of eight selected by a digitally controlled analog multiplexer. Proper choice of the compensation time interval is important since the potentiostat-cell combination represents a closed loop system with two different but finite time constants. The cell time constant is dominant for most dual working electrode cells (including SECM cells) because the cell geometry is typically determined by other constraints. In our case the cell time constant is dominant when the potential of one of the electrodes is changed. Under other circumstances the time constant of the potentiostat (typically less than 100 μs) is dominant. In situations of this sort it is helpful to obtain an estimate of the effective cell time constant. It is inadvisable to make corrections more frequently than once every two cell time constants after a potential change. Additional problems arise when there is any appreciable noise associated with the response signal to be minimized. In our case the dominant noise component is associated with the power line frequency. There are several options to overcome the problem but the best is to eliminate, or at least to minimize, the noise. Signal averaging is a well established noise reduction technique and this is accomplished here by acquiring a fairly large even number of samples at uniform time intervals such that the product of the number of points multiplied by the time between ADC samples is a whole multiple of power line periods, in our case 1024 points in 0.1 s. This has the effect of reducing random noise by a factor 32:1 for 50 or 60 Hz line noise and its multiples are almost totally eliminated. Leakage of the line frequency components is controlled by the jitter in the timing of the individual samples and mismatch between the sampling period and the line frequency period. In our case the individual samples are automatically triggered by a crystal-controlled clock which holds timing jitter to about 20 ns, a negligible value for the time intervals involved. In experiments using resistive-capacitive dummy cells it was possible to suppress currents of several μA while making measurements at the nA full scale range. It is important to note that this is a static compensation and only current components which are time invariant are actually compensated.

The noise reduction algorithm is employed for current compensation and imaging operations while cyclic voltammetry and chronoamperometry are performed without any software noise reduction.

The x–y–z position actuators and their associated drive electronics exhibited some properties which were unexpected and which were uncovered as the project progressed. In order to describe the final form of the instrument and software, it is necessary to briefly discuss some of these properties. The Burleigh Inchworm™ actuators are piezoelectric devices but they operate quite differently from most piezoelectric actuators. In Inchworm™ motors three separate piezoelectric rings successively grip and move the drive shaft in a manner quite similar to that used by a person climbing a rope, thus combining long translation ranges with high positioning resolution. Each actuator action results in a small incremental motion of the motor shaft of approximately 5 nm refered to as "click" below. The velocity of travel is thus controlled by the rate at which these subcycles are performed. These piezoelectric actions are not infinitely repeatable, after 512 steps an internal reset operation is performed by the motor controller. During this operation the change of the clamping piezo ceramic is performed without moving

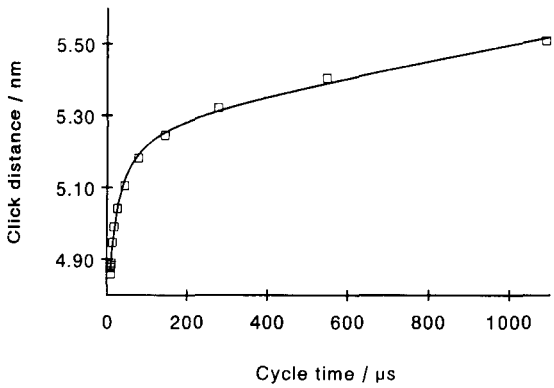

Fig. 4. Dependence of the single click distance from the cycle time for a single axis.

the drive shaft itself. While this reset is in progress (100 μs) the hardware totally ignores any instructions. The actuators, motor controller and interface card used here have no feedback of any sort, including no indication of a reset in progress. However, the motor controller does have signal points which indicate that a reset is in progress although the interface card does not offer provision for accepting this information. Therefore, these signals were brought out to unused digital inputs of the ADC/DAC system.

The hardware also has one additional undocumented and unexpected property. The actual distance travelled per step depends strongly upon the time between step commands, i.e., pulse rate, even when the reset time is taken into account. Fig. 4 shows the click distance versus cycle time function for an individual axis. The behaviour closely resembles the torque limiting characteristics of stepping motors and implies that the step rate must be closely controlled in order to obtain reproducible positioning. The use of the rate generators included in the Burleigh interface card would introduce a serve timing ambiguity, since these circuits are incapable of monitoring the reset condition.

Fig. 5. Signal-time regime for translation and monitoring of the reset period.

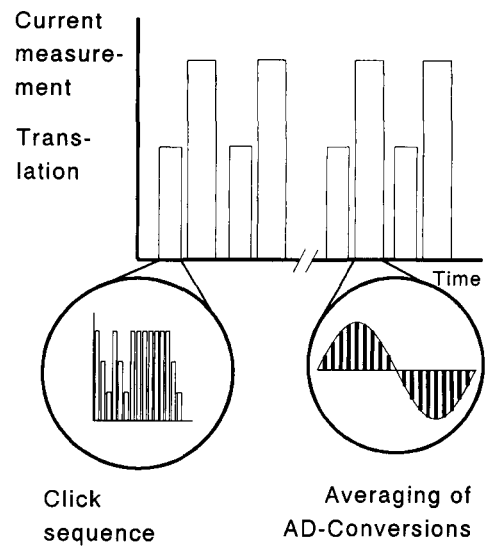

Fig. 6. Coordination of movements and data acquisition.

The approach taken in this project is to implement two basic types of movement. The first form is employed for general positioning and is implemented via assembly language. In this form, the time delay between clicks is controlled by the number of passes through a software delay loop (Fig. 5). The Burleigh controller is monitored via the added signal lines to prevent issuing a step command during reset. Because all applications except the delay loop and the most critical disk operating system (DOS) interrupts were disabled, the software loop is quite constant and reproducible on a particular computer.

The second movement form generates groups of clicks pulses which are produced in the same way as for the general movement case described above. At the end of a movement block a number of AD conversions is acquired at time intervals controlled by the clock of the converter (Fig. 6). These conversions are averaged to provide a single value as discussed above which is subsequently entered into a result array and the process repeats with a new group of movement pulses etc. In normal use a single call to this routine is issued to acquire all points on one line scan of the image.

2.3. Samples

Ultramicroelectrode arrays were manufactured by screen-printing and subsequent eximer laser micromachining techniques (K. Zimmer, Institute of Surface

Modification (IOM), Leipzig): An insulating cover of 20–30 μm thickness was applied on top of the conducting material and subsequently the array was structured by laser ablation ($\lambda = 248$ nm, fluence = 4.1 J cm^{-2}) of the insulating layer to expose square-shaped microelectrodes with dimensions between 6.5 μm and 90 μm. These active areas were arranged hexagonally with an interelectrode distance of 150 μm or as a square with a distance of 500 μm. A set of these array electrodes was kindly provided by B. Stehlitz and H. Kotte (Environmental Research Center Leipzig-Halle, Department of Remediation Research, Leipzig). Concluding the SECM experiments, a scanning electron microscope (SEM) investigation was performed with a DSM 940 (Zeiss, Oberkochen) after coating the array with a gold layer. A gold disk electrode (3 mm diameter, Bioanalytical Systems (BAS), West Lafayette, IN) was polished and one half of it was coated with carbon spray DAG 40 (Acheson Colloiden, Scheemda, Netherlands). The carbon-gold border was cleaned with fine emery paper. The glassy carbon (GC) electrode (0.9 mm diameter) was manufactured at the machine shop of the Institute of Physical Chemistry at the University of Leipzig.

2.4. Chemicals

Trimethylaminomethyl ferrocene perchlorate (TMAMF) was synthesized from trimethylaminomethyl ferrocene iodide (Strem, Kehl) and $NaClO_4$ according to [16] and recrystallized twice from methanol. Mediator solution was prepared daily by dissolving ferrocene monocarboxylic acid FMCA (Sigma, St. Louis, MO), TMAMF or $[Ru(NH_3)_6]Cl_3$ (Aldrich, Milwaukee, WI) in the electrolyte solution to give 0.002 M, 0.004 M and 0.04 M solutions, respectively. In addition, the solution contained 0.1 M KCl (Fisher Scientific, Fair Lawn, NJ) to establish the potential of the AgQRE and was buffered to pH 7.4 with 0.1 M phosphate (KH_2PO_4 from Mallinckrodt, Paris, KY; Na_2HPO_4 from Fisher Scientific).

2.5. Determination of resolution

In order to determine the spatial resolution limit, ultramicroelectrodes of 5 μm and 15 μm radii in 0.04 M $[Ru(NH_3)_6]Cl_3$ solution were scanned across the Au/Si border of a silicon wafer with deposited gold structures. The UME was first placed in the cell in a way that it was still sliding on the wafer. This can be seen in the corresponding current profiles by spikes with tailing, which occur in different numbers and at different locations in the reverse scan. The micropositioning system raised the tip electrode in small steps until a line scan without spikes resulted. The tip-substrate distance at this point was assumed to be 1 μm. Small deviations between assumed and real tip-substrate distances turned out to be irrelevant for the recommended procedure since at small distances the resolution limit depends nearly exclusively on the radius of the tip electrode. The UME was subsequently raised by defined distances and several line scans were recorded at each height. The determination of the resolution limit was carried out in an analogue manner by scanning perpendicularly across the border between a polished GC disk electrode with a diameter of 3 mm in its Kel-F shaft (BAS) in a solution of 0.004 M TMAMF.

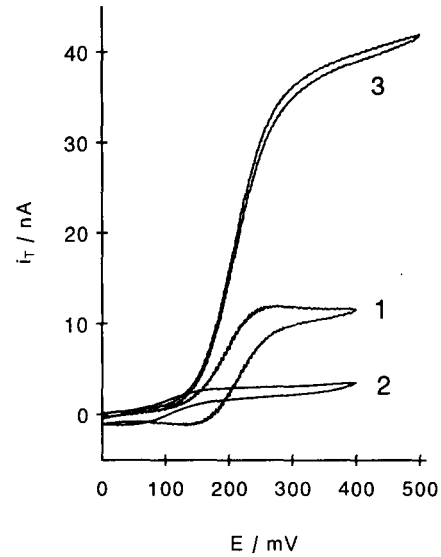

Fig. 7. Cyclic voltammograms of 0.002 M FMCA at a platinum electrode ($r = 15$ μm): (1) at infinity; (2) close to an insulating substrate; (3) close to a conducting substrate; substrate potential −100 mV; $v = 50$ mV s^{-1}.

3. Results and discussion

3.1. Demonstration of the feedback effect

Fig. 7 shows three different cyclic voltammograms recorded with the same tip electrode in the same solu-

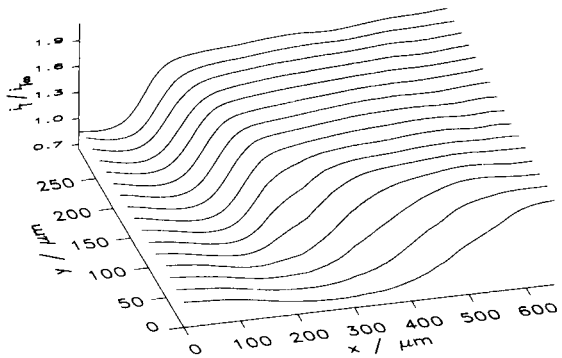

Fig. 8. SECM image of a glassy carbon electrode (0.9 mm diameter); carbon tip ($r = 12.5$ µm) at +400 mV; $i_{T\infty} = 6.5$ nA; mediator 0.002 M FMCA; substrate at open circuit.

tion. Curve 1 corresponds to a batch experiment with the UME located far away from any surface. The vicinity of an insulator (Curve 2) hinders the diffusion of the reactant to the tip electrode, hence smaller currents are recorded with respect to the batch experiment. Positioning of the tip electrode directly over a conducting surface, a GC electrode, establishes the positive feedback effect. As a result, the currents are larger (Curve 3). The large rate of mass transfer leads to nearly steady state diffusion profiles and therefore the forward and reverse potential scan are almost superimposed. The rate of mass transfer competes with the rate of the heterogeneous electrochemical reaction which appears nearly reversible in conventional cyclic voltammetric experiments. The reaction is shifted to a quasi-reversible kinetic regime, which is indicated by the increased potential difference between $E_{1/2}$, where half of the diffusion limited current is obtained, and $E_{1/4}$ or $E_{3/4}$, where one quarter and three quarters of the diffusion limited current are recorded. Mirkin et al. published the theory [17] and applications [18] for the kinetic analysis based on this phenomenon.

Imaging is another application of the feedback mode. Fig. 8 shows an image of one quarter of a GC electrode. Small currents correspond to the polymeric shaft (insulator) and the large currents are caused by the positive feedback over the GC surface. Four different regions can be distinguished in Fig. 9, which displays a measurement of a conventional gold disk electrode of which one half was coated with carbon spray. The small currents in the left foreground are caused by the insulating polymer shaft, the large currents in the left background are due to the positive feedback over the blank gold surface and the righthand side corresponds to the sprayed carbon layer. Although the whole carbon material behaves as a conductor the covered border between the underlying gold and polymer substrates can be located as the curved elongation of the region between Au and polymer shaft on the lefthand side into the righthand part, where it follows the line between the smooth part in the foreground and the more structured response surface in the rear part of the image. No explanation can be given at this point for the smooth appearance of the carbon layer above the polymer shaft. The structures of the carbon layer in the rear part reflect the topographic roughness of the carbon layer. A detailed investigation of this system is presented in [19]. Especially high currents were recorded right above the border between gold and graphite. The sprayed layer has a thickness between 20 µm and 30 µm [19] and the perpendicular side wall contributes to the feedback effect.

3.2. Calibration

As described above, the click distance is a function of cycle time, movement direction and the individual motor used. When performing AD conversions between blocks of single clicks as shown in Fig. 6, the click distance changes with the AD conversion parameters, e.g., the distance between two AD conversion blocks and sampling time. Although the differences were in the 0.1 nm range (2% of one single click) it can cause an offset of the positioning in each forth-and-back movement equal to 2% of the total travel distance and after 50 line scans the endpoint of the scans matches the starting coordinate of the initial scan.

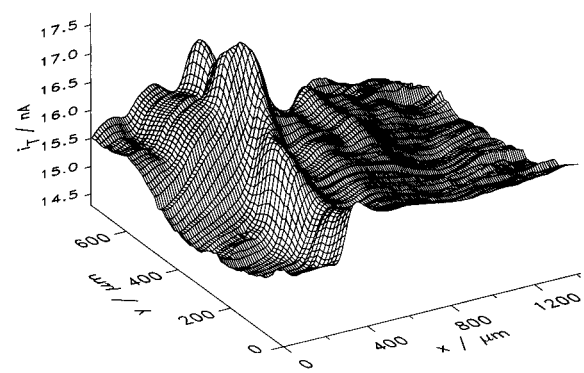

Fig. 9. SECM image of a gold disk electrode half-sprayed with carbon; Pt tip ($r = 15$ µm) at +400 mV, substrate potential 0 mV; mediator 0.002 M FMCA.

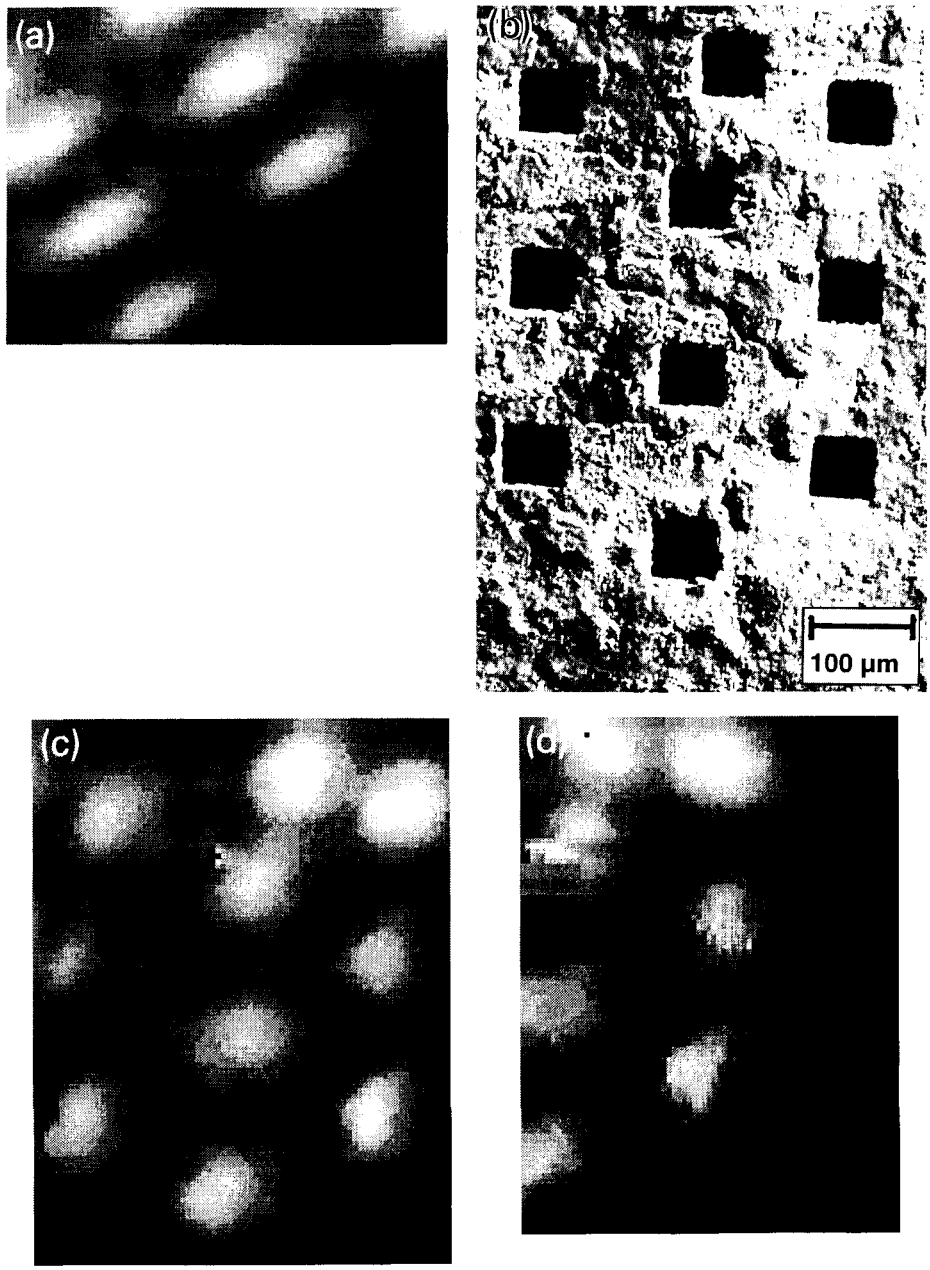

Fig. 10. Investigation of a ultramicroelectrode array of 50 μm × 50 μm square electrodes arranged in an nearly hexagonal pattern; (a) distorted SECM image, size of displayed area 400 μm horizontal, 300 μm vertical, experimental conditions: $E_t = 400$ mV, $E_s = 0$ mV, translation rate = 7 μm s^{-1}, mediator 0.002 M FMCA.; (b) SEM picture, $U = 10$ kV, working distance = 11 mm; (c) SECM image after recalibration, size: 400 μm horizontal, 510 μm vertical, experimental conditions: $E_t = 400$ mV, $E_s = 0$ mV (gray scale inverted relative to (a), other as in a; (d) repetition of (c) with offset of the starting point, size: 375 μm horizontal, 500 μm vertical.

Calibration experiments were performed to measure click distances for different experimental situations. Appropriate calibration data can be chosen before recording an image to ensure that the same settings were used during calibration and imaging.

The relative standard deviation (R.S.D.) of the click distances within 5 consecutive runs was between 0.1% and 0.5%, the difference between the means of one axis for calibration series at different days was between 0.2% and 1.0%. Better accuracy in the calibration could not be achieved with the dial caliper because of its imprecision (measurement of 10.00 mm with a deviation of ± 0.04 mm).

As mentioned above, an inappropriate calibration results in distorted images which are especially obvious for regular structures. Fig. 10a shows the SECM image of a hexagonally structured ultramicroelectrode array, which was recorded using inappropriate calibration data. The distortion of the image against the structure observed with electron microscopy (Fig. 10b) is obvious. Using appropriate calibration data – e.g., values obtained with identical experimental settings as used in the experiment – leads to the image in Fig. 10c. The hexagonal arrangement of the individual electrodes is correctly displayed as well as the out-of-pattern position of the three array elements in the upper right part of Fig. 10b and c. The resolution of the tip electrode with a radius $r = 15$ μm is not high enough to display the approximately square shape of the array electrodes.

The remaining calibration error has two consequences: A slight stretching or compression of the image does not represent a problem for most applications, the difference of the calibration errors of forward and reverse translation of one axis results in a systematic offset of the starting point of each scan, which becomes apparent only if a large number of line scans with a large scan length is carried out. When using Inchworm motors, this remaining distortion cannot be avoided. However, the desired information is often still extractable from those images. Image processing techniques offer a way to an after-run correction of distorted images, but were not applied in this work since they are always accompanied by a loss of information. Once a set of calibration data was established successfully, they have been used in this laboratory for 10 months without loss in accuracy.

3.3. Reproducibility

Reproducibility can be compared with different scopes. Since an image $i_T(x,y)$ consists of n_s line scans, one might compare two subsequently recorded line scans $i_T(x)$ over an identical sample area. The repeatability of these scans is very high and such an approach would neglect the specific problems resulting from a two-dimensional scanning in a finite time of a real sample. Fig. 10d depicts a repetition of the experiment introduced in Fig. 10c which was started 25 min after conclusion of the first run with an intentional offset of the starting point. The identity of the sample can be concluded from the irregular placement of the array elements in the upper left part which is displayed consistently in Fig. 10b–10d. A thorough comparison of corresponding formations in Fig. 10c and Fig. 10d also reveals differences, for example the apparent shape of individual array elements. On one side this is due to the limited spatial resolution of the tip ($r = 15$ μm) and on the other hand an increase in mediator concentration by solvent evaporation, adsorption and inhibition processes at the tip and the substrate as well as partial decomposition of the mediator solution must be considered, since the recording of the images in Fig. 10c and Fig. 10d required 75 min each. Because of the unavoidable changes at the solid/liquid interface of the sample, the determination of a measure for the reproducibility exclusively related to the instrumentation seems very complicated.

3.4. Resolution

The spatial resolution might be defined as the smallest distance between two different areas of the sample which are represented in the SECM image by significantly different currents. This approach has some drawbacks because a so-defined resolution depends on the difference in the properties of the two elements and consequently on the choice of the regarded parts of the sample. Furthermore, a set of test samples would be required to realize different distances.

Similar problems have already been addressed in connection with spatial resolved surface concentration analysis. The general approach taken in [20] seems to be useful for the evaluation of the SECM performance, too. A resolution limit Δx can be estimated by the difference quotient at the inflection point of a current profile of one line scan $i_T(x)$ by Eq. 1

$$\Delta x_0 \approx \frac{\Delta i_T}{\left(\frac{di_T}{dx}\right)_{x = x_{inflection}}} \quad (1)$$

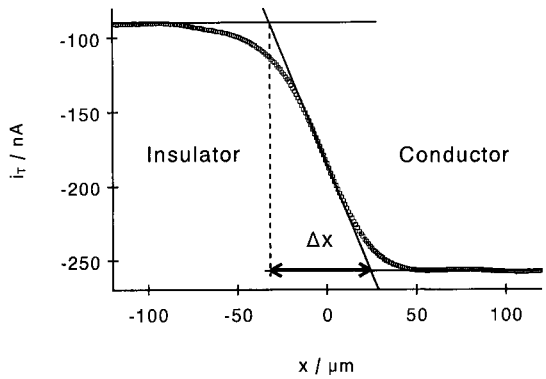

Fig. 11. Definition of the resolution limit using the slope of the tangent at the inflection point of a line scan $i_T(x)$. Parameter of the measurement: $E_t = -500$ mV, $E_s = 100$ mV, $r = 15$ μm, $d = 15$ μm, translation rate = 7 μm s^{-1}, Mediator 0.04 M $[Ru(NH_3)_6]Cl_3$.

The properties of the sample influence Δx via the observed current profile $i_T(x)$. The lowest achievable resolution limit, e.g., the best resolution, is obtained across the border between two quasi-infinite large sample areas, one totally inert and the other with diffusion-controlled positive feedback (electrical conductor), because the deviation of the current $di_T(x)/dx$ reaches its extreme value there. Just this kind of sample is the easiest to realize with the SECM, for example by a commercial microdisk electrode surrounded by a polymer shaft (Fig. 8). The determination of Δx is explained by Fig. 11. Δi_T is the difference between the current above the infinite conducting and insulating regions at a given tip-substrate separation, d. A determination of the resolution limit using a significance limit based upon the standard deviation of the current signals and the tip profile, as exercised for spatial

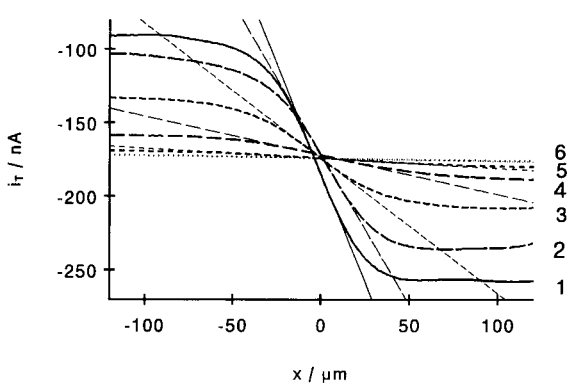

Fig. 12. Set of line scans over a Si/Au border on a wafer with the distances d in μm (1) 15, (2) 30, (3) 45, (4) 75, (5) 120, (6) 150; other experimetal parameters are the same as in Fig. 11.

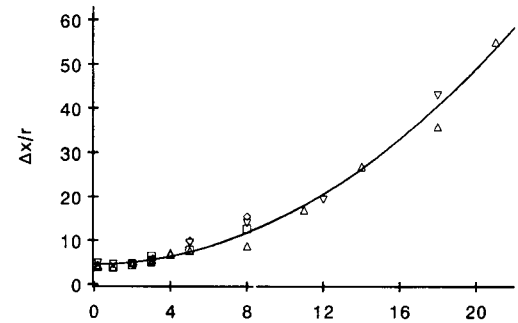

Fig. 13. Resolution limit in SECM feedback experiments as a function of the tip–sample distance. Experimental parameter (Δ) $r = 5$ μm, (◇) $r = 15$ μm, $E_t = 500$ mV, $E_s = 0$ mV, mediator is 0.004 M TMAMF; (▽) $r = 5$ μm, (□) $r = 15$ μm, $E_t = -500$ mV, $E_s = 100$ mV, mediator is 40 mM $[Ru(NH_3)_6]Cl_3$.

resolved concentration analysis [20], was not taken into consideration since the tip profile has not yet been formulated for the SECM tip and the non-linear current–distance relationship contributes via the sample roughness, mechanical vibrations and vertical positioning deviations to the standard deviation of the current signals in a different manner for insulating and conducting sample areas.

One set of experimental line scans above the same sample for different tip–substrate distances is shown in Fig. 12. The tangents at the inflection point were numerically calculated. Their slopes become flatter with increased d and hence Δx is growing. All experimentally determined resolution limits are plotted versus distance in Fig. 13. In order to enable a comparison, both Δx and d were normalized to the radius of the tip electrode r. The curve represents the least-square fit of 36 data pairs to the model

$$\Delta x/r = k_1 + k_2(d/r)^2 \qquad (2)$$

with $k_1 = 4.6 \pm 0.2$ and $k_2 = 0.111 \pm 0.002$. Transformation of Eq. 2 to a function $\Delta x = f(r,d)$ yields two contributions $\Delta x_1 = k_1 * r$ and $\Delta x_2 = k_2 d^2/r$ to the resolution limit. The first contribution Δx_1 can also be regarded as the minimum achievable resolution limit with a given tip radius if d goes towards zero.

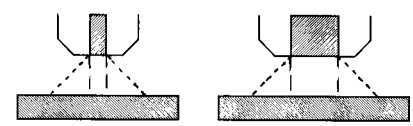

Fig. 14. Schematic representation of the area ("projection area") formed by a perpendicular projection of the tip electrode surface onto the sample and the broadening of the tip profile by the diffusion of the mediator for two tip electrodes having a different radius.

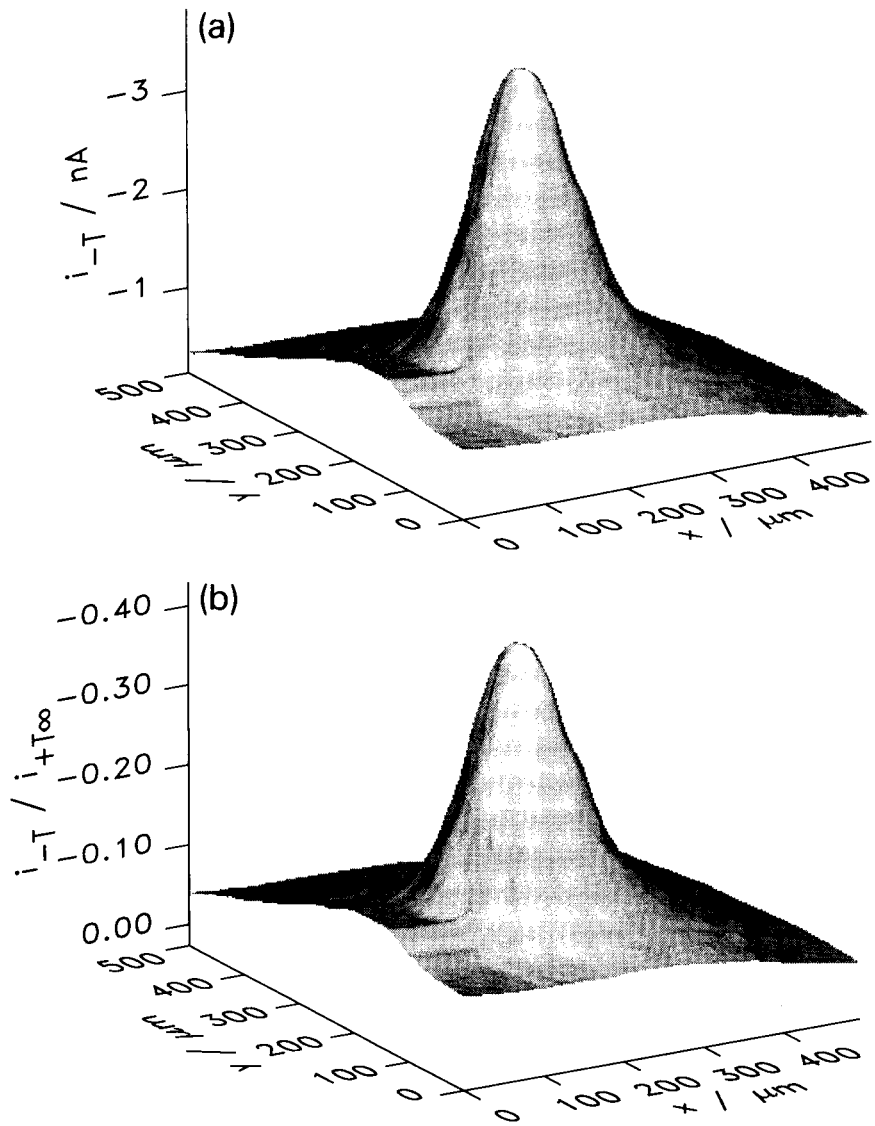

Fig. 15. Sequence a: current profiles $i_{-T}(x,y)$ above elements of ultramicroelectrode arrays with square shape and $h = 90$ µm. Experimental parameters: $E_i = -100$ mV, $E_s = 400$ mV, $r = 15$ µm, mediator 0.002 M FMCA. Sequence b: current profiles of (a) normalized to the steady-state oxidation current of the tip in a batch experiment $i_{+T\infty}$ scaled in the same way for Figs. 15b–21b.

The second contribution Δx_2 describes the broadening of the tip profile by mediator diffusion and depends upon the time necessary for mediator species to cross the gap between tip and substrate. This time can be estimated with $\tau \approx d^2/D$ from the tip–substrate distance d and the diffusion coefficient D of the mediator [21] and Δx_2 could also be expressed as $\Delta x_2 = k_2' \tau / r$ with $k_2' = k_2 D$.

For a larger electrode an increased d causes a smaller increase of the resolution limit than for a smaller tip electrode. As the perimeter-to-area ratio of the tip electrode surface increases with decreasing r, the relative contribution of sample areas outside the "projection area" of the tip is growing (Fig. 14). From Eq. 2 an inversion tip–substrate distance $d_i = [(k_1/k_2) r_1 r_2]^{1/2}$ can be predicted at which two tip electrodes with r_1 and r_2 ($r_1 < r_2$) have the same resolution limit and for all $d > d_i$ the larger tip should give a better resolution (smaller resolution limit). Indeed, this phenomenon has been observed, however, for $d_i = 5$ µm and $d_i = 15$

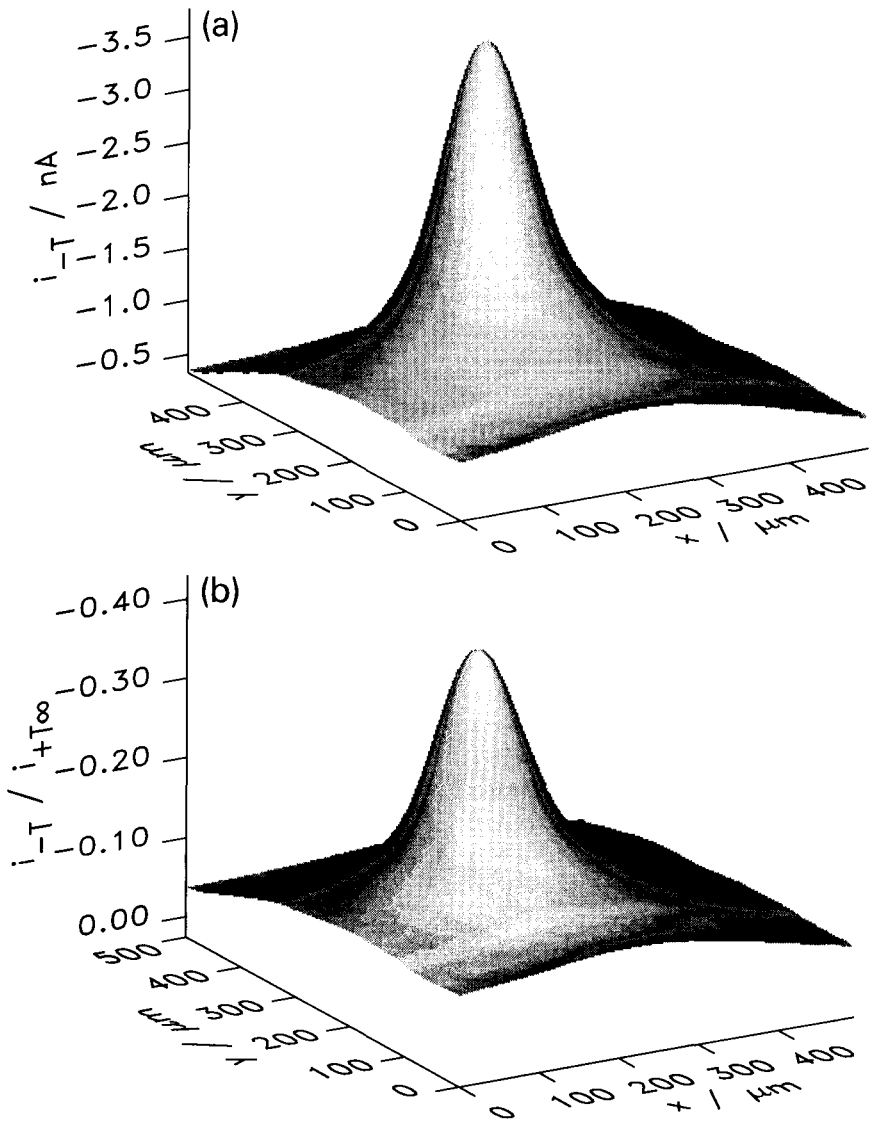

Fig. 16. As Fig. 15, but $h = 70$ µm.

µm this inversion distance $d_i = 56$ µm is so large that, because of the low contrast, imaging with the smaller tip does not seem to be appropriate anyway.

3.5. *Smallest imageable object*

The question about the smallest object imageable with the SECM is closely related but not identical with the problem of resolution limit discussed above. While the resolution limit is a sample-independent quality parameter of the instrumentation and the tip, potential users of microscopic techniques are often more interested in the size h_{min} of the smallest object that causes a current which is significantly different from the variation of the background signal. Of course, this size depends on instrumental parameters such as tip electrode size, tip–substrate distance, positioning quality, bipotentiostat sensitivity and noise suppression effectiveness. Besides that, properties of the sample itself are important. It will be much easier to image a small metal spot surrounded by insulating material with the SECM than to detect the same object in the vicinity of a much

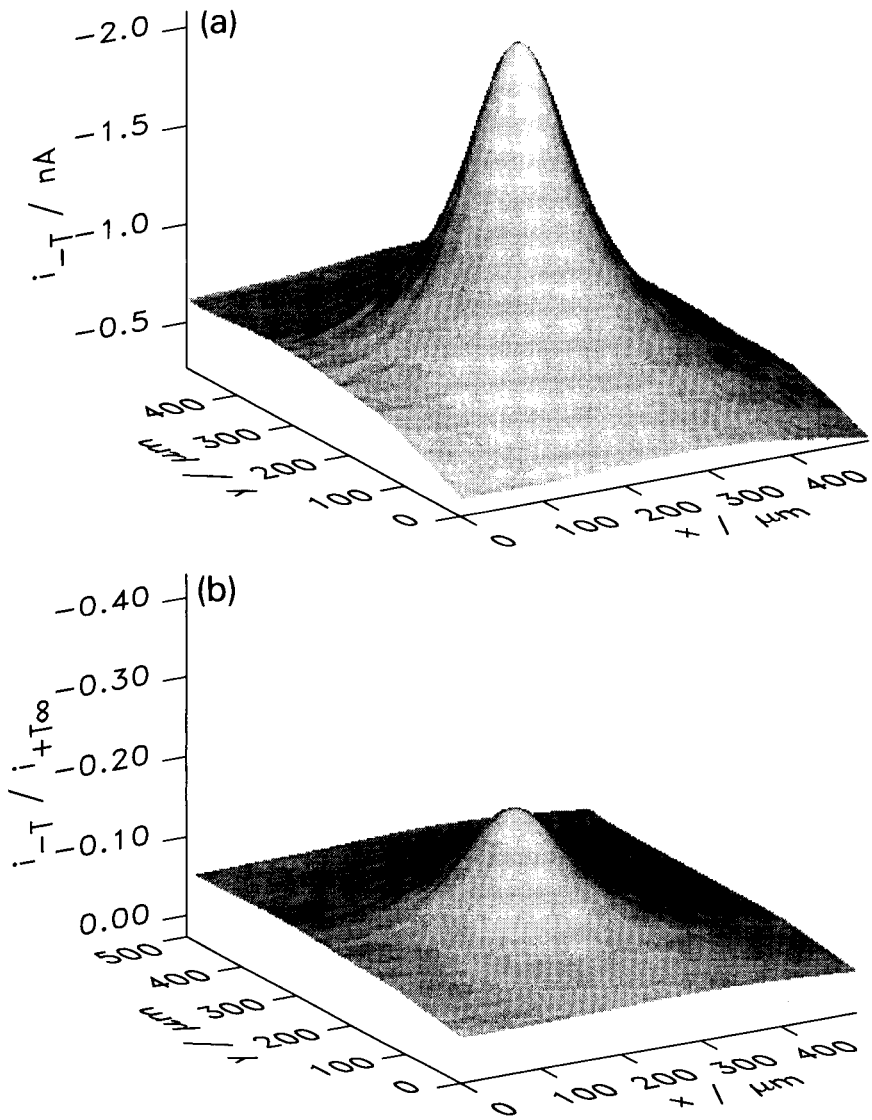

Fig. 17. As Fig. 15, but $h = 50$ µm.

larger metal surface or as one element out of a large number of similar closely-located ones. Based on computer simulations and the assumption of a d/r ratio of 0.1, Bard et al. [22] estimated the smallest identifiable conducting particle embedded in an insulating material to be 10–20 times smaller than the tip electrode diameter. Besides the stated assumptions, this implies furthermore that the sample is perfectly smooth. Otherwise, a small increase in the tip–sample distance over an insulating material can not be distinguished from a small conducting particle. There are, however, quite a number of possible samples with roughnesses in the µm range and other unfavourable sample-specific circumstances.

One of those cases is discussed in the following as an example. Individual square-shaped electrodes out of four-element ultramicroelectrode arrays with constant interelectrode distances of 500 µm and electrode dimensions between 6.5 µm and 90 µm were imaged using a tip electrode with $r = 15$ µm so that radius ratios of substrate and tip between approximately 0.2 and 3 could be realized. An additional difficulty for achieving

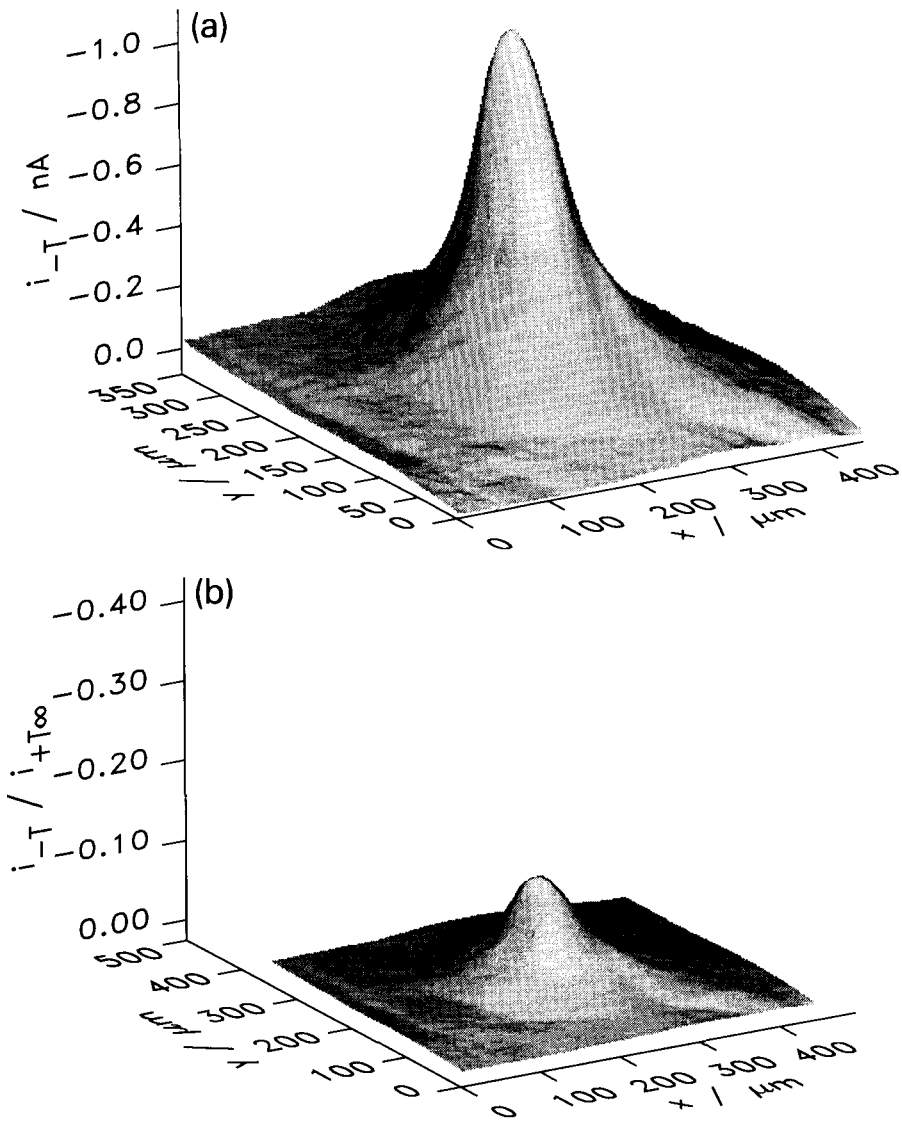

Fig. 18. As Fig. 15, but $h = 30$ µm.

a small h_{min} is the surface roughness of the insulating cover layer (compare with Fig. 10b of an analogous electrode array) and that the active electrode surface is exposed by holes through this cover layer of about 25–30 µm thickness, which prevents a closer tip–substrate distance than $2r$ and an effective exploitation of the feedback effect. Therefore, the substrate was used as anode which continuously oxidized FMCA under diffusion controlled conditions. The product of this reaction was detected cathodically at the tip (i_{-T}). When the tip electrode and the array element were located directly across from each other, the feedback effect was established and increased the signal whereas feedback effects (positive or negative) were completely absent over the insulating part of the array assembly. This operation mode is different from the "substrate-generating/tip-collecting" mode introduced by Zhou et al. [23] only by not recording the currents at the substrate.

The current versus location images are shown in Figs. 15a-21a. For the purpose of an easier comparison between the images and for compensating slightly varying mediator concentrations between the different

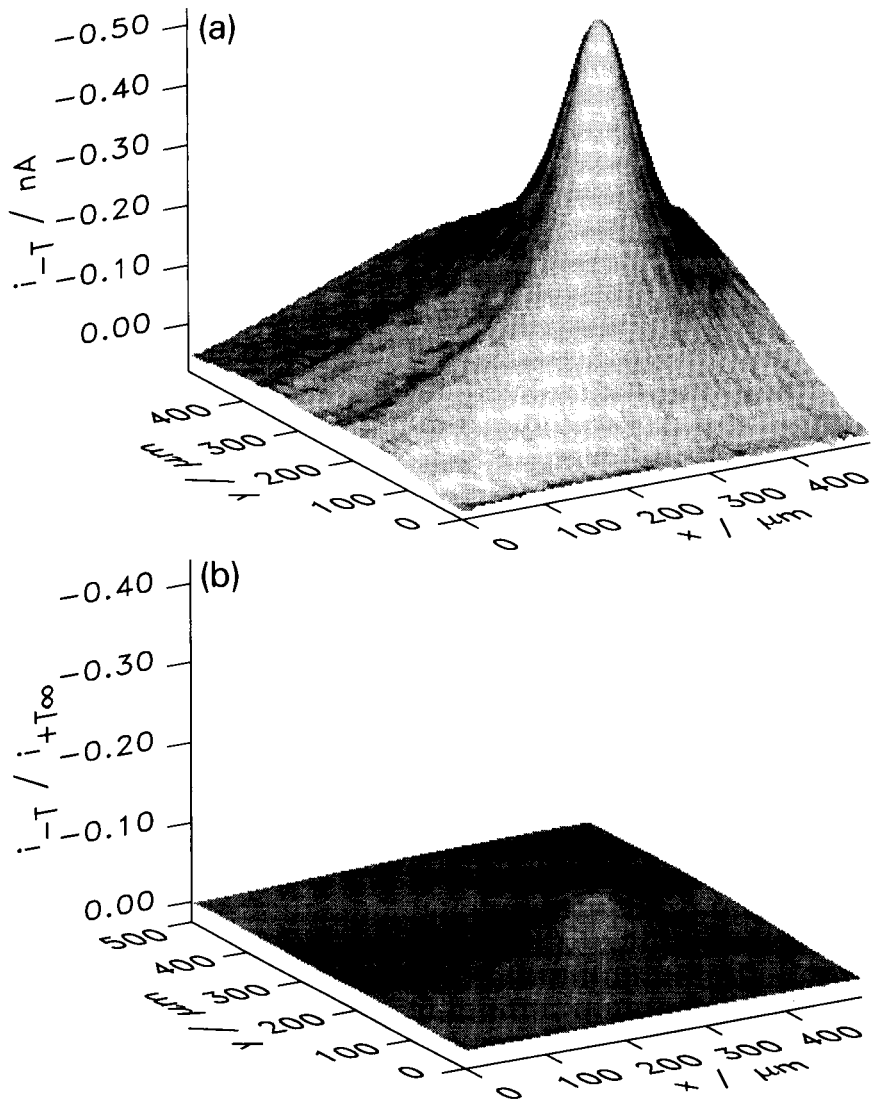

Fig. 19. As Fig. 15, but $h = 20$ µm.

experiments, each image $i_{-T}(x,y)$ was normalized to the steady-state oxidation current in the batch experiment $i_{+T\infty}$ (compare with Fig. 10b of an analogous electrode array) and plotted with unified scales for location and current axes (Figs. 15b–21b).

The array electrodes with dimensions ($2h$) between 10 µm and 90 µm are clearly imaged with the SECM using a tip with $r = 15$ µm. The size of the smallest identifiable object h_{min} is $0.33r$ for this set of samples. The square-shaped area of the array elements is blurred by diffusion of the mediator and indicated slightly only for the largest substrate electrode (Fig. 22). For the electrode with a size of 6.5 µm, a signal is found which cannot be convincingly distinguished from variations of the background signal arising from the roughness of the insulating cover layer of the arrays (compare with Fig. 10b of an analogous electrode array). Variations of the background signal are also visible in Fig. 20. The normalized plots $i_{-T}/i_{+T\infty}(x,y)$ in Figs. 15b–21b reveal that the variation of the background current has approximately the same level in all images and becomes only comparatively larger with the decreasing

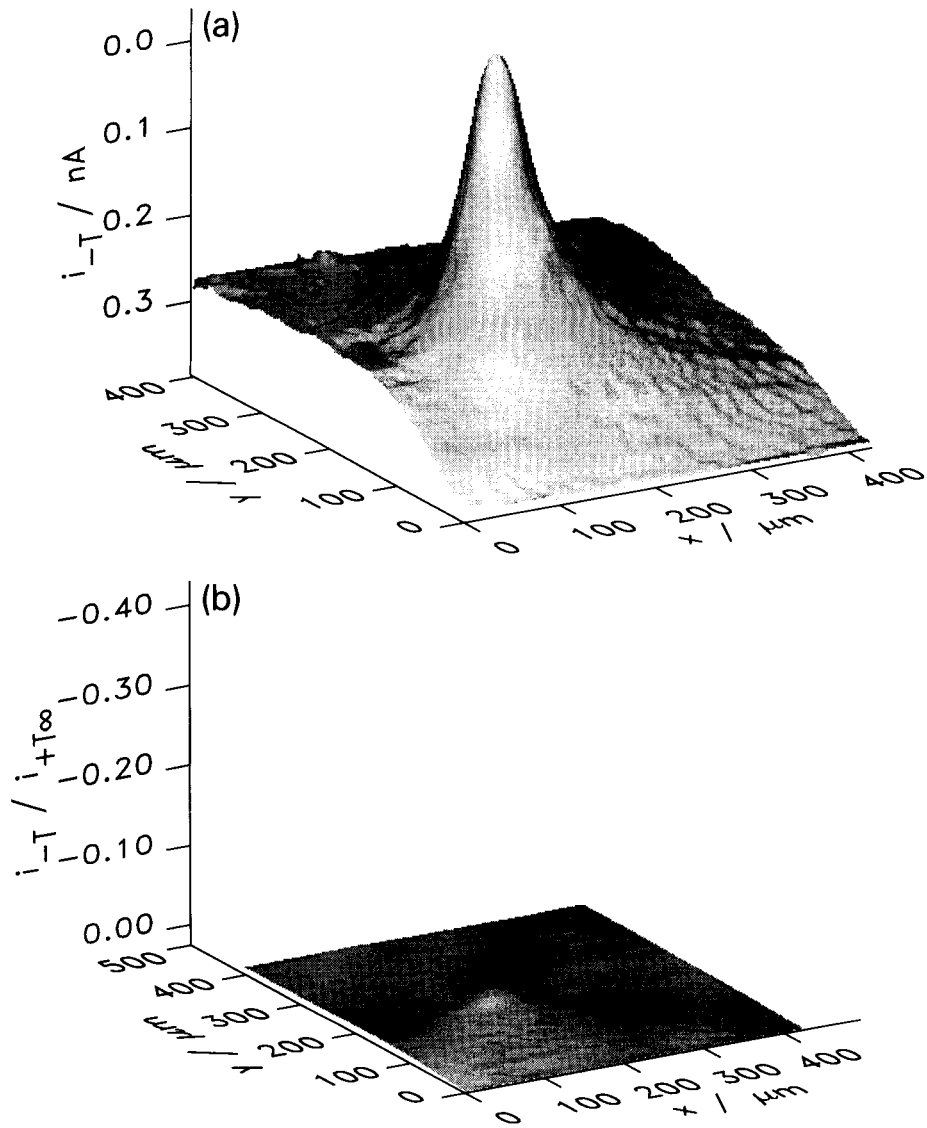

Fig. 20. As Fig. 15, but $h = 10$ µm.

signal for the array electrode. Fig. 23 represents the background-subtracted cross sections of the Figs. 15b–21b along the direction of the line scans through the extrema of the response surfaces. The decreasing size of the substrates for the Curves 1–7 causes first of all a decrease in the signal height rather than a diminished width at half height, because as with any other spatially resolved analytical technique, the spatial signal width is influenced predominately by the width of the tip profile if the imaged object becomes smaller than the width of the profile.

The predicted value for $h_{min} = (0.05–0.1)r$ [22] could not be achieved with this set of samples. As explained above, this is mainly attributed to the unfavourable sample-depending conditions. An experimental verification of the value theoretically derived by Bard et al. [22] seems to be possible if a sample is on hand that meets all the specifications assumed in the estimation of the theoretical h_{min}. The proof of $h_{min} = 0.2r$ also failed in the attempt to image an array of 100 platinum electrodes with 1 µm diameter and 10 µm interelectrode distances on a silicon wafer with a

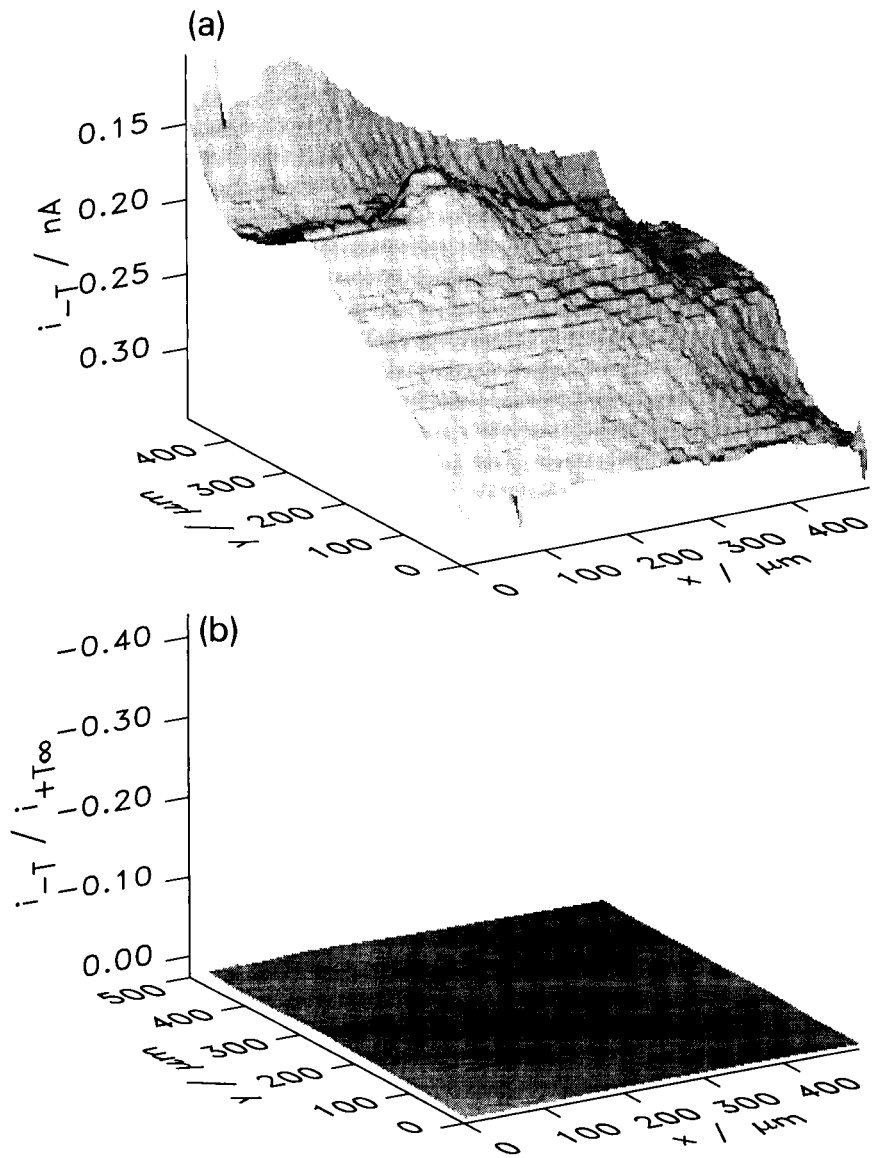

Fig. 21. As Fig. 15, but $h = 6.5$ μm.

tip electrode of $r = 5$ μm. In this case the interelectrode distance might be too small to achieve the predicted h_{min} value.

The difficulties associated with the experimental determination of h_{min} emphasize the usefulness of quantifying the resolution ability of the SECM via the resolution limit Δx as proposed above since the experimental verification is straightforward and does not require special samples.

3.6. Conclusions

A comparatively simple scanning electrochemical microscope was constructed utilizing a commercially available open-loop, Inchworm™ motor-driven micropositioning system, a locally constructed bipotentiostat and AD/DA converter board. A large signal-to-noise ratio and acceptable positioning accuracy of the instrument could be achieved by using tailor-made drivers

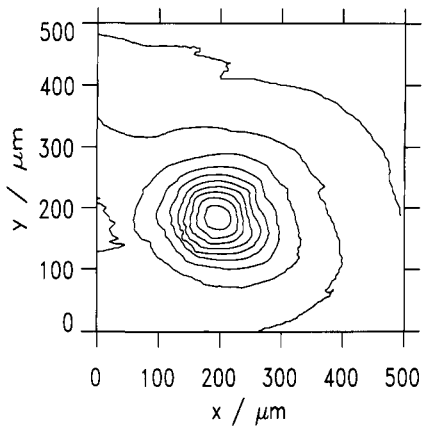

Fig. 22. Contour plot of Fig. 15a.

for the hardware components. Capabilities and limitations of this setup are demonstrated. A new approach was suggested to quantify the ability for spatial resolution of a SECM and its tip. The experimental determination of this parameter requires only a very simple test sample and is in this respect advantageous over the definition of the resolution ability via the smallest imageable object, which requires special sample sets and is strongly dependent not only on the instrument and the tip electrode but also on several sample specifications.

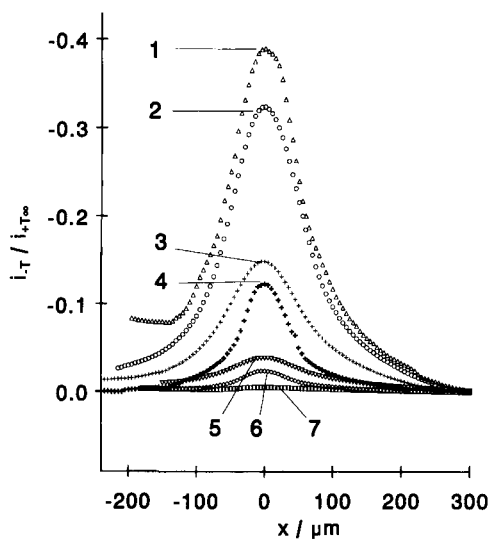

Fig. 23. Background corrected cross-section through the extrema of the response surfaces of Fig. 15b–21b along the main scan direction; size h of the substrate microelectrodes in μm: (1) 90; (2) 70; (3) 50; (4) 30; (5) 20; (6) 10; (7) 6.5.

Acknowledgements

The unselfish support of A.J. Bard and D.O. Wipf in providing information about their SECM systems is gratefully acknowledged. The authors thank B.L. Ramos and F.-M. Matysik for preparation of the ultramicroelectrodes and M. Kummer for providing the spray coated gold electrode. H.E. was Feodor-Lynen Fellow of the Alexander von Humboldt Foundation and Visiting Scholar at the University of Cincinnati. G.W. has received a grant of the German National Scholarship Foundation. Financial support by DOE grant 86ER-60487 (WRH) is gratefully acknowledged.

References

[1] R. Sonnenfeld and P.K. Hansma, Science, 232 (1986) 211.
[2] P. Lustenberger, H. Rohrer, R. Christoph and H. Siegenthaler, J. Electroanal. Chem., 243 (1988) 225.
[3] S. Manne, P.K. Hansma, J. Massie, V.B. Elings and A.A. Gewirth, Science, 251 (1991) 183
[4] P.A. Christensen, Chem. Soc. Rev., 21 (1992) 197.
[5] R.C. Engstrom, M. Weber, D.J. Wunder, R. Burgess and S. Winquist, Anal. Chem., 58 (1986) 844.
[6] H.Y. Liu, F.-R.F. Fan, C.W. Lin and A.J. Bard, J. Am. Chem. Soc., 108 (1986) 3838.
[7] J. Kwak, Ph.D. Thesis, The University of Texas at Austin, 1989.
[8] A.J. Bard, F.-R.F. Fan, J. Kwak and O. Lev, Anal. Chem., 61 (1989) 132.
[9] J. Kwak and A.J. Bard, Anal. Chem., 61 (1989) 1221.
[10] A.J. Bard, F.-R.F. Fan, D.T. Pierce, P.R. Unwin, D.O. Wipf and F. Zhou, Science, 254 (1991) 68.
[11] J. Kwak and A.J. Bard, Anal. Chem., 61 (1989) 1794.
[12] E.A. Blubaugh, G. Russel, M. Racke, D. Blubaugh, T.H. Ridgway and H.B. Mark, Jr., presented at the ACS Symposium on Polymeric Materials for Analysis and Diagnostics, Denver, 1992.
[13] D.W. Paul, Ph.D. Dissertation, University of Cincinnati, 1980.
[14] F.-M. Matysik, Diploma Thesis, University of Leipzig, 1990.
[15] B.L. Ramos, E.A. Blubaugh, T.H. Ridgway and W.R. Heineman, Anal. Chem., 66 (1994) 1931.
[16] M.Gomez and A.E. Kaifer, J. Chem. Educ., 69 (1992) 502.
[17] M.V. Mirkin and A.J. Bard, Anal. Chem., 64 (1992) 2293.
[18] M.V. Mirkin, L.O.S. Bulhões and A.J. Bard, J. Am. Chem. Soc., 115 (1993) 201.
[19] G. Wittstock, H. Emons, M. Kummer, J.R. Kirchhoff and W.R. Heineman, Fresenius' J. Anal. Chem., 348 (1994) 712.
[20] G. Ehrlich, K. Danzer and V. Liebich, in Proceedings of the 2. Tagung Festkörperanalytik, Bd. 1, TH Karl-Marx-Stadt, Karl-Marx-Stadt, 1979, p. 69.
[21] P.R. Unwin and A.J. Bard, J. Phys. Chem., 95 (1991) 7814.
[22] A.J. Bard, M.V. Mirkin, P.R. Unwin and D.O.Wipf, J. Phys. Chem., 96 (1992) 1861.
[23] F. Zhou, P.R. Unwin and A.J. Bard, J. Phys. Chem., 96 (1992) 4917.

ELSEVIER

Analytica Chimica Acta 298 (1994) 303–317

ANALYTICA CHIMICA ACTA

Selection of molecular descriptors used in quantitative structure–gas chromatographic retention relationships I. Application to alkylbenzenes and naphthalenes

N. Dimov [a], A. Osman [b], Ov. Mekenyan [b,*], D. Papazova [c]

[a] *NIHFI, 1756 Sofia, Bulgaria*
[b] *Bourgas Technological University, Bourgas, Bulgaria*
[c] *Neftochim AD, Bourgas, Bulgaria*

Received 21 January 1994; revised manuscript received 9 June 1994

Abstract

The descriptors used in quantitative structure–gas chromatographic retention relationships are chosen among the physico-chemical properties and calculable indices of the compounds studied. In order to overcome the problems related to this choice, a suitable classification of molecular descriptors would be beneficial. The classification in this study is based on the extent of correlation of the corresponding descriptor with the retention by linear modelling. The idea is illustrated with a set of more than 35 descriptors and gas chromatographic retention data for 16 alkylbenzenes and 13 naphthalenes chromatographed on three stationary phases with different polarities. Four groups, namely substantial, important, likely and specific descriptors, were defined. The descriptors from the substantial group correlate with the retention index of the compounds studied to a very high extent, above 0.99. Some of the descriptors from the next group, important, are suitable for modelling, if tuned with the descriptors from the specific group. None of the descriptors from the likely group is able to be combined either with substantial or specific descriptors in order to give an adequate model, despite the proved applicability of many of them in quantitative structure–activity relationships. Very good correlations between some indicator variables and quantum chemical indices were also established. Owing to the fact that the indicator variables (descriptors) can be easily designed and interpreted, their use instead of the more complicated quantum chemical indices is promising, thus making modelling with them well suited for practical chromatography.

Keywords: Gas chromatography; Alkylbenzenes; Molecular descriptors; Naphthalenes; Structure–GC-retention relationship

1. Introduction

Retention in chromatography is due to the integral effect of molecular interactions between the analyte and both mobile and stationary phase molecules. All components of these Van der Waals interactions depend on the distance between the charges in the molecules. The exact orientations of interacting molecules in a solution is unknown, however, and can be only presumed [1]. Besides, the existing numerical methods for determining the preferred

* Corresponding author.

SSDI 0003-2670(94)00280-Y

conformation are limited to the approximation of the isolated molecule. As a result the quantum chemical calculations of intermolecular interactions in solutions are very limited.

Investigations with another approach, the quantitative structure–retention relationship (QSRR), led to several promising results [2,3]. According to the basic QSRR assumption, the structure of a solute molecule can be quantitatively described by suitable numerical descriptors. One would expect that some of these structural descriptors can mimic, although indirectly, the intermolecular interactions decisive for the retention under defined chromatographic conditions. Thus, the combination of QSRR methodology with the experience and intuition of practising gas chromatographers could facilitate the development of analytical methods, allowing a better understanding of the intimate retention mechanism and eventually a positive peak identification with only chromatographic data.

This stimulated the use of a variety of descriptors (e.g., [2–9]) for the calculation of chromatographic retention, some of which are connected with the electrical properties of the analyte molecules (such as atom charges and bond charges) and others with the geometry and topology of the solute molecule. Good correlations were found also between the relative retention and some of the solute properties such as boiling point and molecular refraction [10–13]. Nowadays, both calculable indices and indicator variables (describing the presence or absence of particular structural fragments at a specific site) are used as descriptors for correlation with solute chromatographic relative retention (e.g., [6,14]).

Kováts [15] first studied the relationship between molecular structure and retention index (RI). His encouraging results were confirmed by Chovin [16], Baron and Maume [17] and Zulaica et al. [18] and since then many workers have studied this area. Their investigations, however, have had only limited success, mostly owing to the poor reproducibility of the experimentally obtained retention data. These data are, however, only one of the components in QSRR investigations. The descriptors of the solute physico-chemical properties and molecular structure are the second component of the modelling process. Further, these decriptors are used for deriving regression, linear (e.g., [7,10,13]) or non-linear (e.g., [19,20]). The regression obtained has to obey the classical statistical rules for reliability: high correlation coefficient, high F value, to satisfy Student's t-test, and also some non-traditional tests such as the statistical requirement of Topliss and Edwards [21] for chance correlation and the cross-validation (''leave-one-out'') procedure [22]. One should also pay attention to the requirement for a minimum discrepancy between experimental and calculated values of retention, assessed by the maximum values of the discrepancy for a derived regression equation (Δ_{max}).

Computerized modern equipment and software already provide precise retention data, which can be used for a reliable QSRR. The available packages of software allow one to manipulate the data in different ways. The selection of descriptors, however, remains questionable.

It is known from the chromatographic modelling practice that some of the molecular descriptors intercorrelate highly and hence they should not be used together in the same regression equation. This was demonstrated by Buydens and Massart [5]. They found that higher correlation coefficients (above 0.99) can be obtained only when a large set of descriptors, some of which intercorrelate highly, are included in the regression models.

The primary goal of this study is to rank solute descriptors assessing different components of molecular structure from the standpoint of their applicability in quantitative structure–gas chromatographic retention relationship. This is achieved by (i) arranging the different descriptors according to their individual correlation coefficients, r, with the retention, RI, (ii) calculating the intercorrelation between the descriptors within each group and (iii) selecting those descriptors from the different groups which are sufficient for the adequate prediction of the retention observed. The present descriptor ranking is illustrated by a set of 16 alkylbenzenes and 13 naphthalenes separated on stationary phases with different polarity. It is hoped that this paper will enable the reader to appreciate these more pragmatic aspects of QSRR and thus help in selecting the proper approach and suitable parameters for solving particular problems.

2. Brief review of the descriptors used for modelling the gas chromatographic retention of alkylbenzenes and napthalenes

One of the first physico-chemical properties used for the precalculation of the retention indices of alkylbenzenes is the boiling temperature, T_b [23]. It was found [24] that for 39 alkylbenzenes chromatographed on squalane the standard deviation is 4.5 units and for 19 naphthalenes 7.8 units when this parameter was used as a regressor. The greatest discrepancies were observed for *ortho*-substituted alkylbenzenes.

Gassiot-Matas and Firpo-Pamies [25] suggested a function composed of two physico-chemical parameters: the molecular refraction, *MR*, called a bulk term, and a polar term, related to the solute polarity, the dipole moment, μ. The discrepancies were, however, again greater than those acceptable for inter-laboratory reproducibility.

An incremental approach was published [26,27] based on the equation

$$I_{calc.} = 100Z + \Sigma m_i - \Sigma n_i \qquad (1)$$

where Z is the total number of C atoms, m_i accounts for the contribution of the different functional groups and n_i assesses the structural variation in the alkyl substituent as well as the *ortho* effect. The parameters m_i and n_i were related to the so-called indicator variables. The variance for ten alkylbenzenes under investigation was found to be 20.1 units.

Incremental approaches have also been used [6,28]. The appropriate set of descriptors [6] were chosen among a set of 43 topological and quantum chemical indices. Indicator variables used to describe the presence of specific structural fragments were also added in this investigation. It was found that the maximum error in *RI* prediction of 28 alkylbenzenes on seven stationary phases was 3 units when topological and quantum chemical descriptors only are used. The greatest discrepancy of the equations derived by indicator variables only was found to be 5 units [6]. The incremental approach based on fragment additivity [28] provides a maximum discrepancy of about 6 units for 89 alkylbenzenes separated on silicone oil OV-101.

A thermodynamic approach was applied for homologous series of alkylbenzenes [29]. The general equation involves the electrostatic (ΔG_{el}), dispersion–repulsion ($\Delta G_{d,r}$) and cavity (ΔG_{cav}) contributors to the total solvation energy (ΔG_{solv}). One can conclude from the particular equations derived that there exists one basic contributor:

$$I = 125.39 + 31.9\Delta G_{solv} \quad \text{with } r = 0.99986 \qquad (2)$$

or

$$I = 108.17 + 20.34\Delta G_{d,r} \quad \text{with } r = 0.99970 \qquad (3)$$

The equations are valid for homologous series only. For the best regression (C_7–C_{12} monoalkylbenzenes) the maximum error is 4.3 units and the minimum error 1.3 units.

Recently, Woloszyn and Jurs [30] proposed an equation that related different molecular features (topological, geometrical, electronic or physico-chemical in nature) to the observed retention index of 67 hydrocarbons, 43 of which are alkylbenzenes. On a non-polar stationary phase (SE-30) the correlation coefficient (r) was 0.983 and the standard deviation (S.D.) was 18.6. On a polar stationary phase (Carbowax 20 M) $r = 0.987$ and S.D. = 23.3. In both instances molecular mass or boiling temperature were included as significant descriptors.

From this brief survey it appears that the descriptors used in QSRR can be considered from two aspects: (i) global descriptors describing molecular properties related to the whole molecule (e.g., M_m, T_b) and local indices, e.g., indicator variables, electronic charges and atomic polarization, and (ii) significant descriptors with high correlation with gas chromatographic retention and hence with the highest contribution to the *RI* value and insignificant descriptors.

On the other hand, the observed discrepancies between the calculated retention indices and experimentally obtained *RI* values varied significantly. However, values for maximum difference of 5 units for non-polar phases and 10 units for polar phases could be accepted as easily attainable inter-laboratory reproduciblity in practice. Hence one can accept as statistically adequate a regression model for *RI* calculation for which the mentioned magnitudes are the upper limit for the maximum discrepancy (Δ_{max}).

3. Data handling

The structure and data manipulation used in this investigation of the quantitative structure–gas chromatographic retention relationships is based on the OASIS approach [31–33]. It consists of four stages: (i) entry and storage of chromatographic data and associated information for molecular topology of compounds studied, (ii) generation of 3D molecular structure, proceeding from atom connectivity only, (iii) calculation topological, steric and quantum chemical indices and (iv) multiple regression analysis.

As mentioned above, the present study is focused on the ranking of the tested molecular descriptors. The descriptor significance is estimated using the methodology for deriving a mathematical model for the chromatographic retention given elsewhere [13,34]. The contributors to the retention were divided in this model into two groups, basic and tuning:

$$RI_{calc} = b_0 + \sum_{i=1}^{n} b_i B_i + \sum_{j=n+1}^{n+k} b_j T_j \qquad (4)$$

where RI_{calc} represents the corresponding retention, and in gas chromatography this is usually the retention index, RI_{exp}. The lower the value of b_0, the more suitable is the parameters choice. The parameters B_i include those solute descriptors (e.g., experimentally obtained physico-chemical properties, calculated structural indices or indicator variables) which allow the calculation of the $RI_{B.\ calc}$ value closest to the experimental retention. Owing to the restriction of statistically permitted intercorrelations, there is normally one basic descriptor only to be used. The problem is the choice to allow the best combination with tuning contributor(s). The parameters T_j are solute descriptors, which tune the $RI_{B.\ calc}$ value to that of RI_{exp} in such a way that the RI_{calc} values are statistically comparable to the interlaboratory reproducibility of the experimental RI values.

The molecular descriptors analysed in the present investigation were distinguished according to the scheme given in Fig. 1. Starting from their generic names (physico-chemical properties, topological and quantum chemical indices, etc.) two groups relevant

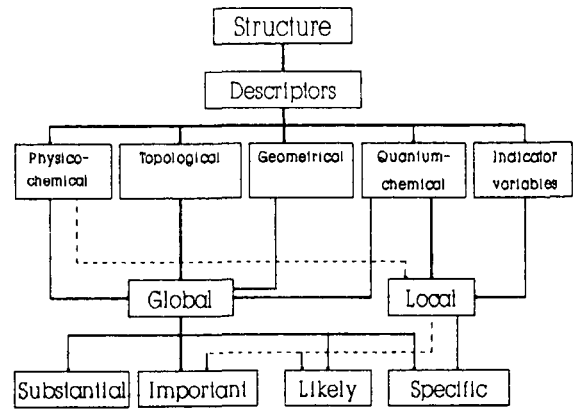

Fig. 1. Scheme of solute descriptors.

the solute features and four groups relevant the significance to the chromatographic retention were formed.

The values of calculable indices were obtained after optimization of the molecular geometry by the PM3 quantum chemical method included in the OASIS package for quantitative structure–activity relationship (QSAR) calculations [32,33]. The values of the Bonastre vapour pressure index I_p [35] and of the physico-chemical index PCI [36] were calculated by using a laboratory-written DBASE-Pascal program. The following criteria for assessing the statistical significance of the regression equation were applied: the value of the greatest discrepancy Δ_{max} between RI_{exp} and RI_{calc} for the studied set of compounds, the confidence interval of regression estimates (statistical significance of parametric estimations) and correlation coefficient.

4. Results and discussion

4.1. Alkylbenzenes

The individual correlation coefficients between chromatographic retention, the RI values of the tested alkylbenzenes (see Table 4) on three stationary phases of different polarity and all studied descriptors are given in Table 1.

According to the r values and the scheme in Fig. 1, the descriptors can be classified into four groups, depending on their individual significance for the

Table 1
Individual correlation coefficients, r, between alkylbenzene retention indices obtained on three stationary phases with different polarities and corresponding descriptors

No.	Descriptor	Abbreviation	Stationary phase		
			OV-101 (16) [a]	UCON LB 550 (118) [a]	C-20M (322) [a]
	Group of substantional parameters				
1	Bonastre index	I_p	0.9997	0.9952	0.9681
2	Log (vapour pressure)	Log p^0	0.9996	0.9952	0.9682
3	Boiling temperature	T_b	0.9993	0.9930	0.9639
4	Physico-chemical index	*PCI*	0.9936	0.9986	0.9875
	Group of important parameters				
5	Vapour pressure	p^0	0.9757	0.9724	0.9481
6	Hydrophobicity	Log *P*	0.9580	0.9300	0.8635
7	Molecular refraction	*MR*	0.9465	0.9177	0.8565
8	Volume polarizability	V_{pol}	0.9425	0.9084	0.6788
9	Geometric info Wiener	GW_{INFO}	0.9259	0.8590	0.5800
10	Info Wiener	W_{INFO}	0.9062	0.8692	0.7883
11	Molecular mass	M_m	0.8984	0.8554	0.7657
12	Molecular connectivity	χ	0.8924	0.8501	0.7615
13	Geometric Wiener index	*GW*	0.8900	0.8485	0.6000
14	Index of Kier and Hall	*K&H*	0.8850	0.8356	0.7549
15	Total electronic energy	E_T	0.8792	0.8383	0.7508
16	Hosoya's index	*Z*	0.8700	0.8290	0.6132
17	Wiener index	*W*	0.8646	0.8142	0.7134
	Group of likely parameters				
18	Zagreb index	*M*1	0.7800	0.7558	0.5438
19	Balaban's index	*D*2	0.7138	0.6548	0.4100
20	Info-Hosoya index	Z_{INFO}	0.7000	0.6935	0.4732
21	Maximum geometric distance	D_{max}	0.6228	0.5732	0.4009
22	Sum of charges at the alkyl substituent	q_T	0.5100	0.4444	0.3151
	Group of specific parameters				
23	Dipole moment	μ	0.2900	0.3490	0.4785
24	Atom charge at C-8 in *o*-alkyl substituents	$q_{7(8)}$	0.2403	0.2674	0.2972
25	*Ortho* effect	"*o*"	0.2056	0.2932	0.4316
26	Number of C atoms in normal substituent chain [b]	*nL*	0.2054	0.2707	0.3669
27	LUMO energy	E_{LUMO}	0.2000	0.2395	0.3800
28	Info-molecular connectivity index	χ_{INFO}	0.1572	0.1700	0.1572
29	Atom charge at C-1 [b]	q_1	0.1375	0.1349	0.1085
30	Atom charge at C-3 [b]	q_3	0.1114	0.1115	0.1197
31	Combined effect of type of substitution	*ST*	0.0728	0.1286	0.2391
32	Atom charge at C-4 [b]	q_4	0.0537	0.0629	0.0551
33	Atom charge at C-7 [b]	q_7	0.0460	0.0743	0.1582
34	HOMO energy	E_{HOMO}	0.0482	0.0882	0.2210
35	Atom charge of CH attached to the ring	CH-Ar	0.0423	0.0994	0.1643
36	Balaban's index	*J*	0.0328	0.0823	0.1300
37	Atom charge at C-2 [b]	q_2	0.0323	0.0483	0.1770
38	Sum of charges at the C-3 and C-4 atoms in the ring	$q_3 + q_4$	0.0030	0.0023	0.0047
39	Number of branching in the alkyl substituent [b]	$CH_{3\text{-}br}$	0.0026	0.0074	0.1615
40	Sum of charges at the C-1 and C-2 atoms in the ring [b]	$q_1 + q_2$	0.0021	0.1099	0.2432

[a] Polarity of stationary phase with respect to benzene according to McReynolds.
[b] See Fig. 2a.

retention studied. These groups are named conventionally as

(i) group of *substantional* descriptors for which $r > 0.99$ (e.g., I_p, T_b for non-polar stationary phases);

(ii) group of *important* descriptors for which $0.989 > r > 0.8$ (e.g., M_m, E_T, W);

(iii) group of *likely* descriptors for which $0.8 > r > 0.5$ (e.g. $M1$, $M2$, Balaban J, D_{max}); despite their general application in QSAR studies, these indices could be assessed as insignificant for the particular series of compounds under investigation;

(iv) group of *specific* descriptors for which $r < 0.5$, i.e., local descriptors such as atomic charges, atomic polarization at a given C_i atom (for the numeration see Fig. 2a) or indicator variables corresponding to specific structural fragments.

The parameters B_i for Eq. 4 can be chosen from Table 1. Owing to the high intercorrelation among descriptors within one group, from a statistical point of view only one representative (descriptor) from the first three groups should be chosen as a regressor for further modelling. There is no restriction, however, on choosing two descriptors, if the accepted criteria can be obeyed.

It can be ascertained that the significance of the descriptors from the first three groups (most of them global descriptors) decreases with increased polarity of the stationary phase under investigation. In contrast, most of the specific descriptors (most of them local descriptors) increase their individual significance with increasing polarity of the stationary phase (presented as McReynolds constants with respect to

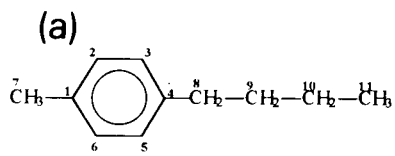

Abbreviation	Numbering of parameter in Table 1	Indicator variable value
q_-	33	calculable
n_L	26	4
"O -"	25	0
CH, br	39	0

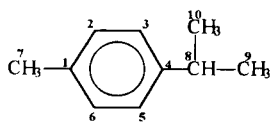

q_+	29	calculable
n_L	26	2
"O -"	25	0
CH, br	39	1

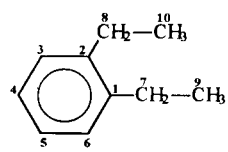

"O -"	25	1
$q_+ + q_-$	40	calculable
$q_-(\bullet)$	24	calculable

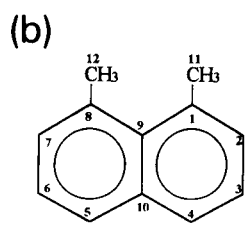

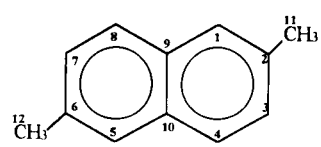

Fig. 2. Abbreviations of some of the descriptors in Table 1 related to the accepted atomic enumeration of alkylbenzenes (a) and enumeration of C atoms in naphthalene ring (b).

benzene). Only three descriptors, namely *PCI*, χ_{info} and $q_3 + q_4$ (Nos. 4, 28 and 38 in Table 1), demonstrate no clear dependence on stationary phase polarity, while q_1 (No. 29 in Table 1), which although being a local parameter, behaves as a global descriptor.

If the individual correlation coefficients obtained for the non-polar stationary phase OV-101 are arranged according to the origin of the descriptors used, one can see that all substantional and some important descriptors with the highest r values belong to the experimentally obtained quantities. The exact reverse, all specific descriptors, except the dipole moment, μ, and χ_{info}, are mostly local, calculable descriptors with a quantum chemical origin or indicator variables.

It seems that the more polar the stationary phase, the smaller is the possibility of using a single regression (only B parameters) in correlation models with acceptable Δ_{max}. On polar phases the retention appears to be due to both steric and electronic factors with an increased role of the latter. Thus, a model with B parameters, even when it is a substantional descriptor, should need always additional tuning descriptors, if the phase is polar.

We tested first the prediction of *RI* on non-polar stationary phases with one substantional descriptor. For example, on the non-polar stationary phase OV-101 and with Bonastre index I_p we obtain the equation

$$RI^{OV-1} = 27.22 + 0.988 I_p \quad (5)$$

which has a correlation coefficient $r = 0.9997$, standard deviation S.D. = 1.6 units and $\Delta_{max} = 3^{135TMB}$ for 1,3,5-trimethylbenzene (135TMB). Evidently, vapour pressure is sufficiently informative and Eq. 5 can be used for practical purposes when the data for p^0 of alkylbenzenes under investigation are known.

With the boiling temperature a high correlation value was again obtained ($r = 0.9993$), but the value of Δ_{max} equals the accepted upper discrepancy limit of 5 i.u. (1,2-diethylbenzene).

No other descriptor allows a single regression with an error less than 5 i.u. Evidently, if another basic parameter has to be used (e.g., owing to a lack of experimentally determined data for p^0 or T_b), the modelling of *RI* with other substantional or important descriptors should be accomplished by adding specific descriptors as tuning parameters in Eq. 4. Table 1 allows one to match the combinations of descriptors according to their correlation coefficients.

The same conclusion can be made if polar stationary phases are used. Even on the medium-polarity stationary phase UCON and with the heaviest sub-

Table 2
Intercorrelation coefficients ($\times 10^2$) between descriptors used in the proposed QSRR models

	I_p	T_b	*MR*	M_m	χ	q_9	$q_{7(8)}$	"*o*-"	*nL*	q_1	*ST*	q_3	q_7	CH-Ar	q_2	$CH_{3\text{-br}}$	$(q_1 + q_2)$
I_p	99	95	89	89	67	23	20	20	15	< 1	13	< 1	< 1	< 1	< 1	< 1
T_b	100	95	90	89	68	22	20	19	14	< 1	11	< 1	< 1	< 1	< 1	< 1
MR		100	96	91	72	17	< 1	< 1	21	< 1	17	< 1	19	21	21	15
M_m			100	97	81	16	13	3	22	25	1	25	23	31	33	26
χ				100	81	23	15	< 1	13	32	7	17	13	31	16	29
q_0					100	22	5	12	9	43	18	39	37	14	40	12
$q_{7(8)}$						100	41	82	16	< 1	36	< 1	18	48	19	47
"*o*"							100	79	12	54	9	26	28	88	29	94
nL								100	28	36	36	23	28	84	29	83
q_1									100	19	63	41	10	46	28	10
ST										100	31	67	22	47	46	45
q_3											100	32	8	41	20	24
q_7												100	25	27	77	13
CH-Ar													100	21	68	28
q_2														100	26	93
$CH_{3\text{-br}}$															100	18

stantional descriptor I_p, Δ_{max} is $\pm 6^{123TMB}$ i.u. (for 1,2,3-trimethylbenzene). Such an RI_{calc} value is inadequate from a practical point of view.

The effect of the stationary phase polarity can be presumed from the r values of Table 1. Although with a preserved greatest weight in the RI_{calc} value, the diminished contribution of substantial descriptors to the retention is clearly demonstrated. This statement is emphasized on the more polar phase Carbowax 20 M. First, all substantional descriptors from the former phases fell into the next important descriptors group. The equation obtained with only one parameter, PCI, with the highest r value was

$$RI^{20\,M} = 249 + 0.981 PCI \quad (6)$$

with $r = 0.9875$, S.D. = 9.6 i.u. and $\Delta_{max} = 24^{123TMB}$. The discrepancy next in magnitude, $\Delta_{next} = 12^{1M2EtB}$, is again for an *ortho*-substituted alkylbenzene. It is clear that a one-parameter equation for the prediction of the retention of alkylbenzenes on Carbowax 20 M is nonsense.

It was recognized that the greatest absolute dis-

Table 3
Values of parametric estimations depending on the basic descriptors used (of tested MR, V_{pol}, GW_{info}, W_{info} and M_m as B descriptors, the best results were obtained with molecular mass, M_m and W_{info}) and on the polarity of the stationary phase

Case A: indicator variables ("*o*", $CH_{3\text{-}br}$ and *nL*) only used

Stationary phase	*B* descriptor		Tuning descriptors						υ		r		b_0	
	M_m	W_{info}	"*o*-"		$CH_{3\text{-}br}$		*nL*		M_m	W_{info}	M_m	W_{info}	M_m	W_{info}
			M_m	W_{info}	M_m	W_{info}	M_m	W_{info}						
OV-101	6.26	278	37	18	−30	−39	−12	−13	43	46	0.996	0.995	203	−429
UCON LB 550X	5.83	260	44	37	−31	−35	−12	−13	61	57	0.993	0.994	347	−244
Carbowax 20 M	5.57	248	58	52	−34	−39	−14	−16	80	66	0.991	0.993	538	−27

Case B: calculable indices only used

Stationary phase	*B* descriptor		Tuning descriptors										υ		r		b_0	
	M_m	W_{info}	q_2		q_3		q_7		$q_{7(8)}$		CH-Ar		M_m	W_{info}	M_m	W_{info}	M_m	W_{info}
			M_m	W_{info}	M_m	W_{info}	M_m	W_{info}	M_m	W_{info}	M_m	W_{info}						
OV-101	6.57	290	−1162	−734	−423	−80	73	731	−180	−230	−1053	−1259	115	109	0.990	0.991	285	−451
UCON LB 550X [a]	6.23	214	−1453	−1153	−550	−423	59	599	−189	−196	−1200	−1378	132	128	0.988	0.988	465	−450
Carbowax 20 M	6.11	210	−1981	−1688	−768	−641	550	650	−225	−233	−1322	−1501	192	163	0.990	0.986	707	−192

Case C: combination of indices and indicator variables used

Stationary phase	*B* descriptor		Tuning descriptors								υ		r		b_0	
	M_m	W_{info}	q_1		q_2		$CH_{3\text{-}br}$		*nL*		M_m	W_{info}	M_m	W_{info}	M_m	W_{info}
			M_m	W_{info}	M_m	W_{info}	M_m	W_{info}	M_m	W_{info}						
OV-101	6.87	298	−1623	−642	−905	−934	−39	−40	−22	−315	51	44	0.995	0.996	443	−383
UCON LB 550X	6.55	283	−2078	−1112	−2210	−1244	−41	−42	−24	−339	57	51	0.994	0.995	644	−150
Carbowax 20 M	6.49	280	−2723	−1707	−2877	−1792	−48	−49	−29	−424	98	68	0.990	0.993	928	126

The dispersion, v, correlation coefficients, r and intersept, b_0 are given too.

[a] For the phases UCON and 20 M GW_{info} give less Δ_{max}.

crepancies occur for *ortho*-substituted alkylbenzenes, whereas Δ_{next} includes also cases with branched alkyl substituents (e.g., isopropylbenzene). Hence it can be expected that specific descriptors reflecting *ortho* substitution could be successfully matched with *B* parameters. Adding another tuning descriptor reflecting the branching in alkyl substituents seems also to be of benefit. If so, the prospective specific descriptors from Table 1 have to be checked for their intercorrelation by the equation

$$\text{Descriptor}\,(i) = a + b \cdot \text{Descriptor}\,(j) \qquad (7)$$

The intercorrelation coefficient values r_i for the descriptors incorporated in the best regression equations presented further in the text are summarized in Table 2. As can be seen, many of them cannot be used together in one equation (e.g., M_m and *MR*) because of their high intercorrelation. On the other hand, the high r values observed between some indicator variables and quantum chemical indices allow the latter to be replaced in the regression by the easily determined indicator variables. To study this possibility, three types of equations were investigated: case A, equations with physico-chemical parameters and indicator variables only; case B, equations with only calculable indices; and case C, mixed type of equations with both calculable and indicator variables.

The values for parameter estimations, and also other statistics, are presented in Table 3. As can be seen, the estimated value of the basic parameters (M_m or W_{info}) does not change significantly (e.g., for M_m the mean value varies by $\pm 6\%$), whereas the estimated values for the descriptor accounting for the branching effect varies 1.2-fold, for *ortho*-substitution (indicator variable or q_2) 1.6-fold and q_7 more than 7-fold (case B) with increase in stationary phase polarity. Hence it was confirmed that the more polar the phase, the greater is the significance of the specific descriptors.

The calculated *RI* values obtained by the different equations are given in Table 4. RI_{exp} values, obtained in our laboratory on OV-101 stationary phase, are presented in column 2. The calculated RI_{calc} values obtained by using the substantional descriptor M_m as a basic parameter in Eq. 4 and applying case A regression are presented in column 3. RI_{calc} values obtained with the W_{info} substantional descriptor as a basic parameter and case B regression are given in column 4 and case C models in column

Table 4
Comparison of the calculated *RI* values (RI_{calc}) according to the parametric estimations for the three types of equations given in Table 3, and also RI_{calc} from Ref. [28] with the experimentally obtained values on OV-101 (RI_{exp})

No. Compound	RI_{exp}	RI_{calc}				
		Case A	Case B	Case C	Eq. 11	Ref. [28]
1 nPrB	947.5	955.6	951	954	949	949.5
2 nBuB	1046	1050	1036	1042	1044	1046.5
3 iPrB	919	921	905	924	918	922
4 tertBuB	986	988	996	984	985	982
5 14DMB	866	860	865	858	863	879
6 13DMB	866	870	869	866	869	876.5
7 1M4iPrB	1016.5	1006	1015	1007	1012	1018
8 1M3iPrB	1010	1014	1023	1018	1017	1014
9 1M4nPrB	1046.5	1045	1043	1042	1047	1046
10 1M3nPrB	1042	1042	1043	1042	1042	1042.5
11 1M2EtB	973	979	983	979	976	972
12 13DEtB	1038.5	1040	1033	1043	1039	1037
13 12DEtB	1051	1048	1046	1048	1049	1051
14 135TMB	969	962	970	970	966	967.5
15 124TMB	988	988	995	993	992	991
16 123TMB	1016	1012	1004	1010	1011	1014
s^2	25 [a]	43	99	51	18	23

[a] Conventionally accepted as mean value S.D. = 5.

5. None of the equations satisfies the accepted upper limit of a 5 i.u. error for any compound. In cases A and B Δ_{max} is 10 i.u. and in case C 9 i.u. Hence, although the tuning descriptors became more important with increase in stationary phase polarity (see their estimated values in Table 3), the variances between the calculated and experimental *RI* also increase. This result is consistent with the well known decrease in inter-laboratory reproducibility of RI_{exp} obtained on polar stationary phases.

The increased value of the intercept b_0, in the case of models with the basic parameter M_m, confirms the failure of tuning descriptors to describe adequately the new intermolecular interactions due to the higher polarity of the stationary phase. From a chromatographic point of view the equation with W_{info} shows less Δ_{max}, but the variances remain statistically equal.

The equations given in Table 3 are those selected from a larger set of equations, not presented here, which have comparable statistics, but with the lowest Δ_{max}. From a chromatographic point of view the accuracy of the results in columns 3–5 is still unsatisfactory. In order to improve the accuracy of the regressions, without increasing the number of descriptors, combinations of different types of descriptors have to be worked out.

The high intercorrelation between some calculable quantum chemical indices and the indicator variables, and also the similar statistics, obtained by the different types of regressions encouraged us to study their interchangeability. A foundation for such an investigation was also the very good correlation between indicator variables and the retentions of more than 80 alkylbenzenes obtained previously [28]. The correction for the *ortho* substitution and the branching effect assumed in certain empirical approximations [28] was verified in the present study. The atom charges at all C atoms are presented in Table 5. A clear quantitative dependence on indicator variables is observed. Designating the charge of the monosubstituted ring C atom by q_1 (Fig. 2a), one can see that this charge, although changed, varies in a limited interval of $\pm 14\%$ (Table 5). Compared with this value, q_2 (when *ortho* substituted) has a lower mean value of $693 \pm 4\%$. The correlation found between the indicator variable "*ortho* effect" and atom charges at C_1 and C_2 is:

$$\text{"}o\text{"} = 6.65 + 37.32.(q + q_2) \qquad r = 0.94 \qquad (8)$$

For *meta* substitution, q_3 has a value of $663 \pm 3\%$ and for *para* substitution $q_4 = 809 \pm 5\%$.

The charges at carbon atoms in alkyl substituents, as seen from Table 5, also show a clear dependence

Table 5
Charges at carbon atoms ($\times 10^{-4}$) in aromatic ring (denoted respectively by q_1, q_2, q_3 and q_4) (see Fig. 2) and in CH_3, CH_2, CH and C attached to aromatic ring

No.	Compound	q_1	q_2	q_3	q_4	CH_3-Ar	CH_2-Ar	CH-Ar(C-Ar)
1	nPrB	774	1004	999	1060	0	558	0
2	nBuB	775	1001	1000	1050	0	544	0
3	iPrB	764	989	1008	1063	0	0	284
4	tertBuB	627	1061	1004	1069	0	0	(64)
5	14DMB	810	962	963	*813* [a]	2×633	0	0
6	13DMB	697	1004	*695*	1136	2×649	0	0
7	1M4iPrB	780	1049	945	*811*	631	0	280
8	1M3iPrB	737	1030	*696*	1045	644	0	284
9	1M4nPrB	782	1030	953	*842*	632	541	0
10	1M3nPrB	686	1153	*631*	1138	646	549	0
11	1M2EtB	792	*675*	1050	1036	675	525	0
12	13DEtB	651	1209	*649*	1134	0	2×550	0
13	12DEtB	755	*758*	1040	1042	0	2×570	0
14	135TMB	660	1069	*647*	1092	3×655	0	0
15	124TMB	841	*682*	958	*771*	3×650	0	0
16	123TMB	685	*659*	727	1087	3×695	0	0
Mean		$740 \pm 14\%$				$654 \pm 6\%$	$547 \pm 4\%$	283

[a] Values in italics are the exceptions from the regular atom charges, specific for the corresponding substitution.

Table 6
Individual correlation coefficients, r, between naphthalene retention indices obtained on three stationary phases with different polarities and corresponding descriptors

No.	Descriptor	Abbreviation	Stationary phase		
			OV-1 (16) [a]	OV-17 (119) [a]	UCON HB 280 × (177) [a]
Group of substantional parameters					
1	Boiling temperature	T_b	0.9969	0.9966	0.9952
2	Total electronic energy	E_T	0.9911	0.9320	0.9781
Group of important parameters					
3	Zagreb index	$M2$	0.9891	0.9435	0.9826
4	Hosoya's index	Z	0.9869	0.9189	0.9734
5	Info Wiener	W_{INFO}	0.9848	0.9275	0.9674
6	Molecular connectivity	χ	0.9843	0.9625	0.9672
7	Index of Kier and Hall	$K\&H$	0.9828	0.9078	0.9678
8	Hydrophobicity	Log P	0.9821	0.8435	0.9541
9	Molecular refraction	MR	0.9819	0.8400	0.9543
10	Geometric info Wiener	GW_{INFO}	0.9792	0.9200	0.9623
11	Molecular mass	M_m	0.9751	0.9486	0.9543
12	Wiener index	W	0.9381	0.8999	0.9079
13	Geometric Winer index	GW	0.9186	0.8345	0.8900
14	HOMO energy	E_{HOMO}	0.8974	0.9137	0.9098
15	Volume polarizability	V_{pol}	0.8914	0.8245	0.8645
16	LUMO energy	E_{LUMO}	0.8896	0.8134	0.8745
Group of likely parameters					
17	Info-moleculecular connectivity index	χ_{INFO}	0.7896	0.8543	0.8234
18	Info-Hosoya index	Z_{INFO}	0.7809	0.7751	0.7700
19	Atom polarizability at 6th C atom [b]	π_6	0.7534	0.7896	0.7506
20	Bond order between the first (C-1) and second (C-2) carbon atoms	p_{1-2}	0.6843	0.7324	0.7241
21	Atom polarizability at C-1	π_1	0.6828	0.7832	0.7109
22	Methyl group at C-1	$1R$	0.5203	0.5781	0.5630
Group of specific parameters					
23	Atom charge at C-1	q_1	0.4623	0.5741	0.5100
24	Atom polarizability at C-7	π_7	0.4532	0.4723	0.4800
25	Dipole moment	μ	0.4451	0.4700	0.4812
26	Atom charge at C-3	q_3	0.3820	0.3442	0.3897
27	*Ortho* effect	"o"	0.2933	0.3323	0.3014
28	Bond order C-7–C-8	p_{7-8}	0.2900	0.3012	0.3000
29	Maximum geometric distance	D_{max}	0.2623	0.1436	0.1899
30	Methyl group at C-2	$2R$	0.2613	0.1581	0.2030
31	Atom charge at C-4	q_4	0.2086	0.3229	0.2451
32	Atom polarizability at C-8	π_8	0.2034	0.1600	0.1600
33	Atom charge at C-9	q_9	0.1543	0.0945	0.1206
34	Atom charge at C-8	q_8	0.1326	0.1209	0.0937
35	Bond order C-8–C-9	p_{7-8}	0.1123	0.0546	0.0549
36	Atom charge at C-7	q_7	0.0812	0.1532	0.0542
37	Atom charge at C-2	q_2	0.0223	0.1000	0.0510

[a] Polarity of stationary phase with respect to benzene according to McReynolds.
[b] See Fig. 2b.

on their location on the benzene ring. A CH_3 group attached directly to the ring has a charge of $-0.0654 \pm 4\%$, one CH_2 group $-0.547 \pm 4\%$, one CH group -0.0283, while a C group has a positive charge of 0.0064. The following regression between the indicator variable "branching" and quantum chemical index atom charge was found to be the best:

$$CH_{3br} = 0.0728 - 0.014[q(-CH-Ar)]^{-1} \quad (9)$$

with $r = 0.94$, where $q(-CH-Ar)$ is the atom charge on a C atom in CH connected to the ring. The verification is given in case B (Table 3).

For the alkyl chains with two or more C atoms in an *ortho* location denoted as *nL*, the charges at C-1, C-2, C-3 and C-4 (Fig 2a) were tested as tuning descriptors. It was found that the equation

$$nL = 2.58 - 24.43q_2 - 12.72q_{7(8)} \quad (10)$$

has the best correlation coefficient, $r = 0.96$; $q_{7(8)}$ represents the atom charge at the α-C atom in an *o*-alkyl substituent with two or more C atoms. Again the data in Table 3 corroborate the possibility of interchanging quantum chemical indices by indicator variables.

For complete support of the proposed interchangeability, we calculated the *RI* values of the alkylbenzenes tested in this work with Eq. 3 in Ref. [28]. The results are compared (Table 4, column 7) with those obtained by using equations presented in the present study. The results obtained by using indicator variables are even better from a chromatographic point of view: only two RI_{calc} values have discrepancies above 5 i.u. Evidently, prediction equations can be obtained by using both calculable or indicative indices, the latter being easier for acquisition and interpretation.

The next step is to increase the accuracy achieved in case C by more suitable combinations. From the analysis of the data presented in Table 5 one can see that the combination of atom charges at first to fourth atoms in the ring seems promising. The following equation with the lowest Δ_{max} was worked out:

$$\begin{aligned} RI^{OV-1} = {} & 334(\pm 45.62) + 6.76(\pm 0.28)M_m \\ & + 1154(\pm 223)(q_1 + q_2) \\ & - 33.7(\pm 4.95)CH_{3br} \\ & + 279.5(\pm 101.9)q_{7(8)} \\ & + 95.21(\pm 64.05)ST \end{aligned} \quad (11)$$

with $r = 0.9984$, S.D. = 4 and $\Delta_{max} = 7^{1M3iPrB}$. The term *ST* is associated with the charges at C-1, C-2, C-3 and C-4 ring atoms and is incorporated to describe the effect of *ortho, meta* or *para* substitution. None of the parameters intercorrelate greater than 0.5. The applicability of Eq. 11 is demonstrated with the RI_{calc} values given in column 6 in Table 4.

The above results can be summarized as follows. It is essential to use one substantional or important descriptor as the basic parameter in Eq. 4 for modelling the gas chromatographic retentions of the studied compounds. Independent of the stationary phase polarity, its contribution to the RI_{calc} value is the

Table 7
Descriptor values used for deriving of regression equations

No.	Naphthalene compound	T_b	$-E_T$	W_{INFO}	χ	Log *P*	M_m	*W*
1	Naphthalene	217.9	6644	5.33	4.97	3.11	128.16	109
2	1-MeNapht	244.2	7986	5.63	5.38	3.60	142.19	140
3	12-DiMeNapht	271.1	9381	5.89	5.79	4.09	156.21	178
4	13-DiMeNapht	265	9320	5.88	5.77	4.09	156.21	179
5	14-DiMeNapht	268.5	9407	5.89	5.71	4.09	156.21	176
6	15-DiMeNapht	270.1	9401	5.89	5.79	4.09	156.21	176
7	16-DiMeNapht	265.5	9302	5.88	5.77	4.09	156.21	181
8	17-DiMeNapht	262.9	9323	5.88	5.77	4.09	156.21	180
9	18-DiMeNapht	276.5	9523	5.90	5.79	4.09	156.21	175
10	2-MeNapht	241.1	7888	5.61	5.36	3.60	142.19	144
11	23-DiMeNapht	268	9284	5.87	5.77	4.09	156.21	182
12	26-DiMeNapht	262	9141	5.86	5.75	4.09	156.21	186
13	27-DiMeNapht	262	9195	5.87	5.75	4.09	156.21	185

greatest. For non-polar phases there are enough sufficient substantional descriptors for adequate *RI* prediction. There is no exact correspondence between the individual correlation coefficient value of the substantional descriptors and their suitability for deriving adequate multivariable QSRR models. A suitable combination of basic and tuning parameters has to be exhaustively searched for among all members of a given group. Several equations with equal statistics could be obtained, but the regression most clearly expressing the retention mechanism should be preferred.

4.2. Naphthalenes

The individual correlation between the retention and descriptors studied, and the intercorrelation coefficients between the regressors, were obtained according to the methods already described for alkylbenzenes. The enumeration of C atoms in the naphthalene rings is presented in Fig. 2b. The individual correlation coefficients of the models obtained are summarized in Table 6. In general, the contribution of the different descriptors to the retention of napthalenes is preserved with the notable exception of the descriptors E_T, $M2$, E_{HOMO} and E_{LUMO}. Their weight in the RI_{calc} value changes to such an extent that some of them even moved from one group into another. The influence of the polarity of the stationary phases on the r values was found to be not so significant as was found for alkylbenzenes. It can be seen from the data in Table 7 that M_m, and log P have a negligible discrimination power. Slightly better is the discrimination power of E_{HOMO} and the best was found for T_b and W. The results from single parametric equations are presented in Table 8. In contrast to alkylbenzenes, neither of the substantional descriptors can adequately describe the experimental retention, even on a non-polar phase. Hence the use of tuning descriptors is essential for the naphthalene test series. We checked both E_T (one calculable substantional descriptor) and M_m (one important, easily determined descriptor) as basic parameters in Eq. 4. The greatest discrepancies (given in Table 8) were for 1,8- and 1,7-methyl substitutions. Thus, descriptors reflecting this type of substitution were checked as tuning parameters. The following equations with the best statistics and least Δ_{max} were obtained:

Table 8
Standard deviations and maximum discrepancies between RI_{exp} and RI_{calc} for the models derived by using only one basic descriptor

Descriptor	s			Δ_{max}		
	OV-1	OV-17	UCON	OV-1	OV-17	UCON
T_b	6	7	18	16^{17DMN}	11^{18DMN}	16^{17DMN}
E_T	10	20	17	18^{18DMN}	42^{18DMN}	34^{18DMN}
χ	14	24	21	31^{18DMN}	56^{18DMN}	47^{18DMN}
M_m	17	28	25	36^{18DMN}	61^{18DMN}	52^{18DMN}
W	27	39	35	51^{18DMN}	79^{18DMN}	69^{18DMN}

For non-polar phase OV-1:

$$RI^{OV-1} = 223.3(\pm 9) - 0.086(\pm 0.0)E_T - 13.98(\pm 6.98)\pi_7 + 27.52(\pm 14.45)\pi_8 - 27.22(\pm 1.24)q_8 + 296.5(\pm 11.93)p_{8-9} \quad (12)$$

with $r = 0.9965$, S.D. = 8 and $\Delta_{max} = 14^{13DMN}$.

With M_m used as a basic parameter, the following equation was obtained:

$$RI^{OV-1} = 2619(\pm 1580) - 8.80(\pm 1.0)M_m - 63.2(\pm 14.0)\pi_7 + 316.4(\pm 156)\pi_8 + 3814(\pm 2391)q_8 - 1629(\pm 833)p_{8-9} \quad (13)$$

with $r = 0.9987$, S.D. = 8 and $\Delta_{max} = 5^{13DMN}$; π stands for atom polarization and p for the bond order of corresponding carbon atoms.

Evidently, r is not the only and the best criterion for searching the suitable series of basic and tuning descriptors; for E_T $r = 0.9911$ whereas for M_m $r = 0.9751$.

For the low-polarity phase OV-17, with M_m as a basic parameter the correlation coefficient was $r = 0.9976$, but Δ_{max} increased to 14^{13DMN} i.u.

For the medium-polarity phase UCON, with M_m used again as the basic parameter in combination with the same tuning descriptors, the following equation was obtained:

$$RI^{UCON} = 3971(\pm 3342) + 9.29(\pm 1.4)M_m - 91.1(\pm 28.6)\pi_7 - 445(\pm 221)\pi_8 + 5263(\pm 3378)q_8 - 2369(\pm 1568)p_{8-9} \quad (14)$$

with $r = 0.9977$, S.D. = 7 and $\Delta_{max} = 9^{13DMN}$.

Table 9
Comparison of the calculated and experimental retention indices for the phases OV-1, OV-17 and UCON HB 280 ×

No.	Naphthalene compound	RI^{exp} OV-1	RI^{calc} Eq. 12	RI^{exp} OV-17	RI^{calc} Eq. 13	RI^{exp} UCON	RI^{calc} Eq. 14
1	Naphthalene	1183.7	1185	1331	1333	1468.2	1471
2	1-MeNapht	1301.7	1297	1463	1456	1592.5	1584
3	12-DiMeNapht	1432	1434	1614	1616	1729	1734
4	13-DiMeNapht	1402.3	1411	1571	1585	1691.8	1701
5	14-DiMeNapht	1419	1420	1596	1596	1711.7	1713
6	15-DiMeNapht	1420.7	1416	1600	1590	1713.1	1708
7	16-diMeNapht	1402.2	1400	1571	1566	1691.2	1687
8	17-DiMeNapht	1409.5	1408	1568	1571	1700	1697
9	18-DiMeNapht	1449	1449	1646	1645	1756.8	1757
10	2-MeNapht	1286.8	1288	1440	1443	1568	1571
11	23-DiMeNapht	1419.6	1415	1591	1589	1712.8	1706
12	26-DiMeNapht	1388.2	1388	1547	1547	1668	1669
13	27-DiMeNapht	1390.1	1393	1547	1548	1671	1675

On account of the presence of five parameters in the equations, modelling the retention of 13 compounds, the rule-of-thumb for this relation to be 1 : 5 was checked for chance correlation by the leave-one-out approach. None of the parameters was discarded, probably owing to their low intercorrelation.

The calculated *RI* values according to these equations are compared with the corresponding RI_{exp} values in Table 9. RI_{calc} values for naphthalenes separated on OV-1 and UCON stationary phases can be accepted as accurate enough, being below the accepted maximum discrepancy of 10 i.u. for naphthalenes.

5. Conclusions

This paper has presented several approaches for canvassing the possibilities for deriving qualitative structure–gas chromatographic retention relationships.

The calculation of *RI* values using substantional, experimentally obtained descriptors (such as boiling point, vapour pressure or its derivatives such as log p^0, I_p or *PCI*) as the basic parameter in Eq. 4 gives accurate enough results when non-polar phases are used for the separation.

If the calculation of *RI* values using important descriptors, including the calculable indices or *RI* values obtained on phases with increased polarity, are the subject, the contribution of the B_i parameters from Eq. 4 to the RI_{calc} value decreases and the use of tuning parameters, describing molecular electronic structure, becomes necessary. The accuracy of the derived equations in this case diminishes, although the significance of the basic contributor to RI_{calc} values is preserved. Neither of the tuning descriptors was able to describe adequately the additional intermolecular forces arising between the solute molecules and polar phase molecules.

There is a specific correspondence between the tuning descriptors and the basic descriptor used, e.g., the best tuning descriptors for the basic parameter B_1 from Eq. 4 could be different from those for basic parameter B_2. The matching of basic and tuning descriptors should not be limited within two descriptor groups only, nor should it be assessed by statistics only. From a chromatographic point of view Δ_{max} must be applied as the ultimate criterion.

The interchangeability between indicator variables and quantum chemical indices due to their high intercorrelation can facilitate QSRR studies, because of the easy determination and interpretation of the indicator variables. Such models ultilize readily available and simple parameters. In practical chromatography this will help in achieving a better understanding of the observed retentions of the solutes of interest and could clear up the dispute about which solute property or functional group increases or decreases the retention.

In cases when neither of the studied descriptors is able to tune the RI_{calc} value to those of RI_{exp}, either

the lack of a suitable descriptor or appropriate conformer of the solute molecule in quantum chemical calculations could be the reason for unsatisfactory accuracy. One could expect that owing to some intermolecular interactions, the descriptor values used, obtained for an ideal molecule conformation, should be corrected by a real number depending on the environment.

References

[1] B. Pullman (Ed.), Intermolecular Interactions: From Diatomics to Biopolymers, Wiley, Chichester, 1978.
[2] R. Kaliszan, CRC Crit. Rev. Anal. Chem., 16 (1986) 323.
[3] R.B. King (Ed.), Chemical Applications of Topology and Graph Theory, Elsevier, Amsterdam, 1983.
[4] D. Bonchev, Information Theory Indices for Characterization of Chemical Structurs, Ellis Horwood, Chichester, 1983.
[5] L. Buydens and D. Massart, Anal. Chem., 55 (1983) 738.
[6] N. Dimov and Ov. Mekenyan, Anal. Chim. Acta, 212 (1988) 317.
[7] C.G. Georgakopoulos, J.C. Kiburis and P.C. Jurs, Anal. Chem., 63 (1991) 2021.
[8] K.B. Woodburn, J.J. Delfino and P.S.C. Rao, Chemosphere, 24 (1992) 1037.
[9] S. Sekusak and A. Sabljic, J. Chromatogr., 628 (1993) 69.
[10] J. Bermejo and M. Guillen, J. High Resolut. Chromatogr. Chromatogr. Commun., 7 (1984) 191.
[11] T.C. Gerbino, G. Castello and G. D'Amato, J. Chromatogr., 609 (1992) 289.
[12] J. Bermejo and M. Guillen, Chromatographia, 17 (1983) 664.
[13] N. Dimov, J. Chromatogr., 119 (1976) 109.
[14] O. Mekenyan, N. Dimov and V. Enchev, Anal. Chim. Acta, 260 (1992) 69.
[15] E. sz. Kováts, Helv. Chim. Acta, 41 (1958) 1915; Fresenius' Z. Anal. Chem., 181 (1961) 351.
[16] P. Chovin, Bull. Soc. Chim. Fr., (1961) 875.
[17] C. Baron and B. Maume, Bull. Soc. Chim. Fr., (1962) 1113.
[18] J. Zulaica, C. Landault and G. Guiochon, Bull. Soc. Chim. Fr., (1962) 1294.
[19] R. Golovnya and O. Grigoryeva, Zh. Anal. Khim., 40 (1985) 316.
[20] K. Heberger, Chromatographia, 25 (1988) 725.
[21] J. Topliss and R. Edwards, J. Med. Chem., 22 (1979) 1238.
[22] R. Cramer, J. Bunce, D. Patterson and I. Frank, Quant. Struct. – Act. Relat., 7 (1988) 18.
[23] D.E. Willis, Anal. Chem., 39 (1967) 1324.
[24] F. Saura-Calixto and A. Garcia-Rasso, J. Environ. Anal. Chem., 17 (1984) 279.
[25] M. Gassiot-Matas and G. Firpo-Pamies, J. Chromatogr., 187 (1980) 1.
[26] C.T. Peng, S.F. Ding, R.L. Hua and Z.C. Yang, J. Chromatogr., 436 (1988) 137.
[27] C.T. Peng and Z.C. Yang, J. Chromatogr., 586 (1991) 85.
[28] N. Dimov and E. Matisova, J. Chromatogr., 549 (1991) 325.
[29] S. Miertus, V. Jahus and E. Matisova, Chromatographia, 30 (1990) 144.
[30] T.F. Woloszyn and P.C. Jurs, Anal. Chem., 65 (1993) 582.
[31] O. Mekenyan and D. Bonchev, Acta Pharm. Yugosl., 36 (1986) 225.
[32] O. Mekenyan, St. Karabunarliev and D. Bonchev, J. Math. Chem., 4 (1990) 207.
[33] O. Mekenyan, St. Karabunarliev and D. Bonchev, Comput. Chem., 14 (1990) 193.
[34] N. Dimov, Thesis, IOH, Bulgarian Academy of Sciences, 1985.
[35] J. Bonastre and P. Grenier, Bull. Soc. Chim. Fr. (1967) 1395.
[36] N. Dimov and D. Shopov, J. Chromatogr., 44 (1969) 170.

ELSEVIER

Analytica Chimica Acta 298 (1994) 319–329

ANALYTICA CHIMICA ACTA

Strategic approach for method selection in high-performance liquid chromatography

T. Hamoir, D.L. Massart *

Vrije Universiteit Brussel, Farmaceutisch Instituut, Laarbeeklaan 103, B-1090 Brussels, Belgium

Received 1 March 1994

Abstract

A strategic approach for the selection of high-performance liquid chromatographic methods in pharmaceutical analysis is outlined. Firstly, on the basis of the acid–base properties of the solute(s) and its hydrophobicity (as reflected by its log P value or total number of carbons), a battery of chromatographic methods is selected. This battery of methods contains first choice, second choice and excluded methods. The chromatographic modes considered are reversed-phase, normal-phase, gradient elution and ion-pair. Afterwards, on the basis of a structure–retention relationship, initial solvent strength conditions (i.e., the percentage of the organic modifier in the mobile phase) can be chosen in the reversed-phase and normal-phase mode corresponding to the chromatographers' needs.

Keywords: High-performance liquid chromatography; Method selection; Pharmaceutical analysis

1. Introduction

Expert systems are becoming increasingly important within analytical chemistry, and more specifically high-performance liquid chromatography (HPLC) [1]. In the area of method selection, which represents the first step within the method development process, Hindriks et al. [2] developed an expert system for a specific group of compounds, namely the central nervous system (CNS) drugs. This system, called DASH, predicts initial chromatographic or first-guess conditions in reversed-phase (RP) on the basis of the structure of the compound. Division of the molecule into structural elements, which correspond with a positive or negative methanol percentage value, leads to an estimation of the solvent strength. However, this system is rather limited in application, since it can only predict initial conditions for single-component samples. Moreover, the system can only estimate the solvent strength on a Nova-Pak RP18 and μBondapak RP18 column.

The expert system LABEL was developed in our laboratory for the label claim analysis of drug formulations [3,4]. Prediction in reversed-phase and normal-phase (NP) is carried out on the basis of the total number of carbons in the molecule using a categorization approach. This system also contains knowledge to select a suitable detection mode (i.e., UV detection or electrochemical detection in the oxidative mode). However, the prediction of a starting mobile phase composition is limited to a single column, namely a LiChrosorb CN column. This system as well as DASH were integrated in a large expert system for HPLC method development to assist the end-user from the initial method selection to selectivity optimization [5,6].

* Corresponding author.

SSDI 0003-2670(94)00256-L

In the expert system EluEx [7,8] the percentage of the organic modifier is predicted on the basis of the calculated log P value of the molecule. By recognition of the acidic/basic groups in the solute the pH of the mobile phase can be selected. EluEx can be applied to acidic, basic and amphoteric drugs. However, this system is not only column-specific, but, it cannot be used for predictions in normal-phase.

Considering these limitations, we investigated several aspects within chromatographic method selection with the aim to develop a more general first-guess system. The usefulness of the descriptor log P incorporated in a quantitative structure-retention relationship (QSRR) for the estimation of initial solvent strength conditions, in reversed-phase as well as in normal-phase [9–11] was reported. The effect of several tailing suppressors was also studied [12]. By structuring this chromatographic knowledge in an arranged scheme, one can develop a strategic approach for method selection, which, afterwards, can be incorporated in a computer system for method selection. The aim of this work is to describe this strategic approach which in the near future will be incorporated in a computer program for method selection.

2. Experimental

2.1. High-performance liquid chromatography

Standards and reagents

All standards were of pharmaceutical grade. The stock solutions (500 μg/ml) were prepared in methanol of analytical grade (Merck, Darmstadt) and diluted to the final concentration with purified water obtained from a Milli-Q water purification system (Millipore). A buffer with pH 4.0 and ionic strength 0.1 was prepared with phosphoric acid and sodium phosphate (Merck). The buffer was adjusted to the final pH with phosphoric acid (85%v/v) using an Orion 520A digital pH meter (Boston, MA). The measured pH corresponds to the pH of the buffer (i.e., without the organic modifier methanol). The electrodes were calibrated with standard buffer solutions (pH 4.00 and 7.00, Merck). Prior to use, the mobile phase was filtered through a membrane filter (0.2 μm) and degassed.

HPLC equipment

The chromatographic system consisted of a Merck-Hitachi L-6200 gradient pump equipped with a Rheodyne injector (sample loop of 100 μl), a Merck-Hitachi L-4000 variable wavelength detector, which was operated at 0.05 a.u.f.s. and 220 nm, and, finally, a Merck-Hitachi D-2500 Chromato-Integrator. The columns used and their corresponding properties are listed in Table 1. The mobile phase was composed of phosphate buffer and methanol as the organic modifier. The flow rate was set at 1.0 ml/min. All experiments were performed in duplicate at constant temperature (30°C). The capacity factors (k') were calculated in the usual manner:

$$k' = (t_r - t_o)/t_o \quad (1)$$

Table 1
Characteristics of the different stationary phases

Type	Name (manufacturer)	Particle size (μm) and shape [a]		Surface area (m^2/g)	Pore size (Å)	Carbon loading (%)	Endcapped (Y/N)
RP-18	Nova-Pak C18 (Waters)	4	S	120	60	7	Y
RP-8	Nucleosil C8 (Machery-Nagel)	5	S	350	100	8	N
CN	LiChrosorb CN (Merck)	5	I	350	100	n.a.	N
	μBondapak CN (Waters)	10	I	300	125	6	Y
	Ultrasphere CN (Beckman)	5	S	n.a.	n.a.	n.a.	Y
	Zorbax CN (Dupont)	5	S	350	70	n.a.	Y
SIL	Suplex pKb (Supelco)	5	S	170	100	– [b]	– [c]

n.a. = Not available.
[a] I(rregular) or S(pherical).
[b] Not applicable.
[c] Electrostatic shielding.

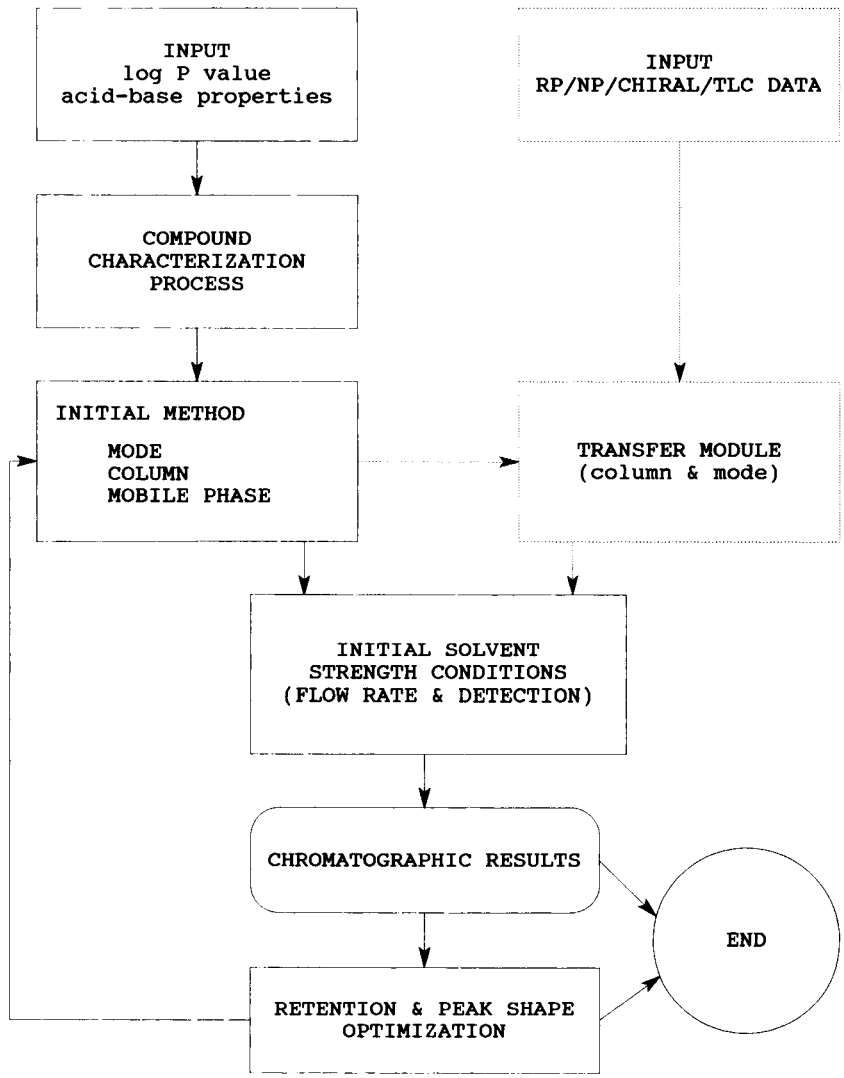

Fig. 1. General structure of the first-guess system.

where t_0 represents the dead time of the system. This value was determined as the first distortion of the baseline after injection of methanol.

3. Results and discussion

The system will consist of four modules. This article describes the first three ones. In the first module we will incorporate the knowledge for the selection of a battery of chromatographic methods (i.e., the mode, the column and the constituents of the mobile phase). The second one will predict the capacity factors (k') for various concentrations of the organic modifier in the mobile phase for the preferred method through structure–retention relationships. The third module will allow to perform retention and peak shape optimization when the initial solvent strength conditions lead to k' values situated outside a postulated range or when the peak shape is unsatisfactory. The last one will permit to transfer a separation between columns and also between modes (for instance, from the first choice method to a second choice one, when the results for the first one are disappointing). This final aspect is under

Table 2
List of the pharmacological groups and their properties

Group	Property [a]	Mode [b]
Alkaloids	B	
Barbiturates	A	
Benzodiazepines	B	
β-Adrenergic blocking drugs	B	
Calcium antagonists	A	
Catecholamines	B	
Cephalosporins	M	IPC
Corticosteroids	N	
Fat soluble vitamines	–	NP
Phenothiazines	B	
Hormones (male and female)	N	
Local anaesthetics	B	
Penicillins	M	IPC
Quaternary ammonium derivatives	–	IPC
Salicylates	A	
Sulphonamides	A	
Tricyclic antidepressiva	B	
Xanthine derivatives	B	

[a] Property: A = acidic, B = basic, N = neutral and M = amphoteric.
[b] Mode: IPC (ion-pair chromatography), NP (normal-phase).

investigation. The general structure of the system is presented in Fig. 1.

3.1. Selection of a global chromatographic method

The purpose of this module will consist in providing several alternatives, i.e., not only first choice methods, but, also second choice methods which can be tried out if the former ones fail, and, finally, the excluded methods. The main source of information for this decision are the properties of a compound as reflected by its acid–base properties and log P value.

Table 3
List of the different functional groups

Acidic functional groups		Basic functional groups	
Strong acidic	Weak acidic	Strong basic	Weak basic
Arsenic	Hydroxamate	Amidines	Aromatic amine
Carboxylic acid	Imide	Aliphatic amine	Aromatic N
Sulphonamide	Nitro		Heterocyclic N
Sulphonamidyl	Oxime		Hydrazine
Sulphonic acid	Phenol		
	Thiol		
	Uracil		

Table 4
Combinations of various functional groups and their corresponding properties

Group	Property [a]
SA + WB	A
SB + WA	B
SA + SB	M
WA + WB	B
None	N

[a] Property: S = strong, W = weak, A = acidic, B = basic, N = neutral and M = amphoteric.

Classification of a drug as a compound with acidic, basic, neutral or amphoteric characteristics is not always straightforward. For this purpose one can check whether the solute belongs to a specific pharmacological group. For instance, a compound belonging to the group of benzodiazepines possesses basic properties. A list of these groups and their characteristics is presented in Table 2. If necessary, the functional groups in the molecule can be identified. For instance, when the solute contains only a –COOH function the compound has acidic properties.

A list of these functional groups and their properties is presented in Table 3. Generally, several functional groups are present in a drug. Their combinations and corresponding acid–base properties are listed in Table 4.

The experimental log P value might be known. Otherwise, one can calculate a theoretical log P value using the hydrophobic fragmental method proposed by Rekker [13]. This method consists in dividing the molecular structure in fragments of which the contribution to the hydrophobicity of a solute is known. Rekker and De Kort [14] proposed an extensive list of fragmental values including also special effects. Special effects are related to, for instance, interactions between some fragments, for which Rekker proposed correction terms [14]. To check whether this division is performed correctly one can verify that by summation of all the fragments the empirical formula is obtained. For some fragments no value is available, for instance, the pteridine fragment [9]. One can then fall back on the total number of carbons in a molecule (n_c) to obtain an estimation of the hydrophobicity. A significant correlation between both parameters was obtained for basic compounds [9,12] as can be observed in Fig. 2. The following regression equation was derived:

$$\log P = 0.327(\pm 0.085) * n_c - 2.285(\pm 1.401) \quad (2)$$

$n = 40$; $s = 0.929$; $r = 0.786$;

$F(\text{eq.}) = 61.3$; $p < 0.00005$

where the regression coefficients are accompanied by their confidence interval. The number of data points (n), the standard deviation of the residuals (s), the correlation coefficient (r), the calculated F value and its significance level (p) are also presented. Similar results were obtained for acidic and neutral compounds. Eq. 2 was included in the system to estimate, if necessary, the log P value on the basis of the total number of carbons.

After this compound characterization process one can select a set of chromatographic methods. The following four modes are considered: reversed-phase, normal-phase, gradient elution and ion-pair chromatography (IPC). The selection of the chromatographic mode, the column and the mobile phase is described in Tables 2 and 5. For some types of compounds or applications the mode is predetermined and very restricted in choice (Table 2). For quaternary ammonium derivatives only IPC can be used, while for compounds insoluble in aqueous phases, namely the fat-soluble vitamins, only the NP mode is allowed.

Of course, NP and IPC are also suitable for other compounds. For instance, NP can be used for neutral compounds, such as steroids, and also for group separations. Numerous publications described the usefulness of IPC on an RP18 type of column for applications usually concerning the chromatography of basic compounds [15,16]. For such compounds the RP mode is considered as the first choice mode, NP and IPC as second choice (Table 5).

Since usually one can observe an increase in selectivity with a larger alkylchain bonded to the stationary phase, one can expect that for samples containing compounds with large differences in hydrophobicity ($\Delta \log P \geq 3.5$) the range in which their k' values is situated will be too large. In such a case one should apply gradient elution. When the differences in hydrophobicity are too large, isocratic conditions can still be selected, but then on a small chain bonded phase, like CN. As can be seen in Table 5, both modes are proposed for such applications, namely a CN type of column in the isocratic mode and an RP18 type of column in the gradient elution mode. In general, we prefer the second approach, since gradient elution presents an important drawback. Indeed, gradient elution requires special laboratory equipment.

A problem generally encountered in the chromatography of basic compounds is peak tailing. Several remedies have been proposed. One can act on the composition of the mobile phase by using a buffer at a sufficiently high ionic strength (a value of 0.05 or 0.1 is currently used) or by adding a tailing suppressor to the mobile phase. Recently, we compared several tail-

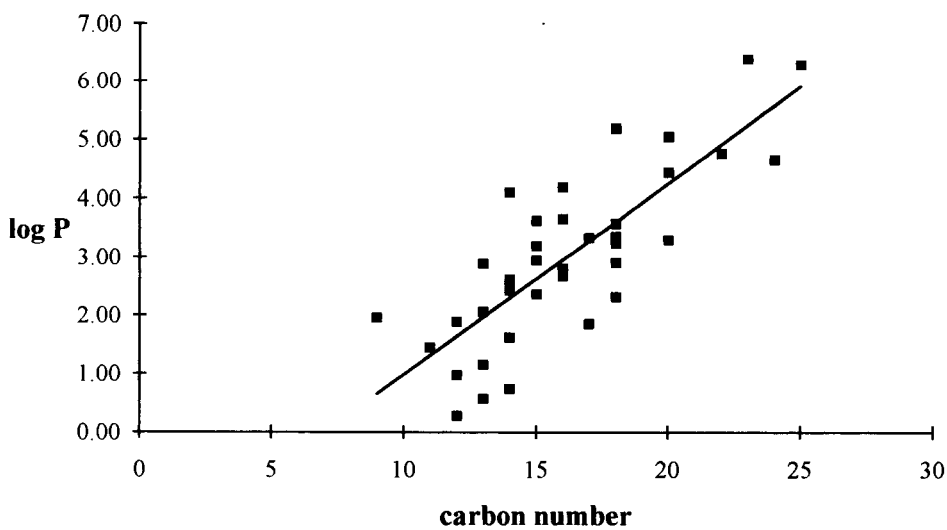

Fig. 2. Relationship between the descriptors log P and n_c for basic compounds.

Table 5
Initial method selection (i.e., mode, column and mobile phase)

Sample	Mode and choice [a]	Column	Mobile phase [b]
Acidic (+ neutral)	RP (I)	Pol-RP18-RP8-Phe-CN	Aqueous buffer pH 4.0, MeOH–ACN–THF
	IPC (II)	RP18-RP8	Aqueous buffer pH 7.0, MeOH–ACN–THF, TBA
	NP (II)	Si-diol-CN-NH_2	Hexane, 2-propanol–$CHCl_2$–$CHCl_3$, HAc
Basic (+ neutral)	RP (I)	RP18-RP8-Phe-CN	Aqueous buffer pH 4.0, MeOH–ACN–THF, DMOA–TEA
	RP (I)	Pol	Aqueous buffer pH 4.0, MeOH–ACN–THF
	IPC (II)	RP18-RP8	Aqueous buffer pH 4.0, MeOH–ACN–THF, SDS–SOS
	NP (II)	Si-diol-CN-NH_2	Hexane, 2-propanol–$CHCl_2$–$CHCl_3$, PA
Acidic and basic (+ neutral)	RP (I)	RP18-RP8-Phe-CN	Aqueous buffer pH 4.0, MeOH–ACN–THF, DMOA–TEA
	RP (I)	Pol	Aqueous buffer pH 4.0, MeOH–ACN–THF
	NP (II)	Si-diol-CN-NH_2	Hexane, 2-propanol–$CHCl_2$–$CHCl_3$, PA and/or HAc
Amphoteric (+ neutral)	RP (I)	RP18-RP8	Aqueous buffer pH 4.0, MeOH–ACN–THF, SDS–SOS
	RP (II)	RP18-RP8	Aqueous buffer pH 7.0, MeOH–ACN–THF, TBA
Neutral	RP (I)	Pol-RP18-RP8-Phe-CN	Water (buffer pH 4.0), MeOH–ACN–THF
	NP (II)	Si-diol-CN-NH_2	Hexane, 2-propanol–$CHCl_2$–$CHCl_3$
$\Delta\log P \geq 3.5$	RP (I)	CN	Aqueous buffer pH 4.0, MeOH–ACN–THF (DMOA–TEA)
	Gradient:		
	RP (I)	Pol-RP18-RP8-Phe-CN	Aqueous buffer pH 4.0, MeOH–ACN–THF
	NP (II)	Si-diol-CN-NH_2	Hexane, 2-propanol–$CHCl_2$–$CHCl_3$

[a] Method of first choice (I) and second choice (II).
[b] TBA = tetrabutylammonium; HAc = acetic acid; DMOA = dimethyloctylamine; TEA = triethylamine; SDS = sodium dodecylsulphate; SOS = sodium octylsulphate; PA = propylamine.

ing suppressors [12]. In reversed-phase, dimethyloctylamine (DMOA) and triethylamine (TEA) were found very efficient in a concentration of 2 and 20 mM, respectively, while in normal-phase propylamine (PA) in a concentration of 0.1% is used. The presence of a tailing suppressor in the mobile phase is recommended, not only for basic compounds, but also for acidic compounds (Table 5). For acidic compounds acetic acid can be used in the mobile phase [17]. This is the only remedy in normal-phase, while in reversed-phase one can also work under ion-suppression conditions. A low mobile phase pH can then be used, in this case a pH of 2.0 to 3.0. Since such conditions are rather detrimental for a silica-based column, in the RP mode a pH of 4.0 is preferred. Acetic acid is only used in the NP mode. For future incorporation in the system the final decision with respect to the use of a tailing suppressor will be left in the hands of the end-user, since it was shown that such mobile phase additives cannot be removed from the column due to irreversible binding [12].

Peak tailing can also be reduced by acting on the column, i.e., by using polymer-based instead of silica-based columns. So-called base-deactivated columns have also been proposed. However, in general, the latter columns show no significant improvement in peak shape for basic drugs [18] and therefore require the presence of a tailing suppressor in the mobile phase as is the case for a classical silica-based column. On polymer or polymer-coated columns ion-suppression conditions can be selected for the chromatography of basic compounds. Indeed, these columns are pH-stable and can be used in the range 0 to 14. This type of column is not only very useful for basic compounds, but, also for the application of optimal gradient conditions for basic compounds, since tailing suppressors offer no remedy in gradient elution. However, the classical silica-based columns can then also be used after pretreatment of the column with DMOA. Indeed, it was shown that this amine cannot be removed from the column [12]. This irreversible binding phenomenon can in fact be used to advantage to improve the peak shape in the gradient elution mode.

3.2. *Selection of the solvent strength of the mobile phase*

Several structure–retention relationships were derived for a large set of β-adrenergic blocking drugs (see further). This group of compounds, which covers a very wide range in log P, was selected by us as a

model set of compounds to study the usefulness of this molecular descriptor for the prediction of solvent strength conditions. Somewhat to our surprise we found that this model (Eq. 3a) is not restricted to β-adrenergic blocking drugs, but that it can also be used for other types of compounds. In other words, this model can be applied as a general retention prediction model. The prediction of the percentage of the organic modifier in the mobile phase is performed on the basis of the log P value or, if necessary, on the basis of the total number of carbons. The log P value of a drug, calculated according to the hydrophobic fragmental method proposed by Rekker [13,14], has been shown to be more appropriate than the total number of carbons to predict initial chromatographic conditions [9]. In cases where the log P value cannot be estimated, the total number of carbons in the solute can still provide a rather accurate estimation of the hydrophobicity of a drug. The estimation of the hydrophobicity of a solute is obtained from the compound characterization process. We are aware that the application of log P or n_c for retention prediction purposes seems rather rudimentary. Indeed, better models have been described [19–22]. However, the purpose of these better models is to provide more insight in the chromatographic retention mechanism. Generally, these models include physical parameters which are not only unknown, but also very difficult to ascertain. These models are therefore unsuitable for application in practical method selection. Clearly, in this domain there is a need to develop a simple and practical approach. In this context one should mention that even the utilisation of log P already frightens some chromatographers.

Importantly, a structure–retention relationship is column-specific, so that for the prediction of solvent strength conditions on any type of column one should develop a procedure to transfer a QSRR from one column to another. This aspect, referred to as the fourth module, is under investigation.

During this research different columns were used for the β-adrenergic blocking drugs. The following QSRRs were derived by multiple regression analysis:

In the reversed-phase mode

for a Nova-Pak RP18 column:

$$\log k' = -0.032(\pm 3.19\times 10^{-3}) * X_m + 0.366(\pm 0.042) * \log P + 0.673(\pm 0.139) \quad (3a)$$

$n = 118$; $s = 0.257$; Mult.$R = 0.898$; Adj.$R^2 = 0.803$; F(eq.) $= 239.6$; $p < 0.05$

and in the presence of 2 mM DMOA:

$$\log k' = -0.029(\pm 2.72\times 10^{-3}) * X_m + 0.337(\pm 0.048) * \log P + 0.620(\pm 0.133) \quad (3b)$$

$n = 114$; $s = 0.153$; Mult.$R = 0.896$; Adj.$R^2 = 0.800$; F(eq.) $= 226.5$; $p < 0.05$

for a Nucleosil C8 column:

$$\log k' = -0.041(\pm 0.024) * X_m + 0.430(\pm 0.099) * \log P + 0.638(\pm 1.235) \quad (4)$$

$n = 15$; $s = 0.171$; Mult.$R = 0.947$; Adj.$R^2 = 0.879$; F(eq.) $= 51.7$; $p < 0.00005$

for a LiChrosorb CN column:

$$\log k' = -0.022(\pm 3.76\times 10^{-3}) * X_m + 0.209(\pm 0.055) * \log P - 0.147(\pm 0.220) \quad (5)$$

$n = 25$; $s = 0.128$; Mult.$R = 0.950$; Adj.$R^2 = 0.895$; F(eq.) $= 102.8$; $p < 0.00005$

for a μBondapak CN column:

$$\log k' = -0.023(\pm 9.09\times 10^{-3}) * X_m + 0.265(\pm 0.094) * \log P + 0.022(\pm 0.447) \quad (6)$$

$n = 15$; $s = 0.122$; Mult.$R = 0.960$; Adj.$R^2 = 0.899$; F(eq.) $= 40.9$; $p = 0.0001$

for a Zorbax CN column:

$$\log k' = -0.027(\pm 3.63\times 10^{-3})*X_m + 0.279(\pm 0.037)*\log P + 0.619(\pm 0.216) \quad (7)$$

$n=35$; $s=0.105$; Mult.$R=0.967$;

Adj.$R^2=0.931$; $F(\text{eq.})=231.5$; $p<0.00005$

for a Suplex pKb column:

$$\log k' = -0.029(\pm 0.011)*X_m + 0.394(\pm 0.091)*\log P + 0.089(\pm 0.639) \quad (8)$$

$n=15$; $s=0.157$; Mult.$R=0.955$;

Adj.$R^2=0.897$; $F(\text{eq.})=62.0$; $p<0.00005$

As mobile phase in RP methanol–phosphate buffer (pH $4.0-\mu=0.1$) was used. The investigation on the effect of the tailing suppressor DMOA resulted in Eq. 3b.

For each of these equations the significance of the interaction term and the quadratic terms was investigated. Generally, the quadratic terms were found insignificant, contrary to the interaction term. However, the contribution of the interaction term was rather limited, so that in all these equations only the pure terms X_m and log P were included. Through comparison of the regression coefficients in Eqs. 3–8 (Fig. 3), one can observe that the coefficients for the terms X_m and log P are strongly correlated. This correlation is in accordance with recent observations [10], where it was shown that the regression coefficient for X_m depends on the hydrophobic character of the solute. Overall, Fig. 3 reflects the differences in the contribution of the hydrophobic interactions for the columns investigated.

In the normal-phase mode

$$\log k' = -0.021(\pm 5.55\times 10^{-3})*X_m - 0.315(\pm 0.076)*\log P + 0.004(\pm 1.78\times 10^{-3})*X_m*\log P + 1.679(\pm 0.237) \quad (9)$$

$n=82$; $s=0.123$; Mult.$R=0.896$;

Adj.$R^2=0.796$; $F(\text{eq.})=106.0$; $p<0.00005$

These results were obtained on an Ultrasphere CN column with a mobile phase of hexane–2-propanol–propylamine (0.1%).

In reversed-phase, the addition of a tailing suppressor has been found to decrease retention considerably, most certainly in the presence of DMOA [12]. Two equations were derived for retention prediction purposes. The first one allows to transfer retention data obtained in the absence of DMOA into retention data obtained in its presence:

$$\log k'_{DMOA} = 0.993(\pm 0.019)*\log k' + 0.082(\pm 5.35\times 10^{-3})*X_m - 8.00\times 10^{-4}(\pm 5.78\times 10^{-5})*X_m^2 - 2.178(\pm 0.125) \quad (10)$$

$n=51$; $s=0.020$; Mult.$R=0.998$;

Adj.$R^2=0.996$; $F(\text{eq.})=4576$; $p<0.05$

Eq. 10 allows to investigate whether an acceptable k' value can still be obtained for a basic compound. If this is not the case, the composition of the mobile phase has to be adapted. For this purpose Eq. 3b is used.

One might prefer to use TEA instead of DMOA. The original QSRR can then be used to perform any predictions, since only a very small decrease in k' was observed in the presence of this tailing suppressor in the mobile phase [12].

Depending on the chromatographic method the second module will predict solvent strength conditions in the absence or presence of a tailing suppressor. The end-user will be able to select solvent strength conditions corresponding to his needs from a list of predicted k' values for various concentrations of the organic modifier. For multi-component samples a k' range will be presented, for instance, 2.6–6.0. The first value corresponds to the k' value for the compound with the smallest log P value and the second one to the k' value for the solute with the highest log P value.

The estimation of the concentration of the organic modifier in the mobile phase is performed in percentage of methanol, in RPLC, or in percentage of 2-propanol, in NPLC. However, in RPLC some chromatographers might prefer acetonitrile or tetrahydrofuran. It is also possible that degradation of the compounds occurs in the presence of methanol. Both problems can be bypassed by calculation of the iso-eluotropic concen-

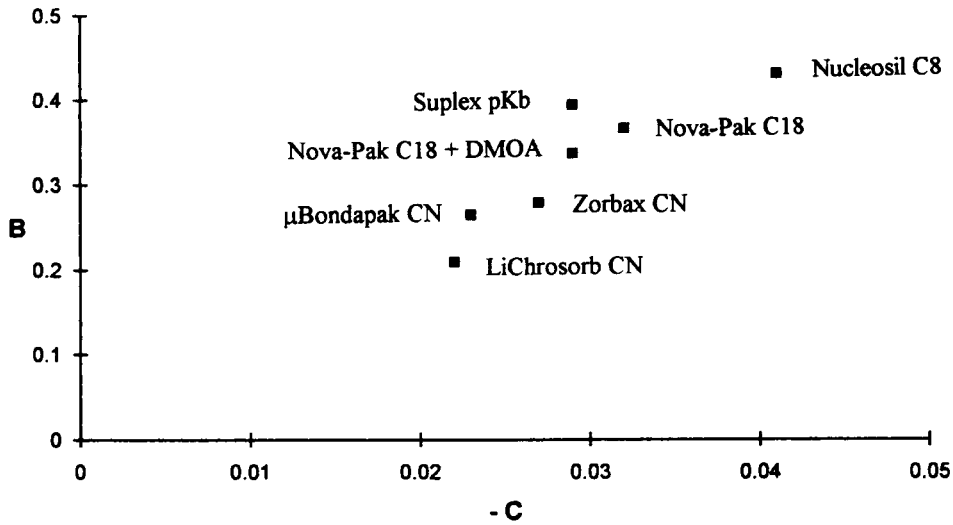

Fig. 3. Plot of the regression coefficients C (for the term X_m) and B (for the term log P) on the different chromatographic columns investigated.

trations for acetonitrile or tetrahydrofuran in the usual manner [23]:

$$S_T = \Sigma s_i * \Psi_i \quad (11a)$$

where S_T is the total solvent strength, s_i the solvent water strength weighting factor for each component ($H_2O = 0$, methanol = 2.6, acetonitrile = 3.2 and tetrahydrofuran = 4.5) and Ψ_i the volume fraction for each organic modifier. Hence, for methanol–water (buffer) one can calculate the percentages acetonitrile (ACN) and tetrahydrofuran (THF) as follows:

$$ACN = MeOH * (2.6/3.2) \quad (11b)$$

and

$$THF = MeOH * (2.6/4.5) \quad (11c)$$

Analogously, in NPLC one might prefer dichloromethane over 2-propanol as organic modifier. To our knowledge both modifiers were never compared. This will be investigated in the near future.

With respect to the prediction of the modifier concentration buffer incompatibility should be considered. Methanol and acetonitrile can never be used in percentages exceeding 70%, whereas for tetrahydrofuran the amount is limited to 45%.

For the estimation of optimal gradient conditions DryLab® [24] can be used. This program can also be used for the prediction of isocratic conditions on the basis of two gradient runs. Since DryLab® cannot predict starting gradient conditions we suggest the following initial gradients:

RPLC	
Methanol gradient	*Acetonitrile gradient*
gradient 1:	*gradient* 1:
0 → 70% in 10 min	0 → 65% in 10 min
gradient 2:	*gradient* 2:
0 → 70% in 40 min	0 → 65% in 40 min
NPLC	
Dichloromethane gradient	
gradient 1: 0 → 100% in 10 min	
gradient 2: 0 → 100% in 40 min	

3.3. Retention and peak shape optimization

On the basis of the chromatographic results (i.e., the dead time of the system, the retention time for each peak and the corresponding asymmetry factor) this module will investigate whether the k' value(s) and *Asf* value(s) are situated within a suitable range. In cases where the initial solvent strength, predicted by a specific QSRR, lead to capacity factors situated outside the required range, the composition of the mobile phase has to be adapted. This retention optimization process

is performed with the same structure–retention relationship. However, then this model is not used to predict k' values versus the concentration of the organic modifier (on the basis of the log P value), but to calculate a 'new' log P value on the basis of the experimental k' value (for a single component) and the composition of the mobile phase for the first experiment. This 'new' log P value can in fact be considered as a chromatographically determined log P value. This value is called log $P_{\text{chrom.}}$. For a multi-component sample the k' value obtained for the first and the last peak are used to determine a log $P_{\text{chrom.}}$ value for the compound eluting first and the one eluting last. Afterwards this value is used to perform retention prediction for various concentrations of the organic modifier in the mobile phase using the same structure–retention relationship.

If the result for the second experiment is still unsatisfactory, then the k' values obtained at both percentages are correlated as follows:

$$\log k' = A * X_m + B \qquad (12)$$

This equation was proposed by Schoenmakers [25] to describe the relationship of log k' versus the concentration of the organic modifier in a binary mobile phase. Using Eq. 12 the appropriate modifier concentration can be determined for a third experiment. Importantly, Eq. 12 has been shown to be only valid for capacity factors situated in the range 0.5 to 15.

Overall, this module will advise mobile phase conditions for a second (or third) experiment, which should permit to obtain an appropriate k' value (single-component samples) or k' values situated in an acceptable range (multi-component samples).

If peak shape is unsatisfactory on a classical silica-based column (*Asf* should be situated in the range 0.8 to 2.0), one should make use of a tailing suppressor as indicated in Table 5. If for performing the initial experiment a tailing suppressor was used in the mobile phase, the concentration of the mobile phase additive should be increased. This is only useful for DMOA (from 2 to 10 mM), since for TEA no further improvements in *Asf* were observed for concentrations exceeding 20 mM (this is the concentration to be used for this tailing suppressor). In cases where the peak shape remains unacceptable, one should verify whether, for instance, overloading effects can be excluded (i.e., troubleshooting). Otherwise, another column should be used, more specifically, a polymer-based type of column.

Generally, short retention times are requested. However, for more complex applications (i.e., multi-component samples), these might yield insufficient separation. To improve selectivity reducing the solvent strength can be very useful. However, for this purpose one can also adapt the concentration of the tailing suppressor (this is only possible for DMOA), since it has been shown that this mobile phase additive has an important effect on selectivity [12,26–28]. Overall, by considering the concentration of as well the organic modifier as the mobile phase additive one can attempt to improve selectivity. Of course, this step can only be investigated once acceptable results are obtained in k' and *Asf* values.

4. Conclusion

Incorporation of this approach in a computer program will be very useful for HPLC method development, not only for single-component, but also for multi-component samples. To identify the limitations of the approach one should validate it. This will be the subject of a separate paper [29].

The several structure–retention relationships allow prediction of solvent strength conditions on different types of columns. Still, one can expect that some applications will need to be performed on other columns than these used in this work. Clearly, there is then a need for a column transfer procedure. This is under investigation.

The selection of initial chromatographic conditions is the first step within HPLC method development, followed by selectivity optimization and method validation. At present, knowledge regarding the latter steps is being implemented in our laboratory. The implementation is carried out using Hypertext text tools, such as Toolbook, which in comparison with the classical expert system building tools, namely expert system shells such as KES, and also the artificial intelligence (AI) languages, such as Prolog present several advantages [1]. Important features are the rapid development of a user-friendly system and the easy maintainability of the system. Toolbook is particularly suitable for the implementation of decision trees, such as the method selection process. In the near future the strategy pro-

posed in this work for chromatographic method selection will be implemented in Toolbook. Afterwards, it would be most useful to link these three systems to assist the chromatographer within these different and complex steps of method development.

Acknowledgements

The authors thank the NFWO and FGWO for financial assistance.

References

[1] T. Hamoir and D.L. Massart, Expert Systems in Chromatography, Advances in Chromatography, Marcel Dekker, New York, Vol. 33, 1993, Chap. 3.
[2] R. Hindriks, F. Maris, J. Vink, A. Peeters, M. De Smet, D.L. Massart and L. Buydens, J. Chromatogr., 485 (1989) 255.
[3] M. De Smet, A. Peeters, L. Buydens and D.L. Massart, J. Chromatogr., 457 (1988) 25.
[4] M. De Smet, G. Musch, A. Peeters, L. Buydens and D.L. Massart, J. Chromatogr., 485 (1989) 237.
[5] T. Hamoir, M. De Smet, H. Piryns, N. Vanden Driessche, F. Maris, H. Hindriks, P.J. Schoenmakers and D.L. Massart, J. Chromatogr., 589 (1992) 31.
[6] P. Conti, T. Hamoir, M. De Smet, H. Piryns, N. Vanden Driessche, F. Maris, H. Hindriks, P.J. Schoenmakers and D.L. Massart, Chemom. Intell. Lab. Syst., 11 (1991) 27.
[7] G. Szepesi and K. Valko, J. Chromatogr., 550 (1991) 87.
[8] EluEx version 2.0 Documentation, Compudrug Ltd., Budapest, Hungary, 1991.
[9] T. Hamoir, B. Bourguignon, H. Hindriks and D.L. Massart, J. Chromatogr., 633 (1992) 43.
[10] T. Hamoir, W. King, S. Kokot, K. Douglas and D.L. Massart, J. Chromatogr. Sci., 31 (1993) 393.
[11] T. Hamoir and D.L. Massart, J. Chromatogr., in press.
[12] T. Hamoir, Y. Verlinden and D.L. Massart, J. Chromatogr. Sci., 32 (1994) 14.
[13] R.F. Rekker, The Hydrophobic Fragmental Constant – Its Derivation and Application, Elsevier, Amsterdam, 1977.
[14] R.F. Rekker and H.M. De Kort, Eur. J. Med. Chem. – Chimica Therapeutica, 14(6) (1976) 479.
[15] S.R. Abbott, J. Chromatogr. Sci., 18 (1980) 540.
[16] L.R. Snyder and J.J. Kirkland, Introduction to Modern Liquid Chromatography, Wiley, New York, 2nd edn., 1979, Chap. 11.
[17] J.W. Dolan, LC-GC Int., 2 (1989) 18.
[18] R. Vervoort, H. Hindriks, M. Vrieling and F. Maris, 18th International Symposium on Chromatography, Amsterdam, 1990, Abstract Mo-P-092.
[19] B.L. Karger, L.R. Snyder and J.J. Kirkland, J. Chromatogr., 125 (1976) 71.
[20] R. Tijssen, H.A.H. Billiet and P.J. Schoenmakers, J. Chromatogr., 122 (1976) 185.
[21] Cs. Horvath, W. Melander and J. Molnar, J. Chromatogr., 125 (1976) 129.
[22] E.D. Katz, K. Ogan and R.P.W. Scott, J. Chromatogr., 352 (1986) 67.
[23] L.R. Snyder, J.W. Dolan and J.R. Gant, J. Chromatogr., 165 (1979) 3.
[24] J.L. Glajch and L.R. Snyder, Computer-Assisted Method Development for High-Performance Liquid Chromatography, Elsevier, Amsterdam, 1990.
[25] P. Schoenmakers, Optimization of Chromatographic Selectivity: A Guide to Method Development, Elsevier, Amsterdam, 1986.
[26] T. Hamoir, F. Cuesta Sanchez, B. Bourguignon and D.L. Massart, J. Chromatogr. Sci., in press.
[27] C.T. Hung, R.B. Taylor and N. Paterson, J. Chromatogr., 240 (1982) 61.
[28] R.W. Roos and C.A. Lau-Cam, J. Chromatogr., 370 (1986) 403.
[29] T. Hamoir, B. Bourguignon and D.L. Massart, Chromatographia, in press.

ELSEVIER

Analytica Chimica Acta 298 (1994) 331–339

ANALYTICA CHIMICA ACTA

Application of SIMPLISMA for the assessment of peak purity in liquid chromatography with diode array detection

F. Cuesta Sánchez, D.L. Massart *

ChemoAC, Vrije Universiteit Brussel, Laarbeeklaan 103, B-1090 Brussels, Belgium

Received 15 April 1994; revised manuscript received 24 June 1994

Abstract

The application of SIMPLISMA for the investigation of peak purity with liquid chromatography and diode array detection (LC-DAD) is proposed. SIMPLISMA is applied in the chromatographic direction, and is used to detect pure zones in the chromatogram. The performance of SIMPLISMA and of an approach based on the Gram-Schmidt orthogonalization technique are compared.

Keywords: Liquid chromatography; SIMPLISMA

1. Introduction

Liquid chromatography (LC) is widely used in many industries, e.g., pharmaceutical industry, due to its simplicity and specificity. For pharmaceutical purposes it is of great importance to assure the purity of each peak. The purity itself is not an absolute term, therefore one can only assess the absence of impurities. Most of the time the impurities are isomers or degradation products of the compound of interest. Their chromatographic behaviour and their spectra can be very similar, which makes the detection of the impurity very difficult. The introduction of hyphenated techniques, mostly LC coupled with a diode array detector (LC-DAD), was an important step forward. Many techniques were developed for the assessment of peak purity. The most widely used techniques such as the ratiogram [1], the absorbance index technique [2], the spectral suppression [3], the purity parameter [4], the spectral correlation [5], the multiple absorbance ratio correlation (MARC) [6], are unable to detect small amounts of impurities ($\sim 0.1\%$) or require that one knows which impurity one is looking for. An improvement was obtained with the introduction of multivariate techniques based on principal component analysis (PCA) such as evolving factor analysis (EFA) [7,8], fixed size window evolving factor analysis (FSW EFA) [9], the heuristic evolving latent projections method (HELP) [10–12], and those based on the Gram-Schmidt orthogonalization technique (see also Theory) [13,14]. SIMPLISMA [15–17] is a self-modelling approach based on the selection of what are called pure variables. A pure variable is defined as a variable of which the intensity is due to only one of the compounds in the mixture under consideration [18,19]. The task of a self-modelling approach is the resolution of the data matrix into the concentration profiles and the pure spectra of the components present. In a self-modelling approach no assumptions about the shape of the pure spectra and/or concentration profiles

* Corresponding author.

SSDI 0003-2670(94)00283-5

are required. In this paper we investigate the application of SIMPLISMA for the detection of impurities under a chromatographic peak when both resolution and the concentration of the impurity are rather low; for instance, $Rs = 0.5$ and 0.5% of impurity. The results are compared with the ones obtained with the orthogonalization technique proposed by us [13,14].

LC-DAD yields a data table $\mathbf{X}$ ($m \times n$) where the m rows are spectra measured at different time intervals, and the n columns are chromatograms measured at different wavelengths. Usually the pure spectra of the components present in the mixture are rather similar, and selective spectral regions are not present. However, often there are selective chromatographic regions, at least for the main compound eluting. We propose to apply SIMPLISMA in the chromatographic direction to search for the purest rows of $\mathbf{X}$, i.e., the analysis times where only one compound is eluting. In this case the "pure spectrum" will provide information about the spectra of the pure components.

2. Theory

SIMPLISMA is based on the selection of pure variables. If pure variables exist, i.e., variables that have an intensity contribution from only one of the components in that data set, they are determined without the use of PCA as is the case in other methods like VARDIA [19] and the KEY SET method [20]. Once the pure variables are known, it is possible to determine the pure spectrum of each component by a least squares procedure. In our context UV spectra are measured and we are interested in situations where the spectra are similar, so that no pure zones in the spectrum are expected. However, it is probable that there are zones in the chromatogram when only one substance will be present; therefore, we look for analysis times (objects) where only one compound is eluting. We will call, following Windig's terminology, first "pure spectrum" the spectrum with the highest purity. The purity, p_i, of each object $\mathbf{x}_i$ (for $i = 1,\ldots,m$) is calculated as the ratio between its standard deviation σ_i and its mean μ_i, multiplied by a weight, w_i. The value of w_i depends on the number of the "pure spectra" selected and on the normalization applied to the data matrix and, initially, is equal to one:

$$p_i = w_i \frac{\sigma_i}{\mu_i} \quad \text{for } i = 1,\ldots,m \tag{1}$$

To explain this approach, some further explanations are required:

2.1. Mean and standard deviation vectors

The mean vector of each spectrum $\mathbf{x}_i$ is a vector $\boldsymbol{\mu}_i = (\mu_i,\ldots,\mu_i)$ with n elements, where

$$\mu_i = \frac{x_{i1} + x_{i2} + \ldots + x_{in}}{n} \tag{2}$$

A vector $\mathbf{v}_i$ can be defined by

$$\mathbf{v}_i = \mathbf{x}_i - \boldsymbol{\mu}_i = (x_{i1} - \mu_i, x_{i2} - \mu_i, \ldots, x_{in} - \mu_i) \tag{3}$$

The vector standard deviation $\boldsymbol{\sigma}_i$ of each spectrum $\mathbf{x}_i$ is defined as

$$\boldsymbol{\sigma}_i = \frac{1}{\sqrt{n-1}}(x_{i1} - \mu_i, x_{i2} - \mu_i, \ldots, x_{in} - \mu_i) \tag{4}$$

therefore

$$\boldsymbol{\sigma}_i = \frac{1}{\sqrt{n-1}} \mathbf{v}_i \tag{5}$$

In SIMPLISMA, for reasons explained below, Windig chose to divide by n instead of $n-1$

$$\boldsymbol{\sigma}_i = \frac{1}{\sqrt{n}}(x_{i1} - \mu_i, x_{i2} - \mu_i, \ldots, x_{in} - \mu_i) = \frac{1}{\sqrt{n}} \mathbf{v}_i \tag{6}$$

The length of the standard deviation vector $\boldsymbol{\sigma}_i$, also called standard deviation of the object $\mathbf{x}_i$, is equal to

$$\|\boldsymbol{\sigma}_i\| = \sigma_i = \sqrt{\frac{\sum_{j=1}^{n} (x_{ij} - \mu_i)^2}{n}} \tag{7}$$

For graphical illustration let us consider a data matrix reduced to two variables $\mathbf{X}$ ($m \times 2$). Each spectrum $\mathbf{x}_i$ is represented as a point with coordinates x_{i1} and x_{i2} in the two-dimensional space spanned by the two variables (Fig. 1). Vectors $\boldsymbol{\mu}_i$ and $\mathbf{v}_i$ are orthogonal ($\boldsymbol{\mu}_i \cdot \mathbf{v}_i = 0$), therefore:

$$\|\boldsymbol{\mu}_i\|^2 + \|\mathbf{v}_i\|^2 = \|\mathbf{x}_i\|^2 \tag{8}$$

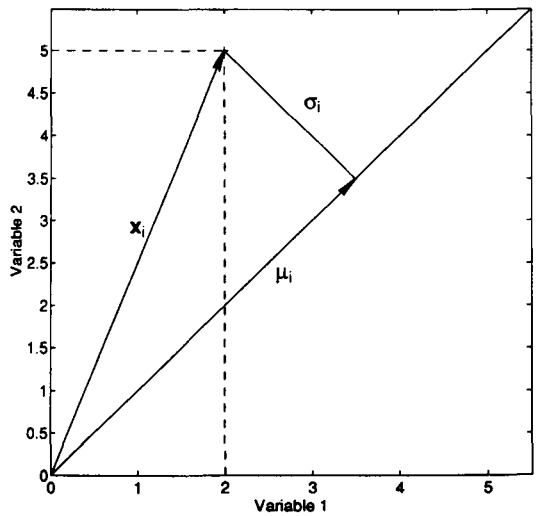

Fig. 1. A spectrum $\mathbf{x}_i$ in a 2-dimensional space, together with its mean vector $\boldsymbol{\mu}_i$ and its standard deviation vector $\boldsymbol{\sigma}_i$.

and

$$\|\boldsymbol{\mu}_i\| = \|\mathbf{x}_i\| \cos \alpha_i \tag{9}$$

$$\|\mathbf{v}_i\| = \|\mathbf{x}_i\| \sin \alpha_i \tag{10}$$

where α_i is the angle between the vectors $\mathbf{x}_i$ and $\boldsymbol{\mu}_i$.

$$\|\boldsymbol{\sigma}_i\| = \sigma_i = \frac{1}{\sqrt{n}}\|\mathbf{v}_i\| = \frac{1}{\sqrt{n}}\|\mathbf{x}_i\| \sin \alpha_i \tag{11}$$

$$\|\boldsymbol{\mu}_i\|^2 + n\|\boldsymbol{\sigma}_i\|^2 = \|\mathbf{x}_i\|^2 \tag{12}$$

2.2. Normalization of $\mathbf{x}_i$

Each spectrum $\mathbf{x}_i$ is normalized by dividing each element of a row, x_{ij} (for $j = 1,..,n$) by the length of the row $\|\mathbf{x}_i\|$:

$$z_{ij} = \frac{x_{ij}}{\|\mathbf{x}_i\|} \tag{13}$$

Taking into account Eq. 12 and that

$$\|\boldsymbol{\mu}_i\|^2 = n\mu_i^2 \tag{14}$$

Eq. 13 can be expressed in the following way

$$z_{ij} = \frac{x_{ij}}{\sqrt{n(\sigma_i^2 + \mu_i^2)}} \tag{15}$$

This definition of $\|\mathbf{x}_i\|$ (Eq. 12) will be very important in the next steps, when an offset is included. The normalized spectra $\mathbf{z}_i$ have a length equal to one. The normalized spectra of the data matrix reduced to two wavelengths (244 and 280 nm) obtained with $Rs = 1$ and 10% of impurity (see data) are shown in Fig. 2.

2.3. Weight vector w

The weight vector is a vector with m elements containing the weights of each spectrum $\mathbf{x}_i$. Each element of the weight vector, w_i, is defined as the determinant of the dispersion matrix of $\mathbf{Y}_i$, which contains all the "pure spectra" selected and each normalized spectrum $\mathbf{z}_i$. If for instance, one "pure spectrum" has been determined then $\mathbf{Y}_i$ contains two rows, the "pure spectrum" and, for each i, $\mathbf{z}_i$.

When no "pure spectrum" has been determined yet:

$$\mathbf{y}_i = \mathbf{z}_i$$

$$w_i = \det(\mathbf{y}_i * \mathbf{y}_i^{\mathrm{T}}) = \|\mathbf{z}_i\|^2 \tag{16}$$

When the first "pure spectrum", $\mathbf{p}_{1i}$, has been determined:

$$\mathbf{y}_{1i} = \mathbf{p}_{1i}$$

$$\mathbf{y}_{2i} = \mathbf{z}_i$$

$$w_i = \det(\mathbf{Y}_i * \mathbf{Y}_i^{\mathrm{T}}) = \|\mathbf{p}_{1i}\|^2 \|\mathbf{z}_i\|^2 (\sin \alpha_{1i})^2 \tag{17}$$

where α_{1i} is the angle determined between the first "pure spectrum" and the spectrum $\mathbf{x}_i$.

When two "pure spectra", $\mathbf{p}_{1i}$ and $\mathbf{p}_{2i}$, have been determined:

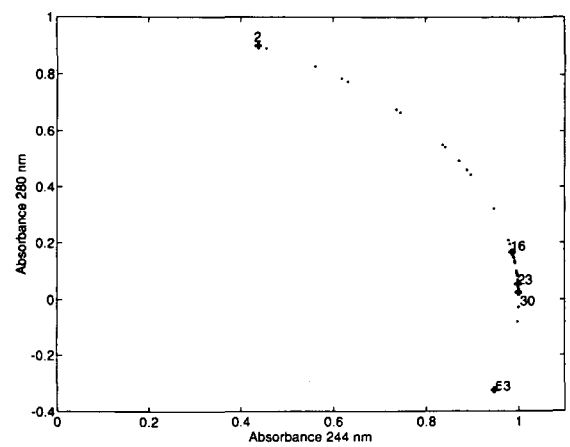

Fig. 2. Normalized spectra of the data matrix reduced to two wavelengths (244 and 280 nm) obtained for $Rs = 1$ and 10% of impurity.

$$\mathbf{y}_{1i} = \mathbf{p}_{1i}$$

$$\mathbf{y}_{2i} = \mathbf{p}_{2i}$$

$$\mathbf{y}_{3i} = \mathbf{z}_i$$

$$w_i = \det(\mathbf{Y}_i * \mathbf{Y}_i^{\mathrm{T}})$$

$$= \|\mathbf{z}_i\|^2 \|\mathbf{p}_{1i}\|^2 \|\mathbf{p}_{2i}\|^2 \times [(\sin \alpha_{12})^2 - (\cos \alpha_{1i})^2 - (\cos \alpha_{2i})^2 + 2 \cos \alpha_{12} \cos \alpha_{1i} \cos \alpha_{2i}] \quad (18)$$

Taking into account the concepts explained above (Eqs. 9, 11, 14 and 16), the purity of each spectrum (Eq. 1) can be expressed as

$$p_i = \|\mathbf{z}_i\|^2 \frac{\frac{1}{\sqrt{n}}\|\mathbf{x}_i\| \sin \alpha_i}{\frac{1}{\sqrt{n}}\|\mathbf{x}_i\| \cos \alpha_i} = \tan \alpha_i \quad (19)$$

Before the selection of the first "pure spectra", the value of w_i is equal to one, since each vector is normalized to length equal to one (Eq. 15). The purity of each spectrum is a measure of the angle α_i determined between each spectrum $\mathbf{x}_i$ and the mean vector $\boldsymbol{\mu}_i$. The plot of p_i ($i = 1,\ldots,m$) versus the analysis time is called purity chromatogram.

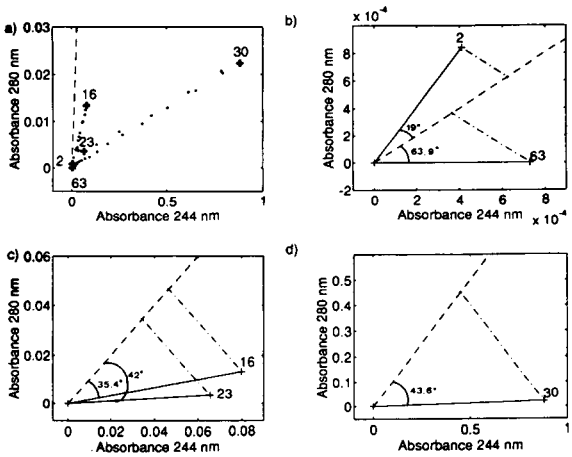

Fig. 3. (a) Absorbance data at 280 nm vs. absorbance data at 244 nm for the case of $Rs = 1$ and 10% of impurity, together with the line of slope 1 (the mean vector); mean (– – –) and standard deviation (–·–·–) vector for (b) times 2 and 63, (c) times 16 and 23, and (d) 30.

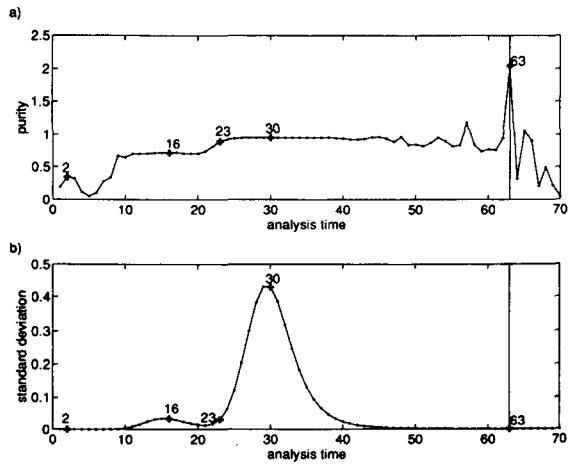

Fig. 4. (a) First purity chromatogram obtained for the reduced data matrix for $Rs = 1$ and 10% of impurity without offset, (b) standard deviation chromatogram.

For illustration, the data matrix obtained for $Rs = 1$ and 10% of impurity (see data) is reduced to two wavelengths (244 and 280 nm) of which we know that they differentiate rather well between the two analytes. In Fig. 3a each spectrum is plotted in the two dimensional space spanned by the two wavelengths, together with the line of slope one where the mean vector is situated. The numbers indicate the analysis times. Times 2 and 63 represent noise, 16 impurity, 30 main compound and 23 mixture. In Figs. 3b–d are shown the mean and standard deviation vectors, together with the angles α_i, for the times mentioned above (2, 63 (b), 16, 23 (c) and 30(d)).

In Fig. 4a is given the purity chromatogram (Eq. 19), together with the first "pure spectrum" selected, the analysis time 63. In Fig. 4b is shown the purity-corrected standard deviation chromatogram, which is the standard deviation of each spectrum σ_i multiplied by its weight w_i, versus the analysis time.

In this case, it is known that 63 is a "pure spectrum", since only the main compound is left, but this spectrum represents mostly noise. Therefore, the purity of a spectrum may be high due to the small value of its mean. To avoid such an effect, an offset is introduced. An offset equal to 1 means that one adds to each mean μ_i ($i = 1,\ldots,m$) 1% of the maximum mean ($\max(\boldsymbol{\mu})$), where $\boldsymbol{\mu} = (\mu_1,\ldots,\mu_m)$:

$$\mu_i' = \mu_i + (\text{offset}/100) * \max(\boldsymbol{\mu}) \quad (20)$$

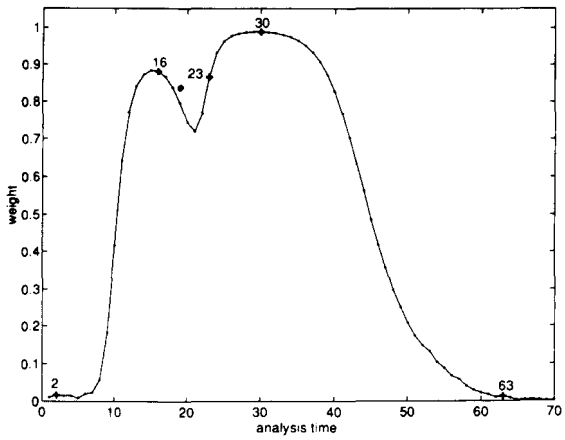

Fig. 5. Weight of each variable for the reduced data matrix obtained for $Rs = 1$ and 10% of impurity with an offset equal to 1, before the selection of the first pure spectrum.

When an offset is added, it is also included in the normalization of the spectra in the following way:

$$z_{ij} = \frac{x_{ij}}{\sqrt{n(\sigma_i^2 + \mu_i'^2)}} \qquad (21)$$

The length of all the spectra is lower than 1 (Fig. 5). The highest length corresponds to the spectra at which the maximum mean absorbance is situated (time 29), and very small for the vectors representing noise, since their mean is very small compared with ($\max(\boldsymbol{\mu})$) and the offset will be an important factor.

When an offset is included, the purity of each spectrum, p_i, is determined by:

$$p_i = w_i \frac{\sigma_i}{\mu_i'}$$

$$\text{for } i = 1, \ldots, m \qquad (22)$$

The result obtained is given in Fig. 6a. The purity of the spectra representing noise is decreased by the weight, since now the weight of the vectors representing noise is small ($w_i = \|\mathbf{z}_i\|^2$), and by the inclusion of the offset in the denominator. When the offset is included the purity chromatogram has more similarity with the purity-corrected standard deviation chromatogram (Fig. 6b), i.e., the standard deviation of each spectrum multiplied by its weight, pstd_i.

The first "pure spectrum", $\mathbf{p}_{1i}$, is the spectrum at analysis time 30, which corresponds to the elution of the main compound.

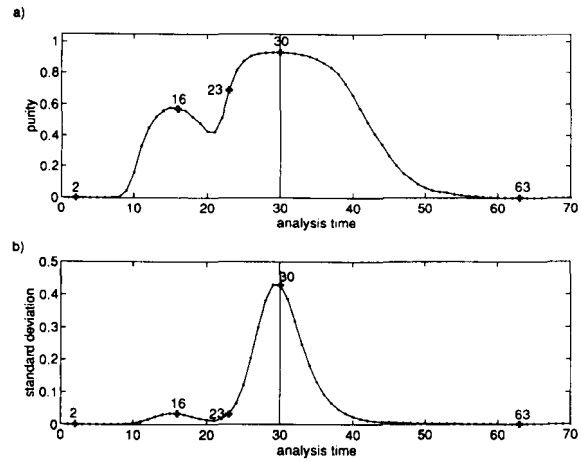

Fig. 6. (a) First purity chromatogram obtained for the reduced data matrix for $Rs = 1$ and 10% of impurity with an offset equal to 1, (b) standard deviation chromatogram.

The next step is the subtraction of the information contained in the first "pure spectrum". For this purpose, the weight vector is calculated in the way explained above (Eq. 17). In the weight vector the length of each spectrum normalized $\mathbf{z}_i$ and the dissimilarity between the first "pure spectrum" and each object is considered (Fig. 7). The value of w_i will be small when the length of the spectrum considered is small (e.g., vectors representing noise), or when the spectrum is correlated with the first "pure spectrum" ($\sin \alpha_{1i}$ close to zero). This step is similar to the orthogonalization methods [13,14]. In the orthogonalization methods one calculates the length of the orthogonal

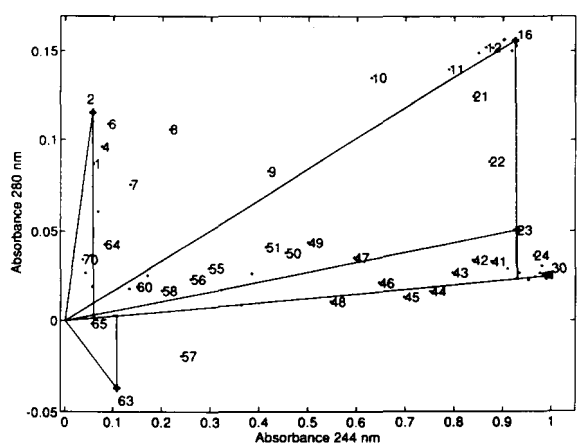

Fig. 7. Normalized spectra with an offset equal to 1 of the reduced data matrix obtained for $Rs = 1$ and 10% of impurity, together with the first pure spectrum (time 30) and the weights for times 2, and 63 (noise), 16 (impurity) and 23 (mixture).

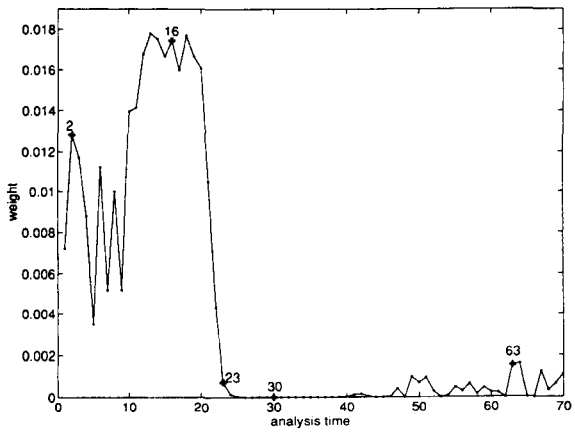

Fig. 8. Weight for the reduced data matrix obtained for $Rs = 1$ and 10% of impurity with an offset equal to 1, after the selection of the first pure spectrum.

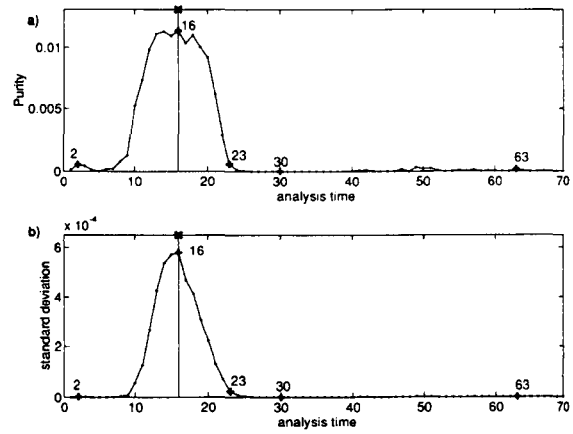

Fig. 9. (a) Purity chromatogram obtained for the reduced data matrix for $Rs = 1$ and 10% of impurity with an offset equal to 1 after the selection of the first pure spectrum, (b) corrected standard deviation chromatogram.

projection of each normalized spectrum $\mathbf{z}_i$ onto the "base" vector. The length of the projection is calculated, which is equal to $\|\mathbf{z}_i\| \sin \alpha_i$, α_i is the angle determined between $\mathbf{z}_i$ and the "base" vector. The sine of the angle between each spectrum and the "base" vector is called dissimilarity, while the correlation coefficient, i.e., the cosine, is the similarity. The weight w_i of the spectrum $\mathbf{x}_i$ is equal to $\|\mathbf{p}_{1i}\|^2(\|\mathbf{z}_i\|(\sin \alpha_{1i}))^2$ and $\|\mathbf{p}_{1i}\|$ is practically 1 (Fig. 8).

The new purity chromatogram and purity-corrected standard deviation chromatogram are calculated (Fig. 9):

$$p_{i\,\mathrm{new}} = p_{i\,\mathrm{old}} \|\mathbf{p}_{1i}\|^2 (\sin \alpha_{1i})^2 \tag{23}$$

$$\mathrm{pstd}_{i\,\mathrm{new}} = \mathrm{pstd}_{i\,\mathrm{old}} \|\mathbf{p}_{1i}\|^2 (\sin \alpha_{1i})^2 \tag{24}$$

In this case $\|\mathbf{p}_{1i}\|^2 = \|\mathbf{z}_{30}\|^2$.

The weight vector subtracts the information contained in the first "pure spectrum". The process is repeated, and the spectrum with the highest p_i will be the second "pure spectrum". In this case $\mathbf{p}_{2i} = 16$, which corresponds to the maximum elution time of the impurity.

The weight vector is calculated (Eq. 17). In Fig. 10 is shown that w_i is practically zero for all the spectra, which means that all the variance of the data is explained by the two "pure spectra" selected. The weight vector is very useful for the detection of the number of components presents.

The purity chromatogram and the purity-corrected standard deviation chromatogram are calculated and plotted in Fig. 11. One can see that only noise is left.

3. Data

The application of the algorithm was studied on a LC-DAD data set published by Keller et al. [21]. The samples consisted of hydrocortisone and different concentrations of prednisone. The latter was considered as impurity and its relative concentration ranged from 0.1 to 100%. Chromatographic separation quality between the two analytes was varied from $Rs = 0.1$ to 1.

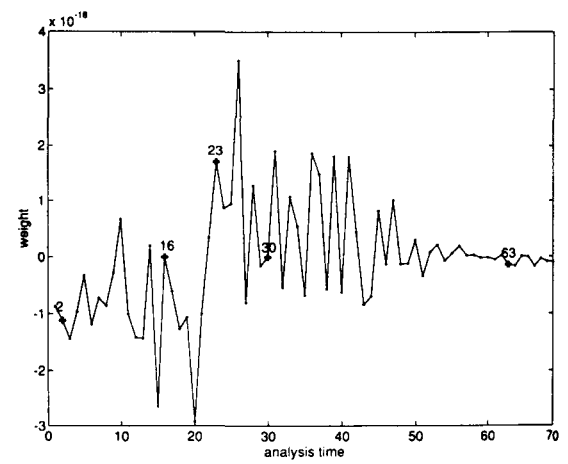

Fig. 10. Weight for the reduced data matrix obtained for $Rs = 1$ and 10% of impurity with an offset equal to 1, after the selection of the second pure spectrum.

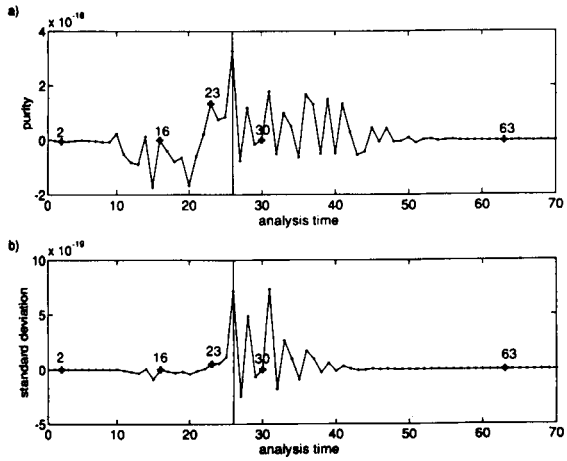

Fig. 11. (a) Purity chromatogram obtained for the reduced data matrix for $Rs = 1$ and 10% of impurity with an offset equal to 1 after the selection of the second pure spectrum, (b) corrected standard deviation chromatogram.

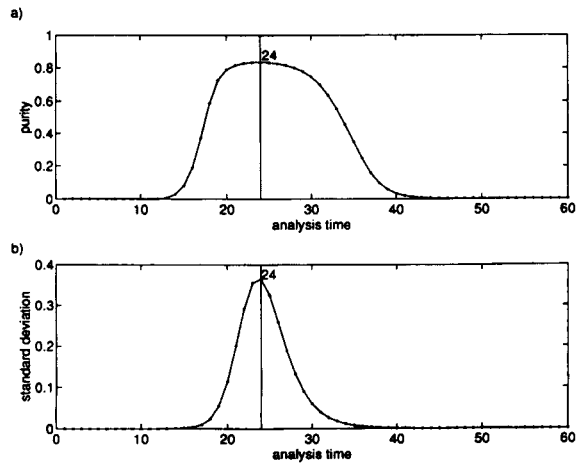

Fig. 12. (a) Purity chromatogram obtained for the data matrix for $Rs = 0.5$ and 1% of impurity with an offset equal to 1, (b) standard deviation chromatogram.

4. Results

The performance of SIMPLISMA for the assessment of peak purity was investigated with the LC-DAD data sets described above. The results obtained for the case of $Rs = 0.5$ and 1% of impurity will be discussed in detail. The purity of each spectrum is calculated with an offset equal to 1 (Fig. 12a). The first "pure spectrum" is selected at time 24. In the corrected standard deviation chromatogram (Fig. 12b) one can see that at time 24 the largest standard deviation is found. The weight vector is determined to subtract the information contained in the first "pure spectrum". In Fig. 13 the corrected second purity chromatogram (Fig. 13a) and the corrected second standard deviation chromatogram (Fig. 13b) are plotted. The spectra correlated with the first "pure spectrum" have very small purity, since the angle determined between them is very small. The second "pure spectrum" is located at analysis time 16. As before, one can see that at this time the standard deviation has a large value (Fig. 13b). The new weight vector is calculated; the corrected third purity and standard deviation chromatograms are plotted in Fig. 14. After the selection of the two "pure spectra" only noise is left. To confirm that all the information has been subtracted with the two "pure spectra" determined, analysis times 24 and 16, SIMPLISMA offers several tools. The first one is the visualization of the pure spectrum profile each time that a "pure spectrum" is determined. In Fig. 15 is shown the spectra at time 24 and 16. Another possibility is to calculate the total signal of each wavelength by adding all the intensities of each column. The total signal spectrum, $\mathbf{t}$, is a linear combination of the pure spectra of the compounds present in the mixture, so that in this case,

$$\mathbf{t} = c_M \mathbf{s}_M + c_I \mathbf{s}_I$$

where c_M and c_I are the total concentration of the main compound and of the impurity in the mixture, respectively; $\mathbf{s}_M$ and $\mathbf{s}_I$ are the molar absorptivities at the different wavelengths of the main compound and of the

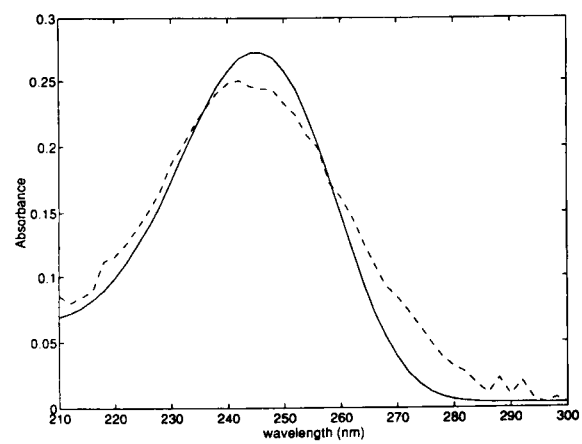

Fig. 13. (a) Purity chromatogram obtained for the data matrix for $Rs = 0.5$ and 1% of impurity with an offset equal to 1 after the selection of the second pure spectrum, (b) corrected standard deviation chromatogram.

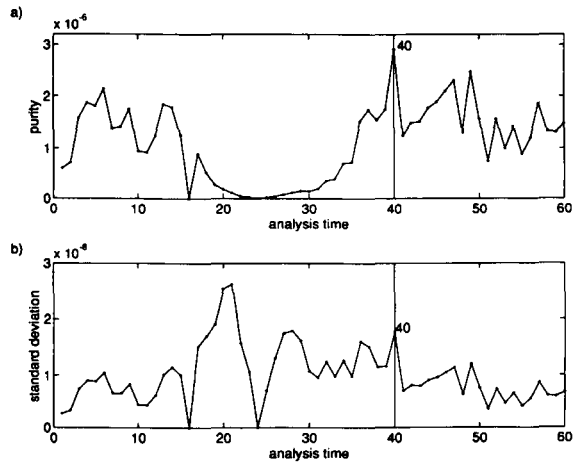

Fig. 14. (a) Purity chromatogram obtained for the data matrix for $Rs = 0.5$ and 1% of impurity with an offset equal to 1 after the selection of the first pure spectrum, (b) corrected standard deviation chromatogram.

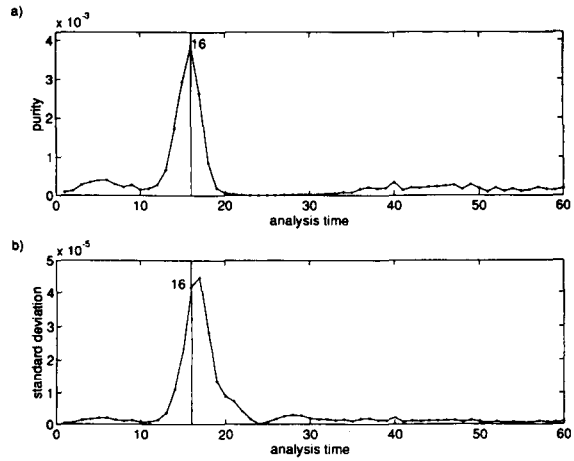

Fig. 15. Pure spectra at time 24 (solid line) and at time 16 (dashed line).

impurity, respectively. The total signal spectrum, **t**, is projected onto the space determined by the "pure spectra" selected and the contribution of each "pure spectrum" to the total signal spectrum, c_M and c_I, are determined. The values obtained for c_M and c_I are used to calculate the least square approximation of the total intensity spectrum. When the proper number of "pure spectra" has been chosen, the least square approximation should be equal to **t**. The criterion used to measure the difference is the square root of the relative sum of squares differences between the two functions. By definition, each "pure spectrum" is the spectrum of the pure compound eluting at the selected analysis time, therefore it is equal to the molar absorptivities at the different wavelengths of the compound eluting multiplied by the concentration of that compound at the analysis time selected. Therefore, the coefficients, c_M and/or c_I, calculated are equal to the total concentration of the main compound and/or impurity divided by the concentration of the main compound and/or impurity at the analysis time selected. For example, in our case the first "pure spectrum" selected is the spectrum at analysis time 24 and at this time only the main compound is eluting. The spectrum at analysis time 24 is proportional to the molar absorptivities of the main compound at the different wavelengths and the proportionality constant is the concentration of the main compound at time 24. The second "pure spectrum" selected is time 16. The spectrum at time 16 is a mixture spectrum, since there are no selective regions for the impurity, or if there is a small region it is at the beginning of the elution of the impurity, where the concentration is very low. However, the spectrum at time 16 is the most dissimilar with respect to the spectrum of the main compound. The coefficient c_I determined for the impurity, equal to 17.06; while the one for the main compound, c_M, is 6.93. The relative root of squares of the residuals between the total intensity spectrum and its least square approximation is equal to 0.0022. If any of the coefficients were negative, it would indicate that too many "pure spectra" have been selected. The positive value of the coefficients, together with the low value of the relative root of squares of the residuals, indicate that the correct number of "pure spectra" have been selected.

Another parameter used in SIMPLISMA is the relative total intensity of the standard deviation chromatogram, since the standard deviation has a close relation with the initial data [15]. The relative total standard deviation is determined by adding all the elements of

Table 1
Relative total intensities of the weight function (first column), of the purity chromatogram (second column) and of the purity-corrected standard deviation chromatogram.

Pure spectrum selected	Weight	Purity	S.D.
–	100	100	100
24	0.7723	0.1482	0.0099
16	0.0039	0.0005	0.0000

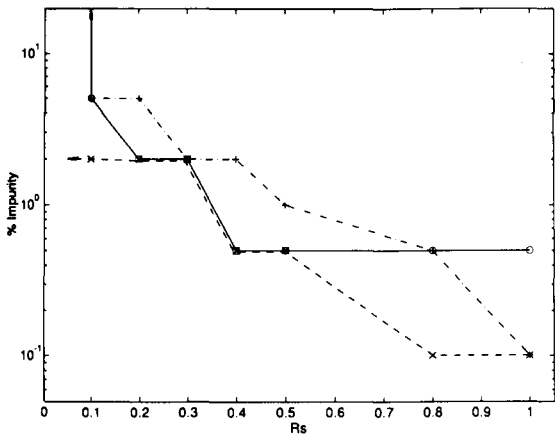

Fig. 16. Limits of detection for an impurity with SIMPLISMA (solid line) and with two modifications of the orthogonalization technique for untransformed data: (a) the "base" vector is the row vector with the highest length (–·–·) and (b) the "base" vector is the mean spectrum (– – –).

the standard deviation vector and dividing by the value before the selection of the first "pure spectrum". The final value is given in percent, therefore before the selection of the first "pure spectrum", the relative total standard deviation has a value of 100. When the correct number of "pure spectra" has been selected the value should be zero. In Table 1 one can see that after the selection of the second "pure spectrum" (time 16) the relative standard deviation has a value virtually equal to zero. In the same way one calculates the relative total intensity of the weight vector and of the purity chromatogram.

The detection limits reached with SIMPLISMA, i.e., the concentration of impurity detected in function of the resolution, are compared with the ones obtained with the approach based on the Gram-Schmidt orthogonalization technique [13,14] (Fig. 16). It seems that with SIMPLISMA the limiting factor for the detection of the impurity is the concentration of the impurity, more than the quality of the chromatographic separation between the two components.

5. Conclusion

SIMPLISMA can be used for the detection of impurities under a chromatographic peak. The results obtained are similar to the ones obtained with other methods as evolving factor analysis (EFA) [7,8], fixed size window evolving factor analysis [9] and the orthogonalization technique developed by us [13,14]. However, the latter seems to be somewhat more sensitive when the concentration of impurity is rather low (~0.1%). To determine which of the methods is superior in which aspects it would however be necessary to organize a broad intercomparison, using different examples and different instruments. Indeed, noise characteristics certainly have an effect on some of these methods. This intercomparison is now being organized.

Acknowledgements

The authors thank W. Windig for providing the software.

References

[1] A.C.J.H. Drouen, H.A.H. Billiet and L. De Galan, Anal. Chem., 56 (1984) 971.
[2] A.F. Poile and R.D. Conlon, J. Chromatogr., 204 (1981) 149.
[3] A.F. Fell, H.P. Scott, R. Gill and A.C. Moffat, J. Chromatogr., 282 (1983) 123.
[4] M. Joseph, Varian Instrument Applications, 20 (1991) 13.
[5] L. Huber, Hewlett-Packard Co., 1989, p. 90.
[6] J.G.D. Marr, G.G.R. Seaton, B.J. Clark and A.F. Fell, J. Chromatogr., 506 (1990) 289.
[7] H. Gampp, M. Maeder, C.J. Meyer and A.D. Zuberbühler, Talanta, 32 (1985) 1133; 33 (1986) 943.
[8] M. Maeder and A. Zilian, Chemom. Intell. Lab. Syst., 3 (1988) 205.
[9] H.R. Keller and D.L. Massart, Anal. Chim. Acta, 246 (1991) 379.
[10] O.M. Kvalheim and Y.Z. Liang, Anal. Chem., 64 (1992) 936.
[11] Y.Z. Liang, O.M. Kvalheim, H.R. Keller, D.L. Massart, P. Kiechle and F. Erni, Anal. Chem., 64 (1992) 946.
[12] H.R. Keller, D.L. Massart, Y.Z. Liang and O.M. Kvalheim, Anal. Chim. Acta, 267 (1992) 63.
[13] F. Cuesta Sánchez, M.S. Khots, D.L. Massart and J.O. De Beer, Anal. Chim. Acta, 285 (1994) 181.
[14] F. Cuesta Sánchez, M.S. Khots and D.L. Massart, Anal. Chim. Acta, 290 (1994) 249.
[15] W. Windig and J. Guilment, Anal. Chem., 63 (1991) 1425.
[16] W. Windig, C.E. Heckler, F.A. Agblevor and R.J. Evans, Chemom. Intell. Lab. Syst., 14 (1992) 195.
[17] W. Windig and D.A. Stephenson, Anal. Chem., 64 (1992) 2735.
[18] W. Windig, Chemom. Intell. Lab. Syst., 4 (1988) 201.
[19] W. Windig, J.L. Lippert, M.J. Robbins, K.R. Kresindke and A.P. Snyder, Chemom. Intell. Lab. Syst., 9 (1990) 7.
[20] E.R. Malinowski, Anal. Chim. Acta, 134 (1982) 129.
[21] H.R. Keller, D.L. Massart and J.O. De Beer, Anal. Chem., 65 (1993) 471.

ELSEVIER

Analytica Chimica Acta 298 (1994) 341–349

ANALYTICA CHIMICA ACTA

Magnetic circular dichroism analysis of nitrogen contaminants in crude oil

J.A. Warner, B.R. Hollebone *

Ottawa-Carleton Chemistry Institute, Carleton University, 1125 Colonel By Drive, Ottawa, Ontario K1S 5B6, Canada

Received 23 May 1994

Abstract

Nitrogen pollution of air can occur from combustion of fossil fuels contaminated with fossilized nitrogen bearing organic molecules. Upgrading and refining processes have been designed to remove nitrogen but analytical monitoring feedstocks and products in real time is impractical with standard analytical techniques for nitrogen. In this study, magnetic circular dichroism (MCD) detection and quantitation of fossil porphyrins is shown to correlate well with total nitrogen in fractions representing over 80% of crude oil. Non-linear correlation in the heaviest fraction due to non-porphyrin neutral substances can be recognized and corrected. The resulting MCD procedure has the potential to become a fast on-site quality control system for upgrading crude oil.

Keywords: Crude oil; Magnetic circular dichroism; Nitrogen; Oil

1. Introduction

The level of nitrogen found in crude oils is in the range of 1% by weight [1]. It occurs principally as a heteroatomic replacement of carbon in unsaturated, cyclic or aromatic structures [2]. Regardless of its speciation however, nitrogen in all fossil fuels interferes with the sequence of processes used for upgrading and refining to final products [3]. As well, when fuels are used, the trace nitrogen species are converted to mixed nitrogen oxides regardless of the design of the combustion system [4]. In these forms, it becomes a contribution to urban smog and acid rain.

To avoid these problems, the initial upgrading steps have been designed to remove the bulk of nitrogen species during the coking process which precipitates the aromatic materials as amorphous carbon [5]. This succeeds because the nitrogen substituted species are similar thermodynamically to the aromatics and often contain fossilized porphyrins or its degradation fragments [6–8]. The most common of these are listed in Table 1 together with their standard enthalpies of formation.

The nitrogen level of crude oils varies widely and controlling the upgrading process to ensure complete removal of nitrogen is difficult with current techniques. Typically the feedstock passes through the

* Corresponding author.

SSDI 0003-2670(94)00301-7

Table 1
Stabilities of nitrogen contaminants of crude oils

Name	Molecular formula	Standard enthalpy formation (kJ/mol) H_f (298.15 K)
Pyrrole	C_4H_5N	63.1
Indole	C_8H_7N	86.1
Carbazole	$C_{12}H_9N$	125.1
Pyridine	C_5H_5N	100.2
Isoquinoline	C_9H_7N	144.5
Acridine	$C_{13}H_9N$	200.9
Phenanthridine	$C_{13}H_9N$	148.9
21*H*,23*H*-Porphin	$C_{20}H_{14}N$	−1106.9
Etioporphyrin I	$C_{32}H_{38}N_4$	−25.2
Etioporphyrin II	$C_{32}H_{38}N_4$	1.6
Octaethylporphyrin	$C_{36}H_{46}N_4$	−183.2

upgrades in 10–15 min. Attempts to control the process with traditional Kjeldahl analysis for nitrogen become impractical since it typically requires several hours to perform the analysis [10]. Recent introduction of inductively coupled plasma mass spectrometry (ICP-MS) methods, based on observation of NO [11] still requires sample preparation and analysis at a remote laboratory.

Because practical, real-time, on-site analysis for nitrogen has not been available upgrading plants tend to be overbuilt to allow for the most extreme conditions [12]. They are also operated to overcompensate the coking. This raises the initial capital cost and wastes some feedstock which could otherwise be recovered as final products.

To overcome these problems a chemical analysis for nitrogen which completes the determination routinely within the hold-up time of the process is needed. These requirements essentially preclude all but the simplest and most rapid manipulations and strongly suggest that direct spectroscopic determination on the crude oil itself is necessary. Several types of spectroscopy are available but the chemical and physical constraints of this problem preclude most of them.

The major chemical problems arise from the variability of the chemical components and the suspended solids in the crude oil. These make it very difficult to establish a reference material for absorbance spectrometry or to normalize backgrounds for fluorimetry. At the same time, the major physical difficulties arise from the intense, broad band spectra of crude oils. Detection of signals from trace contaminants against these intense backgrounds involves detection of small differences between large signals for either absorbance or fluorescence.

The most promising spectrometric technique for this application is magnetic circular dichroism (MCD) [13]. In this form of spectroscopy, the signal measures the preferential absorption of left or right circularly polarized light by a sample held in a strong magnetic field. This preferential absorption may be plotted as a positive (LCP) or negative (RCP) signal. The signal arises from the rotation of electrons around the applied field during excitation by the light to an excited state. For practical purposes, this means that molecules capable of magnetic response can become highly visible against a background of magnetically silent substances, even if the background has a high electronic absorption [14]. In the present case, the nitrogen occurring as a porphyrin is easily detected because of the strong magnetic signal of this structure in several bands in the visible and near ultraviolet regions [15]. This overcomes the basic physical difficulties since the MCD spectra of the deeply coloured oil background are very weak. At the same time, MCD also, in effect, overcomes the chemical problem of the reference. Right and left hand light scatter equally from suspensions so MCD spectrometry is not sensitive to sample turbidity. As well, the differential absorbance means that the concentration is estimated, using Beer's law, as a difference in intensities of the two handed beams of light. In this sense, one beam acts as a reference for the other and MCD appears to provide single-beam analysis. In fact, a baseline correction may be needed [14], but the characteristic porphyrin signal is easily recognized against poorly defined and weak spectra of other oil components.

In spite of this ability to discriminate and quantify the signal from porphyrins, MCD can only become a reliable indicator of nitrogen contamination if total nitrogen is correlated strongly to porphyrin content of oil. The processes of fossilization and metamorphosis which lead to oil formation suggest that such a correlation is possible [16,17]. The porphyrins occur in the original life forms and may also serve as the thermodynamically stable end point of anaerobic metamorphosis. To test this hypothesis a synthetic crude oil obtained from oil sand deposits has been

studied. In particular, fractions separated by solution in homologous alkane solvents were analyzed to determine the reliability of the proposed correlation.

2. Experimental

2.1. Crude oil

A sample of synthetic crude oil was obtained from a Clark hot water extractor operated by Syncrude Canada at Mildred Lake, Alberta. This viscous material was diluted with benzene, and filtered through sintered glass to remove the entrained sand and clay particles. The benzene was then removed by rotary evaporation.

2.2. Fractionation of crude oil

Crude oil is known to contain alkanes, cycloalkanes, aromatics and heteroatomic compounds [2,18]. In general, these are separable by their solubilities in increasingly polarizable alkane solvents [19]. A very convenient series of these solvents is the straight chain hydrocarbons from propane to heptane. In this series, the polarizability increases linearly with the number of carbon atoms, as shown in Fig. 1. Thus, these solvents can be used to extract increasingly polar or polarized components of crude oil [19]. In particular, this discrimination should include the nitrogen-bearing contaminants. The working scheme of the fractionation sequence is shown in Figs. 2 and 3. Because of the specific design, no explicit extraction with butane is included. The corresponding fraction is the maltene resins, isolated here as soluble in pentane but insoluble in propane at $-80°C$.

After solvent separations, all fractions except the heptane asphaltenes were dissolved in cyclohexane and subjected to cation exchange on Amberlist 15 cation-exchange resin columns (Rohm and Haas). The columns were washed with four volumes of cyclohexane. The retained bases were then eluted successively with benzene, then benzene–methanol azeotrope and finally the benzene–methanol–isopropylamine azeotrope, to separate the weak, medium and strong bases. The non basic faction in cyclohexane was subjected to anion exchange on the base form of Amberlyst 29 anion exchange resin (Rohm and Haas). The acids were eluted with 5% acetic acid–95% benzene. Finally, the neutral fraction was recovered from the cyclohexane, redissolved in dichloromethane and loaded onto Davisil, silica gel 150A (Aldrich). The dichloromethane was evaporated and the silica gel eluted with cyclohexane to remove saturates, then with the benzene–methanol azeotrope to remove the aromatics.

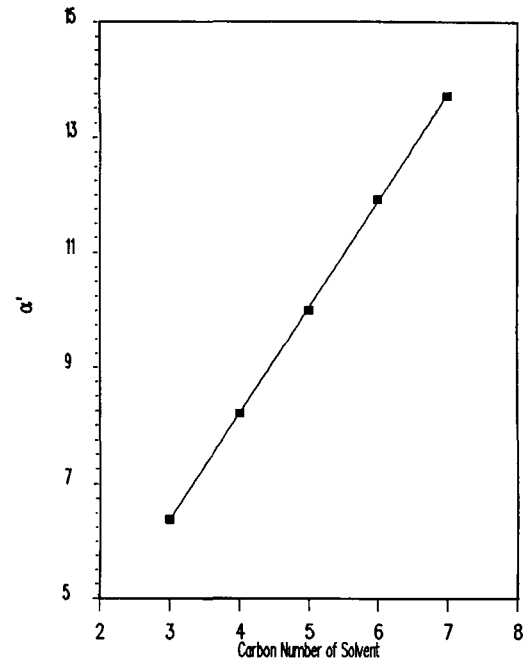

Fig. 1. Relationship between the average electric polarizability volume (10^{-24} cm^3) of homologous alkane straight chain solvents and the number of carbon atoms.

2.3. Analyses

The recoveries of all of the separable components were analysed first by gas chromatography (GC) then GC–MS. The preliminary data were obtained on a Varian 3400 gas chromatograph with a 1045 injection system and 30-m DB5 column with a thermionic detector. Final data were determined on a Varian Saturn GC/MS system with a 30-m DB5 column programmed with a rapid ramp to 300°C and a 70 V ion trap source.

With each fraction and subfraction where possi-

ble, analyses for C, H and N were performed by Canadian Microanalytical Services.

The porphyrin analyses were performed by MCD spectrometry on a custom-built system in this laboratory. Data were obtained in the Q band and when possible, the B band. This technique was calibrated with cobalt sulphate [13] and then with vanadyl porphyrin. The latter was chosen since it is the dominant porphyrin found in these oil sand deposits. It was synthesized by well defined procedures [20]. From the known absorbance extinction coefficient [21] and the cobalt sulphate calibration of MCD intensities, the differential extinction coefficients were determined for the Q and B bands of vanadyl porphyrin. From these, two calibration curves were determined, following the relations;

$$[VOP]_Q = \frac{A_Q - 3.0228 \times 10^{-6}}{0.0193}$$

$$[VOP]_B = \frac{A_B - 2.7577 \times 10^{-7}}{0.01332}$$

These calibrations are shown in Fig. 4.

3. Results

The recoveries of fractions from the crude oil and the analyses of elements and vanadyl porphyrin in

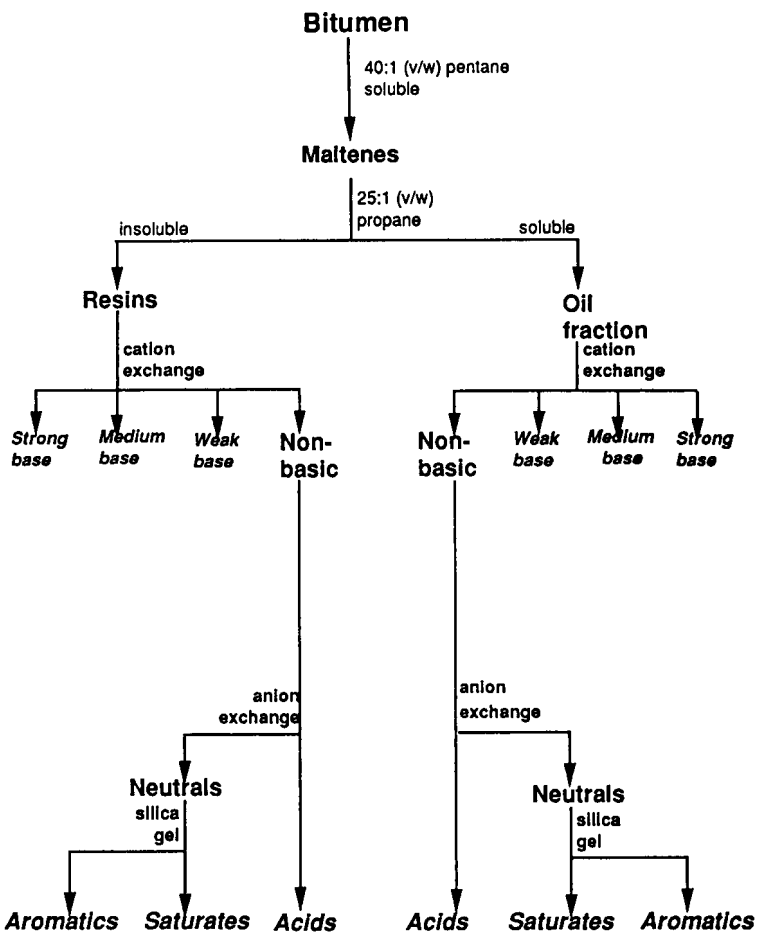

Fig. 2. Experimental scheme for separating maltene fractions from bitumen.

these fractions are all reported in Table 2. In several instances, the fractions represent very small recoveries and full analyses were not possible from the quantities obtained. In particular, the hexane fraction was so small that only C, H and N analyses together with porphyrin determinations were possible. The porphyrin analyses rely essentially on the Q band data, both because it is stronger and because the B band is often obscured by other transitions.

These data can be used to determine whether the porphyrin content of these fractions is correlated to the total nitrogen levels. In Fig. 5, the total porphyrin content is plotted against the total level of nitrogen in each of the fractions obtained by homologous alkane solvent separations. The four successive fractions extracted by C_3 up to C_6 solvent yield a good correlation of the porphyrin determination to the nitrogen content. In the remainder fraction from heptane, the porphyrin level is much lower than predicted by the trend of the first four data points.

The reason for this decreased porphyrin level in the heptane fraction can be examined in the subfractionation data for bases, acids and neutrals, in Table 2. The porphyrin content tends to be concentrated in the basic subfractions, particularly in those subfractions denoted as either weak or medium bases. The total nitrogen however is found distributed over most of the subfractions. From these observations, the

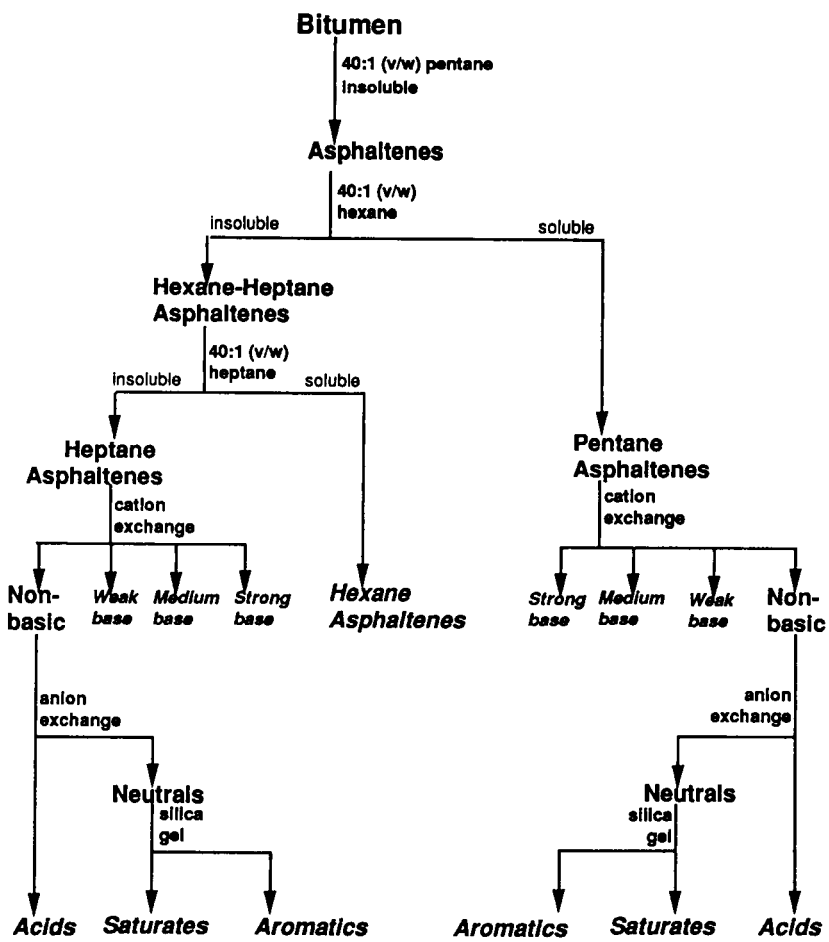

Fig. 3. Experimental scheme for separating asphaltene fractions from bitumen.

total porphyrin content of a solvent fraction should correlate to the proportion of nitrogen found in these basic subfractions. This is illustrated by a plot of total fraction porphyrin against the nitrogen content of medium base subfractions, corrected for their relative subfraction yield, in Fig. 6. In this plot, the porphyrin of the extracted heptane fraction (C_7) correlates closely with that of the other fractions for which subfraction data were available.

This result shows that the distribution of elemental nitrogen amongst various types of molecules is reasonably constant through fractions soluble in C_3

Table 2
Analysis of crude oil fractions

Bitumen	Recovery as % bitumen	Fraction	Recovery as % fraction	C	H	N	Porphyrin content	
							MCD Q band	MCD B band
Description	wt.% ±0.5	Description	wt.% ±0.5	wt.% ±0.8	wt.% ±0.1	wt.% ±0.03	wt.% ±0.05	wt.% ±0.05
Dephased oil	34 ±0.3			84.8	10.5	0.15	0.17	0.22
		Weak bases	8	–	–	–	0.14	0.13
		Medium bases	9	66.4	8.91	0.88	0.13	0.00
		Strong bases	1.0	–	–	–	0.00	0.00
		Acids	7	52.8	7.65	1.43	0.00	0.00
		Saturates	69	85.6	11.5	–	0.00	0.28
		Aromatics	7	–	–	–	0.00	0.00
Resins	35 ±0.3			83.1	9.8	0.44		2.69
		Weak bases	3.0	82.4	8.37	0.85	4.2	0.00
		Medium bases	15	71.9	8.49	0.99	2.97	0.00
		Strong bases	7	81.4	9.21	1.49	1.56	0.00
		Acids	21	55.8	7.03	0.92	0.39	0.00
		Saturates	0	–	–	–	0.00	0.52
		Aromatics	54	78.8	8.07	1.17	0.41	0.00
Pentane asphaltenes	4.0 ±0.1			81.9	9.09	0.76	5.5	0.00
		Weak bases	15	79.3	7.94	0.81	8.3	1.65
		Medium bases	23	68.2	7.80	1.00	6.8	3.13
		Strong bases	4.0	–	–	–	4.7	0.00
		Acids	52	–	–	–	0.010	0.06
		Saturates	< 1	–	–	–	0.00	0.00
		Aromatics	< 1	–	–	–	0.00	0.00
Hexane asphaltenes	1.0 ±0.1			80.7	8.53	0.96	10.23	2.28
Heptane asphaltenes	19 ±1			80.2	7.94	1.2	1.85	0.00
		Weak bases	32	79.3	7.53	1.35	0.99	0.00
		Medium bases	14	78.5	6.13	0.77	3.9	2.90
		Strong bases	7.0	78.0	8.14	1.44	2.51	0.00
		Acids	6	71.3	7.72	1.02	1.0	0.84
		Saturates	28	84.7	11.3	–	0.00	0.53
		Aromatics	12	79.0	9.25	0.57	4.1	4.24

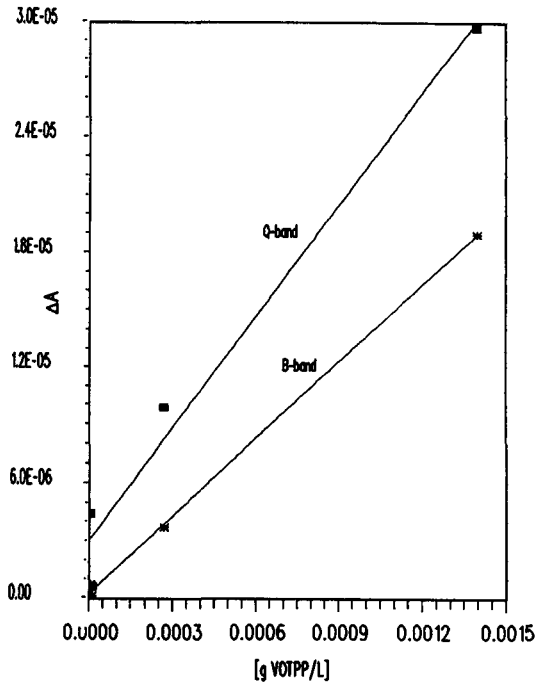

Fig. 4. Calibration curves for MCD quantification of vanadyl porphyrin using both Q and B band correlations.

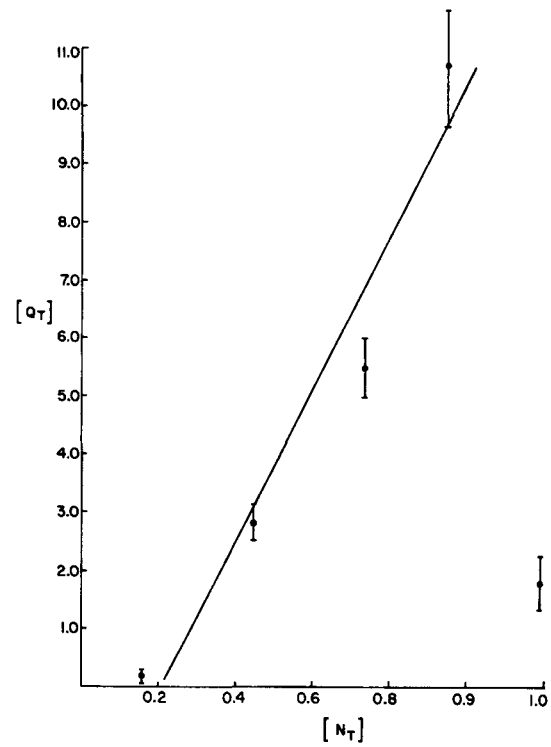

Fig. 5. The dependence of % total porphyrin for successive fractions on % total nitrogen.

up to C_5 solvents. Beyond this point however, the distribution appears to change. This is illustrated in Fig. 7, using all the available subfraction data.

4. Discussion

The correlation in Fig. 5 shows that an MCD assay of total porphyrin is a good indicator of the total nitrogen content of fractions representing more than 80% of the total synthetic crude oil. The correlation in Fig. 6 shows that the MCD assay continues to be valid when applied to the basic subfraction of the heptane-soluble fraction. The excess nitrogen content of this fraction appears to arise in the high aromatics and acids content, as shown in Fig. 7.

This distribution of aromatics into the heptane fraction follows the increasing polarizability of the solvent. The least polarizable solvent, propane, dissolves saturates and small amounts of permanently polar acids and bases. With increasing polarizability, the solubility of saturates drops quickly, that of polar bases and acids rises continuously and the aromatics

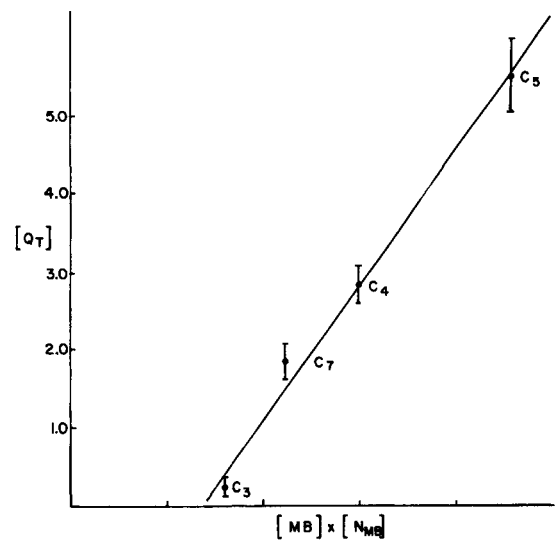

Fig. 6. The dependence of % total porphyrin for successive fractions on % nitrogen present as medium bases in each fraction.

appear to split into two different groups, those soluble at butane and those in heptane. Significantly, the aromatics soluble in butane carry on unusually low nitrogen content, while those soluble in heptane have a nitrogen content ten times higher. Since these substances emerged from the subfractionation process as apparent aromatic neutral species, they are most probably, nitrogen heteroaromatic compounds in which the nitrogen is fully substituted. The non-basic nitrogen compounds typically found in these synthetic crude oils [22] include the indoles, carbazoles, benzocarbazoles and substituted pyrroles shown in Fig. 8. There may be some complexes of nitrogenous molecules with metals which would also fall into this group but none have been positively identified [23,24].

These conditions suggest that an MCD assay of porphyrins in oils could be used in process control. The scan time for the Q band region is typically 2 to 3 min, depending on the gain required. Thus, the only limitation to real-time, on-line data would arise from sample preparation. Since the results show that porphyrin content correlates linearly to total nitrogen up to the hexane fraction, a rapid, one-step hexane extraction could be performed to prepare a representative sample at a dilution appropriate to good MCD signal to noise. Since this is such a sample operation, it should be readily automated with a robotic extraction apparatus. Presuming this would require only a few minutes, feed stock data could be available to plant operators at 10 min intervals. This would provide the real-time data needed for continued optimization of denitrification operations.

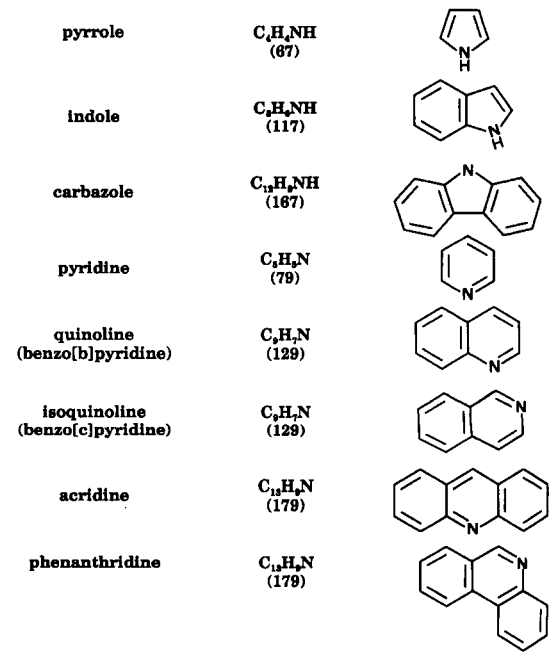

Fig. 8. Non-porphyrin nitrogen contaminants commonly found in crude oils.

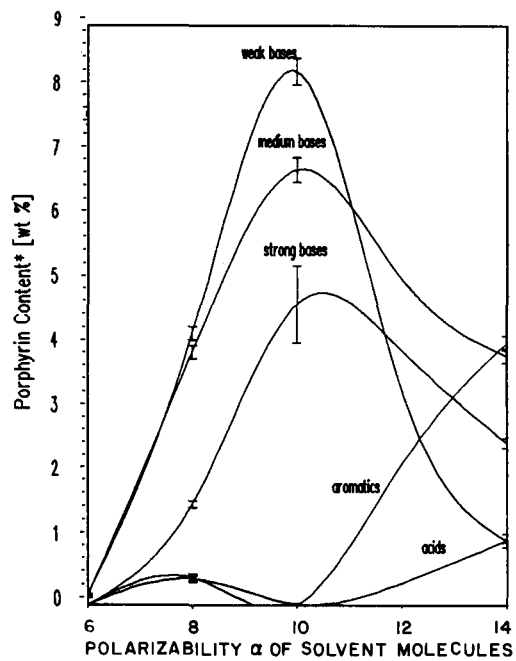

Fig. 7. The dependence of % total porphyrin in each fraction on polarizability of each solvent for components of each subfraction.

References

[1] O.P. Strausz, in D.A. Redford and G.A. Weinstock (Eds.), The Oil Sands of Canada–Venezuela, CIM Special Volume 17, 1977, pp. 146–152.
[2] J.G. Speight and S.E. Moschopedis, Adv. Chem. Ser., 195 (1981) 1.
[3] C.D. Ford, S.A. Holmes, L.F. Thompson and D.R. Latham, Anal. Chem., 53 (1981) 831.
[4] Z.R. Ismagilov and M.A. Kerzhentsev, Catal. Rev. Sci. Eng., 32 (1990) 51.
[5] M. Dorbon, I. Ignatiadis, J.M. Schmitter, P. Arpino, G. Guiochon, H. Toulhoat and A. Huc, Fuel, 63 (1984) 565.

[6] J.M. Schmitter, Z. Vajta and P. Arpino, in A.G. Douglas and J.R. Maxwell (Eds.), Investigation of Nitrogen Bases in Petroleum, Advances in Organic Geometry 1979, Pergamon Press, Oxford, 1980, pp. 67–76.
[7] Z. Frakman, Y. Ignasiak, D. Montgomery and O.P. Strausz, AOSTRA, J. Res., 3 (1987) 131.
[8] J.M. Schmitter, P. Garrigues, I. Ignatradis, R. De Vazelkes, F. Perin, M. Ewald and P. Arpino, Org. Geochim., 6 (1984) 579.
[9] J.B. Pedley, R.D. Nayler and S.B. Kirby, Thermodynamic Data of Organic Compounds, Chapman Hall, London, 2nd edn., 1986.
[10] D.A. Skoog and D.M. West, Fundamentals of Analytical Chemistry, Saunders, Philadelphia, PA, 4th edn., 1982, pp. 249–251.
[11] C. Gregoire, personal communication.
[12] M. Nagai, T. Masunaga and N. Hanu-oka, Energy and Falls, 2 (1988) 645.
[13] B. Holmquist and B.L. Valee, Methods Enzymol., 49 (1978) 149.
[14] B.R. Hollebone, Spectrochim. Acta. Rev., 15 (1994) 493.
[15] J.B. Lambert, H.F. Shurovell, L. Verbit, R. Cooks and G.H. Stout, Organic Structural Analysis, McMillan, New York, 1976.
[16] A.H. Whittaker and P. Dyson, Oil Gas J., 28 (1980) 141.
[17] I. Ignatiadis, M. Ewald, P. Arpino and G. Guiochon, Org. Geochem., 7 (1984) 111.
[18] B. Tissot and D.H. Welte, Petroleum Formation and occurrance, Springer Verlag, Berlin, Part IV, Chap. 2, 2nd edn., 1981.
[19] L.W. Corbett and V. Petrozzi, Ind. Eng. Chem. Prod. Rev. Dev., 17 (1978) 342.
[20] J.W. Buchler, G. Eikelmann, L. Puppe, K. Rohbock, H.H. Schneehage and D. Weck, Justus Liebis Ann. Chem., 745 (1971) 135.
[21] M.M. Barbooti, E.Z. Said, E.B. Hassan and S.M. Abdul-Ridah, Fuel, 68 (1989) 84.
[22] Z. Frakman, T.M. Ignasiak, D.S. Montgomery and O.P. Strausz, AOSTRA, J. Res., 3 (1987) 131.
[23] J.G. Reynolds, W.R. Biggs and S.A. Bezman, ACS Symp. Ser., 344 (1987) 205.
[24] Z. Frakman, T.M. Ignasiak, D.S. Montgomery and O.P. Strausz, AOSTRA, J. Res. 4 (1988) 171.

ELSEVIER

Analytica Chimica Acta 298 (1994) 351–361

ANALYTICA CHIMICA ACTA

Analysis of sodium polyacrylate absorbent dust using ultra-trace sodium analysis — a seven-company collaborative study

P.A. Forshey [a,*], T.S. Turan [a], J.S. Lemmo [b], S.S. Cutiè [c], D.L. Pytynia [d]

[a] *Procter and Gamble Co., Cincinnati, OH, USA*

[b] *Johnson and Johnson WAPMR, Dayton, NJ, USA*

[c] *Dow Chemical Co., Midland, MI, USA*

[d] *Nalco Chemical Co., Naperville, IL, USA*

Received 24 February 1994; revised manuscript received 7 July 1994

Abstract

Seven companies that either manufacture cross-linked polyacrylate absorbents (PA) or manufacture products that contain PA have developed in situ methods to measure trace levels of PA dust. The method uses sodium present in PA as the tracer element and involves careful pre-cleaning of sampling cassettes and filters. Cassette and filter pre-cleaning as well as sample collection, extraction, and analysis are carried out in a sealed cassette assembly, hence the term "in situ". Inadvertent contamination of the cassette assembly during shipping and handling or during solution transfer is thereby eliminated. Limits of detection for PA range from 0.11 to 2.4 $\mu g/m^3$ and the seven companies averaged 0.7 $\mu g/m^3$. This report contains the results of an inter-company collaborative trial conducted to assess the accuracy, precision, and limits of detection for the in situ methods used by the seven companies.

Keywords: Atomic absorption spectrometry; Atomic emission spectrometry; Gravimetry; Inter-laboratory comparison; Polyacrylates; Sodium; Ultratrace

1. Introduction

The sodium salts of cross-linked polyacrylate (see Fig. 1) are commonplace in a variety of disposable personal products where absorption of aqueous fluids is a key product attribute. Cross-linked polyacrylate absorbents (PA) are typically added to a disposable product in a granular form with average particle diameters of 400 to 800 μm. During the production, handling, and shipping of these materials, airborne PA dust can be generated.

Particles in the 100 to 1000 μm range quickly fall out of the air, but smaller particles, which are present in the PA powder, may stay suspended for longer periods of time and may contribute to the concentration of dust in a manufacturing plant. Because of the potential for inhalation, methods have been developed that can measure PA dust in industrial atmospheres. Initial attempts to quantify PA dust involved the measurement of sodium by either atomic absorption spectroscopy (AAS) or atomic emission spectroscopy (AES) or involved the formation of propyl ester of PA followed by base hydrolysis of the ester and gas chromatographic (GC) analysis of the resultant alcohol [1,2]. The sample pretreatment employed in these methods involved the digestion, ashing, or derivatization of PA dust samples and filters. Cutiè and co-workers, of Dow Chem-

* Corresponding author.

SSDI 0003-2670(94)00304-1

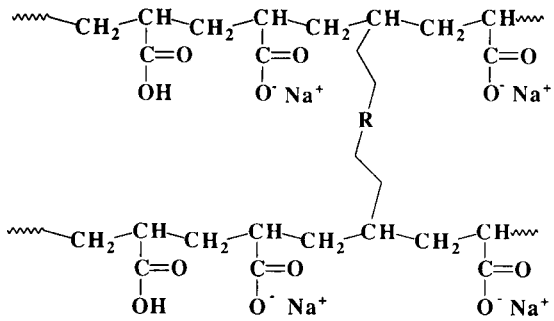

where R = Cross-linker

Fig. 1. Polyacrylic acid, sodium salt.

ical [3,4], developed a method involving sodium determination using a sodium ion-selective electrode. Tucker [5] developed a method that involved the interaction of copper with PA followed by inductively coupled plasma AES analysis of copper. Limits of detection (LODs) typically ranged from 4 to 50 μg PA and were often dependent on the sodium present from non-PA sources. Another problem with most of these methods was that only the dust that was collected on the filter was analyzed and not the dust that might be deposited on the interior surfaces of the collection cassettes. Analyses at several laboratories have indicated that, on average, about 30% of the collected dust was deposited on interior surfaces other than the filter and, more importantly, the amount could range from 5% to 95% [6,7]. This was believed to be due to electrostatic charge build-up on the polystyrene cassette which then caused significant wall losses of PA dust. The electrostatic effect on dust samples collected in polystyrene cassettes has been documented for a variety of dust types [8–10].

In an effort to overcome the limitations of existing methods, seven companies that either manufacture PA or products that contain PA have developed methods that can measure microgram amounts of PA dust. Most were using very similar methods that involved the trace analysis of sodium by either AAS or AES. Two companies were using sodium ion-selective electrodes but eventually abandoned these methods in favor of AAS or AES to achieve the necessary analytical sensitivity. Through a collaborative effort these companies developed in situ methods with the necessary sensitivity, precision, and accuracy to measure ultra-trace levels of PA dust. A key feature of these methods is that cassette and filter pre-cleaning as well as sample collection, extraction, and analysis are carried out in a sealed cassette assembly, hence the term "in situ". Inadvertent contamination of the cassette assembly during shipping and handling or during solution transfer is thereby eliminated. This report contains the results of an inter-company collaborative trial by the seven companies.

The study was conducted with the aid of the Inhalation Toxicology Research Institute (ITRI) of Albuquerque, NM, USA. ITRI had the facilities, experience, and expertise necessary to generate and to sample controlled PA dust clouds. Each of the participating companies delivered to ITRI 20 to 50, carefully cleaned closed face air sampling cassettes (CFCs). Some were randomly selected as control samples and were used to sample a dust chamber that contained no PA dust. The rest were used to sample the PA dust chamber for a sufficient length of time and flow-rate to collect target dust loadings of 1, 5, or 25 μg of PA. All were returned to the appropriate company for analysis.

2. Experimental

2.1. Data analysis and outlier rejection

In some data sets at least one result seemed out of line with the remainder of the data set. The Q-test [11] was used to determine which data points should be rejected from each data set. Throughout this paper the rejected data points are shown in parentheses and were treated as outliers.

Two methods were used to calculate averages in this paper, an average of averages method and a global average method. The global average was calculated by averaging all data reported for a given group. Using this method, each result from each company had identical statistical weight. Therefore, because some companies reported more results than others, those companies had greater statistical weight than others in the calculation of the global average. For the average of averages method, the results for each company were first averaged then the average values for each company were averaged. In this way the data from each company was given equivalent statistical weight.

It was apparent that the collaborative study data from Company G were skewed high and were imprecise, particularly at the lower dust levels. This was deter-

mined to be due to contamination during the extraction step of the sodium analysis. Contamination was apparently caused by the use of a thick plastic filter support pad which did not allow some of the cassette assemblies to be completely sealed. As a result of inconsistent sealing, sodium extraction solution leaked from the cassette and came in contact with external sources of sodium. Because of this, the results from Company G have been excluded from the calculation of the means and standard deviations. However, for completeness, these results are shown in this paper.

2.2. Dust collection devices

Dust samples for the participating companies were collected in 37-mm polystyrene CFCs (Gelman Part No. 225-3). The samples were collected on Zefluor filters (2 μm pore size, Gelman Part No. P5PJ037) supported by either porous plastic (Nuclepore Part No. 220800) or cellulose pads. Reference samples for the determination of chamber concentration or PA moisture content were collected by ITRI using a Total Dust Monitor (TDM) which consisted of a 25-mm in-line Zefluor filter (2 μm pore size).

2.3. Dust generation

The PA test material was a commercially available material from one of the participating companies. It was micronized to significantly increase the amount of material of small particle size. The milled bulk PA was repackaged into lots of ~1 kg at ITRI. These lots were sealed in moisture-proof containers and stored at ambient room conditions for the duration of this study. The test system consisted of an H-2000 exposure chamber (Lab Products, Maywood, NJ, USA), a Wright Dust Feeder (WDF) generation system (BGI, Waltham, MA, USA) with a 6-μm effective cut-off diameter (ECD) cyclone, and an aerosol delivery system (see Fig. 2). The exposure chamber was operated at a total flow-rate of ~15 cubic feet per minute. Chamber environmental conditions (temperature, relative humidity, pressure, and flow-rate) were monitored by a computer-based environmental system.

The PA was compressed into a 2″-diameter stainless-steel cup at 3000 p.s.i.g. using a laboratory hydraulic press and the test aerosol was generated using a WDF. The WDF was operated with dry, clean compressed air

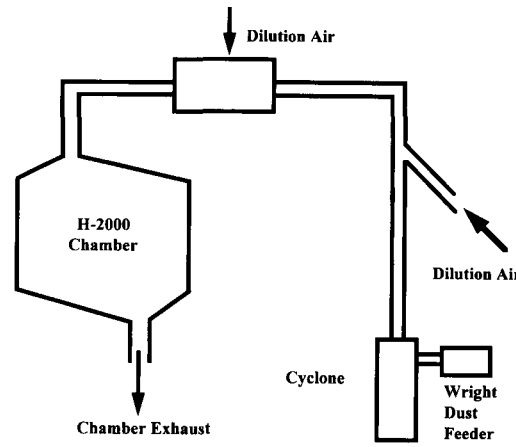

Fig. 2. Dust generation system and chamber.

at ~30 LPM. The output of the WDF exited the generator directly into a 6-μm ECD cyclone which was used to remove the large fraction (>6 μm) of the aerosol. Dust in this particle size range should be collected by CFCs and TDMs with a collection efficiency of 100%. The aerosol was then diluted with clean, compressed air and further diluted with filtered air (approximately 50% relative humidity) prior to delivery to the chamber. Samples were extracted from the chamber using one of eight sample probe assemblies. The homogeneity, size distribution, and stability of the test aerosol in the chamber were evaluated and found to be acceptable prior to the collection of samples.

The target dust chamber concentration was 200 μg/m^3. Based on this chamber concentration, the sampling flow-rate of 1.9 LPM, and the target filter loadings of 1, 5, and 25 μg PA per cassette filter, sample times for the cassettes were calculated to be 2.5, 13, and 65 min, respectively. A second chamber, through which was drawn only filtered air, served as a control and was used for collecting 37-mm background samples. These controls were later used to correct both gravimetric and sodium analyses for background levels of non-PA dust that might be in the chamber.

2.4. Analysis of bulk micronized PA

Each participating company was supplied with a 0.5-g sample of bulk PA for sodium and moisture analyses. The moisture levels were determined by weighing before and after oven-drying at 105°C for 3 h. The moisture level of bulk PA was calculated to be 8.1% (±1.0%) by averaging each company's average

results (average of averages approach). This moisture value applies to the bulk material but not necessarily to the sample after it had been aerosolized.

Samples of the dried bulk PA were analyzed for sodium content and the average was determined to be 15.8% (±0.6%) using the average of averages approach. The reagents and equipment used in these analyses are identical to those used in each company's in situ method (to be discussed later). The sodium content was used to calculate a gravimetric factor of 6.34 μg PA/μg Na (6.34 = 1/0.158). All sodium values presented herein have been converted to the equivalent PA value using this gravimetric factor as shown in Eq. 1.

$$\text{PA}\ (\mu\text{g}) = 6.34 \times \text{Na}_x \qquad (1)$$

where Na_x is the amount of sodium (in μg) found on each filter from company "x". Since the presence of sodium is to some degree ubiquitous, some trace sodium was found in most samples regardless of whether or not PA was present.

2.5. Moisture content of PA dust

Since PA is very hygroscopic, it may rapidly acquire moisture while aerosolized in the atmosphere of the dust chamber. Thus, the gravimetric determination of PA dust samples would be biased high by moisture acquired during dust generation, sampling, and analysis. To quantify the impact of moisture on PA dust, six dust samples and two control samples were collected using the ITRI total dust monitor. These samples were analyzed first gravimetrically, then via AAS for sodium. The target levels for dust samples were significantly higher than those in the comparative study to avoid difficulties associated with ultra-trace analysis. The results of these analyses are listed in Table 1.

The gravimetric results for both control samples suggested either that 4 μg of background dust were collected or that there was a 4-μg weighing error. Regardless of the cause, 4 μg were subtracted from the gravimetric results for each of the six dust samples to correct for this offset. The sodium analyses of the control samples were not significantly different from the reagent background.

The dust weights determined gravimetrically for these samples were significantly greater than the equivalent PA dust weights calculated using the results of sodium analyses and Eq. 1. On average, the corrected gravimetric results are 150% more than the sodium equivalent PA dust weights suggesting that the gravimetric samples have a 33% moisture content. These results are consistent with the hygroscopic nature of PA and with the results of earlier Institute for Polyacrylate Absorbents (IPA) studies [1,2]. The data suggest that micronized PA dust concentrations determined gravimetrically overestimate the true PA concentration, especially at very low dust levels.

The background- and moisture-corrected PA dust concentration was calculated to be 115 $\mu g/m^3$, as

Table 1
Moisture content of TDM dust samples

Chamber sampled	Volume sampled (m^3)	As sampled gravimetric PA dust weight (μg)	Background corrected gravimetric PA dust weight (μg)	Sodium equivalent PA dust weight by AAS (μg)
Control	0.145	4	0	0
Control	0.595	4	0	0
Sample	0.068	24	20	7.1
Sample	0.086	19	15	9.5
Sample	0.308	52	48	34.6
Sample	0.417	89	85	55.9
Sample	0.465	84	80	56.4
Sample	0.595	98	94	64.5
Sample chamber total volume = 1.99 m^3			Total weight = 342	Total weight = 228

Ratio = 342/228 = 1.50.
%Moisture = (342 − 228)/342 = 114/342 = 33%.
Chamber concentration = 228/1.99 = 115 $\mu g/m^3$.

Table 2
Delivered PA dust levels

Sample group	Target PA dust weight (μg)	Average sodium equivalent PA dust weight (μg)	Standard deviation (μg)	Number of samples
Control	0	0.00	0.00	90
Low level	1	0.54	0.01	90
Mid level	5	2.82	0.06	78
High level	25	14.1	0.3	78

shown in Table 1. Based on this concentration and the corresponding sampling times and flow-rates, the loading levels for the CFC samples prepared for the collaborative study were calculated. The results are shown in Table 2.

2.6. Recovery of sodium from PA dust

The quantitative recovery of sodium from PA dust was demonstrated by comparing the results of AAS and neutron activation analysis (NAA). Samples of the PA powder (approximately 50 mg) were extracted with three different concentrations of an ammonia–ammonium chloride solution. These solutions were analyzed by AAS and NAA. The results indicated that 99% of the sodium contained in the PA samples was quantitatively extracted from the polymer using a dilute ammonium chloride solution. A separate set of experiments were carried out in which samples of PA dust ranging from 5 to 50 μg were extracted with an ammonia–ammonium chloride solution. The extracts were analyzed by AAS and NAA. The results from the two instruments correlated well and, again, indicated that the sodium contained in the PA samples was quantitatively extracted. Although a comprehensive study of extracting reagents has not been done, it is assumed that the reagents and conditions used by the participating companies will also quantitatively extract sodium from the study polymer.

3. Results and discussion

3.1. In situ analysis

There was not a single, detailed, analytical method in use for this study. Rather, each company had developed slightly different methods and, therefore, solvents and reagents varied slightly. Details of the pre-cleaning, extraction, analysis reagents, and conditions used by each company are listed in Table 3.

All laboratories used a unique in situ analysis, that is, the extraction or "solubilization" of the sodium from the PA was done within the cassette assembly. Throughout the extraction and analysis procedure the cassette assemblies were sealed. Extracting solutions were added through the 4-mm inlet of the CFC. The inlet plug was then replaced and the cassette assemblies were shaken for a predetermined length of time. Solutions from the interior of the cassette were aspirated directly into the AES or AAS. The in situ method insured that all the PA present in the cassette was extracted including any dust that may have collected on the cassette walls. Furthermore, all extraction steps occurred within the cassette thus decreasing the chance of sodium contamination from external sources.

In the course of investigations several sources of trace levels of sodium sufficient to cause interferences were found. These sources included filters, support pads, the cassette interiors, and reagents. It was found that interferences were minimized by carefully washing the cassettes, filters, and support pads with sodium-free solutions. Also, all equipment and chemicals used during these operations were ultra-low in sodium to avoid sodium contamination, including gloves (if used), extracting solvents, and wash bottles.

Other modifications were necessary in order to perform the in situ, ultra-trace analysis of sodium. Some companies chose to pre-wet the PTFE filters with isopropanol during analysis to further guarantee the complete extraction of sodium from the filters. These companies found it necessary to replace the normal cellulose support pad with one made of pre-washed porous plastic. The companies that did not wet the PTFE filters with a non-aqueous solvent were able to use a cellulose support pad.

Table 3
Pretreatment and extraction conditions of participating companies

	Company A	Company B	Company C	Company D	Company E	Company F	Company G
Equipment							
Filter	2-μm Zefluor (Gelman)	2-μm Zefluor (Gelman)	2-μm PTFE (SKC)	2-μm Zefluor (Gelman)	2-μm Zefluor	5-μm PTFE (MSI)	2-μm Zefluor
Support pad	Porous plastic (SKC)	Cellulose	Cellulose	Porous plastic	Porous plastic	Porous plastic	Porous plastic
Pre-wash							
Solution (vol.)	0.5 ml ipa [a] + 9.5 ml 0.01% ISA [b]	Same as extraction solution (10 ml)	Same as extraction solution (10 ml)	ipa [a] (0.5 ml) + 0.2% KCl; fill cassette	ipa [a] (0.5 ml); fill with deionized water	Components washed, then assembled	ipa [a] (0.5 ml) + 10 ml 10% HNO_3
Procedure	Shake 1 h	Shake 2 h, deionized water rinse	Shake 1 h, deionized water rinse	Fill, let stand > 15 min, rinse 4× deionized water	Pull water through with vacuum; repeat 4× with deionized water	Filters; methanol/2% H_2SO_4/methanol cassettes; H_2O, 16 h at 75°C	Set 15 min, distilled, deionized water rinse
Drying	Vacuum oven 60–70°C 20–25 in.Hg	Dry open, upside down, covered overnight	Dry open, upside down on Kimwipes®	Pull air through use HEPA filter	Pull air through use HEPA filter	Dry 50°C oven (non-forced air)	Vacuum oven 50°C overnight
Extraction							
Pre-wet (vol.)	ipa [a] (0.5 ml)	No alcohol	No alcohol	ipa [a] (0.5 ml)	ipa [a] (0.5 ml)	ipa [a] (0.2 ml)	ipa [a] (0.5 ml)
Solution (vol.)	9.5 ml of 0.01% ISA [b]	3% HNO_3 + 0.1% K as KCl (10 ml)	2% H_2SO_4 + 0.1% KCl (10 ml)	0.2% KCl (4.5 ml)	0.5% HCl (4.5 ml)	2% H_2SO_4 + 0.1% CsCl (5 ml)	10% HNO_3 + 0.5% KNO_3
Procedure	Shake 1 h	Shake 1 h	Shake 1 h	Shake 1 h	Swirl every 15 min for 2 h	Shake 1 h	Shake 15 min
Analysis							
Method	AAS at 589 nm	AAS at 589 nm	AES at 589 nm	AAS at 589 nm	AAS at 589 nm	AAS at 589 nm	AAS thermal
Linear range (μg/ml)	0 to 1 μg/ml	0.005 to 0.05 (low), 0.01 to 0.30 (high)	0.004 to 0.06 (low) 0.01 to 0.15 (medium)	Up to 2.0 μg/ml	0–1 μg/ml	0.005 to 0.30 μg/ml	0 to 1 μg/ml
Notes				Quadratic fit of data			
	Integrate 5 s		Signal avg., 2 s	Signal avg., 3 s		Signal avg., 3 s	Avg. of five readings
	Avg. of three readings	Use avg. of ten readings	Use avg. of three readings	Use avg. of three readings	Use avg. of two readings	Use avg. of at least two readings	589.6 nm (1-nm band pass)
			Change to 820 nm for higher working range	Dilute sample for higher working range		Sequence, sample/standard/sample/standard	

[a] ipa = isopropanol.
[b] ISA = 0.4 M NH_4Cl + 0.4 M NH_4OH.

3.2. Collaborative study

Each company pre-cleaned, assembled, and shipped to ITRI sufficient numbers of CFCs for this study. ITRI split the CFCs into four groups to be used to collect control, low-level, mid-level, and high-level PA dust samples. The CFCs were then returned to the appropriate company for sodium analysis. The results for

each of the four groups are presented and discussed below.

Analysis of control group

Samples collected from the control chamber were believed to contain no PA dust and in most cases yielded extremely low, but measurable, levels of sodium. Sodium levels were converted to "equivalent PA dust weight" using Eq. 1 and the results are listed in Table 4.

Extracting reagents were used to "zero" the AAS or AES instrument before measurements were made; as a result, some negative numbers were obtained for the control samples. Each company analyzed six control samples, except Company G which had one broken cassette. The control levels, indicative of sodium contamination or background dust, cover a wide range with company averages from 0.038 to 0.913 μg of PA. This suggests that some participating companies had greater success than others in minimizing sodium in the filters, cassette assemblies, and reagents. The relative standard deviation for the control group was calculated to be 101% (using the average of averages). This is indicative of the variability in the analysis when working at ultra-trace sodium levels. It is also indicative of the difficulties of some of the participating laboratories in achieving ultra-low sodium blank levels. For example, the standard deviation of the control chamber results calculated for Companies E and G were significantly higher than those calculated for the other participating companies. Also, the control chamber averages calculated for Companies D, F, and G were more than double the values calculated for the other companies.

Limit of detection

The definition of the LOD used in this study was three times the standard deviation of the background [12]. In keeping with this definition LODs were calculated for each company using the control group data. The results are listed in Table 5. For each company two LODs are listed, one based upon sodium levels and the other calculated as the equivalent PA levels using Eq. 1. In two cases, Companies D and F, the company mean for the control group is higher than the LOD for that company. This is indicative of a relatively high but consistent sodium contamination and was probably due to trace levels of sodium present in the extracting solution or some other reagent. The seven-company average LOD can be calculated as 0.11 μg of Na or 0.68 μg of PA.

It is important to note that the LODs listed in this table were achieved in a non-industrial environment

Table 4
Equivalent PA dust results for the control group

	Equivalent PA dust weight (μg)						
	Company A	Company B	Company C	Company D	Company E	Company F	Company G [b]
1	0.000	0.38	0.127	0.761	−0.571	0.520	0.000
2	0.000	0.95	0.159	0.888	−0.425	0.520	0.190
3	0.063	0.139	0.178	0.951	−0.279	0.520	0.507
4	0.063	0.139	0.209	0.951	0.159	0.520	0.888
5	0.063	0.139	0.279	1.014	0.456	0.666	1.078
6	[1.205]	[2.029]	0.444	[1.720]	1.553	[0.888]	
Average	0.038	0.110	0.232	0.913	0.149	0.549	0.533
S.D.	0.035	0.045	0.116	0.096	0.787	0.065	0.454
Lab bias [a]	−0.292	−0.222	−0.095	0.581	−0.183	0.217	
Avg. of avgs. 0.332					Global mean 0.323		
S.D. of avgs. 0.336					Global S.D. 0.443		
R.S.D. 101%					R.S.D. 137%		

Q-Test outliers shown in brackets, e.g. [1.205].
[a] Lab bias = (company average − average of averages).
[b] Results for Company G not included in averages.

Table 5
Limits of detection (μg)

	Company						
	A	B	C	D	E	F	G
LOD as Na	0.018	0.021	0.054	0.045	0.372	0.030	0.220
LOD as PA [a]	0.11	0.13	0.34	0.29	2.36	0.19	1.37

[a] PA values calculated using Eq. 1.
Average PA LOD = 0.68 ($\pm$0.86), R.S.D. = 126%.

and may not be achievable during routine dust monitoring. Samples were taken in a well controlled dust chamber that contained no significant extraneous dust. In comparison, during routine monitoring the sampling cassettes (1) will have an increased chance of contamination during sampling and handling, (2) may collect non-PA sodium containing dust, and (3) may not receive the same level of attention that the samples received in this controlled study. Therefore, the LOD determined during routine dust monitoring in an industrial setting may be higher than those reported here.

Analyses of low-, mid-, and high-level sample groups

Low-level group

The target level of PA dust for the low-level group was 1 μg per cassette. The delivered PA dust level as listed in Table 2 was 0.54 μg. The PA results for the low-level group are shown in Table 6. These equivalent PA values were calculated from sodium analysis results using Eq. 2.

$$\text{PA}\ (\mu\text{g}) = 6.34 \times [\text{Na}_x - \text{C}(\text{Na}_x)] \qquad (2)$$

where Na_x represents each individual sodium result from company "x" and $\text{C}(\text{Na}_x)$ represents the average sodium results for the control samples analyzed by company "x".

The average of averages for the six companies was 0.52 ($\pm$0.19) μg of PA which is in reasonable agreement with the delivered PA dust level of 0.54 μg. The inter-company agreement was good with a relative standard deviation (R.S.D.) of 37%, especially considering the proximity to the LOD.

The low-level group results were compared to the control group results using a Student's *t* comparison of means approach on a company-by-company basis. For each company, the low-level group was found to be statistically different from the control group. This indicates that each company was able to detect PA on the low-level samples.

Mid-level group

The target level of PA dust for the mid-level group was 5 μg per cassette. The equivalent PA results for the mid-level group are shown in Table 7. These values were calculated from sodium analysis results using Eq. 2. The average of averages for the six companies was 2.05 ($\pm$0.29) μg of PA which is in reasonable agreement with the delivered PA dust level of 2.82 μg (see Table 2). The inter-company agreement was good with an R.S.D. of 14%.

High-level group

The target level of PA dust for the high-level group was 25 μg per cassette. The equivalent PA results for the high-level group are shown in Table 8. These values

Table 6
Equivalent PA dust results for low-level group

Company	Average sodium equivalent PA dust weight (μg)	Standard deviation (μg)	Lab bias [a] (μg)
A	0.40	0.08	−0.12
B	0.40	0.07	−0.12
C	0.29	0.04	−0.23
D	0.77	0.09	+0.26
E	0.72	2.11	+0.20
F	0.53	0.09	+0.01
G [b]	4.88	3.92	+4.36
Avg. of avgs. 0.52		Global mean 0.50	
S.D. of avgs. 0.19		Global S.D. 0.78	
R.S.D. 37%		R.S. D. 156%	

[a] Lab bias = (company average − average of averages).
[b] Results for Company G not included in averages.

Table 7
Equivalent PA dust results for mid-level group

Company	Average sodium equivalent PA dust weight (μg)	Standard deviation (μg)	Lab bias [a] (μg)
A	2.28	0.17	+0.23
B	1.95	0.15	−0.10
C	2.51	0.41	+0.46
D	1.92	0.26	−0.13
E	1.95	0.17	−0.10
F	1.69	0.31	−0.36
G [b]	5.36	2.37	+3.32
Avg. of avgs. 2.05		Global mean 2.11	
S.D. of avgs. 0.29		Global S.D. 0.38	
R.S.D. 14%		R.S.D. 18%	

[a] Lab bias = (company average − average of averages).
[b] Results for Company G not included in averages.

Table 8
Equivalent PA dust results for high-level group

Company	Average sodium equivalent PA dust weight (μg)	Standard deviation (μg)	Lab bias [a] (μg)
A	12.69	2.34	−1.43
B	12.41	1.08	−1.71
C	18.43	2.54	+4.31
D	14.99	1.64	+0.87
E	14.22	1.61	+0.10
F	11.98	0.80	−2.14
G [b]	18.28	2.43	+4.16
Avg. of avgs. 14.1		Global mean 14.6	
S.D. of avgs. 2.4		Global S.D. 3.0	
R.S.D. 17%		R.S.D. 21%	

[a] Lab bias = (company average − average of averages).
[b] Results for Company G not included in averages.

Table 9
Results summary: moisture corrected gravimetric versus in situ AAS or AES

Target level (μg)	Six-company average via in situ method (μg)	Corrected gravimetric results [a]	Ratio gravimetric results versus six-company average
0	0.00	0.00	NA
1	0.52	0.54	1.04
5	2.05	2.82	1.38
25	14.12	14.08	1.00

[a] See Table 2.

were calculated from sodium analysis results using Eq. 2. The average of averages for the six companies was 14.1 ($\pm$2.4) μg of PA, which is in excellent agreement with the delivered PA dust level of 14.1 μg (see Table 2). The inter-company agreement was good with an R.S.D. of 17%.

Comparison of gravimetric levels versus sodium equivalent PA levels

The second column of Table 9 contains the equivalent PA levels as determined by sodium analysis using in situ AAS or AES. The third column contains the PA levels determined by gravimetric analysis and corrected for a moisture content of 33%. The agreement between the two data sets is good. The ratios of gravimetric results to the six company average for the low-, mid-, and high-level groups were 1.04, 1.38, and 1.00, respectively.

3.3. Environmental sources of sodium

One problem commonly cited for methods that rely on sodium analysis is that sodium is ubiquitous and that any ultra-trace analysis would be seriously affected by environmental sodium. The methods described in this paper successfully addressed these concerns as follows:

1. Ultra-low sodium reagents were used.
2. Sampling cassettes were pre-cleaned with these reagents to reduce sodium content to ultra-low levels.
3. Analyses were performed in situ to avoid contact of reagents with extraneous sources of sodium.

The in situ analytical method was tested in a real manufacturing plant situation to evaluate the effect of environmental sodium. Table 10 contains the results for respirable dust samples collected at sites around a manufacturing plant that uses PA. For these measurements the CFCs were equipped with 9 LPM cyclones so that only dust of small particle size (approximately less than 5 μm) was collected. The first two lines of Table 10 contain the results for samples collected in areas free of PA dust and therefore are a measure of background and environmental sodium. The average sodium equivalent PA dust concentration for these samples was found to be 0.29 and 0.32 $\mu g/m^3$. These results suggest that, by using an in situ method, sodium interferences and environmental sources of sodium can be minimized so they are not a major source of error.

Table 10
Equivalent PA dust levels near PA sources

Location	Distance to PA source (ft)	Number of samples	Average sodium equivalent PA dust concentration ($\mu g/m^3$)	Standard deviation ($\mu g/m^3$)	Maximum ($\mu g/m^3$)	Minimum ($\mu g/m^3$)
Office	Remote	9	0.32	0.13	0.52	0.15
Roof of plant	Remote	12	0.29	0.14	0.49	0.06
Warehouse	1000	3	0.91	0.13	1.01	0.76
Plant floor	100	3	1.88	0.33	2.18	1.52
Plant floor	3	9	4.27	2.73	10.16	1.91

Samples were also taken in a warehouse 1000-ft distant from known PA sources but in locations where trace levels of airborne PA dust may be present. The average sodium equivalent PA dust concentration in these samples was 0.91 $\mu g/m^3$ which is three-fold higher than in PA free samples. This demonstrates the ability to measure low levels of PA dust above the environmental sodium background levels.

Samples were also collected close to a PA dust source and the results are also shown in Table 10. The average sodium equivalent PA dust concentration for samples collected 100 ft from a known PA dust source was 1.9 $\mu g/m^3$. The concentration for samples collected 3 ft from a known PA dust source was 4.3 $\mu g/m^3$ which is more than an order of magnitude higher than the sodium levels found for the environmental samples.

4. Conclusions

A seven-company collaborative study was successfully conducted which compared the results generated for the analysis of cross-linked polyacrylate absorbent dust. Each company received samples collected from a PA dust chamber using 37-mm polystyrene closed face cassettes. Each company also received samples collected from a control chamber to assess the background sodium content of materials and reagents.

The seven companies used similar, but not identical, analytical methods based on the ultra-trace analysis of sodium. In the course of developing trace sodium methods, participating companies independently identified cassettes, filters, support pads, and reagents as possible sources of sodium contamination from non-PA dust sources. Cassette clean-up procedures and a unique in situ analysis were developed and were shown to be effective in significantly reducing sodium contamination.

By paying strict attention to details in all aspects of cassette clean-up and sample analysis, participating companies were successful in lowering LODs. The six-company average LOD for this highly controlled study was 0.68 μg of PA. LODs determined during routine monitoring at manufacturing plants might typically be higher than those reported here if contamination from environmental sources of sodium is present.

PA dust loading determined gravimetrically and via sodium analysis were in good agreement when the gravimetric results were corrected for moisture content of the hygroscopic PA dust. The company-to-company agreement in this study is excellent considering the ultra-trace level sodium analyses used.

Air samples were collected at sites at varying distances from a manufacturing plant that used PA. Environmental sources of sodium were measured and found to be low enough to permit ultra-trace PA dust measurements without significant sodium interferences. Samples were taken inside a manufacturing plant and PA dust levels increased as the distance to the PA dust source decreased.

The analytical methods described in this report represent significant improvements in determining ultra-trace levels of PA dust. Individual companies now have optimized methods capable of measuring much lower levels of PA dust than previously available methods.

Acknowledgements

This work was sponsored by the Institute for Polyacrylate Absorbents (IPA). The authors gratefully acknowledge the other members of the IPA Analytical/Industrial Hygiene Task Force and the scientists at ITRI

for their assistance and guidance: Mark Anderson (Chemdal), Al Blanchette (Johnson and Johnson), Michael Dupuis and John Jurgiel (Dow Chemical), Mark Holcomb and Andy Wegner (Kimberly Clark), James Michels (Nalco Chemical Company), Mike Jayjock (Rohm and Haas), Van Fidino (Weyerhaeuser Company), Margaret Macomber (Procter and Gamble), Edward Barr and Yung-Sung Cheng (ITRI), Darryl Whitmore (Hoechst-Celenese Corporation) and Rick Opatick (IPA). In addition, the authors thank the following scientists for their assistance and efforts in conducting analytical work for this study; Herb Emmel and Ward Rigot (Dow Chemical), Roger Jutte (Nalco Chemical), Lee Chambers and Stephanie Wauligman (Procter and Gamble), Rudy Del Gavio (Johnson and Johnson).

References

[1] T.S. Turan, Round Robin Study of Analytical Methods for Polyacrylate Absorbent (PA) Dust, Institute for Polyacrylate Absorbents Report, Washington, DC, 1989.

[2] J.D. Wendlick, Sampling for Polyacrylate Absorbent (PA) Dust in Air at Low Concentrations, Institute for Polyacrylate Absorbents Report, Washington, DC, 1990.

[3] S.S. Cutiè, R.M. Van Effen, D.L. Rick and B.J. Duchane, Anal. Chim. Acta, 260 (1992) 13.

[4] S.S. Cutiè, W.C. Buzanowski and J.A. Berdasco, J. Chromatogr., 513 (1990) 93.

[5] S.P. Tucker, presented at the American Industrial Hygiene Conference, Salt Lake City, UT, May 1991; S.P. Tucker, M.B. Millson and D.D. Dollberg, Anal. Lett., 26 (1993) 965.

[6] D. Whitmore, Hoechst-Celenese Corporation, 1992, personal communication.

[7] T.S. Turan, Procter and Gamble, S.S. Cutiè, Dow Chemical and A.R. Blanchette, Johnson and Johnson, 1991, personal communication.

[8] M.A. Puskar, J.M. Harkins, J.D. Moomey and L.H. Hecker, Am. Ind. Hyg. Assoc. J., 52 (1991) 280.

[9] J.K. Briant and O.R. Moss, Am. Ind. Hyg. Assoc. J., 45 (1984) 440.

[10] S. Turner and B.S. Cohen, Am. Ind. Hyg. Assoc. J., 45 (1984) 745.

[11] D.A. Skoog and D.M. West, Fundamentals of Analytical Chemistry, Holt, Rinehart and Winston, New York, 3rd ed.

[12] ACS Committee on Environmental Improvement, Anal. Chem., 55 (1983) 2210.

ELSEVIER

Analytica Chimica Acta 298 (1994) 363–374

ANALYTICA CHIMICA ACTA

The adaptation of the dichromate digestion method for total mercury determination by cold-vapor atomic absorption spectrometry to the analysis of soils, sediments and sludges

Silvio Landi *, Francesco Fagioli

University of Ferrara, Department of Chemistry, Via Borsari, 46, 44100 Ferrara, Italy

Received 4 January 1994; revised manuscript received 24 June 1994

Abstract

Previous research demonstrated the overall validity of a two-component wet digestion procedure based on the action of $K_2Cr_2O_7 + H_2SO_4$ (50%, v/v) at boiling temperature (180°C) with vapors refluxing in an air condenser in the treatment of biological samples to be analyzed for total mercury by cold-vapor atomic absorption spectrometry (CVAAS). This study explored the ability of this procedure to cope with soils, sediments and sewage sludges. After demonstrating that cinnabar (HgS) is completely dissolved under the experimental conditions employed, a set of nine standard reference materials having a mercury content ranging from 0.0568 to 9.49 $\mu g\ g^{-1}$ was analyzed. One difficulty was posed by chloride containing samples and was due to the formation of chlorine, a strong inhibitor of the spectrometric signal. Evidence is given that this effect is ascribable to the re-oxidation of elemental mercury by the chlorine present inside the reduction–aeration system. The elimination of chlorine by simply running the digestion without a condenser proved effective in some cases. However, when the samples had a high content of organic matter or carbonates the absence of the condenser caused mercury losses. A study employing mercuric nitrate and methylmercury chloride showed that the escape of mercury from the digestion tube not surmounted by the condenser is related to the rapid release of CO_2 when organic matter and carbonates react with the digestion mixture at its boiling point; high temperature alone is not sufficient for mercury to be lost. Therefore, the digestion procedure was duly reconsidered and split in two parts: (a) an initial 60 min period with the condenser in place during which the destruction of all organic matter and carbonates takes place followed by (b) a 30 min span without condenser to allow chlorine and other potential interfering vapors and gases to leave the digest. The modified procedure was applied to the same reference materials as above and additionally to a biological standard of mussel tissue. The analytical results showed that total mercury could be determined in all samples with consistently good precision and accuracy (R.S.D.% range = 1.2 − 4.5; error %range = −3.8 to +8.7).

Keywords: Atomic absorption spectrometry; Total mercury determination; Cold-vapor atomic absorption spectrometry; Environmental analysis; Solid wastes

1. Introduction

Mercury is a toxic element sparsely distributed in the lithosphere, its average concentrations having been indicated to be 0.08 and 0.4 mg kg^{-1} (ppm) in igneous and sedimentary rocks respectively [1]. Since soils and sediments have as their main constituents the particles derived from the mechanical and chemical weathering of rocks they also would be low in mercury if left undisturbed by civilization. Natural soils, in fact, have

* Corresponding author.

SSDI 0003-2670(94)00286-X

Table 1
Layout of digestion procedures validated by scientific organizations and government agencies for the determination of total mercury by CVAAS in a variety of matrices

Proponent organization	Sample type	Glassware; reagents; working conditions
American Society of Agronomy (ASA) [9]	Soils/sediments	Open vessel [a]. $H_2SO_4 + HNO_3 + HCl$ (10 + 5 + 2); at 55°C for 2–3 h; + $KMnO_4 + K_2S_2O_8$; at 25°C for 12 h
Inland Waters Directorate, Ottawa [10]	Sediments	Same as above
U.S. EPA [11A]	Soils/sediments/sludges	Open vessel [a]. $HNO_3 + HCl$ (1 + 3); at 95°C for 2 min; + $KMnO_4$; at 95°C for 30 min
U.S. EPA [11B]	Mainly sludges	Open vessel [a]. $H_2SO_4 + HNO_3$ (2.5 + 1) + $KMnO_4$ + $K_2S_2O_8$; at 95°C for 2 h
Association of Official Analytical Chemists (AOAC) [12A]	Food in general	Modified Liebig (water) condenser. $H_2SO_4 + HNO_3$ + $HClO_4 + Na_2MoO_4$; boil for 1 h
AOAC [12B]	Fish	Modified Liebig condenser. $H_2SO_4 + HNO_3$ (1 + 1); + V_2O_5; boil for 16 min; + H_2O_2

[a] No condenser in use.

been found to contain mercury in the range 0.01–0.5 ppm [2]. Anthropogenic activities continuously worsen this picture by dispersing a variety of mercury-containing wastes into the environment [3]. Because soils and sediments are the principal sinks of most of these discharges [3,4], they appear good indicators of the extent of environmental contamination and its trend [4].

Among the array of refuses produced by man on a very large scale, sewage sludge certainly requires a strict analytical monitoring of the levels of mercury, likely to be present at exceptionally high concentrations. For instance, a study on 53 American sludge treatment stations reports mercury concentrations ranging between 1 and 10,600 ppm (dry-weight basis) [5]. Given the usual destinations of this by-product, i.e. dumping at sea or in land or application as organic amendment to agricultural soils, its long-term disposal concurs to posing mercury-related toxicity problems to man via aquatic [6] and terrestrial [3] nutritional chains. Clearly the control of life quality with respect to mercury pollution entails its determination in a wide spectrum of wastes and environmental systems.

Instrumentally, the cold-vapor atomic absorption spectrometric technique (CVAAS) has gained generalized acceptance for routine mercury determination. Conversely, little agreement has been reached on the issue of the chemical pretreatment of the sample, that is its acid–oxidant digestion necessary to bring all inorganic and organic forms of mercury in solution as Hg^{2+}, whose subsequent reduction to Hg^0 makes the spectrometric determination possible. Two digestion techniques [7,8] have been screened among the many proposed, to become the basis of procedures officially accepted by prominent scientific associations [9] and state agencies [10,11] for dealing with environmental and sludge samples. These official methods have been summarized in Table 1 together with those approved by AOAC [12] for biological (food) materials. From the breadth of prescriptions offered to operators, with differences concerning so many practical as well as chemical aspects it would appear to be reasonable trying to develop one simple procedure capable to tackle widely different matrices with uniformly good precision and accuracy. Pursuing this idea, we resumed a digestion method which this laboratory had satisfactorily used in the analysis of vegetal [13] and animal [14] tissues for total mercury, and tested it unaltered on a number of standard reference samples of soils, sediments and sludges. Briefly, this wet-ashing procedure, hereafter denominated ODP (old digestion procedure), found its action on the oxidizing properties of $K_2Cr_2O_7$ in diluted (1 + 1) H_2SO_4 in contact with the sample for 60 min at boiling temperature (180°C) with vapors refluxed with the aid of an air condenser. Encouragement for the outlined investigation came from the preliminary tests that proved that the ODP procedure totally recovered Hg from cinnabar, a compound whose presence in geological samples [15] causes concern in the determination of mercury for its resistance to solubilization [8,16,17]. This study continued with the analysis of a range of soils, sediments

and sewage sludges with officially certified mercury content. The ODP procedure was found unsuccessful in the analysis of three sediments, when the analyte signal was suppressed to a serious extent. Chlorine derived from the oxidation of chlorides by dichromate was identified as the interferent. In this paper the mechanism of the depressive effect of chlorine on the mercury signal is clarified. A simple operation is proposed for the effective elimination of the interference without resort to chemical agents. This has been incorporated into the digestion scheme and the modified procedure (NDP) has been tested by the use of the standard reference materials previously employed and also of an additional one consisting in an all-organic biological matrix.

2. Experimental

2.1. Apparatus [14]

A 100-ml calibrated borosilicate glass tube was used as the digestion vessel, to be connected when required to an air condenser made of a simple glass tube. The condenser had in its lowest part a female side neck for the introduction of the acid by means of a separatory funnel. A magnetic stirrer was used whenever the mixing of the reacting mass was necessary. The digestions were carried out in a block digestor. Hg determinations were performed on a Perkin-Elmer Model 603 atomic absorption spectrometer mounting a Hg electrodeless discharge lamp (EDL) and equipped with a D_2 background corrector. The absorption wavelength was set at 253.7 nm (resonance line) and the spectral bandwidth at 0.7 nm. The experimental set-up was completed with a Perkin-Elmer Model 303-0832 apparatus for the recirculation of Hg vapors.

2.2. Reagents and standards

All reagents were of analytical grade. A special treatment was applied to $K_2Cr_2O_7$ to render it virtually mercury-free: the salt was heated at 350°C for 4 days, then the temperature was raised to 410°C and the mass kept melted for 24 h; the solidified salt was homogenized by ball-milling. The reducing agent $SnCl_2$ $2H_2O$ was dissolved in 10% (v/v) H_2SO_4 to give a 25% (m/m) solution; the solution was bubbled with N_2 for 20 min to strip away any residual Hg and O_2. A diluting solution containing 1.2% (w/v) $K_2Cr_2O_7$ in 20% (v/v) H_2SO_4 was prepared; this solution contains the same amounts of oxidant and acid as those employed for the digestion and was used to construct the calibration curve and to dilute digests when necessary as explained below. Ultrapure water obtained from a Millipore Model Milli-Q2 purification system was used throughout.

The following standard reference materials were utilized: National Institute of Standards and Technology (NIST) Standard Reference material (SRM) 2704 Buffalo River Sediment and SRM 1646 Estuarine Sediment; National Research Council of Canada BCSS-1 Estuarine Sediment and PACS-1 Harbour Sediment; European Community Bureau of Reference BCR 141 Calcareous Loam Soil, BCR 142 Light Sandy Soil, BCR 143 Sewage Sludge Amended Soil, BCR 144 Sewage Sludge of Domestic Origin, BCR 146 Sewage Sludge of Mainly Industrial Origin, CRM 278 Mussel Tissue. The sample intake was always equal or higher than the minimum amount recommended by the instructions given in the certificate of analysis; instructions were also followed for the determination of the moisture content of the materials, whose knowledge is necessary to adjust results to a dry-weight basis.

2.3. Analytical procedure

0.5–2 g soil (sediment) or 0.1 g sewage sludge was placed in a digestion tube having a magnetic bar resting at its bottom. 1.2 g $K_2Cr_2O_7$ and 20 ml H_2O were added, the condenser was connected and the separatory funnel set in place with 20 ml H_2SO_4 in it. This assembly was placed on the magnetic stirrer, stirring was started and all acid run dropwise into the tube (the slow addition of the acid has a two-fold aim: to avoid froth rising high in the tube when treating carbonate- and/or organic-rich samples and to disperse the heat which might cause the organic matter to char, thus favouring the loss of mercury by reduction to Hg^0. [18] The funnel was removed, the lateral opening on the condenser closed with a stopper and the assembly transferred to the hot-block preheated at 180°C. The digestion was allowed to proceed for 60 min to completion, the subsequent operations being necessary just to expel gases and vapors capable of causing interference during the spectrometric determination. The

assembly was extracted from the block and kept 5 min at room temperature to be slightly cooled. The condenser was removed, rinsed with three 5 ml portions of H_2O and washings added to the digest. The mass was briefly mixed to prevent subsequent bumping and the open tube (no condenser on it) replaced in the block for a further 30 min boiling span. Dilution to about 90 ml, mixing and cooling, extraction and washing of the stirring bar were the last manipulations before bringing the digest to the 100 ml mark (the error of dilution due to the presence of a solid residue can be overlooked if the indicated sample sizes are processed).

Mercury analyses by CVAAS were performed in the recirculation mode employing the same reduction vessel, briefly washed with H_2O between subsequent analyses. The premature reduction of Hg by residual stannous chloride adhering to the glass walls of the apparatus is prevented by the excess of oxidant in the digest. The usual amount of digest analyzed was 25 ml (1/4 of the diluted final digest) but whenever the linearity range was exceeded, a smaller volume of digest was taken and made up to 25 ml by way of the diluting solution. 3 ml of the stannous chloride solution as reductant were constantly used; this quantity was enough to bring about the reduction of the mercuric ions after that of the dichromate present in the standards and the analyses (≤ 0.3 g).

2.4. Calibration curve and detection limit

The appropriate volumes of the Hg working standard solution were added to 25 ml of the diluting solution and the resulting standards were analyzed to work out the calibration function. A typical 5 point (blank included) calibration function took the form $\text{Abs} = (1.2 \pm 0.09)m$ (μg) with $s_{y/x}\% = 2.1$ and $r = 0.9994$. Linearity was verified in the concentration range of 0.004–0.2 μg Hg. The detection limit of 0.004 μg Hg/sample weight was calculated from the blank signals ($n = 15$) according to UPAC ($k = 3$) [19]. The method of standard additions for the determination of Hg concentration in samples was found unnecessary.

3. Results and discussion

3.1. Solubilization of cinnabar (HgS) by the ODP procedure

Mercuric sulfide may enter the composition of soils and sediments as a primary mineral owing to its geochemical association with many other metals in hydrothermal sulfide ores [20]. HgS can also originate in mercury containing media under anaerobic conditions, consequence of biochemical reduction of higher (0–VI) valence state sulfur compounds to hydrogen sulfide. [21] With a water solubility as low as 1.1×10^{-16} μg l^{-1}, its presence in the environment would not appear to pose a health danger. However, microorganisms have been shown to mobilize HgS using it as substrate for the production of the much more soluble $HgSO_4$ [22] and CH_3Hg^+ [22,23] thus making the determination of HgS meaningful. HgS solubilization for CVAAS determination can be successfully accomplished with HNO_3–HCl (1+3) [8], H_2SO_4–$K_2S_2O_8$ [17], H_2SO_4–HNO_3 (3+2) [17], H_2SO_4–HNO_3–HCl (10+5+2) [16] with speed depending on temperature [17]. The assessment of the efficacy of the H_2SO_4–$K_2Cr_2O_7$ mixture in the decomposition of cinnabar under the conditions here proposed was introductory to the analysis of samples. The purity of the commercially available cinnabar was controlled (and found to be 99.26%) by dissolving it in aqua regia at 90°C on a water-bath and EDTA titrating the resulting solution according to Flaschka [24]. The standardized HgS was digested at two different weight levels. Data in Table 2 indicate that the digestion mixture reacts with HgS, dissolving it completely and that Hg losses are nil.

Table 2
Determination of mercury from HgS (cinnabar) at two weight levels by ODP procedure [a]

Hg present [b] (μg)	Hg found (μg)	Recovery (%)
59.3	59.4	100
113.0	114.1	101
97.6	98.4	101
8.4	7.9	94
5.1	4.7	92
10.7	11.7	109

[a] The amount of $K_2Cr_2O_7$ used in all analyses was 1.2 g.
[b] Calculated from the HgS purity determined as described in the text. HgS was weighed on a Sartorius Model 4504 MP8 balance with a readability to 1×10^{-7} g.

3.2. Determination of Hg in Standard Reference Materials by the ODP procedure

The first approach to the treatment of actual samples was to extend the ODP procedure without substantial

Table 3
Determination of mercury in soil, sediment and sewage sludge Standard Reference Materials by the ODP procedure [a]

Sample	Sample weight [b] (g)	Hg present (certified) ($\mu g\ g^{-1}$)	Confidence limits (95%) (certified) ($\mu g\ g^{-1}$)	Hg found ± S.D. ($n=4$) ($\mu g\ g^{-1}$)	R.S.D. (%)	e [c] (%)
Soils						
BCR 141 Calcareous Loam Soil	2	0.0568	0.0525–0.0611	0.0577 ± 0.0015	2.6	+1.6
BCR 142 Light Sandy Soil	2	0.104	0.0917–0.1163	0.1026 ± 0.0020	2.0	−1.3
BCR 143 Sewage Sludge Amended Soil	0.5	3.92	3.69–4.15	3.92 ± 0.082	2.1	0
Sediments						
SRM 1646 Estuarine Sediment	2	0.063	0.051–0.075	~0	–	~ −100
SRM 2704 Buffalo River Sediment	0.25	1.44	1.37–1.51	1.57 ± 0.022	1.4	+9.0
BCSS-1 Coastal Marine Sediment	2	0.129	0.117–0.141	0.108 ± 0.0059	5.5	−16.3
PACS-1 Harbor Marine Sediment	0.5	4.57	4.41–4.73	2.55 ± 0.939	36.8	−44.2
Sludges						
BCR 144 Sewage Sludge (Domestic)	0.1	1.49	1.27–1.71	1.52 ± 0.024	1.6	+2.0
BCR 146 Sewage Sludge (Mainly Industrial)	0.1	9.49	8.73–10.25	9.62 ± 0.32	3.3	+1.4

[a] The amount of $K_2Cr_2O_7$ used in all analyses was 1.2 g.
[b] These quantities have been the same throughout this study.
[c] The error (e), % was calculated as $100(Hg_{found} - Hg_{present})/Hg_{present}$.

modifications to the analysis of soils, sediments and sludges. Being in search of a method of extensive applicability, the reference materials to be examined were selected within each sample category, so as to cover the widest possible range of sample origins and mercury concentrations. Table 3 presents the data obtained for the nine matrices. While an amply acceptable analytical picture was obtained in the case of soils, sludges and the river sediment (R.S.D. (%), 1.4–3.3; e%, −1.3 to +9.0), the three sediments from marine environments SRM 1646, BCSS-1 and PACS-1, are conspicuous for the severe hindrance produced on the Hg signal. A most prominent feature of these last samples is their richness in chlorides, the Cl^- content being 1.68, 1.12, 2.39% (w/w) respectively. Cl_2 is produced by the action of dichromate on chlorides under the given experimental conditions. In the ODP procedure the reflux condenser rests on the digestion tube until the end of the operation; consequently, a (variable) portion of the formed Cl_2 is kept trapped inside the apparatus and washings partly return it into the digest, adding to that already present. When N_2 was blown through the digest, until an *o*-toluidine impregnated paper at the tube's mouth did not reveal Cl_2 any more, the digests could be analyzed satisfactorily. The above observations led to suspect Cl_2 to be responsible for the interference observed and its influence on the spectrometric signal was specifically investigated.

3.3. Interferences by chlorine

The formation of chlorine from chloride containing samples has been previously observed when $KMnO_4$ and $K_2S_2O_8$ were employed for the sample digestion preceding the CVAAS determination of mercury [25,26]. In these occasions chlorine was found to absorb at the same wavelength as mercury (273.7 nm) [10,11,25,26] and consequently was indicated as being an interferent which produces an enhancement of the analyte signal. We aimed to demonstrate that the

Table 4
Interferences of chlorine in the determination of mercury

Type of interference	Type of test [a]	Chlorine concentration in test solutions [b] (mg 100 ml^{-1})	Absorbance D_2 lamp OFF	Absorbance D_2 lamp ON	Relative absorbance, % of absorbance with no interference
Spectral	(Cl)	97	0.004	0	
		153	0.010	0	
Non Spectral	(Cl + Hg) [c]	0.125			100
		0.25			80
		0.5			62
		1			50
		5			18
Non Spectral	(Cl/Hg) [c]	0.125			92
		0.25			84
		0.5			73
		1			64
		5			24

[a] (Cl) = only chlorine present in the solution; (Cl + Hg) = chlorine and Hg^{2+} (as nitrate) present in the test solution; (Cl/Hg) = air was first recirculated across the Cl_2 solution and a pure Hg^{2+} (as nitrate) standard solution was subsequently analyzed (see text).
[b] Amounts (mg) of chlorine in the analysis were 1/4 of the figures given in the column.
[c] Tests were performed on 0.1 μg Hg.

involvement of chlorine in the determination of mercury has in fact two aspects since chlorine is responsible not only for the spectral interference already evidentiated but also for the suppression of the mercury response to such an extent to account for our analytical results.

To adopt realistic conditions for the interference studies the amount of Cl_2 dissolved in the digests at the end of the digestion step was determined. N_2 was blown through the diluted digests to transfer Cl_2 into a NaOH solution which was titrated iodometrically. It could be seen that Cl_2 left in the digests was usually lower than 5 mg; in particular for SRM 1646, four replicate digests exhibited residual Cl_2 in the range 1.3–2.3 mg.

Interference tests were carried out employing 25 ml of Cl_2 water solution of appropriate concentration pipetted into the reduction–recirculation apparatus for the spectrometric measurements. Operationally these tests were conducted in three different ways: (i) by starting the recirculation pump air was bubbled through a Cl_2 solution and the resulting signal was registered. These runs, hereafter dubbed (Cl), allowed to quantify the spectral interference due to the gaseous chlorine stripped from the solution by the air stream; (ii) a Cl_2 solution was spiked with Hg^{2+} and analyzed in the usual way by the addition of the reductant. These runs have been dubbed (Cl + Hg); (iii) a Cl_2 solution was processed as in (i) for a few seconds, discarded and substituted with a Hg^{2+} standard solution which was analyzed. These runs have been dubbed (Cl/Hg). Results are summarized in Table 4.

Data from (Cl) tests indicate that Cl_2 indeed absorbs at the 273.7 nm wavelength but the signal becomes just barely appreciable at a Cl_2 concentration of about 100 mg 100 ml^{-1}, more than 20 times the value characterizing our digests. Therefore, the spectral interference from Cl_2 can in no way be a problem in the Hg determinations, more so because it can be fully corrected by the simple use of the deuterium (D_2) lamp (Table 4).

Both the (Cl + Hg) and (Cl/Hg) tests showed that Cl_2 did cause a drastic suppression of the Hg response and it can be calculated that a Cl_2 concentration of 1 mg 100 ml^{-1} reduces the Hg signal by an amount equivalent to 0.04–0.05 μg of Hg. This allows to quantitatively justify the null recovery of mercury reported in Table 3 in relation to the SRM 1646 digests, for the Cl_2 concentration in these digests was in fact in the order of 1 mg 100 ml^{-1} while the amount of mercury in the analyses was equal to 0.0315 μg.

The (Cl/Hg) tests give evidence that the Cl_2–Hg interaction takes place inside the liquid-free part of the recirculation loop, hence that chlorine action is exerted upon elemental mercury. A likely mechanism for the interference can consequently be envisaged, which

involves the oxidation of Hg^0 back to Hg^{2+} by the Cl_2 stripped by the air from the digest into the recirculation loop. From the observation that following any (Cl/Hg) test the mercury signal could be restored up to its uninterfered value only by air-purging the opened loop for several minutes (data not shown), it can be inferred that the oxidation of Hg is brought about, at least partially, by Cl_2 adsorbed upon the loop walls.

Bromine [27] and iodine [27,28] formed in the course of acid digestions of bromide and iodine containing samples with final $KMnO_4$ oxidation have been previously found to depress most severely the absorbance of mercury. While the authors did not further dwell on the issue, in the light of the present findings we are inclined to suspect these two halogens as being able to act on Hg^0 in the same way as chlorine.

3.4. Open-tube digestion

The spectral interference by Cl_2 in the course of the CVAAS determination of mercury is routinely dealt with by reducing this gas selectively with hydroxylamine before the mercury vapor is produced [10,11]. Of course, this measure would also effectively eliminate the second kind of interference mentioned above. However, because additional reagents are a complication and often a source of mercury contamination, as indicated in the very case of hydroxylamine, [29] we preferred to solve the entire Cl_2 problem physically by simply expelling it out of the digest.

As already pointed out, the removal of Cl_2 from the digest by bubbling N_2 through it leads to a correct determination. However, this is not a practical expedient when several digests are to be processed simultaneously and a different solution was needed. Currently, Hg determination is considered to be difficult because many mercury compounds are highly volatile and likely to be lost during the digestion. For this reason digestion is run in an open vessel, i.e. not equipped with a reflux condenser, only when it is conducted at low temperature ($\leqslant 100°C$); in the case high temperatures are preferred to speed up the process, the use of an efficient condenser is the rule (Table 1). Nonetheless a few authors reported good results when treating biological [30–32] and environmental samples [30,33] in open vessels at 140–180°C. If this were true, the open-vessel digestion would be a simple solution for eliminating Cl_2 and other volatile interfering compounds (e.g., bromine, iodine, aromatic hydrocarbons [3]) without suffering mercury losses. To check this possibility the three marine sediments were digested in the usual way except in that the condenser was omitted. The open-tube approach seemed to be the right solution since it had got rid of chlorine without losing mercury, as testified by the good R.S.D.% and *e*% values (Table 5). Once the artifice was extended to the remaining six standard materials, a mixed response was obtained (Table 6). In three cases, BCR 141–144–146, for which the ODP method had worked fine (Table 3), the absence of the condenser led now to above-normal R.S.D.s and to low mercury recoveries. These facts might have been explained by a prevalence in these samples of mercury species of particularly high volatility (e.g., dimethylmercury), unable to condense within the digestion tube. Instead, we favoured the view that the comparatively high contents of carbonates in BCR 141 (a calcareous soil) and of organic matter in BCR 144 and 146 (Tables 5 and 6) were involved. The idea of mercury losses being related to an abundant/rapid CO_2 evolution at high temperature, with mercuric vapors being dragged out of the tube, had to be substantiated.

3.5. CO_2 production and Hg losses

The two mercury(II) compounds of different volatility, $Hg(NO_3)_2$ and the much more volatile CH_3HgCl,

Table 5
Determination of mercury in marine environment sediment Standard Reference Materials by the open-tube digestion [a]

Material	C_{org} (%)	Hg found ± S.D.(n), $\mu g\ g^{-1}$	R.S.D. (%)	e [b] (%)
SRM 1646	2.33	0.064 ± 0.0020(6)	3.2	+1.6
BCSS-1	2.47	0.146 ± 0.0066(11)	4.5	+13.2
PACS-1	5.24	4.55 ± 0.14(6)	3.1	−0.4

[a] The amount of $K_2Cr_2O_7$ used in all analyses was 1.2 g.
[b] The error (e), % was calculated as $100(Hg_{found} - Hg_{present})/Hg_{present}$.

Table 6
Determination of mercury in soil, river sediment and sewage sludge Standard Reference Materials by the open-tube digestion [a]

Material	C_{org} (%)	Hg found ± S.D. (n), $\mu g\ g^{-1}$	R.S.D. (%)	e [b] (%)
Soil				
BCR 141	2.21	0.0484 ± 0.011(6)	22.1	−14.8
BCR 142	1.99	0.102 ± 0.0049(6)	4.8	−1.9
BCR 143	9.58	3.9 ± 0.10(6)	2.6	0
Sediment				
SRM 2704	4.16	1.50 ± 0.028(10)	1.9	+4.2
Sludges				
BCR 144	37.37	1.36 ± 0.14(9)	10.2	−8.7
BCR 146	21.00	8.9 ± 0.69(9)	7.7	−5.5

[a] The amount of $K_2Cr_2O_7$ used in all analyses was 1.2 g.
[b] The error (e), % was calculated as $100(Hg_{found} - Hg_{present})/Hg_{present}$.

were digested in the open-tube mode, alone and as spikes of $CaCO_3$ or egg powder in their quality of CO_2 producers. When $CaCO_3$ was used, it was observed that not all of it reacted during the initial addition of the acid (maybe because of the formation of a sulfate film on the surface of the particles) so that CO_2 evolution continued energically during the subsequent heating. From the results given in Table 7 the fact stands out that the boiling of the digest in an open tube is a perfectly harmless operation, neither mercury compounds can be said to have been lost in detectable amounts, provided CO_2 does not evolve. However, when a rapid disengagement of CO_2 takes place, relevant losses of both inorganic and organic mercury ensue; and it may marginally be observed that the speed and not the abundance of the CO_2 emission is the factor to be blamed for these losses, because the digestion of the $Hg(NO_3)_2 + CaCO_3$ mixture at low temperature (100°C) gave a full Hg recovery (Table 7). For all that precedes it is evident that in a high-temperature digestion method of general applicability as that we aimed at, the condenser is an essential part of the apparatus and must be kept in place until the matrix decomposition is over. Thereafter the condenser can be safely taken away and boiling continued until all undesirable gases and vapors are dispersed into the atmosphere. This sequence is the very element characterizing the present method hereafter called NDP (new digestion procedure).

Table 7
Recovery of mercury in open-tube digestion [a] of $Hg(NO_3)_2$ and CH_3HgCl pure and in Admixture with $CaCO_3$ (0.5 g) and egg powder (0.4 g) [b]

Test solution composition [c]	Mean recovery (n), %
$Hg(NO_3)_2$	98.2(8)
CH_3HgCl	98.8(8)
$Hg(NO_3)_2 + CaCO_3$	48.9(4)
$CH_3HgCl + CaCO_3$	48.4(4)
$Hg(NO_3)_2 + CaCO_3$ [d]	100.9(4)
$Hg(NO_3)_2$ + egg powder	88.7(4)
CH_3HgCl + egg powder	66.5(4)

[a] The amount of $K_2Cr_2O_7$ used in all analyses was 1.2 g.
[b] Egg powder is a matrix devoid of Hg (see Ref. 14).
[c] Hg present in total digest = 0.2 g.
[d] Digestion was run at 100°C for 60 min.

3.6. The NDP procedure – Amount of $K_2Cr_2O_7$ and sample size

Mercuric ions are quite easily reduced to elemental mercury during digestion and lost to the atmosphere, a most serious difficulty in mercury analysis which has long been appreciated [34]. Losses of mercury have been frequently observed even from solutions of mercuric salts in distilled water at ppb levels [35–37] and invariably ascribed to the reducing properties of uncheckable traces of organic impurities. Quite properly this difficulty has been stressed [30,37] when low-mercury, high organic-carbon matrices are to be dealt with for mercury determination. To overcome this hurdle very strong oxidizing conditions must be adopted and maintained throughout and after the digestion. The NDP procedure satisfies these requirements by employing $K_2Cr_2O_7$ in (slight) excess with respect to the quan-

tity needed for the complete oxidation of the sample. The amount of dichromate to be used is then a function of sample size and its organic matter content, a widely variable factor in soils, sediments and sludges. It might consequently appear difficult to find the correct analytical conditions without avoiding several trials. However, some considerations may help to overcome the uncertainty and to fix parameters valid in most cases. With the exclusion of histosols, the majority of soils contains $\leqslant 10\%$ (w/w) of organic matter (OM) [38] and this, with a rougher approximation, can be held true for most sediments as well [39]. Assuming, as it is currently done for soils [40], that OM contains at most 58% organic carbon (C_{org}) and that C_{org} has an average oxidation state of zero and an equivalent weight of 3 g, it can be calculated conservatively that 1 g of air-dried soil (sediment) at 10% OM would reduce 0.95 g $K_2Cr_2O_7$. Consequently, the analysis of 1 g of sample under the prescribed conditions (1.2 g $K_2Cr_2O_7$ used) would mean a 0.2 g surplus of dichromate, enough in our experience to deal with accessory reductants (e.g., Cl^-, Fe^{2+}, Mn oxides) and still leaves 0.05–0.1 g of oxidant unreacted. As for sewage sludges, much richer in OM, their C_{org} content may be deemed not to exceed 50% (w/w, dry-weight basis) [5,30]. If a sample size of 0.1 g (dry) sludge were taken as suggested here, the calculation shows that at least 0.4 g of dichromate would be present at the end of the digestion; and 0.1 g of sludge should not be considered too small an amount to be analyzed for Hg but, indeed, amply sufficient, as it becomes evident from the simple comparison of the detection limit of the analysis (0.004 μg Hg/sample weight) with the Hg levels of these materials, likely exceeding 1 $\mu g\ g^{-1}$ (dry) even if originated from the treatment of waste waters from uncontaminated rural areas [41]. Nevertheless, cases may be encountered when the prescribed amount of $K_2Cr_2O_7$ is all consumed. This situation is easily detected by the analyst simply noting the absence of the distinctive yellow shade that even a quantity of $K_2Cr_2O_7$ as small as 0.05 g imparts to the diluted digest. If doubt persists, a few drops of the digest may be retrieved from the tube and treated with a 0.1% *N*-phenylanthranilic acid solution in 0.1% Na_2CO_3 and the presence of $K_2Cr_2O_7$ revealed by the development of a red-violet coloration. If dichromate is absent, the analyst may decide, on Hg detection grounds, to repeat the analysis increasing the dichromate instead of lowering the sample weight. In this case he must, of course, accordingly augment the quantity of $K_2Cr_2O_7$ in the diluting solution. This poses a problem in the construction of the calibration curve and when digests too concentrated in the analyte have to be diluted with the diluting solution: the previously mentioned 3 ml of the 25% (w/w) stannous chloride solution would be insufficient to completely reduce the new amount of dichromate and consequently the mercuric ions too. According to the quantitative increase of $K_2Cr_2O_7$, two ways out are at hand. A moderate increase, up to 1.6 g in all, can be compensated by the use of 3 ml of a 30% (w/w) stannous chloride solution with no fear of modifying the slope of the calibration line (in fact, at constant air recirculation flow-rate, sensitivity depends on the volume of the solution from which the mercury vapors disengage [14] and on the heat which develops when the dichromate is reduced and make the temperature of the solution rise). For quantities of dichromate larger than 1.6 g, the diluting solution should instead be prepared by partial reduction of dichromate by way of a suitable organic substance as described in the previous paper [14].

3.7. *The NDP procedure – Analytical results*

Before being applied to the materials under consideration, the NDP procedure was tested to evaluate if the good performance of its ODP predecessor in digesting all-organic, biological samples was retained. The CRM 273 Mussel Tissue reference material was chosen to work on, on the special ground that its 3.55% (w/w) chloride content is high. The ODP and the open-tube methods were also tried in order to gain a confirmation of the preceding findings. The pertinent data are presented in Table 8. With a R.S.D.% = 1.4 and $e\% = +4.2$, the new method shows its ability to cope with samples of high organic content while overcoming the disastrous influence of Cl_2, whose presence in the analysis (ODP) zeroed the mercury response. Once more the claims regarding the viability of the complete abolition of the condenser as a permanent feature in high temperature treatments are disproved by the poor results achieved in the open-tube runs.

Table 9 provides the full picture of the experiments on soils, sediments and sludges. For each sample five experiments were run in rapid succession under identical circumstances so that the reported R.S.D. values

Table 8
Determination of mercury in CRM 278 mussel tissue [a,b] (Hg content = 0.188 ± 0.007 μg g^{-1})

Digestion procedure	Hg found ± S.D. (n = 4), μg g^{-1}	R.S.D. (%)	e [c] (%)
NDP	0.196 ± 0.0027	1.4	+4.2
ODP	0	–	−100
Open-tube	0.15 ± 0.015	10.3	−20.2

[a] Cl^- content = 3.55% (w/w).
[b] 0.5 g of the product were analyzed; 4.3 g $K_2Cr_2O_7$ were introduced in the digestion mixture and the diluting solution was prepared according to Ref. 14.
[c] The error (e), % was calculated as $100(Hg_{found} - Hg_{present})/Hg_{present}$.

are an estimation of repeatability. The R.S.D. values actually achieved did not exceeded the value of 4.5%, they were in fact notably lower in most cases. Considering the small amounts of mercury involved in every digestion (0.1–2 μg, Table 9) this dispersion of results is quite acceptable, particularly so in view of the very different nature of the materials. Variability would be expected to decrease as the absolute amount of the analyte processed increases. This was not true in our case, as evidenced in Table 9. The discrepancy may likely be attributed to the variability as being inherent to the CVAAS recirculation technique alone, which had previously been indicated for contributing 3.6% in terms of R.S.D. to the variance of the entire (ODP digestion + spectrometric determination) procedure [14]. Mean Hg contents from this study (Table 9) fell within the declared 95% confidence limits (CL) of the reference materials (Table 3) in seven of the nine instances; the relative errors (e%) varied from −3.8% (SRM 1646) to +8.7% (BCSS-1) with a mean value of +1.6%. Moreover, among the 45 single determinations only four fell outside the certified CL. In two of the nine instances, i.e. sediments SRM 2704 and PACS-1, the mean concentrations slightly overshot the upper limit of the corresponding CL and e% was +5.5 and 5.0, respectively, for the two products. We believe

Table 9
Determination of mercury in soil, river sediment and sewage sludge Standard Reference Materials by the NDP procedure [a]

Sample	Hg present in digest (μg g^{-1})	Hg found ± S.D. (n = 5) (μg g^{-1})	Range (μg g^{-1})	R.S.D. (%)	e [b] (%)
Soils					
BCR 141 Calcareous Loam Soil	0.1136	0.058 ± 0.0019	0.056–0.060	3.3	+2.1
BCR 142 Light Sandy Soil	0.208	0.111 ± 0.0026	0.108–0.113	2.3	+6.7
BCR 143 Sewage Sludge Amended Soil	1.96	3.96 ± 0.12	3.78–4.07	3.1	+1.7
Sediments					
SRM 1646 Estuarine Sediment	0.126	0.061 ± 0.0013	0.059–0.062	2.1	−3.8
SRM 2704 Buffalo River Sediment	0.36	1.53 ± 0.069	1.44–1.63	4.5	+5.5
BCSS-1 Coastal Marine Sediment	0.258	0.140 ± 0.0017	0.138–0.143	1.2	+8.7
PACS-1 Harbour Marine Sediment	2.28	4.81 ± 0.12	4.72–4.99	2.5	+5.0
Sludges					
BCR 144 Sewage Sludge (Domestic)	0.149	1.50 ± 0.054	1.45–1.56	3.6	+0.5
BCR 146 Sewage Sludge (Mainly Industrial)	0.95	9.14 ± 0.39	8.63–9.49	4.3	−3.7

[a] The certified Hg content of the samples with the 95% confidence limits are given in Table 3.
[b] The error (e), % was calculated as $100(Hg_{found} - Hg_{present})/Hg_{present}$.

that, as a whole, these numbers give credit to the present method in terms of accuracy. However, the *e%* columns in Tables 8 and 9 point to mean Hg concentration values most frequently with a positive bias. The same impression is given by Table 3 (ODP) if only the results not flawed by chlorine are considered. This might be indicative of a bias with respect to the slope of the calibration line. A control excluded a systematic error related to the Hg bulk standard solution (a product purchased as such and not prepared by ourselves from a solid salt). Then the slope comparison investigation was resumed, now between the regression line from a series of aqueous standards prepared as described in "Reagents and standards" and each one of the regression lines obtained with the standard addition method applied to SRM 2704, BCR 142 and BCSS-1 digests (worse positive *e%* values). Since no significant differences at a 95% probability level were detected between the slopes, the matter remains undecided.

4. Conclusions

The digestion method presented in this paper is based on the action of the $K_2Cr_2O_7$–H_2SO_4 mixture used at its boiling point. The heating treatment consists of two successive phases, the first carried out with an air condenser resting on the digestion tube and the second without it. The initial step completes the digestion without the mercury losses which would be caused by the disengagement of CO_2 if the condenser were absent. In the second step the Cl_2 produced by the oxidation of chlorides possibly present in the sample is expelled from the digest and its involvement in the abatement of the analyte signal is avoided. The digestion procedure recovered all Hg from HgS; it dealt with soil sediments and sludges of various origin and composition allowing good precision and accuracy; it also proved to be satisfactory for the determination of mercury in tissues of marine organisms.

Acknowledgements

This work was financially supported by the Ministry for University, Scientific and Technological Research (MURST).

References

[1] A.A. Levinson, Introduction to Exploration Geochemistry, Applied Publishing, Calgary, 1974.
[2] H.J.M. Bowen, Environmental Chemistry of the Elements, Academic Press, London, 1979.
[3] D. Purves, Trace-Element Contamination of the Environment, Elsevier, Amsterdam, 1985, p. 66.
[4] U. Förstner, in I. Thornton (Ed.), Applied Environmental Geochemistry, Academic Press, London, 1983, p. 395.
[5] T.M. McCalla, J.R. Peterson and C. Lue-Hing, in L.F. Elliott and F.J. Stevenson (Eds.), Soils for Management of Organic Wastes and Waste Waters, Soil Science Society of America (SSSA), American Society of Agronomy (ASA), Crop Science Society of America (CSSA), Madison, WI, 1977, p. 33.
[6] M.D. Turner, D.O. Marsh, J. Crispin-Smith, J.B. Inglis and T.W. Clarkson, Arch. Environ. Health, 35 (1980) 367.
[7] I.K. Iskandar, J.K. Syers, L.W. Jacobs, D.R. Keeney and J.T. Gilmour, Analyst, 97 (1972) 388.
[8] L.W. Jacobs and D.R. Keeney, Environ. Sci. Technol., 8 (1974) 267.
[9] J.W.B. Stewart and J.R. Bettany, in A.L. Page, R.H. Miller and D.R. Keeney (Eds.), Methods of Soil Analysis, Part 2, American Society of Agronomy (ASA), Soil Science Society of America (SSSA), Madison, WI, 1982, p. 367.
[10] Inland Waters Directorate, Water Quality Branch, Analytical Methods Manual, Part 4, Naquadat No. 80050, Ottawa, 1979.
[11] U.S. Environmental Protection Agency, Test Methods for Evaluating Solid Wastes, SW 846, Vol. 1, Washington, DC, 3rd edn., 1986, Sec. A, (A) Method 7471, (B) Method 7470.
[12] Association of Official Analytical Chemists (AOAC), Official Methods of Analysis, K. Helrich (Ed.), Arlington, VA, 15th edn., Vol. 1, 1990, (A) Sec. 971.21, (B) 977.15.
[13] S. Landi, F. Fagioli, C. Locatelli and R. Vecchietti, Analyst, 115 (1990) 173.
[14] S. Landi, F. Fagioli and C. Locatelli, J. Assoc. Off. Anal. Chem. Int., 75 (1992) 1023.
[15] L. Frieberg and J. Vostal, Mercury in the Environment, CRC Press, Cleveland, OH, 1972.
[16] H. Agemian and A.S.Y. Chau, Analyst, 101 (1976) 91.
[17] A. Kuldvere, Analyst, 115 (1990) 559.
[18] R.W. Marts and J.J. Blaha, J. Assoc. Off. Anal. Chem., 66 (1983) 1421.
[19] International Union of Pure and Applied Chemistry (Analytical Chemistry Division), Spectrochim. Acta, 33B (1978) 242.
[20] J.A. Plant and R. Raiswell, in Ref. 4, p. 8.
[21] J.R. Postgate, The Sulphate-reducing Bacteria, Cambridge University Press, Cambridge, 1984.
[22] T. Fagerström and A. Jernelöv, Water Res., 6 (1972) 1193.
[23] J.M. Wood, in J.R. Kramer and H.E. Allen (Eds.), Metal Speciation, Theory, Analysis and Application, Lewis Publishers, Chelsea, MI, 1991, p. 309.
[24] H.A. Flaschka, EDTA Titrations, Pergamon Press, Oxford, 1964, p. 93.
[25] H. Agemian and A.S.Y. Chau, Anal. Chem., 50 (1978) 13.

[26] A.A. El-Awady, R.R. Miller and M.J. Carter, Anal. Chem., 48 (1976) 110.
[27] G. Lindstedt, Analyst, 95 (1970) 264.
[28] A.M. Ure and C.A. Shand, Anal. Chim. Acta, 72 (1974) 63.
[29] T.C. Rains and O. Menis, J. Assoc. Off. Anal. Chem., 55 (1972) 1339.
[30] J. Ross Knechtel and J.L. Fraser, Anal. Chem., 51 (1979) 315.
[31] F.D. Deitz, J.L. Sell and D. Bristol, J. Assoc. Off. Anal. Chem., 56 (1973) 378.
[32] M.R. Hendzel and D.M. Jamieson, Anal. Chem., 48 (1976) 926.
[33] G.S. Caravajal, K.I. Mahan, D. Goforth and D.E. Leyden, Anal. Chim. Acta, 147 (1983) 133.
[34] O. Lindström, Anal. Chem., 31 (1959) 461.
[35] T.Y. Toribara, C.P. Shields and L. Koval, Talanta, 17 (1970) 1025.
[36] C. Feldman, Anal. Chem., 46 (1974) 99.
[37] D.R. Christmann and J.D. Ingle, Anal. Chim. Acta, 86 (1976) 53.
[38] F.J Stevenson, Humus Chemistry, Wiley, New York, 1982, p. 1.
[39] R. Pelet, Bull. Soc. Geol. France, 8th Series, Tome I (1985) 1075.
[40] See Ref. 9, p. 561.
[41] See Ref. 3, p. 82.

ELSEVIER

Analytica Chimica Acta 298 (1994) 375–379

ANALYTICA CHIMICA ACTA

Determination of manganese by electrothermal atomisation atomic absorption spectrometry following coprecipitation with yttrium hydroxide

Kikuo Takeda *, Chikashi Akamatsu, Yoshihiro Ishikawa

Ehime Research Laboratory, Sumitomo Chemical Co., Ltd., 5-1, Soubiraki-cho, Niihama, Ehime 792, Japan

Received 5 June 1994

Abstract

Coprecipitation is applied to the determination of trace amounts of manganese by electrothermal atomisation atomic absorption spectrometry. Manganese (0.05–1 μg) is coprecipitated quantitatively from the sample solution (50–500 ml) with yttrium hydroxide at pH 9.0–11.3. The atomic absorbance of manganese is increased about 3 times by using an yttrium-impregnated graphite cuvette. The calibration curve is linear from 0.002 to 0.04 μg ml^{-1} of manganese. Twenty-three different ions investigated did not produce serious interferences. The proposed method was successfully applied to the determination of trace amounts of manganese in zinc metal.

Keywords: Atomic absorption spectrometry; Coprecipitation; Electrothermal AAS; Manganese

1. Introduction

Preconcentration procedures utilizing the collection of trace elements by coprecipitation have often been used to improve the sensitivity and/or selectivity of a given analytical method. Their major advantage over other preconcentration techniques lies in simplicity. Moreover, relatively high enrichment factors can be achieved. A variety of coprecipitants for the concentration of manganese have been proposed, including metal hydroxides [1–17], sulphide [18], phosphate [19], and organic precipitants [20–28]. For preconcentration prior to the determination of manganese by atomic absorption spectrometry (AAS) using graphite tube atomisation, indium hydroxide has recently been reported [29].

In a previous paper [30], the present authors proposed that yttrium hydroxide was effective as a collector for trace amounts of tin. In this work, we used yttrium hydroxide as a coprecipitant for manganese prior to the determination by electrothermal atomisation AAS. It was found that yttrium hydroxide could quantitatively collect trace amounts of manganese. Furthermore, the presence of yttrium enhanced the atomic absorbance of manganese in the determination of manganese by electrothermal atomisation AAS.

* Corresponding author. Present address: Sumika Chemical Analysis Service, Ltd., 3-1-43, Shinden-cho, Niihama, Ehime 792, Japan.

SSDI 0003-2670(94)00294-0

2. Experimental

2.1. Apparatus

A Hitachi Z-7000 Zeeman-effect atomic absorption spectrophotometer equipped with a manganese hollow-cathode lamp (Hitachi 2082019-21) was used for the atomic absorption measurements. A Horiba M-8S glass electrode pH meter was utilized for pH measurements. Glass material was previously washed with hydrochloric acid and deionized water to prevent trace contamination.

2.2. Reagents

All reagents were of analytical-reagent grade and deionized water prepared with a Milli-Q system (Millipore) was used throughout.

A stock solution of manganese (1 mg ml^{-1}) was prepared by dissolving 0.360 g of manganese(II) chloride tetrahydrate (Wako) in 0.02 M hydrochloric acid and diluting the solution to 100 ml with deionized water.

An yttrium solution (10 mg ml^{-1}) was prepared by dissolving 1.270 g of yttrium oxide (Wako, 99.99%) in small amounts of nitric acid and diluting the solution to 100 ml with deionized water.

2.3. Impregnation of cuvette

Tube-type graphite cuvettes were employed throughout this study. A 20 μl aliquot of an yttrium solution (10 mg ml^{-1}) was placed in a new graphite cuvette and carried through the atomisation cycle given for the measurements of manganese. This step was repeated three times.

2.4. General procedure

A 1-ml volume of an yttrium solution (10 mg ml^{-1}) is added to a sample solution (50–500 ml) containing 0.05–1 μg of manganese. The pH of the solution is adjusted to about 10.5 with aqueous ammonia. To let the yttrium hydroxide settle, the solution is allowed to stand for more than 1 h. The precipitate is filtered by suction using a 3G4 sintered-glass filter, washed with small amounts of deionized water and dissolved with 5 ml of 3 M nitric acid. After the solution is diluted to 25 ml with deionized water, manganese is determined by electrothermal atomisation AAS using an yttrium-impregnated cuvette. The operating conditions for atomic absorption measurements are shown in Table 1. A blank is also run, using deionized water instead of the sample solution.

Table 1
Instrumental conditions for the determination of manganese

Analytical wavelength	279.6 nm
Slit width	0.4 nm
Lamp current	7.5 mA
Argon flow rate	
Carrier gas	200 ml min^{-1}
Interrupted gas	30 ml min^{-1}
Injection volume	10 μl
Cuvette	Yttrium-impregnated graphite tube
Furnace programme	
Drying	80–120°C, 30 s
Ashing	800°C, 30 s
Atomisation	2500°C, 10 s

3. Results and discussion

3.1. Enhancing effect of yttrium

The enhancing effect of yttrium on the atomic absorbance of manganese was investigated with untreated graphite cuvettes by measuring the response to 0.02 μg ml^{-1} of manganese solution in the presence of 0.4 mg ml^{-1} yttrium and in the absence of yttrium. In the presence of yttrium, it was observed that the atomic absorbance of manganese gradually increased with injection times and reached almost constant absorbance. This value was almost equal to the atomic absorbance of manganese measured using yttrium-impregnated graphite cuvettes. The enhancement factor was about 3 as shown in Fig. 1. This phenomenon can be explained as the enhancing effect by formation of yttrium carbide on the inner surfaces of the graphite cuvettes such as the impregnation of graphite surfaces with lanthanum or zirconium [31]. For these results, we decided to use the yttrium-impregnated graphite cuvettes for sensitive measurements of the atomic absorbance of manganese.

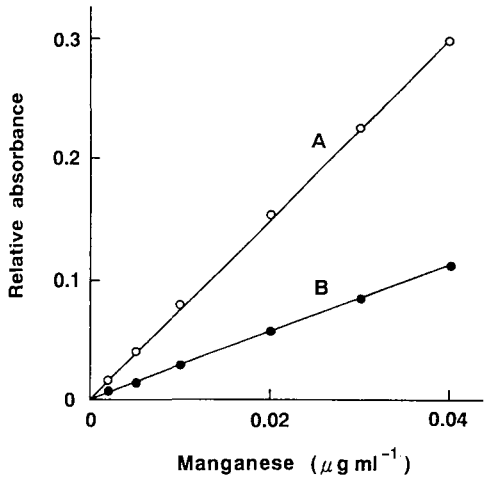

Fig. 1. Response–concentration graphs for manganese in the presence of 0.4 mg ml^{-1} of yttrium with an yttrium-impregnated cuvette (A) and in the absence of yttrium with an untreated graphite cuvette (B).

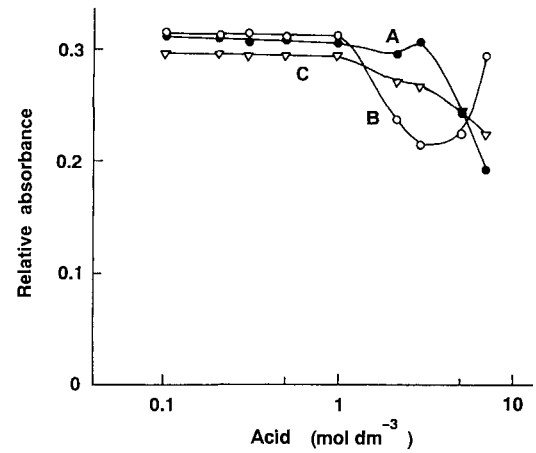

Fig. 2. Influence of hydrochloric acid (A), nitric acid (B) and sulphuric acid (C) on the atomic absorbance of manganese.

3.2. Optimum conditions for measurements

The optimum operating conditions for the determination of manganese by electrothermal atomisation AAS with the yttrium-impregnated graphite cuvette were investigated.

The effect of the concentration of nitric, hydrochloric and sulphuric acid on the atomic absorbance of 0.02 $\mu g\ ml^{-1}$ of manganese was examined. In the range 0.1–1 M of nitric acid, 0.1–3 M of hydrochloric acid and 0.1–1 M of sulphuric acid, the atomic absorbance of manganese was almost constant. At higher concentrations of these acids, the atomic absorbance gradually decreased. The results are shown in Fig. 2. In further experiments, 0.6 M nitric acid was used.

The heating programme for the drying, ashing and atomisation stages was examined by using 0.6 M nitric acid solution containing 0.02 $\mu g\ ml^{-1}$ of manganese and 0.4 mg ml^{-1} of yttrium. A setting of 80–120°C/30 s was sufficient for drying. At the ashing stage, the atomic absorbance of manganese was almost constant from 400 to 1100°C, and then decreased steeply at higher temperature. The results are shown in Fig. 3, together with those by using an untreated graphite cuvette and the manganese solution (0.02 $\mu g\ ml^{-1}$) not containing yttrium. With an increase in the atomisation temperature, the atomic absorbance of manganese increased and remained almost constant for temperatures of more than 1900°C. The results are shown in Fig. 4, together with those by using an untreated graphite cuvette in the absence of yttrium. The optimum instrumental parameters are summarized in Table 1.

3.3. Effect of pH on coprecipitation

To determine the optimum pH of the coprecipitation with yttrium hydroxide, the recovery of man-

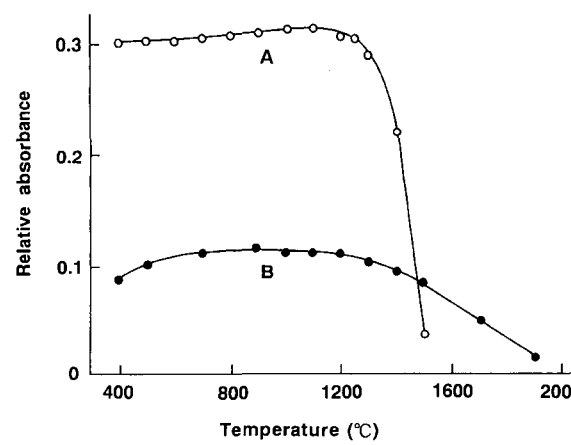

Fig. 3. Effect of the ashing temperature examined with 0.6 M nitric acid solution containing 0.02 $\mu g\ ml^{-1}$ of manganese, in the presence of 0.4 mg ml^{-1} of yttrium with an impregnated graphite cuvette (A), and in the absence of yttrium with an untreated graphite cuvette (B).

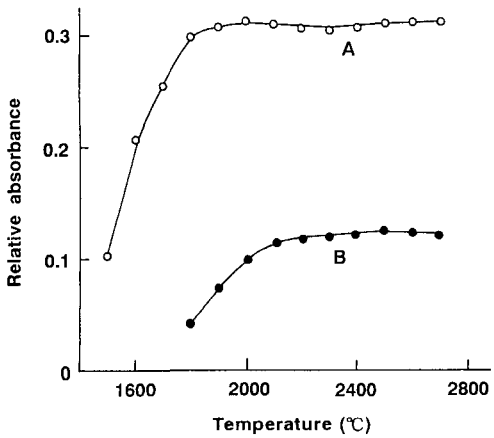

Fig. 4. Effect of the atomisation temperature examined with 0.6 M nitric acid solution containing 0.02 μg ml^{-1} of manganese, in the presence of 0.4 mg ml^{-1} of yttrium with an impregnated graphite cuvette (A), and in the absence of yttrium with an untreated graphite cuvette (B).

ganese was studied in the pH range 8.4–11.3 with the solutions (100 ml) containing 0.5 μg of manganese, according to the general procedure. The results indicated that maximum and almost constant recoveries were obtained at pH 9.0–11.3. The pH was therefore adjusted to about 10.5 for the coprecipitation.

3.4. Effect of amounts of coprecipitant

The necessary amounts of yttrium for the coprecipitation were examined with solutions (100–500 ml) containing 0.5 μg of manganese. More than 3 mg of yttrium should be added to 100 ml of the solutions for quantitative collection. This amount should increase to 5 mg, when the volume of sample solution increased to 500 ml. From these results, an yttrium amount of 10 mg was used for the coprecipitation.

3.5. Effect of standing time

The relation between the recovery of 0.5 μg of manganese and the standing time of the precipitate was investigated. The recovery of manganese was almost 100% at about 1 h after the formation of yttrium hydroxide and remained almost constant while standing for 6 h. From these results, the precipitate was allowed to stand for more than 1 h.

3.6. Calibration curve

A straight line was obtained over the concentration range of 0.002–0.04 μg ml^{-1} of manganese. The reproducibility, expressed by the relative standard deviation obtained from ten repeated determinations, was 4.2% for 0.02 μg ml^{-1} of manganese. The detection limit, defined as three times the standard deviation for 20 measurements of the reagent blank, was 0.7 ng ml^{-1} of manganese if a volume of 10 μl was taken.

3.7. Interferences

The influence of 23 different ions on the determination of 0.5 μg of manganese was examined by coprecipitating manganese from about 100 ml of sample solution. Aluminium(III), Si(IV), Ti(IV), V(V), Fe(III), Co(II), Ni(II), Cu(II), Zn(II), Ga(III), Sr(II), Sb(III), Ba(II), Pb(II), Bi(III), Cl^-, NO_3^-, SO_4^{2-}, and PO_4^{3-} did not interfere in a 2000-fold amount relative to manganese, within 5% relative error values. Na, Mg, K, and Ca did not interfere even in 100,000-fold excess.

3.8. Application to the determination of manganese in zinc metal

To evaluate the usefulness of the proposed method, the determination of manganese in zinc matal was carried out. The sample (0.5 g) was dissolved in a mixture of 20 ml of hydrochloric acid and 0.1 ml of nitric acid. The resulting solution was diluted to 100 ml with deionized water and treated according to the general procedure. The sample solu-

Table 2
Analytical results of manganese in zinc metal (0.5 g) and recovery

Added (μg)	Found (μg) [a]	Recovery (%)
–	0.07	–
0.10	0.17	100
0.25	0.33	104
0.50	0.55	96

[a] The mean of triplicate measurements.

tions spiked with manganese were also examined. The results obtained are shown in Table 2. From these results, it was found that the proposed method is applicable to the concentration and determination of trace amounts of manganese in zinc metal.

4. Conclusion

A quantitative method for the preconcentration of trace amounts of manganese has been developed. Coprecipitation with yttrium hydroxide was suitable for preconcentration prior to the determination of manganese by electrothermal atomisation AAS. The use of an yttrium-impregnated graphite cuvette increased the atomic absorbance of manganese. The present method was useful for the determination of manganese in zinc metal.

References

[1] P.N.W. Young, Analyst, 99 (1974) 588.
[2] Y. Harada and N. Kurata, Bunseki Kagaku, 35 (1986) 641.
[3] M. Hiraide, Y. Yoshida and A Mizuike, Anal. Chim. Acta, 81 (1976) 185.
[4] R. Ko and P. Anderson, Anal. Chem., 41 (1969) 177.
[5] J.M. Scarborough, C.D. Bingham and P.F. DeVries, Anal. Chem., 39 (1967) 1394.
[6] Y. Harada, N. Kurata and G. Furuno, Bunseki Kagaku, 36 (1987) 526.
[7] K. Himeno, K. Yanagisawa, T. Yuki and Y. Nakamura, Bunseki Kagaku, 33 (1984) T43.
[8] T. Akagi, K. Fuwa and H. Haraguchi, Anal. Chim. Acta, 177 (1985) 139.
[9] T. Akagi and H. Haraguchi, Anal. Chem., 62 (1990) 81.
[10] E. Bruninx, A.V. Eenbergan and A. Schouten, Anal. Chim. Acta, 109 (1979) 419.
[11] H. Yoshikawa, K. Isobe, H. Iwata, N. Benitani, K. Saito and H. Seno, Bunseki Kagaku, 38 (1989) 535.
[12] F. Koroleff, Acta Chem. Scand., 1 (1947) 503.
[13] Y. Shigetomi, Bunseki Kagaku, 24 (1975) 699.
[14] A. Tsuyama and S. Nakashima, Bunseki Kagaku, 29 (1980) 81.
[15] A.S. Buchanan and P. Hannaker, Anal. Chem., 56 (1984) 1379.
[16] H.L. Polak, J. Radioanal. Chem., 9 (1971) 241.
[17] Y. Harada, Bunseki Kagaku, 31 (1982) 130.
[18] V. Simeonov, I. Karadzhova and S. Aleksandrov, Fresenius' Z. Anal. Chem., 320 (1985) 330.
[19] J. Holzbecher and D.E. Ryan, J. Radioanal. Chem., 74 (1982) 25.
[20] S. Brueggerhoff and E. Jackwerth, Fresenius' Z. Anal. Chem., 326 (1987) 528.
[21] H. Bem and D.E. Ryan, Anal. Chim. Acta, 166 (1984) 189.
[22] H. Watanabe, S. Berman and D.S. Russell, Talanta, 19 (1972) 1363.
[23] E. Yamada and M. Sato, Bunseki Kagaku, 32 (1983) 654.
[24] C. Bergerioux and W. Haerdi, Analusis, 8 (1980) 169.
[25] W. Zmijewska, H. Polkowska-Motrenko and H. Stokowska, J. Radioanal. Nucl. Chem., 84 (1984) 319.
[26] J.M. Eckert, K.E.A. Leggett, J.B. Keene and K.L. Williams, Anal. Chim. Acta., 222 (1989) 169.
[27] I. Atsuya and K. Itoh, Fresenius' Z. Anal. Chem., 329 (1988) 750.
[28] K. Akatsuka and I. Atsuya, Anal. Chim. Acta, 202 (1987) 223.
[29] M. Hiraide, Z.-S. Chen and H. Kawaguchi, Anal. Sci., 7 (1991) 65.
[30] K. Takeda, C. Akamatsu and Y. Inoue, Fresenius' J. Anal. Chem., 339 (1991) 50.
[31] J.H. Runnels, R. Merryfield and H.B. Fisher, Anal. Chem., 47 (1975) 1258.

ELSEVIER

Analytica Chimica Acta 298 (1994) 381–386

ANALYTICA CHIMICA ACTA

Enzymatic method for the determination of tellurite ions

Dai-Eun Sok [a,*], Mee Ree Kim [b]

[a] *Daejeon Machine Depo, P.O. Box 35, Daejeon, South Korea*

[b] *Department of Food Science and Nutrition, Chungnam National University, Daejeon 305–764 South Korea*

Received 16 February 1994; revised manuscript received 27 June 1994

Abstract

A simple method for the quantitative determination of tellurite ions in aqueous media including blood plasma or serum is described. This assay is based on the selective and potent inhibition of a Zn^{2+}–glycerophosphocholine phosphocholine phosphodiesterase by tellurite ions in the presence of tetramethylammonium ions. The assay method, which showed a good relationship between the enzyme inhibition and the amount of tellurite ions (50 nM–5 μM), was found to be rapid (< 5 min), reproducible (mean C.V., 6.5%), and at the same time, sensitive, showing a low limit of detection (50 nmol). Based on this technique, the removal of tellurites by thiols, and the kinetics for the uptake of tellurite ions in blood were investigated.

Keywords: Enzymatic methods; Tellurite ions

1. Introduction

Tellurite ions have been reported to induce alterations of red cell membranes at concentrations $\leqslant 5$ μM [1], or to be responsible for the tellurium-induced neuropathy [2], where demyelination was supposed to be partially due to the decreased biosynthesis of cholesterol. In further studies, tellurites were suggested to inhibit the cholesterol epoxidase [3]. Recently, Zn^{2+}-glycerophosphocholine phosphocholine phosphodiesterase activity [4] was found to be inhibited by tellurite ions, a hydrolysis product of tellurium(IV) tetrachloride. Its inhibition was shown to be due to the competition between substrates and tellurites for the enzyme, and to be enhanced by organic cations such as tetramethylammonium chloride. In addition to the toxicity of tellurites to mammalian cells, the susceptibility of most gram-negative bacteria to the inhibitory role of tellurite (0.01–1.5 mM) was also reported [5]. Although the toxicity of tellurite has been examined at the cellular level [3,5], the in vivo study on the fate of tellurites has been hampered by the lack of a sensitive and selective assay.

The radiometric assay, which has been used to study cellular interaction with tellurites [6], includes disadvantages such as high costs of the isotope and a difficulty in its use. Atomic absorption spectrometric methods [7] as well as electrochemical determination may be more accurate, but require a long sample preparation time and a large sample volume. Although complexation reagents such as diethyldithiocarbamate, thioglycollic acid and dithizone have been used for assays of tellurite ions, these assay procedures involve a time-consuming extraction process

* Corresponding author.

SSDI 0003-2670(94)00289-4

[8,9]. Recently, a spectrophotometric method requiring no solvent extraction has been reported [9]. However, the limit of detection was 4 μM, which is above the lowest concentration (1 μM) of tellurites required for colloid osmotic lysis of erythrocytes depleted of glutathione [1], and there is interference from excess oxyanions such as tellurite, selenite or arsenite, or biological materials showing UV absorption at 340 nm. Therefore, a more sensitive (detection limit < 1 μM) and selective method for the assay of tellurites was required.

This study demonstrates that tellurites in aqueous samples can be determined conveniently and selectively by this enzymatic assay.

2. Experimental

2.1. Materials

p-Nitrophenylphosphocholine, potassium tellurite, potassium tellurate, sodium sulfite, cysteine and thioglycollic acid were obtained from Sigma. Sodium selenite, tetramethylammonium chloride (TMA) and dimethylaminoethanethiol were from Aldrich. Bovine serum was from Gibco. Zn^{2+}–GPC phosphocholine phosphodiesterase was prepared according to a previous report [10]; the phosphodiesterase was solubilized from brain membranes by microbial phospholipase C, and purified sequentially by chromatography on concanvalin A Sepharose and CM Sephadex columns. Finally, the major fraction from CM Sephadex chromatography was further purified on Sephadex G-150. Although the enzyme preparation from concanavalin A Sepharose chromatography was generally used in this experiment, either Triton X-100 solubilized [11] or phospholipase C solubilized enzyme [10] is suitable for the purpose of tellurite measurement.

2.2. Assay of phosphodiesterase activity

Zn^{2+}–glycerophosphocholine phosphocholine phosphodiesterase activity was determined by monitoring the absorbance of *p*-nitrophenol released from *p*-nitrophenylphosphocholine [11]. Absorbance changes were followed on a spectrophotometer (Gilford 250) at 410 nm ($\varepsilon = 1.35 \times 10^4$ M^{-1} cm^{-1}). Unless otherwise described, assays were conducted in 1 ml of 0.1 M glycine buffer (pH 10) containing 150 μM *p*-nitrophenylphosphocholine (*p*-NPPC) at 20°C. One unit of enzyme activity was expressed as the ability to generate 1 μmol of *p*-nitrophenol per hour.

2.3. Enhancing effect of TMA

Unless stated otherwise, the phosphodiesterase (ca. 20 milliunits) was incubated with tellurite ions (1 μM) in 0.1 M glycine buffer (pH 10) containing tetramethylammonium chloride (TMA) of various concentrations (0–2 mM) at 20°C, and the remaining activity was measured as described above.

2.4. Standard curves for the enzymatic assay

Potassium tellurite was dissolved in distilled water to yield the stock solution (10 mM). The Zn^{2+}–GPC phosphocholine phosphodiesterase (20 milliunits) was incubated with potassium tellurite of various concentrations (50 nM–4 μM) in 0.1 M glycine buffer (pH 10) containing 1 or 10 mM TMA, and the remaining activity was expressed as the percentage of control, where tellurites were not included. Lower concentrations (50–800 nM) of tellurites were used to establish a standard curve with 6 replicates for 10 mM TMA, and higher concentrations (0.25–4 μM) used for the standard curve with 11 replicates for 1 mM TMA. Separately, the serum sample containing tellurites was freshly prepared by dissolving tellurites of various concentrations in bovine serum. The aliquot (50 μl) was used for the enzyme inhibition as described above. Intra-assay (within-day assay) was determined at four concentrations (50, 100, 200 and 400 pmol ml^{-1}) in six analyses, and inter-assay (between-day assay) for reproducibility was singly at the same four concentrations in triplicate runs.

2.5. Effect of oxyanions or thiols on the enzymatic assay.

The phosphodiesterase (20 milliunits) was incubated with 150 μM *p*-NPPC in the presence of oxyanions (1–10 mM) or thiols (1 mM), and the remaining activity was measured as described above. In a separate experiment to investigate interferences,

the enzymatic assay of tellurites at 50 or 100 nM was carried out in the presence of oxyanions (0.1 mM) or thiols (0.1 mM).

2.6. Removal of tellurite ions by thiols.

Tellurite ions (2, 20 or 100 μM) were incubated with cysteine or dimethylaminoethanethiol of two concentrations (100 or 500 μM) in 30 mM Tris buffer, pH 7.5 at 20°C, and 10 s later, the aliquot was taken for the assay of the remaining tellurite ions using the enzymatic method employing 1 mM TMA.

2.7. Uptake of tellurites into blood of mouse.

Mice (approximately 30 g weight, either sex) were injected intraperitoneally with potassium tellurite (3 or 10 mg kg^{-1} weight), and blood (20–40 μl) from the tail vein was taken into capillary tubes, and centrifuged with a Autocrit centrifuge (Clay Adams). Plasma (10–20 μl) was used for the inhibition of the phosphodiesterase, and the amount of tellurite was estimated from the standard curve for tellurite inhibition.

3. Results and discussion

3.1. Enhancing effect of TMA on the tellurite inhibition.

As demonstrated in Fig. 1, a Zn^{2+}–glycerophosphocholine (GPC) phosphocholine phosphodiesterase was inhibited by potassium tellurites, and the inhibitory action of tellurites was enhanced in a concentration-dependent manner by TMA. In the presence of 1 and 10 mM TMA, the inhibitory potency of tellurites was increased by approximately 10- and 50-fold, respectively.

3.2. Calibration

A typical standard curve for the inhibition of a Zn^{2+}–GPC phosphocholine phosphodiesterase by tellurite ions is shown in Fig. 2. Over a broad range of tellurite concentrations, 50–800 nM in the presence of 10 mM TMA, or 0.25–4 μM in the presence

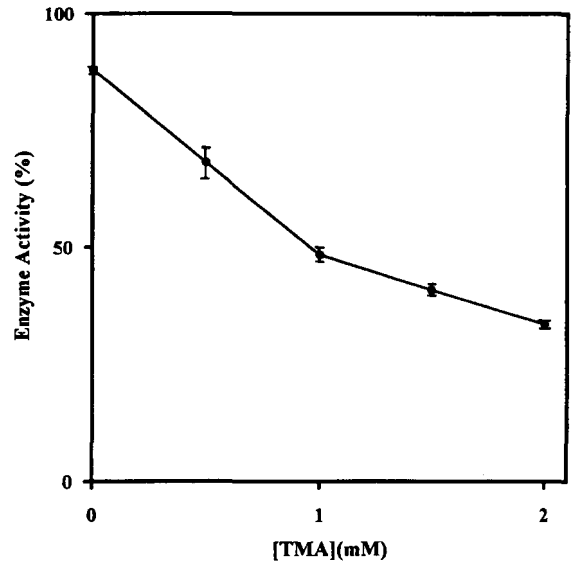

Fig. 1. Enhancing effect of TMA on the inhibition of a Zn^{2+}–GPC phosphocholine phosphodiesterase by tellurites. The phosphodiesterase (20 milliunits) was incubated with 150 μM *p*-NPPC in either the absence or presence of TMA of various concentrations (0–2 mM) in 0.1 M glycine buffer (pH 10) containing 1 μM potassium tellurite. Enzymatic activity was measured as described in Experimental, and the inhibitory effect was expressed as the percentage of control, where the inclusion of tellurites was omitted. Each point was the average ±S.D. of three determinations.

of 1 mM TMA, we observed a linear inhibition of the phosphodiesterase activity with an increasing log concentration of tellurites. Results for linear regression analyses of the data show a good relationship: $y = -261 - 52 \log x$, $r = 0.993$, $n = 6$, where the concentration of TMA was 10 mM (Fig. 2), and $y = -3474 - 59 \log x$, $r = 0.998$, $n = 11$, where the concentration of TMA was 1 mM. The detection limit of this method employing 10 mM TMA was 50 pmol, and the precision under the conditions used was estimated to be 5.5%. In comparison with the spectrophotometric method [9] which had been reported to cover the concentration range of 4 to 200 μM, this enzymatic assay possessing a detection range of 0.05–4 μM was at least 80 times more sensitive. It is therefore favored over the previously-reported assay methods [8,9].

3.3. Precision and accuracy

This assay procedure was repeated at least six times using the samples of tellurite ions dissolved in

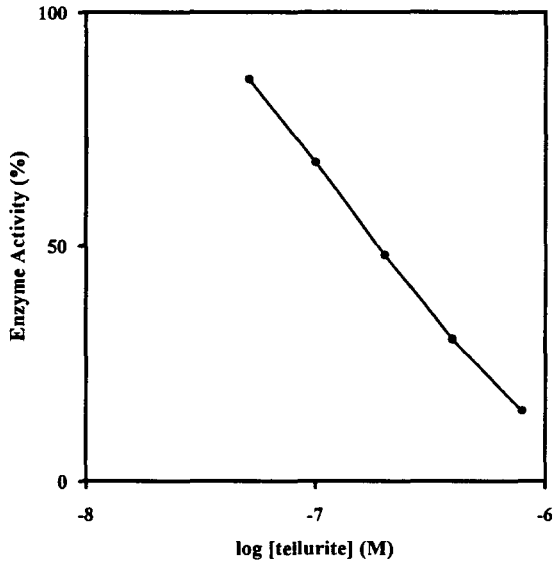

Fig. 2. Standard curve for the inhibition of a Zn^{2+}–GPC phosphocholine phosphodiesterase by tellurites in the presence of TMA. The phosphodiesterase (20 milliunits) was incubated with 150 μM *p*-NPPC in the presence of tellurite (50–800 nM) in 0.1 M glycine buffer (pH 10) containing 10 mM TMA. The inhibition degree was expressed as the percentage of control. Each point was expressed as the average ±S.D. of 6 determinations. The maximum standard deviation for any of five points used was within 6.5% of the average percentage.

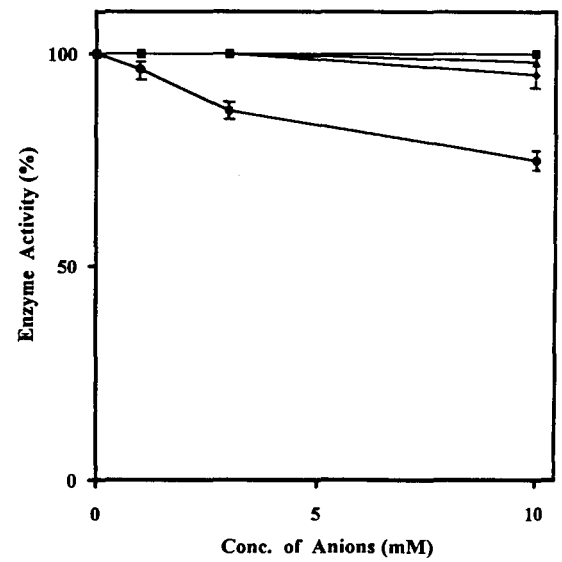

Fig. 3. Inhibitory effect of oxyanions on a Zn^{2+}–GPC phosphocholine phosphodiesterase activity. The phosphodiesterase (20 milliunits) was incubated with 150 μM *p*-NPPC in the presence of anions of various concentration (1–10 mM), and the activity was measured as described in Experimental. Each point was the average ±S.D. of three determinations. (■) Phosphate; (▲) sulfite; (♦) salenite; (●) tellurate.

bovine serum, and was also carried out at different days. The data presented in Table 1 show the precision and accuracy of this assay. The precision of the method was 6.0% and 6.5% for intra- and inter-assay, respectively. The accuracy for the values of recovered standards was 0.8–11.5% over the concentration range investigated. Thus, reliable and reproducible inhibition of phosphodiesterase activity is observed with the range of concentrations used, although the extended exposure of tellurites to bovine serum resulted in a gradual loss of tellurites.

Table 1
Precision and reproducibility data for the present method in the quantitation of tellurite ions

Amount of tellurite added to plasma (pmol/ml)	Within-day assay		Between-day assay	
	Mean ($n=6$) ±S.D.	C.V. (%)	Mean ($n=3$) ±S.D.	C.V. (%)
50	49.3± 2.6	5.3	49.3± 2.9	5.9
100	100.8± 7.9	7.8	102.3± 8.3	8.1
200	218.5±15.8	7.0	220.0±19.5	6.1
400	445.8±17.9	4.0	441.7±26.4	6.0

Potassium tellurite was added to bovine serum to be at various concentrations (50–400 pmol ml^{-1}). The aliquot was taken, and subjected to the enzymatic assay of the tellurite ions as described in Fig. 1.

3.4. Selectivity

The inhibitory action of various oxyanions such as phosphate, selenite, sulfite or arsenite ions was examined. As shown in Fig. 3, these anions, at the concentrations used, expressed no significant inhibition of the phosphodiesterase activity, and even tellurate ions had no inhibitory effect below 1 mM. These results indicate that the enzymatic method has an advantage over the previous spectrophotometric methods [8,9].

3.5. Interferences

Thiols such as cysteine or glutathione were examined for any interference of this enzymatic assay. Under the assay conditions used, these thiols ($\leq$ 100

μM) had no significant interfering effect on the enzymatic assay of tellurites at concentrations close to the detection limit. In a separate experiment, where oxyanions such as tellurite or selenite were included in the assay system, it was found that these compounds did not show any significant interference at 100 μM.

3.6. Removal of tellurites by thiols

The removal of tellurites by thiols during a short incubation time (10 s) was investigated. As demonstrated in Table 2, most of the tellurite ions at 100 μM appeared to be removed rapidly after contact with excess thiols (500 μM). Meanwhile, the inclusion of a lower amount (100 μM) of cysteine caused a negligible (< 3%) removal of tellurite (2, 20 or 100 μM). It is therefore suggested that the removal of tellurites by thiols is dependent on the concentration of thiols and tellurites, and that the molar ratio of tellurites to thiols is consistent with the previous observation [1]. This might explain why thiols at a lower concentration (100 μM) caused no significant interference on this enzymatic assay.

3.7. Uptake of tellurites into blood of mouse.

Subsequently, this assay method has been applied to the analysis of plasma samples of mice administered intraperitoneally with potassium tellurites. Blood samples were collected in triplicate before the injection and at intervals up to 2 h after treatment.

Table 2
Removal of tellurites by thiols

Concentration of tellurite (μM)	Added	Amount of tellurite remaining (%)
2	100 μM glutathione	99.0 + 2.5
20	100 μM glutathione	98.3 ± 2.0
20	100 μM cysteine	98.7 ± 8.0
100	100 μM cysteine	97.7 ± 5.5
100	500 μM cysteine	7 ± 4
100	500 μM dimethyl-aminoethanethiol	≤ 5

Tellurite (2, 20 or 100 μM) was incubated with 100 or 500 μM cysteine or 500 μM dimethylaminoethanethiol, and after 10 s the aliquot (50 μl) was taken and used for the assay of the remaining tellurite as decribed in Experimental. Each value was the average ±S.D. of three determinations.

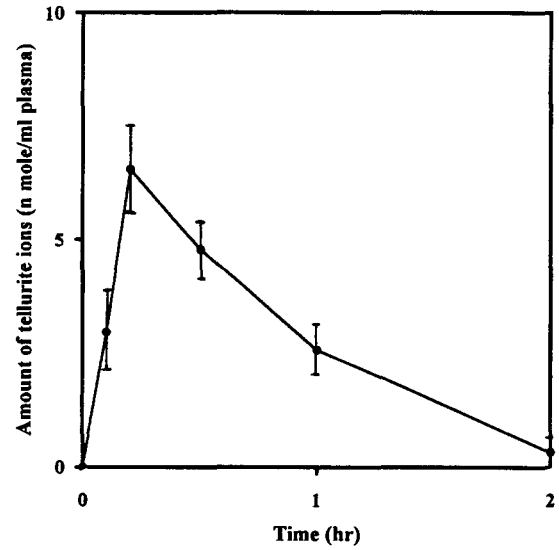

Fig. 4. Tellurite uptake into plasma of mouse injected intraperitoneally with potassium tellurite. Mice were injected intraperitoneally with potassium tellurite (3 or 10 mg kg^{-1}). The amount of tellurite present in plasma was measured according to the enzymatic assay as described in Experimental. Each point was the average ±S.D. of three determinations.

Fig. 4 shows a profile for the change of the tellurite level in blood. The experimental data presented indicated that the initial disposition is relatively short, and the maximum plasma concentration of 6.5 nmol ml^{-1} was observed 10 min after the administration. Subsequently, plasma levels declined gradually, remaining above 1 nmol ml^{-1} plasma, a lower limit of quantitation, for at least 60 min. The biological half life and the maximum uptake percentage of tellutrite in the body were estimated to be 69 min and about 3.3%, respectively. In an additional experiment where blood samples were collected after injection with 10 mg tellurite kg^{-1} weight, the plasma concentration at 10 min was estimated to be about 20 nmol ml^{-1} plasma. Separately, when 50 μM tellurite in plasma was stored at 30°C, it was found that the amount of tellurite did not change significantly (< 5%) during 1 h incubation, but decreased to about 80% of the starting level after 2 h. From these results, it is supposed that the disposal of tellurites is relatively rapid in an in vivo system, and that a minor portion of tellurite removal may be due to the complexation of tellurites with thiols in blood. Since this enzymatic assay is highly specific for tellurite ions, this method would be useful for the selective monitoring

of tellurite ions in in vivo systems, for which the conversion of tellurites has been reported [1].

4. Conclusion

The enzymatic assay described in this article, which is based on the selective inhibition of Zn^{2+}–GPC phosphocholine phosphodiesterase by tellurites in the presence of TMA, has a low detection limit (50 pmol), a small sample volume (10–50 μl) and a short incubation time (< 5 min). This method overcomes limitations imposed by spectrophotometric methods previously reported: the detection sensitivity was 80-fold higher, and the assay was not interfered by the presence of excess oxyanions or UV-absorbing materials. The method can be used for the analysis of aqueous samples including plasma specimens.

References

[1] B. Deuticke, P. Lutkemeier and B. Poser, Biochim. Biophys. Acta, 1109 (1992) 97.
[2] G.J. Harry, G.F. Goodroom, T.W. Bouldin, M. Wagner-Recio and A.D. Towes, J. Neurochem., 52 (1989) 938.
[3] M. Wagner-Recio, A.D. Towes and D. Morell, J. Neurochem., 57 (1991) 1891.
[4] D.-E. Sok and M.R. Kim, Biochem. J., 284 (1992) 641.
[5] D.E. Bradley, K.K. Grewal, D.E. Taylor and J. Whelan, J. Gen. Microbiol., 134 (1988) 2009.
[6] G. Lloyd-Jones, D.A. Ritchie and P. Strike, FEMS Microbiol. Lett., 81 (1991) 19.
[7] J.F. Walper, F.L. Tucker and M.D. Appleman, Anal. Biochem., 3 (1962) 298.
[8] G.F. Kirkbright and W.K. Ng, Anal. Chim. Acta, 35 (1966) 116.
[9] R.J. Turner, J.H. Weiner and E.T. Diane, Anal. Biochem., 204 (1992) 292.
[10] D.-E. Sok and M.R. Kim, Biochem. J., 286 (1992) 435.
[11] D.-E. Sok and M.R. Kim, Anal. Biochem., 203 (1992) 201.

ELSEVIER

Analytica Chimica Acta 298 (1994) 387–392

ANALYTICA CHIMICA ACTA

Direct determination of the cation-exchange capacity of soils with automatic sample pretreatment in a flow system

Zheng-liang Zhi [1], Angel Ríos, Miguel Valcárcel *

Department of Analytical Chemistry, University of Córdoba, E-14004, Córdoba, Spain

Received 18 March 1994; revised manuscript received 9 June 1994

Abstract

An automatic method for the determination of the cation exchange capacity (CEC) in soils by use of a flow-injection system coupled to an open/closed loop sample pretreatment unit was developed. Cations were displaced from exchange sites on soil colloids by dissolved barium, excess reagent being subsequently removed and the solid retained in a filter cartridge located in the open/closed loop unit. The barium fixed in soil was then exchanged with magnesium(II) by adding magnesium sulphate, which aided to further remove barium as a sulphate precipitate. The clear liquid filtrate in the open/closed loop was finally driven to the loop of the injection valve and inserted into a flow system designed for the spectrophotometric determination of residual magnesium(II) with Eriochrome Black T. CEC values ranging from 6.6 to 20 mmol/100 g air-dried soil were obtained with an average relative standard deviation of ±2.9%. About 10 samples per hour can be processed in this way.

Keywords: Flow injection; Ion exchange; Spectrophotometry; Soil samples; Cation exchange capacity; Automatic analysis

1. Introduction

Automatic flow systems offer interesting possibilities for the analysis of liquid (aqueous) samples, physico-chemical pretreatment of which is relatively simple. Only a few approaches to the analysis of gaseous [1–3] and solid [4–9] samples, however, have so far been reported, in the form of straightforward automated procedures for implementation of the preliminary operations of the analytical process, which is a big challenge today [10]. In this context, various units and approaches have been developed, most of which are based on non-chromatographic continuous separation techniques [11], in order to simplify processing of samples prior to the determination of the analytes. Thus, various on-line filtration units have been designed and incorporated into continuous-flow systems for developing precipitation-based applications. The potential of automatic on-line precipitation–dissolution was demonstrated in 1989 [12], particularly for the indirect determination of both organic and inorganic anions, and preconcentration determination of metal traces by atomic absorption spectroscopy. Recently, Kubán [13] reviewed continuous precipitation techniques in flow-injection analysis (FIA).

The analysis of soil samples is of great agricultural and environmental interest, but is confronted with sample problems arising from the complex matrices of soils. In response, great endeavours are being devoted to automating or at least simplifying preliminary oper-

* Corresponding author.

[1] Permanent address: China Pharmaceutical University, Nanjing, 210009, China.

SSDI 0003-2670(94)00278-T

ations for this type of sample [6,9,14]. In the present study, a direct determination for the cation-exchange capacity (CEC) of soils was developed that simplifies sample pretreatment by using an open/closed flow system prior to the manifold employed for the analytical determination proper. The open/closed system includes a filter for retaining solid soil particles, and passing barium(II) and magnesium(II) solutions successively. The clear liquid filtrate obtained is introduced in the determination manifold, where the concentration of residual magnesium(II) is used to indirectly determine the CEC of the sample.

2. Experimental

2.1. Apparatus

A Hewlett-Packed HP 8452A diode-array spectrophotometer furnished with a Hellma 178.012-QS flow-cell of 18 μl inner-volume and 10 mm path-length, and interfaced to a Vectra ES/12 computer which delivered results through a HP Think-Jet printer, was used for absorbance measurements ($\lambda = 525$ nm). Two peristaltic pumps (four channel Gilson Minipuls-3 Model), a Rheodyne 5401 injection valve, two Rheodyne 5011 six-way switching valves (SV), and a cartridge filter holder of 38 mm diameter (Pat. No. 2,879,207, supplied by Millipore, MA) furnished with Whatman No. 1 filter paper were employed to build the flow-injection and open/closed loop sample pretreatment manifolds. Polytetrafluoroethylene (PTFE) tubing of 0.5 mm i.d. and perspex connectors were also used.

2.2. Reagents

All reagent solutions were prepared from analytical-reagent grade chemicals and distilled water. A standard magnesium sulphate solution (0.05 M) was prepared by dissolving 3.081 g of $MgSO_4 \cdot 7H_2O$ (Merck) in water and diluting to 250 ml in a volumetric flask. This solution was used either for leaching (exchange) or preparation of the working solutions used to run the calibration curve for the determination of magnesium.

A barium chloride solution (0.25 M) was made by dissolving 62 g of $BaCl_2 \cdot 2H_2O$ (Merck) in 500 ml water, adding 25 ml triethanolamine (Merck), diluting to about 800 ml, adjusting the pH to 8.1 with 1 M HCl, and finally diluting to 1 l.

A buffer solution of pH 8.0 was prepared daily from 3.0 g NH_4Cl in 400 ml water, the pH being adjusted by adding a few drops of concentrated ammonia.

Eriochrome Black T (Merck), 0.030%, solution was freshly prepared in methanol, and was degassed in an ultrasonic wave generator for about 5 min prior to use.

2.3. Manifold

The manifold used consisted of two distinct blocks, namely: the open/closed loop sample pretreatment system and the flow-injection analysis system for the CEC determination (Fig. 1). The former was used to accomplish cation replacement and exchange automatically. It consisted of one peristaltic pump, one cartridge filter furnished with Whatman No. 1 filter paper where the weighed sample was placed, and two switching valves of which, SV_1 inserted Ba(II) or Mg(II), whereas SV_2 linked the pretreatment flow unit with the CEC determination manifold. Position 1 in SV_2 was used to led the barium filtrate to waste, while position 2 allowed the flow circuit to be closed with the $MgSO_4$ solution inside, the solution being circulated through the closed-loop and repeatedly passed through the soil sample retained on the filter for as long as required to reach the exchange equilibrium and remove all precipitating $BaSO_4$ in the connecting coil and pump tubing. Position 3 was used to drive the filtrate solution to the loop of the flow-injection valve. Magnesium was determined in this filtrate. On injection of this solution, the sample plug was first mixed with a diluting stream (H_2O) and

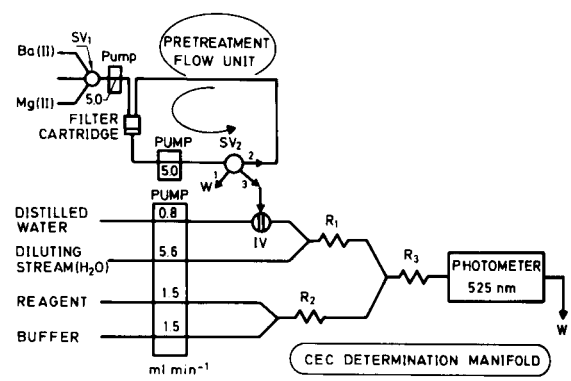

Fig. 1. Overall flow configuration used for the CEC determination including the sample pretreatment unit and the CEC determination manifold (for details, see text).

then with the Eriochrome Black T–buffer stream. Because the dye was unstable in the basic buffer solution, methanol was used as solvent (it was subsequently merged with the NH_4Cl–NH_3 buffer stream). The coloured complex thus formed along reactor R_3 was monitored spectrophotometrically at $\lambda = 525$ nm on passage through the flow-cell.

3. Results and discussion

The automatic soil sample pretreatment and the determination step must be studied and optimized separately and then integrated in a single, synchronized manifold.

3.1. Pretreatment flow unit

The manual determination of CEC operation has been addressed by using various procedures, most of which involve using a cation, (e.g., ammonium, sodium, potassium, barium), to saturate the soil colloids in the initial extractant. After washing with water and alcohol, adsorbed cations are displaced by a leaching solution in which the cation released is subsequently determined [15]. Because the washing step is the main source of error in the estimation of CEC, several other procedures using the Cu^+–thiourea or Ag^+–thiourea complex to saturate the soil and analysing the supernatant solution by AAS [16], for example, have been developed. The procedure, originally reported by Bascombe [17], seems to be the most precise and simple. The soil was saturated with barium salt, excess extractant was discarded and washing was avoided by adding magnesium sulphate to precipitate adsorbed barium, which was then exchanged for magnesium, and the magnesium remaining in solution was finally determined. This procedure was used in an automated form in this work. The final determination of magnesium was performed in a flow-injection system by complexation with Eriochrome Black T and spectrophotometric measurement [18,19].

Sample pretreatment was done in an open/closed loop system that bears some resemblance to an on-line leaching system [11] for analysis of solid samples using a mini-leaching cell. However, a cartridge filter holder furnished with Whatman No. 1 filter paper was used as a leaching cell to facilitate addition of the soil sample and replacement of the filter, and use of larger sample sizes. Filtration was performed with the aid of a peristaltic pump included in the open/closed system. The $BaCl_2$ and $MgSO_4$ solution were successively added to the sample in the filter cartridge (5 ml, introduced via SV_1 in Fig. 1), at pH 8.1 according to the reference method [20]. The effects of the concentrations of $BaCl_2$ and $MgSO_4$ used and the time during which the magnesium solution was circulated along the loop system were studied and optimized experimentally. The results showed an almost negligible influence of barium for concentrations in the range 2.5–12.5%; a 6% $BaCl_2 \cdot 2H_2O$ solution (0.25 M) was finally chosen. This solution was adjusted to pH 8.1 with 2.5% triethanolamine–HCl buffer. At this pH, almost all exchangeable cations, including H^+, would be displaced by Ba^{2+}. The circulation time of the magnesium solution along the closed flow system was important in order to ensure that the exchange equilibrium was reached and the barium sulphate precipitate produced in the system was removed. Experiments showed 2-min circulation time to be sufficient to obtain a clear, homogeneous filtrate solution. However, as expected, the concentration of $MgSO_4$, which was used to saturate exchangeable sites in place of barium, had a critical effect on the final results. In fact, the CEC value for the soil samples increased with increasing concentrations of magnesium in the range of 0.025–0.25 M. Table 1 shows the results obtained for two different soil samples by using different concentrations of $MgSO_4$. A suitable concentration of $MgSO_4$ for the determination of absolute CEC values was quite difficult to find. In any case, a 0.05 M $MgSO_4$ solution was selected for consistency with the reference manual method. An attempt at estimating the CEC by directly determining residual barium after saturation with soil in order to simplify the procedure proved ineffective and inadvisable since inorganic anions commonly found in soil

Table 1
Influence of the magnesium concentration on the CEC obtained (in mmol/100 g soil) for two different soil samples

Soil sample	$[Mg^{2+}]$ (M)				
	0.125	0.100	0.075	0.050	0.025
A	19.50	16.90	14.43	14.03	13.35
B	9.75	9.36	7.72	6.67	4.92

(e.g., sulphate, phosphate and carbonate), co-precipitated with barium under the experimental conditions used.

3.2. Flow-injection system

In order to use a simpler approach for the automatic determination of residual magnesium(II) from the open/closed flow unit, the reaction between alkaline Eriochrome Black T and magnesium to yield a pink complex was selected [18]. Formation of the complex was monitored spectrophotometrically at 525 nm.

Optimization of FIA variables

The configuration shown in Fig. 1 was designed on the basis of the following considerations for the direct determination of magnesium in the filtrated solution (up to 0.05 M) with adequate sensitivity: the sample plug should be properly diluted after injection, so a diluting stream was included. The flow rate ratio between sample carrier stream and diluting stream was set to 1:7 (0.8 ml min^{-1} vs. 5.6 ml min^{-1}), in order to increase dilution of the sample plug. A high pumping rate of the reagent stream resulting from mixing of the Eriochrome Black T and buffer stream relative to the sample was also used for the same purpose. This was also the reason for the relatively small sample volume employed (ca. 13 μl). The effect of the reactor lengths was also studied. The length of R_3 was found to hardly influence the signal over the range of 20–200 cm, because of the fast formation kinetic of the colouring reaction. Therefore, a length of 50 cm was chosen for R_3 to facilitate the mixing. The same length was considered optimal for R_1 and R_2 for appropriate mixing conditions. The overall flow rate was not critical for the signals. A value of 9.4 ml min^{-1} was adopted as a compromise between a high sampling rate and low reagent consumption.

Optimization of chemical variables

By using the configuration described above, the effects of the buffer pH, ionic strength (adjusted with NH_4Cl) and Eriochrome Black T concentration on the calibration curve were studied in a series of magnesium standards.

The effect of the buffer pH was studied over the range of 7.5–9.0, the linear range of the calibration curve was found to decrease with increasing pH. Lower pH values resulted in lower sensitivity, whereas higher pH values were only suitable for determining lower concentrations of analyte. A pH 8.0 for the buffer was finally selected to get the best possible results. The effect of the ionic strength was investigated over the range of 0.01–0.5 M; ca. 0.1 M NH_4Cl solution (adjusted in the buffer solution) provided the highest sensitivity. The concentration of Eriochrome Black T also had a critical influence, as can be seen in Fig. 2. However, the dye concentrations above 0.030% resulted in poor reproducibility in the signals; so a compromise between sensitivity and precision of measurements was made by using a 0.030% Eriochrome Black T concentration in the reagent stream. This solution provided a reasonably high absorbance (ca. 0.8 units) for the initial magnesium solution.

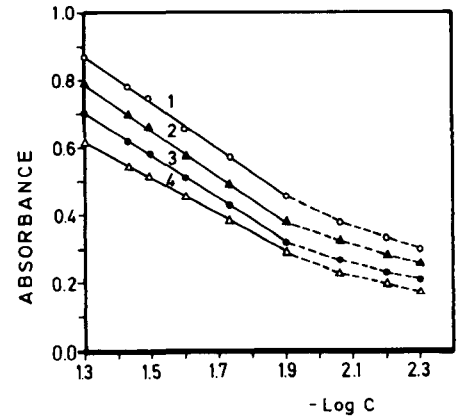

Fig. 2. Effect of the Eriochrome Black T concentration on the determination of Mg(II): (1) 0.035%; (2) 0.030%; (3) 0.025%; (4) 0.020%. C = Mg(II) in mol l^{-1}.

Calibration curves

Standard solution containing magnesium concentrations in the range 0.005 M and 0.05 M were used to construct the calibration graph by the FI manifold. Good linearity between the absorbance and the logarithmic concentration of the analyte was observed over the concentration range 0.0125–0.05 M. The regression equation obtained for the linear portion of the curve was:

$$A = 1.637 - 0.6588(-\log C)$$

where C is the magnesium concentration (in mol l^{-1}). The linear calibration range is sufficiently broad for application to real sample. The correlation coefficient was 0.9992, and the relative standard deviation for 11

Table 2
Maximum tolerable concentration of common species in soils in the determination of 0.05 M magnesium

Foreign species	Maximum tolerated concentration tested ($\mu g\ ml^{-1}$)
K^+	2000
Na^+	2000
NH_4^+	5000
Ca^{2+}	80
Mg^{2+}	15
Mn^{2+}	5
Zn^{2+}	10
Fe^{3+}	1
Al^{3+}	10
CO_3^{2-}	3000
SO_4^{2-}	5000
NO_3^-	1000
PO_4^{3-}	500
Cl^-	2000

replicate injections of 0.05 M Mg^{2+} was 1.3%. A sampling frequency of 90 h^{-1} was achieved.

Study of interferences

A systematic study of the effect of potentially interfering species on the determination of magnesium commonly found in soils was performed by using the CEC determination manifold. The results obtained were shown in Table 2, tolerated limits were taken as the largest amounts yielding a relative error of less than 5% in the absorbance. No interference is to be expected in practice because saturating the soil with barium chloride before the magnesium solution to be added is bound to avoid interferents when processing real samples. In this way, most interferents present in soil (including soluble Ca^{2+} and Mg^{2+}) are removed by the excess of barium, and residual barium in the soil is retained on the filter as precipitated $BaSO_4$ after $MgSO_4$ is added. As a result, any residual interferents should be at concentrations below the tolerated limit for magnesium determination and thus have a negligible effect on the results in most of instances.

3.3. Application to real samples

The proposed method was applied to the determination of CEC in various types of soils by using 0.5 g of accurately weighed, previously air-dried, powdered and homogenized soil sample (particle size i.e. <2 mm), and transferring it to the filter cartridge, through which the barium(II) solution was added over an interval equivalent to using a volume of 5 ml, selected via SV_1, this solution was circulated in the closed loop unit during this period, after which, the filtrate produced was sent to waste by switching SV_2 to position 1, and after about 2 min, switching to the magnesium solution (5 ml) via SV_1 in order to treat the soil retained in the filter cartridge. SV_2 was then switched to position 2 so that the solution was circulated through the closed-loop system. After 2 min, SV_2 was switched to position 3, the filtrate was driven to the loop of the injection valve and residual magnesium in the filtrate was determined spectrophotometrically in the CEC determination manifold. The CEC of the soil concerned can be calculated from the difference between the Mg^{2+} concentrations (in mol l^{-1}) in the initial and residual solution: CEC (mmol/100 g air-dried soil) $= \{([Mg^{2+}]_{init} - [Mg^{2+}]_{res})/m\}V \cdot 100$, where m is the weight of soil sample (in gram) and V is the volume of extractant used (5 ml).

As can be seen in Table 3, the results thus obtained were consistent with those provided by the reference manual method [15,20]. The sampling frequency was about 10 h^{-1} which is quite high relative to the manual method. The reproducibility of the determination, evaluated from repeated detection of a soil sample containing 13.99 mmol/100 g soil of CEC, was 2.9%, expressed as the R.S.D. ($n=6$). After finishing each

Table 3
Determination of the CEC of soils by the proposed and the reference method (exchanged by Mg^{2+})

Soil sample	pH [a]	CEC (mmol/100 g soil) ($n=3$)	
		Proposed method	Reference method
1 (franco I)	8.47	9.95 ± 0.05	9.75 ± 0.05
2 (franco III)	8.52	8.65 ± 0.10	8.35 ± 0.45
3 (clayey)	8.49	19.80 ± 0.25	20.05 ± 0.40
4 (clayey)	8.61	14.00 ± 0.45	13.90 ± 0.15
5 (franco II)	8.26	7.85 ± 0.20	7.95 ± 0.30
6 (clayey)	8.55	13.95 ± 0.40	14.00 ± 0.20
7 (clayey)	8.64	11.75 ± 0.25	11.45 ± 0.10
8 (sandy)	8.54	6.65 ± 0.05	6.65 ± 0.20
9 (sandy)	8.76	7.00 ± 0.10	6.95 ± 0.30

[a] Determined by the method recommended in Ref. [15].

determination, the filter could be regenerated a few times by removing accumulated soil with gentle water washing; otherwise, the low cost of filter paper and the simplicity of the filter cartridge design facilitate replacement of the filter.

4. Conclusions

The proposed method, based on the joint use of a sample pretreatment unit and a flow manifold for the photometric determination of residual Mg^{2+}, provides satisfactory results in the determination of soil CEC, that are consistent with those obtained by using the reference manual method. In comparison with the manual method, this proposed procedure is simpler, faster and more reliable, because the manipulation of the soil samples is dramatically reduced due to the fact that the entire pretreatment is done in the filter cartridge included in the flow system.

Acknowledgements

Financial support provided by the CICyT (Project No. PB93-0717) is gratefully acknowledged.

References

[1] S.M. Ramasamy and H.A Mottola, Anal. Chem., 54 (1982) 283.
[2] A. Ríos, M.D. Luque de Castro, M. Valcarcel and H.A. Mottola, Anal. Chem., 59 (1987) 666.
[3] F. Cañete, A. Ríos, M.D. Luque de Castro and M. Valcárcel, Anal. Chim. Acta, 224 (1989) 127.
[4] H.F.Bergamin, F.J. Krug, E.A.G. Zagatto, E.C. Arruda and C.A. Coutinho, Anal. Chim. Acta, 190 (1986) 177.
[5] H.F. Bergamin, F.J. Krug, B.F. Reis, J.A. Nobrega, M. Mesquita and I.G. Souza, Anal. Chim. Acta, 214 (1988) 397.
[6] F. Lázaro, M.D. Luque de Castro and M. Valcárcel, Anal. Chim. Acta, 242 (1991) 283.
[7] S. McLeod, Anal. Chim. Acta, 266 (1992) 107.
[8] S. McLeod, Anal. Chim. Acta, 266 (1992) 113.
[9] Z. Zhi, A. Ríos and M. Valcárcel, Anal. Chim. Acta, 293 (1994) 167.
[10] M. Valcárcel, M.D. Luque de Castro and M.T. Tena, Anal. Proc., 30 (1993) 276.
[11] M. Valcárcel and M.D. Luque de Castro, Non-chromatographic Continuous Seperation Technique, The Royal Society of Chemistry, Cambridge, 1991.
[12] M. Valcárcel and M. Gallego, Trends Anal. Chem., 8 (1989) 34.
[13] V. Kubán, Fresenius' J. Anal. Chem., 346 (1993) 873.
[14] Z. Zhi, A. Ríos and M. Valcárcel, Int. J. Environ. Anal. Chem., 54 (1994) 1.
[15] S.E. Allen, H.M. Grimshaw, J.A. Parkinson and C. Quarmby, Chemical Analysis of Ecological Matericals, Blackwell, Oxford, 1974, pp. 50–51.
[16] L.P. Little, Aust. J. Soil Res., 27 (1989) 117; Anal. Abstr., 52 (1990) 4G2.
[17] C.L. Bascombe, J. Sci. Food Agr., 15 (1964) 821; Chem. Abstr., 62 (1965) 15369-F.
[18] Z. Marczenko, Spectrophotometric Determination of Elements, Ellis Horwood, Chichester, 1976, p. 332-4.
[19] F. Cañete, A. Rios, M.D. Luque de Castro and M. Valcárcel, Analyst, 112 (1987) 267.
[20] E. Primo and J.M. Carrasco, Determinación del Cambio Catiónico de los Suelos, in Química Agrícola, Alhambra, Madrid, 1986, p.273.

ELSEVIER

Analytica Chimica Acta 298 (1994) 393–399

ANALYTICA CHIMICA ACTA

A fast, highly efficient, continuous degassing device and its application to oxygen removal in flow-injection analysis with amperometric detection

Jairo J. Pedrotti, Lúcio Angnes, Ivano G.R. Gutz *

Instituto de Química, Universidade de São Paulo, Caixa Postal 20780, 01498 - 970 São Paulo, SP, Brazil

Received 5 April 1994; revised manuscript received 22rd June 1994

Abstract

A new continuous degassing device, based on the permeation of gases dissolved in a liquid through the walls of a narrow-bore polymeric tube, is described. The key innovation, responsible for the superior efficiency in relation to other designs, consists in maintaining a reduced pressure of an inert gas (N_2, ca. 1600 Pascal) in the degassing chamber that contains the coiled polymeric tube wandered by the solution. When applied to the continuous removal of oxygen from an electrolyte in flow-injection analysis, FIA, with amperometric detection (flow of 1.0 ml/min, 34 s residence time), a decrease of at least 99.97% in the oxygen reduction current is experienced. Routine determination of 80 samples per hour of heavy metals like cadmium is afforded with a detection limit of about 10 ppb (1.8×10^{-12} mol of Cd(II) for 20-μl injections), by using a sessile drop mercury electrode. FIA with pre-concentration followed by voltammetric stripping extends the detection limit to the sub-ppb level, as illustrated by monitoring lead and cadmium in samples of drinking water.

Keywords: Amperometry; Flow injection; Flow system; Degassing; Oxygen removal; Trace metal determination

1. Introduction

Degassing of liquids and, more specifically, oxygen removal from an aqueous or non-aqueous solution, is a requirement of many analytical procedures. In voltammetric and polarographic analysis, the interference of oxygen results from its electroreduction to H_2O_2 or water, beginning near to the NHE potential and extending in the direction of negative potentials. This is one of the reasons why the application of amperometric and voltammetric detectors in flow-injection analysis (FIA) and liquid chromatography (LC) is growing rapidly only for species electroactive at potentials where oxygen does not interfere, using solid electrodes [1–3]. These low-cost techniques are very versatile, presenting a good selectivity, a wide dynamic concentration range, a rapid response and a high precision even at very low concentrations. Main drawbacks are related to long-term solid electrode performance, not observed with renewable mercury drop electrodes. Robust mercury drop electrodes that fit to low-volume flow cells are available [4,5], but for them the problem is oxygen removal.

In batch voltammetric analysis, oxygen is usually removed by the classical procedure of bubbling the sample solution with nitrogen or a noble gas. This method is time consuming (typically 10 min/sample) and not well suited for application in FIA. Even care-

* Corresponding author.

SSDI 0003-2670(94)00303-3

fully deoxygenated carrier electrolyte solutions and samples suffer recontamination during the injection operation. Diffusion of oxygen through the walls of the polymeric plastic tubing widely used in FIA is also significant. Substitution of plastic tubing by stainless steel, as done in LC, avoids this problem [6], but in aggressive medium it can be a source of metal ion contamination. Other available methods for oxygen removal from flow systems can be classified as chemical, electrolytic, photochemical and physical methods.

Chemical methods rely on the reaction of dissolved oxygen with a reagent added to the solution or immobilized in a reactor. No ideal reagent has been found and its choice depends on the pH of the solution. In neutral or alkaline solutions, sulfite is frequently used [7,8]. Ascorbic acid [9] or a column packed with zinc particles [10] are alternatives for acidic media. Introduction of impurities into the flowing solution, eventually increasing the background current, can be a drawback.

The base of electrolytic methods is the electrochemical reduction of oxygen (and other reducible impurities) of the electrolyte before it reaches the injection valve. A scrubber based on this principle and employing a porous silver electrode results in a 100-fold reduction of background current in comparison to nitrogen purge [11]. A coulometric cell with a mercury-coated reticulated vitreous carbon electrode can be used for the same purpose [12]. In general, these methods are unable to remove oxygen that accompanies the injected sample, because they act prior to the injector. The scrubbing cell can be placed between the injector and the detector only when the reduction of the species of interest in the sample sets in at potentials more negative than the oxygen reduction. The determination of Zn(II) constitutes a favorable example [12].

Photochemical methods are based on the reaction of oxygen with an organic acid like formic, citric and oxalic acid under UV irradiation. This kind of reaction has been applied to stationary cells [13] or continuous removal from flowing solutions [14], combined with anodic stripping voltammetry. A high concentration of the acid must be added to the electrolyte (1 M) and an irradiation time of many minutes is required to attain an acceptable efficiency.

Physical methods embrace: decrease in the concentration of oxygen in the solution by displacement with an inert gas under heating to 40°C to keep the dissolved gas concentration low [15]; mixing of sample solutions with excess of deaerated supporting electrolyte [16]; combination of previous inert gas bubbling with the gas-segmented stream [17,18]; nebulization of the sample with nitrogen followed by collection of the drops [19]; exposition of a thin layer of sample flowing over a surface to a counter flow of inert gas [20] and permeation of oxygen through membranes. For this last approach, the partial oxygen pressure at the side opposed to the solution has been lowered by maintaining the tubing in a nitrogen atmosphere [21], under vacuum [22] (available also in commercial LC systems [23,24]) or immersed in solution with a reducing agent [25].

A new design of a gas permeation unit, the continuous deoxygenating device, CDD, will be presented in this paper and its superior performance demonstrated. It combines the external renewable nitrogen atmosphere concept with the reduced pressure approach. Fast and effective deoxygenation of flowing solutions was obtained in FIA with CDD and amperometric detection. Determination of cadmium(II) with a detection limit around 10 ppb (200 pg of Cd(II) for 20 μl injections) at a frequency of 80 samples/h was attained. Higher sensitivity was obtained after pre-concentration followed by stripping voltammetry, rendering the proposed system well suited for fast heavy metals surveillance in drinking water.

2. Experimental

2.1. Continuous deoxygenating device, CDD

Fig. 1 shows a schematic diagram of the degassing unit. The chamber that contains the permeation tube is a 100-ml Duran^R glass flask (A), Model no. 82.2.1330.4 from Schott. A length of 3 m silicone tube (B) with 0.5 mm I.D. and 0.2 mm wall thickness is coiled around a 2.5 × 9.5 cm metal plate (D) covered with a thick silicone tube at the edges (C). This arrangement is attached to the flask cap. Four orifices in the cap consent the inlet (G) and the outlet (E) of the flowing solution, the nitrogen inlet (H) and the gas outlet (F). The larger orifice (F) is connected to a mechanical vacuum pump. The deoxygenated solution is carried to the micro-cell through a fused-silica tube coated with polyimide (E), with 0.5 mm I.D., of the

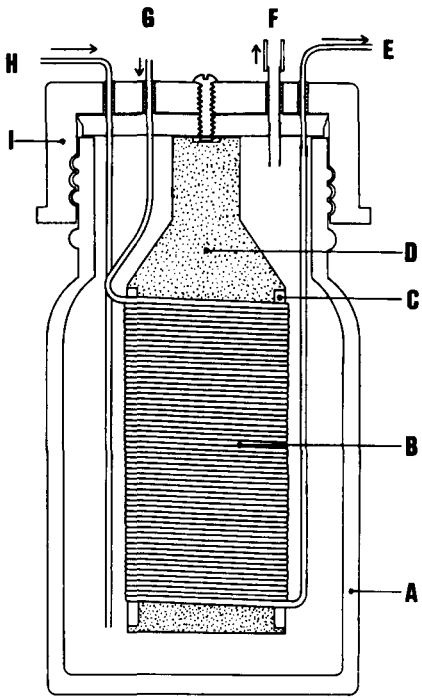

Fig. 1. Cross-section of the CDD. (A) Vacuum chamber (borosilicate glass flask); (B) permeation coil (silicone rubber tube); (C) edge protector (silicone rubber tube, with longitudinal slit); (D) coil support (brass plate fixed to the flask cap); (E) solution outlet (fused silica tube covered with polyimide); (F) connection to the vacuum pump; (G) solution inlet; (H) nitrogen inlet; (I) glass flask cap.

type used as capillary column in gas chromatography. This prevents the re-contamination of the test solution with atmospheric oxygen.

2.2. Apparatus

The flow-injection system is constituted of a Ismatec peristaltic pump Model MS REGLO, a home-made injector with a 20- or 500-μl loop, the CDD (Fig. 1), the automatic mercury electrode [4] and voltammetric microcell previously described [5]. Amperometric and stripping experiments were performed by using an EG&G PAR Model 273 potentiostat or Model 264A voltammetric/stripping analyzer, connected to an *X–t* recorder model L6512B from Linseis or to an *X–Y* recorder Model RE0089 from Houston. The potential values applied to the mercury drop electrode were measured against a small sized Ag/AgCl (sat. NaCl) reference electrode. A stainless steel tube placed downstream to the working electrode acts as an auxiliary electrode. The injection valve was operated manually. Reduced pressure in the CDD chamber was obtained with a Leybold 52 (E. Leybold's Nachfolger) mechanical vacuum pump. All measurements were performed at room temperature (25 ± 2°C).

2.3. Reagents

Solutions of $Cd(NO_3)_2$, $Pb(NO_3)_2$, $NaClO_4$ and $HClO_4$ were obtained from analytical grade reagents. Water used as solvent was filtered, distilled, and purified with a Nanopure system. Sodium perchlorate for the electrolyte was recrystallized twice from water. 1.0×10^{-2} M Cd(II) and Pb(II) stock solutions were prepared by dissolving the nitrates in 25 mM perchloric acid solution. Synthetic samples were obtained just before use by dilution of the metal stock solutions with 10 mM $NaClO_4$ + 2.5 mM $HClO_4$ solution, also used as the carrier electrolyte. Tap water samples were collected in the laboratory. $NaClO_4$ and $HClO_4$ were added to match the concentration of the carrier. Mercury for the electrode was chemically purified and doubly distilled under vacuum.

3. Results and discussion

The oxygen interference on a huge part of the potential window accessible to mercury electrodes has been an obstacle to more extensive use of electrochemical detection with this electrode in FIA and LC. A hydrodynamic voltammogram of oxygen for a solution in equilibrium with air, obtained with the FIA system described in the experimental section, is shown in Fig. 2A.

The oxygen wave hinders the observation of the response of electroactive species present at low concentrations. The electrochemical reduction generates H_2O_2 and/or OH^-, and can lead to secondary products, as hydroxy complexes, or act as an oxidant of the analyte, with consequent disturbance of the analytical information [26]. The oxygen wave and associated interferences are virtually eliminated after intercalating the CDD between the sample injector and the electrochemical cell, as shown in Fig. 2B. The true O_2 reduction current is even lower than recorded in this figure because the capacitive current originated from the linear potential scan has not been subtracted.

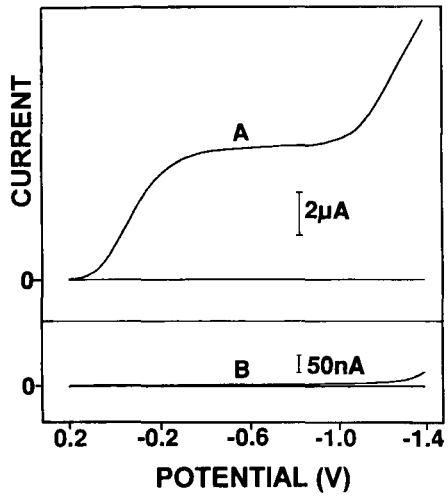

Fig. 2. Hydrodynamic voltammogram of a 10 mM $NaClO_4$ solution (A) without oxygen removal (CDD open to the atmosphere) and (B) continuously degassed with CDD. Scan rate, 10 mV/s; sessile mercury drop electrode; flow-rate, 1.0 ml/min.

The CDD allows direct comparison of the efficiency of exposing the permeation tube to nitrogen at atmospheric pressure, vacuum or nitrogen at low pressure. The dynamic response for oxygen removal from flowing solutions was evaluated by measuring the O_2 reduction current at the AME starting with the chamber opened to the air and switching to one of the mentioned conditions. Sodium perchlorate at a flow-rate of 1 ml/min was used as electrolyte. All i versus t curves present a nearly exponential decay of the current but the time constants and final steady state currents depend on the working condition. Table 1 summarizes data extracted from these curves and presents the estimated efficiencies of O_2 removal.

Three minutes are necessary to reduce the amperometric signal to nearly 10% of its initial value when nitrogen flows through the chamber at ambient pressure (condition A). When the CDD is operated at reduced pressure (conditions B, C and D), this happens in less than 50 s, revealing faster achievement of steady state operation. Efficiencies were evaluated from the ratio of the initial current (no degassing) and constant currents measured after 20 min of operation. For condition A, the efficiency decays by using flow-rates below 90 ml N_2/min and shows no improvement at higher values. Table 1 reveals that evacuation of the CDD to 400 Pascal (ca. 3 mmHg) without N_2 flow (condition B) is less effective then condition A. A significantly higher efficiency is obtained at the N_2 flow-rate of condition A, with the CDD maintained at ca. 2700 Pascal, proving the advantages of the combination of both resources. It is possible to optimize the efficiency of O_2 removal for a given vacuum pump, by adjusting the N_2 flow. This was done in condition D where an efficiency of 99.97% was attained.

As mentioned, the performance of the device increases by lowering the pressure in the chamber, under continuous inert gas purging. If necessary, the presented results can be probably improved by employing a more efficient vacuum pump. The evaluation of O_2 concentrations at the ppb level based on the reduction current can be affected to an unknown extent by the presence of traces of other species contaminating the electrolyte, electroreducible at -0.8 V. As a consequence, the efficiency presented in Table 1 can even be underestimated.

The residence time of the solution in the CDD for the conditions of Table 1 (flow-rate of 1.0 ml/min) is

Table 1
Amperometric examination of the CDD efficiency under different experimental conditions, for a 10 mM $NaClO_4$ solution at flow-rate of 1 ml/min, residence time of 34 s with cathodic current measured at -0.800 V

Parameter	CDD operation conditions				
	Open	A	B	C	D
Pressure inside CDD chamber (kPascal)	93	93	0.40	2.70	1.60
N_2 flow (ml/min)	0	90	0	90	20
CDD response time (90% decrease in current) (s)	–	180	45	37	37
Steady state ($t > 20$ min) current (nA)	6.19×10^3	12.4	18.8	5.9	2.0
Current decrease factor	1	500	330	1050	3100
O_2 removal efficiency (%)	0	99.80	99.70	99.90	99.97
Residual dissolved O_2 (ppb)	1.6×10^4	32	49	15	5.2

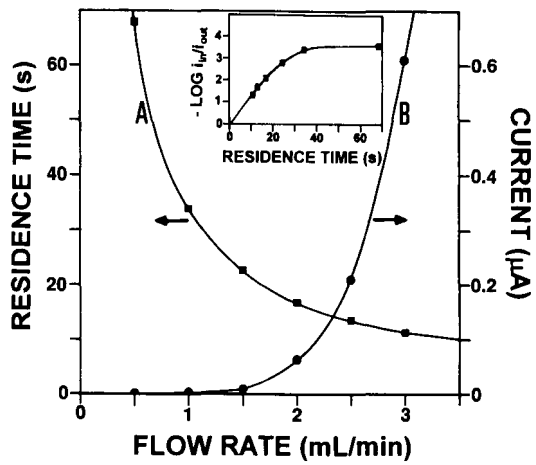

Fig. 3. Effect of solution flow-rate and residence time on the O_2 removal efficiency. (A) Residence time of the solution in the CDD; (B) amperometric O_2 reduction current; (inset) efficiency of O_2 removal. 10 mM $NaClO_4$ electrolyte, −0.80 V vs. Ag/AgCl, degasser at 400 Pascal and 20 ml/min N_2 input flow.

approximately 34 s. As expected, the oxygen removal efficiency is dependent on this residence time. Its effect was investigated by changing the peristaltic pump speed and, consequently, the flow-rate. Experimental results obtained over the range of 0.5 to 3.0 ml/min appear in Fig. 3. A nearly exponential increase in the residual O_2 concentration (proportional to i_d) with the flow-rate appears on curve B. The logarithm of the ratio of the O_2 i_d measured without and with degassing is plotted versus the residence time in the inset of Fig. 3 to show that at residence times higher than 25 s (flow-rate below 1.3 ml/min), more than 99.9% of the original O_2 is removed. Comparable residence times and efficiencies can be obtained at higher flow-rates by using longer silicone tubing coil. The upper limit is dictated by pressure build up in the CDD or peak broadening in FIA operation.

Unnecessary to say that the degassing efficiency is affected by other parameters, maintained constant in the present study, such as the internal diameter and the thickness of the walls of the tube, the O_2 permeability of the polymer, the operating temperature and the viscosity of the fluid. In very alkaline medium, or in non-aqueous solvents, it may be necessary to substitute the silicone tube for another chemically resistant material. In comparison with silicone, most other polymers are much less permeable to gases [2]. To attain comparable O_2 removal efficiency, longer pathways (or residence times) are required, eventually leading to significant peak broadening, as a result of increased sample dispersion. This problem can be alleviated by using two CDDs, with gas lines connected in series. The first unit, with extended tube length, is placed just before the injector, and the second one, with a shorter path, at the input of the detector cell.

An intrinsic advantage of a CDD operated under reduced gas pressure is the removal of bubbles and the decrease in dissolved gas content of the flowing solution. This characteristic is interesting not only for electroanalytical but also for spectrophotometric and some other detection techniques.

To demonstrate the practical application of the CDD, experiments of FIA with amperometric detection were performed with and without oxygen removal. Without oxygen extraction, a high background current is present (5.5 μA) and the lowest detectable cadmium concentration is of the order of 5×10^{-5} M, as shown in Fig. 4A. When the dissolved oxygen is eliminated, the background current decreases to less 5 nA, part of it originated by the reduction of a minimum fraction of the H^+ present in the electrolyte (absent in Fig. 3). So, for injections of 1×10^{-5} M of cadmium, the sharp peaks shown in the Fig. 4B are obtained. Under these conditions, a detection limit of 1×10^{-7} M can easily be attained.

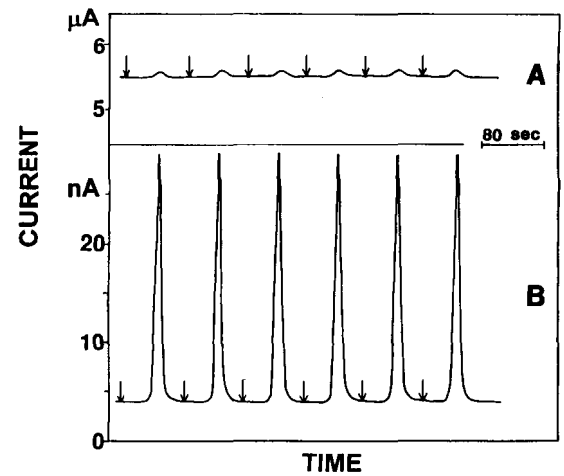

Fig. 4. FIA with amperometric detection of: (A) 50 μM of cadmium, without oxygen removal (CDD open to the atmosphere) and (B) 10 μM of cadmium, with continuous oxygen removal (CDD at 400 Pascal, 20 ml/min N_2 input flow). Arrows indicate sample injections. 10 mM $NaClO_4$ + 2.5 mM $HClO_4$ electrolyte.

Fig. 4 also demonstrates the remarkable dynamics of the whole CDD FIA system. Using a 20-μl sample loop and a flow-rate of 1 ml/min, the time interval between the injection (indicated by arrows on the figure) and the rise of the amperometric signal is of 34 s. In this short time the solution travels from the injector valve to the detector, passing the 3-m silicone tube, where the oxygen elimination takes place. Slight solvent loss by evaporation is expected in the CDD. However, as standards and samples are subjected to the same conditions, no relative errors are observed. The short tails after the peaks and the stability of the base line are good indications of the absence of memory effects. Under these conditions, successive determinations can be performed in 45 s, allowing the injection of 80 samples per hour. In cases where the flow-rate is not critical and a higher O_2 content can be tolerated, a substantial increase in the sample throughput is achievable.

Other important features of the described system are the high reproducibility and long-term stability. A series of 20 successive injections of 20-μl samples of 1×10^{-5} M cadmium was done during 19 min. The current was monitored amperometrically on the same mercury drop and the peak heights (31.9 nA) present a relative standard deviation of 0.7%. For these injections at nearly every minute, the base line was also very stable and reproducible (4.86 ± 0.19 nA). The residual current is somewhat higher here then shown in Table 1 because the electrolyte was acidified with $HClO_4$.

The observed performance compares favorably with other analogous FIA systems and suffers no degradation when mercury drops are renewed between sample injections, thanks to the high reproducibility of the mercury sessile drop electrode [4], with negligible contribution to the overall standard deviation. This result confirms the advantages of renewable mercury drop electrodes when compared to solid ones.

Increased sensitivity of the CDD FIA system can be obtained by using well-known preconcentration and stripping techniques. The potentiality of this approach was demonstrated by monitoring lead and cadmium (in sub-ppb levels) in tap water by the stripping analysis technique. Well-defined peaks are observed for concentrations of metals in the nanomolar range and standard additions to the sample lead to linear peak height plots. The analysis of a sample of drinking water serves as an example. The straight lines defined by the experimental points (sample plus four standard additions) presented very similar slopes for both metals, with small standard deviation. For cadmium it was 0.46 nA/nM ($s=0.020$) and for lead 0.45 nA/nM ($s=0.013$). The corresponding correlation coefficients were 0.994 and 0.997. Extrapolated concentrations and confidence levels (90%) of lead(II) and cadmium(II) in the sample were 0.69 ± 0.13 ppb (ca. 3.3×10^{-9} M) and 0.16 ± 0.05 ppb (ca. 1.5×10^{-9} M).

4. Conclusion

Evaluation of the proposed CDD has revealed expressive progress in lowering the dissolved oxygen content of flowing solutions, in comparison to previously described permeation devices. The association of the CDD with a trustworthy and long lasting automatic mercury electrode with a PTFE tip, adapted to a microcell with very low response volume, previously developed in the authors' laboratory [4,5], resulted in an FIA system with excellent characteristics. It allows rapid and sensitive determinations of electroactive species at trace level or, in combination with pre-concentration, ultra-trace level, and presents great potentiality for surveillance purposes. The system is also sufficiently light and rugged to be considered in field operation. An automated, microcomputer controlled version, now in final stage of development, will support a high sample throughput and permit synchronous execution of fast techniques as square wave voltammetry. The sensitivity and selectivity of methods using adsorptive pre-concentration can also be explored.

The proposed design of the CDD combines simplicity with efficiency. Although designed originally for electroanalytical application, the concept of the proposed CDD will probably find use in other branches where oxygen removal is necessary, like in LC and in fluorimetric analysis.

In short, it was demonstrated that a permeation CDD operated under reduced pressure and fluxed with renewable inert gas, proportionates higher efficiency than using vacuum alone (preferred in commercial systems) or nitrogen at atmospheric pressure, (described in the literature).

Acknowledgements

The authors acknowledge CNPq (Conselho Nacional de Desenvolvimento Científico e Tecnológico, Brazil), for grants (I.G.R.G. and L.A.) and scholarship (J.J.P.).

References

[1] K. Stúlik and V. Pacáková, CRC Crit. Rev. Anal. Chem., 14 (1984) 297.
[2] K. Stúlik and V. Pacáková, Electroanalytical Measurements in Flowing Liquids, Ellis Horwood, Chichester, 1987.
[3] D.C. Johnson, M.D. Ryan and G.S. Wilson, Anal. Chem., 60 (1988) 147R.
[4] J.J. Pedrotti, L. Angnes and I.G.R. Gutz, Electroanalysis, 4 (1992) 635.
[5] I.G.R. Gutz, L. Angnes and J.J. Pedrotti, Anal. Chem., 65 (1993) 500.
[6] J.B.T. Lloyd, Anal. Chim. Acta, 199 (1987) 161.
[7] B. Persson and L. Rosén, Anal. Chim. Acta, 123 (1981) 115.
[8] A.M. Bond, H.A. Hudson P.A. and Van Den Bosch, Anal. Chim. Acta, 127 (1981) 121.
[9] T.M. Florence and J.Y. Farrar, J. Electroanal. Chem., 41 (1973) 127.
[10] W.A. McCrehan and W.E. May, Anal. Chem., 56 (1984) 625.
[11] H.B. Hanekam, W.H. Voogt, P. Bos and R.W. Frei, Anal. Chim. Acta, 118 (1980) 81.
[12] J. Wang and H.D. Dewald, Anal. Chem., 55 (1983) 933.
[13] E.A. Zakharova and V.N. Volkova, J. Anal. Chem. USSR, 39 (1984) 508.
[14] J.N. Barisci and G.G. Wallace, Electroanalysis, 4 (1992) 323.
[15] U. Baltensperger and R. Eggli, Anal. Chim. Acta, 123 (1981) 107.
[16] S. Silvestri, Pharm. Acta. Helv., 47 (1972) 209.
[17] L.F. Cullen, M.P. Brindle and G.J. Papariello, J. Pharm. Sci., 62 (1973) 1708.
[18] W. Lund and L. Opheim, Anal. Chim. Acta, 79 (1975) 35.
[19] C. Yarnitzky and E. Ouziel, Anal. Chem., 48 (1976) 2024.
[20] C.N. Yarnitzky, Electroanalysis, 2 (1990) 581.
[21] A. Trojánek and K. Holub, Anal. Chim. Acta, 121 (1980) 23.
[22] R.E. Reim, Anal. Chem., 55 (1983) 1188.
[23] Hewlett Packard, Product Brief, publication number 12-5091-2870E.
[24] Knauer, On-line Solvent Degassing, Brief of Product no. A1050.
[25] M.E. Rollie, G. Patonay and I.M. Warner, Anal. Chem., 59 (1987) 180.
[26] J. Wang, Stripping Analysis: Principle, Instrumentation and Applications, VCH Publishers, Deerfield Beach, FL, 1985.

ELSEVIER

Analytica Chimica Acta 298 (1994) 401–404

ANALYTICA CHIMICA ACTA

Flow-injection spectrofluorimetric determination of sulphate using calcein and zirconium

N. Chimpalee [a], D. Chimpalee [a], S. Suparuknari [a], B. Boonyanitchayakul [a], D. Thorburn Burns *,[b]

[a] *Department of Chemistry, Faculty of Science, Silpakorn University, Nakorn Pathom 73000, Thailand*
[b] *Department of Analytical Chemistry, The Queen's University of Belfast, Belfast BT9 5AG, UK*

Received 25 April 1994

Abstract

Sulphate can be determined spectrofluorimetrically ($\lambda_{em} = 505$ nm, $\lambda_{ex} = 410$ nm) based on the formation of a ternary complex between sulphate, zirconium and calcein in a flow-injection system. The carrier stream was deionised water and the reagent streams were 100 μg ml^{-1} Zr (as $ZrOCl_2$) in 1% (v/v) hydrochloric acid, and 40 μg ml^{-1} calcein in 0.1 M potassium hydroxide. The injection rate was 50 h^{-1}. The calibration graph was linear up to 25 μg ml^{-1} SO_4^{2-} based on 250-μl injection volumes. The relative standard deviation ($n = 10$) was 1.95% for 10 μg ml^{-1} SO_4^{2-}; the detection limit was 0.82 μg ml^{-1} SO_4^{2-}. The system has been applied to the determination of sulphur in NIST coal samples after oxygen bomb combustion.

Keywords: Flow injection; Fluorimetry; Calcein; Sulphate; Zirconium

1. Introduction

Pollution of the environment has become a major concern to the general community. One aspect is the release of SO_2 into the atmosphere as a result of the burning of fossil fuels. The emitted SO_2 is oxidised and is then present as solid sulphate salts or as sulphuric acid mist. Both the gaseous forms and aerosol forms of atmospheric sulphur have detrimental effects on the environment. Buildings, vegetation and fresh water fish are damaged by acid rain and some human respiratory complaints are made worse by quite low concentrations of atmospheric SO_2 [1,2].

The analysis of coal for sulphur is used to evaluate potential sulphur emissions from combustion of coal or other conversion processes and to check sulphur levels against contract specifications for fuels. The most commonly used spectrophotometric procedures are based on turbidimetric measurements on dispersed barium sulphate, spectrophotometric measurements using barium chloranilate, methylthymol blue, dimethylsulphonazo III, 2-aminoperimidine, or nitrochromazo [3,4] or on spectrofluorimetric measurements using calcein blue [5], morin [6] or biacetyl monoxime nicotinylhydrazone (BMNH) [7].

* Corresponding author.

SSDI 0003-2670(94)00298-3

Of the 4000 or so papers published on flow-injection analysis (FIA) so far 23 deal with the determination of sulphate [8], usually based on spectrophotometric determination after competitive reaction with barium chelates such as those of methylthymol blue [9–16], dimethylsulphonazo III [7–19], nitrochromazo [20] 3-{2-carboxyphenylazo[-6-(2-sulphophenylazo)]-4,5-dihydroxynaphthalene}-2,7-disulphonic acid [21], sulphanazo III [22], or after reaction with barium chloranilate [23,24], or formation of $[Fe(III)SO_4]^+$ [25] or turbidimetrically using dispersed barium sulphate [9,10,26–36]. Only BMNH has been used for the fluorimetric FI determination of sulphate [37]. We now report on the first use of calcein for the spectrofluorimetric determination of sulphate in FIA, based on the formation of a ternary complex between zirconium, calcein and sulphate.

2. Experimental

2.1. Apparatus

Fluorescence intensities were measured at 505 nm (excitation wavelength 410 nm) with a Shimadzu RF-540 spectrofluorimeter fitted with a 25 μl, 1.5 mm quartz Suprasil 1 flow cell (Hellma) and recorded with a Shimadzu DR-3 data recorder. Solutions were pumped using a variable-speed peristaltic pump (MS-Reglo, Ismatec) fitted with Tygon pump tubes for all solutions. Samples were injected using an Omnifit four-way valve fitted with a by-pass coil. Flow lines were PTFE tubing (0.8 mm i.d.). Omnifit three-way connectors (''Hex'') were used for mixing the solutions. The flow system is shown in Fig. 1.

2.2. Reagents and solutions

For the sulphate standard solution (1000 μg ml^{-1} SO_4^{2-}), 0.7400 g anhydrous sodium sulphate (puriss, Fluka) was dissolved in 500 ml of deionized water. Working standard solutions were prepared by suitable dilution as required.

The calcein stock solution (1000 μg ml^{-1} calcein) was prepared by dissolving 0.2500g of calcein (puriss, Fluka) in 250 ml of 0.1 M KOH. This solution was stored in a plastic bottle and kept in a refrigerator.

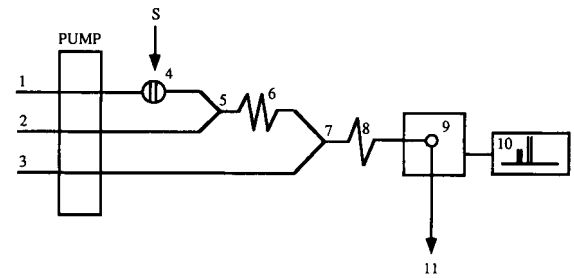

Fig. 1. Schematic diagram of the flow-injection system: (1) deionized water at 1.80 ml min^{-1}; (2) 100 μg ml^{-1} zirconium solution at 1.80 ml min^{-1}; (3) 40.0 μg ml^{-1} calcein solution at 1.80 ml min^{-1}; (4) sample injector (250 μl); (5, 7) mixing points (Omnifit three-way connector, ''Hex''); (6) mixing coil (200 cm × 0.8 mm i.d.); (8) reaction coil (100 cm × 0.8 mm i.d.); (9) spectrofluorimeter; (10) recorder, (11) waste.

The calcein working solution (40 μg ml^{-1} calcein) was prepared daily, as required, by dilution of 15 ml of calcein stock solution to 250 ml with 0.1 M KOH.

The zirconium solution (100 μg ml^{-1} Zr as $ZrOCl_2$) was prepared by dissolving 0.176 g of $ZrOCl_2 \cdot 8H_2O$ in 500 ml of 1% (v/v) HCl.

Deionized water was used throughout and reagents were of analytical-reagent grade unless indicated otherwise.

2.3. General procedure

Samples and standard were examined using the flow system and conditions given in Fig. 1.

2.4. Bomb combustion procedure for coal samples

The procedure is based on the ASTM D 3177 ''Total Sulphur in the Analysis Sample of Coal and Coke'' [38] and ASTM E 144 ''Standard Practice for Safe Use of Oxygen Combustion Bombs'' [39].

Place accurately weighed 0.2–0.4g of pelleted coal powder in a fused-silica ignition capsule, add a fuse wire, and 10 ml of deionised water as absorbing liquid. Assemble following the bomb manufacturer's instructions and pressurise with 20 atm of oxygen. Ignite, allow the bomb to cool in water for 10 min before release of pressure. Filter the solution and washings into a 100-ml volumetric flask and make up to volume with deionised water. Dilute further as

necessary with water to achieve suitable sulphate concentrations for measurement.

2.5. Examination of the main experimental variables

The optimum experimental conditions were determined in univariate searches using a 20 μg ml^{-1} sulphate sample solution.

2.6. Effect of reagent concentrations

With the concentration of zirconium fixed at 100 μg ml^{-1} it was found that peak heights increase with increasing calcein concentration up to 40 μg ml^{-1} and decreased slowly thereafter. A calcein concentration of 40 μg ml^{-1} was therefore used in further work.

With the concentration of calcein and zirconium fixed at 40 and 100 μg ml^{-1}, respectively, the hydrochloric acid concentration in the zirconium solution was varied from 0.02 to 5% (v/v). Peak heights were found to increase with increasing acidity up to 1% (v/v) and to rapidly decrease above that, a hydrochloric acid concentration of 1% (v/v) was selected for further work.

With the concentration of calcein and acid in the zirconium solution fixed at 40 μg ml^{-1} and 1% (v/v), respectively, the concentration of zirconium was varied from 10 to 1000 μg ml^{-1}. The peak heights were found to increase with increasing the zirconium concentration up to 100 μg ml^{-1} and to decrease slowly thereafter; a 100 μg ml^{-1} zirconium concentration was thus selected.

2.7. Effect of operation variables

The effect of flow rate, reaction coil length, mixing coil length and sample injection volume were each studied under the above optimised reagent conditions.

The total flow-rate was varied from 4.0 to 8.5 ml min^{-1}. The peak heights increase with increase in the total flow-rate up to 5.5 ml min^{-1}, then remain constant up to 7.0 ml min^{-1} and decrease slowly thereafter. A total flow-rate of 5.5 ml min^{-1} was selected.

When the length of the mixing coil was fixed at 200 cm, the peak heights were found to decrease slightly with increase in length of reaction coil from 100 to 200 cm. A 100 cm reaction coil (0.8 mm i.d.) was therefore selected. Similarly, 200 cm was found to be the optimum mixing coil length.

The volume of sample injected was varied from 100 to 1000 μl by changing the length of the loop in the injection valve. The peak heights increased non-linearly with increase in sample size and the peak widths became broader. A volume of 250 μl was a compromise between sensitivity and sample injection rate.

2.8. Effect of sample acidity

The effect of hydrochloric acid in 10 μg ml^{-1} SO_4^{2-} sample solution was examined over the range 0–0.1% (v/v). Peak heights were constant up to 0.03% hydrochloric acid and increased with increase in acid concentration thereafter. In subsequent work the acid concentration was kept below 0.03%.

3. Results and discussion

A linear calibration graph ($r = 0.998$, $n = 6$) was obtained up to 25 μg ml^{-1} sulphate. The relative standard deviation for the determination of 15 μg ml^{-1} SO_4^{2-} was 1.95% (10 replicates). The effect of possible interferents in the determination was examined using 10 μg ml^{-1} sample solutions. The results are summarised in Table 1. The method is thus most suitable for use after separation of SO_4^{2-} from ma-

Table 1
Effect of diverse ions on the determination of 10 μg ml^{-1} SO_4^{2-}

Ion	Ratio to SO_4^{2-} (w/w)	Change in peak height (%)
Fe^{3+}	1	−14
Ca^{2+}	1	+62
Mg^{2+}	1	+41
Cu^{2+}	1	+19
Co^{2+}	1	+59
Ba^{2+}	1	−59
Ni^{2+}	0.5	−47
PO_4^{3-}	1	+45
F^-	0.10	+38
NO_3^-, Na^+, K^+, Cl^-	10	0

Table 2
Determination of sulphur in NIST coal samples

Samples	Certified values [%(w/w)S]	Sulphur found [a] [%(w/w)S]
NIST-SRM 1682a Subbituminous	0.49	0.486 ± 0.006
NIST-SRM 2692 Bituminous	1.11	1.12 ± 0.02
NIST-SRM 1632b Bituminous	1.89	1.89 ± 0.06
NIST-SRM 2685a Bituminous	4.73	4.73 ± 0.05

[a] Mean ± standard deviation for five replicates.

trix elements by, for example, ion exchange or by absorption of gaseous products of combustion.

The results for the analysis of sulphur in coal samples (Table 2) were in acceptable agreement with certified or prior measured values. The method is sensitive, simple to operate and more rapid (50 injections h^{-1}) than when using the method in a manual format.

References

[1] P. O'Neill, Environmental Chemistry, 2nd edn., Chapman and Hall, London, 1993.
[2] P. Brimblecombe, Air Composition and Chemistry, Cambridge University Press, Cambridge, 1986.
[3] W.J. Williams, Handbook of Anion Determination, Butterworth, London, 1979.
[4] F.D. Snell, Photometric and Fluorometric Methods of Analysis, Non Metals, Wiley, New York, 1981.
[5] L.A. Tan and T.S. West, Analyst, 96 (1971) 281.
[6] J.C. Guyon and E.J. Lorah, Anal. Chem., 38 (1966) 155.
[7] S. Rubio, A. Gomez-Hens and M. Valcarcel, Talanta, 32 (1985) 203.
[8] D. Chen, M.D. Luque de Castro and M. Valcarcel, Analyst, 116 (1991) 1095.
[9] J. Müller and B. Winter, Fresenius' Z. Anal. Chem., 320 (1985) 451.
[10] A.B. Marsden and J.F. Tyson, Anal. Proc., 26 (1986) 157.
[11] B.C. Madsen and R.J. Murphy, Anal. Chem., 53 (1981) 1924.
[12] B. Koch, Fresenius' Z. Anal. Chem., 321 (1988) 707.
[13] J.F. van Staden and A. van Rensburg, S. Afr. J. Chem., 43 (1990) 78.
[14] E.A. Jones, Anal. Chim. Acta, 156 (1984) 313.
[15] W. Ripl and J. Michel, Int. J. Environ. Anal. Chem., 34 (1988) 109.
[16] M. Karlsson, J.Å. Perrson and J. Müller, Anal. Chim. Acta, 244 (1991) 109.
[17] O. Kondo, H. Miyata and K. Tôei, Anal. Chim. Acta, 134 (1982) 353.
[18] S. Nakashima, M. Yagi, M. Zenki, M. Doi and K. Tôei, Fresenius' Z. Anal. Chem., 317 (1984) 29.
[19] H.F.R. Reijnders, J.J. van Staden and B. Griepink, Fresenius' Z. Anal. Chem., 300 (1980) 273.
[20] V. Kuznyecov and H.M. Magdolna, Magy. Kem. Foly. 88 (1982) 569.
[21] J.D. Eremina, L.K. Shpigun and Yu. Zolotov, Zh. Anal. Kim., 42 (1987) 1631.
[22] T. Korenaga, K. Okada, T. Takahashi and T. Moriuake, Bunseki Kagaku, 39 (1990) T129.
[23] J. Tôei, Analyst, 112 (1987) 1067.
[24] K. Ueno, F. Sagara, R. Higashi, K. Yakata, I. Yoshida and D. Ishii, Anal. Chim. Acta, 261 (1992) 241.
[25] A. Kojło, J. Michałowski and M. Trojanowicz, Anal. Chim. Acta, 228 (1990) 287.
[26] F.J. Krug, B. Filho, E.A.G. Zagatto and S.S. Jørgensen, Analyst, 102 (1977) 503.
[27] S. Baban, D. Beetlestone, D. Betteridge and P. Sweet, Anal. Chim. Acta, 114 (1980) 319.
[28] J.F. van Staden and W.D. Basson, Lab. Pract., 29 (1980) 1279.
[29] J.F. van Staden and W.D. Basson, Water Res., 15 (1981) 333.
[30] J.F. van Staden, Fresenius' Z. Anal. Chem., 310 (1982) 239.
[31] J.F. van Staden, Fresenius' Z. Anal. Chem., 312 (1982) 438.
[32] F.J. Krug, E.A.G. Zagatto, B.F. Reis, O. Bahia and A.O. Jacintho, Anal. Chim. Acta, 145 (1983) 179.
[33] J.F. van Staden, Water S.A., 12 (1986) 43.
[34] B. Xia and L. Zhang, Fenxi Huaxue, 15 (1987) 465.
[35] D.L. Heanes, Anal. Lett., 23 (1990) 675.
[36] K. Sonne and P.K. Dasgupta, Anal. Chem., 63 (1991) 427.
[37] B. Fernandez-Band, P. Linares, M.D. Luque de Castro and M. Valcarcel, Analayst, 116 (1991) 305.
[38] Annual Book of ASTM Standards 1992, Volume 5.05, Gaseous Fuels; Coal and Coke, D 3177 Total Sulphur in the Analysis Sample of Coal and Coke, ASTM, p. 327.
[39] Annual Book of ASTM Standards 1992, Volume 14.02, General Test Methods, E 144-64, Standard Practice for Safe Use of Oxygen Combustion Bombs, ASTM, p. 123.

ELSEVIER

Analytica Chimica Acta 298 (1994) 405–413

ANALYTICA CHIMICA ACTA

Kinetic determination of the surfactant sodium dodecyl sulphate by use of mixed micelles

D. Sicilia, S. Rubio, D. Pérez-Bendito *

Department of Analytical Chemistry, Faculty of Sciences, University of Córdoba, 14004 Córdoba, Spain

Received 11 March 1994; revised manuscript received 27 June 1994

Abstract

A kinetic-photometric method for the determination of the anionic surfactant sodium dodecyl sulphate (SDS) is proposed. The method is based on the accelerating effect of micelles of the surfactant on the reaction between iron(II) and 1,10-phenanthroline, which is monitored via the ferroin complex formed. While Triton X-100 micelles have no catalytic effect on the reaction, this non-ionic surfactant forms mixed micelles with SDS, thereby considerably reducing the anionic surfactant concentration at which catalysis of the complex formation reaction starts. SDS was determined over the range 50–400 μg/ml (detection limit 15 μg/ml) with a relative standard deviation of 3% for 200 μg/ml. The proposed method was applied to the direct determination of the surfactant in pharmaceuticals (three shampoos, a toothpaste and a rectal solution) with satisfactory results. The main advantages of using micellar catalysis instead of monomer properties for the determination of the surfactant include enhanced selectivity and experimental convenience (use of organic solvents is avoided), whereas its most serious disadvantage is the increased detection limit of the micellar catalysis method.

Keywords: Kinetic methods; Micelles; Sodium dodecyl sulphate

1. Introduction

Formulated detergent products for household, cosmetic, pharmaceutical and industrial utilization have become increasingly complex, particularly with the current common practice of using mixtures of surfactants in their manufacture. Qualitative and quantitative analysis of one or more surfactants in these products can be quite difficult and research in this area continues in search of more straightforward, rapid and better alternatives to existing procedures.

Two-phase titration with a surfactant of opposite charge remains the most widely used method for quantification of total ionic surfactants [1]. This technique is reliable, requires little, and inexpensive equipment, and is easy to use for product development or quality control applications. However, the procedure is fairly slow and laborious, the end-point is somewhat subjective and the toxic hazard arising from the use of chloroform is undesirable.

Spectroscopic methods have also contributed significantly to the analysis of surfactant materials [2] and, whilst UV–visible and infrared spectrometers are very common, more expensive techniques such as nuclear magnetic resonance and mass spectrometry are also available in many laboratories. Spectrophotometric methods are widely used for ionic surfactants and involve the formation of a solvent-extractable compound between the surfactant and an intensely coloured species of the opposite charge. In this context, Meth-

* Corresponding author.

SSDI 0003-2670(94)00288-6

ylene Blue is one of the most frequently used cationic dyes for the determination of anionic surfactants [3] in spite of the fact that the ensuing method is very troublesome and its sensitivity very low because of the small extractability of the ion associates of Methylene Blue with anionic surfactants.

Nearly all of the methods developed to date for the determination of surfactants are based on reactions or physico-chemical properties of their monomers in solution. This paper is the first in a series reporting a systematic study on the analytical potential of the properties of micelles and other organized media for the determination of surfactants. The study is intended to improve the analytical features of surfactant determinative methods as regards rapidity, operational simplicity and selectivity. With regard to sensitivity, the lowest surfactant concentration that can be determined by using surfactant micelles is given by its critical micelle concentration (cmc). Since the concentration at which non-ionic and ionic surfactants form micelles normally range from 10^{-2} to 10^{-5} M, new strategies for lowering the detection limits of these surfactant determinative methods need be developed. Such detection limits can be lowered by decreasing the concentration at which the surfactant aggregates into micelles through solubilization of reagents in the micelle, electrolyte effects, addition of organic solvents, modification of the solution temperature, etc. Thus, reductions by about one order of magnitude have been observed for surfactants acting as reaction catalysts [4]. One other, more effective alternative, involves using mixed micelles [5], with which the detection limit for the surfactant determination will be given by the minimum number of monomers needed in the mixed micelles for the monitored property to be observed.

Several properties exhibited by micellar aggregates can in principle be used for determining surfactants: micellar catalysis, increases in the apparent absorptivity or fluorescence of various compounds, the relation between the cmc of mixed micelles and the surfactant mole fraction, etc. In this work, the micellar catalysis of sodium dodecyl sulfate (SDS) on the reaction between 1,10-phenanthroline and iron(II) yielding the ferroin complex was used to determine the surfactant. Micellar catalysis has been frequently exploited in the last few years for improving the features of both catalytic and non-catalytic kinetic methods for the determination of inorganic and organic compounds [6]. Three assets of this property of micellar aggregates make it attractive for surfactant determinations, namely: (a) a decreased cmc in the reaction medium by about one order of magnitude relative to an aqueous solution, which should permit the determination of relatively low surfactant concentrations; (b) most reactions take place and are monitored in an aqueous medium, thus avoiding use of the organic solvents typically utilized when monomer properties are exploited for determining the surfactant; (c) since the extent of substrate solubilization in the micelle depends on the surfactant structure, some selectivity in the determination of these compounds by using micellar properties can be expected.

As shown elsewhere [7], anionic SDS micelles catalyse the Hg(II)-accelerated reaction between hexacyanoferrate(II) and 1,10-phenanthroline, which is monitored via the ferroin complex formed. These micelles allow the ferroin complex to be formed under more acidic conditions, which results in a more selective determination of Hg(II) relative to water. Since micellar catalysis by SDS was ascribed to the effect of this surfactant on the reaction between the iron(II) released from hexacyanoferrate(II) [under the catalytic action of Hg(II)] and 1,10-phenanthroline, for simplicity and expeditiousness we chose the complex-formation reaction between iron(II) and 1,10-phenanthroline for the determination of the surfactant. The non-ionic surfactant Triton X-100, which has no catalytic effect on the reaction, forms mixed micelles with SDS that permit the direct determination of the anionic surfactant at the microgram-per-millilitre level in pharmaceutical products.

2. Experimental

2.1. Apparatus

Kinetic measurements were made on a Philips PU 8625 UV/vis spectrophotometer fitted with a stopped-flow module [8] (Quimi-Sur Instrumentation, Seville). The module, furnished with an observation cell of 0.3-cm pathlength, was controlled by the associated electronics via a 640 K Mitac computer for acquisition and processing of kinetic data. The solutions in the stopped-flow module and cell compartment were kept at a constant temperature by circulating water

from a thermostated tank. A conventional stalagmometer was used for surface tension measurements in order to determine the critical micelle concentration of the surfactants [9].

2.2. Reagents

Commercially available highest grade reagents were used throughout, without further purification. A 4.0×10^{-3} M aqueous solution of 1,10-phenanthroline was made from 1,10-phenanthroline chloride monohydrate (Merck). A 1.0×10^{-3} M Fe(II) solution was prepared by dissolving 0.0392 g of $(NH_4)_2Fe(SO_4)_2\cdot6H_2O$ (Merck) in 100 ml of 5.6×10^{-2} M H_2SO_4. Aqueous solutions of sodium dodecyl sulphate (1.000 g/l, SDS, Aldrich), and Triton X-100 (3.47×10^{-2} M, Serva) were also made. The other surfactants tested, viz. sodium octylsulphate (Fluka), sodium decylsulphate (Merck), sodium dioctylsulphosuccinate (Aerosol OT, Aldrich), sodium dodecylbenzenesulfonic acid (SDBS, Aldrich), sodium 3,9-diethyl-6-tridecyl sulphate (Tergitol 7, Fluka) and Brij-35 (Merck) were prepared in a similar way.

2.3. Procedure for the determination of SDS

Two solutions (A and B) were used to fill the two 10-ml reservoir syringes of the stopped-flow module. Solution A contained between 50 and 400 μg/ml of SDS, 1 ml of 4.0×10^{-3} M 1,10-phenanthroline, 0.6 ml of 3.47×10^{-2} M Triton X-100, and distilled water to a final volume of 10 ml. Solution B contained 1 ml of 1.0×10^{-3} M Fe(II) and distilled water. After the two 2-ml drive syringes had been filled with the corresponding solutions from the reservoir syringes, 0.15 ml of each was mixed in the mixing chamber in each run. The reaction was monitored at 500 nm by recording the variation of the absorbance as a function of time at 50 ± 0.1°C. Absorbance data were collected and processed by the microcomputer using a linear regression program for application of the initial rate method. The reaction rate was determined within 2 s. Blank solutions were prepared in the same way as the samples (without SDS), and their signals subtracted from those obtained for the samples.

2.4. Determination of SDS in pharmaceutical preparations

Several pharmaceutical samples, both commercial and magistral formulations, were analysed. Their compositions are shown in Table 1. An amount of sample containing ca. 0.05 g of SDS was accurately weighed and diluted with about 50 ml of distilled water. In order to assure representativity the amount weighed for shampoo samples was that containing ca. 0.12 g of SDS. Magnetic stirring and heating at about 60°C for 30 min were used to aid dissolution of some samples. If any insoluble material was present in the solution after this treatment, it was removed by centrifugation and washed several times with distilled water. Solutions were made to 100 ml with distilled water. For shampoo samples solutions were diluted to 250 ml. The final concentration of SDS in all samples was ca. 500 μg/ml. Aliquots of 4 ml of each sample were analysed as described above. In order to obtain maximum accu-

Table 1
Determination of SDS in pharmaceuticals

Type of sample	Sample [a]	SDS nominal value	SDS found (S.D.) [b]
Commercial formulation	Binaca (toothpaste)	20 μg/mg	19.7 (0.2) μg/mg
	Micralax (rectal solution)	9 μg/mg	8.4 (0.07) μg/mg
Magistral formulation	Bacteriostatic shampoo	180 mg/ml	177 (2) mg/ml
	Antiscurf shampoo	180 mg/ml	182 (5) mg/ml
	Antifungal suspension	20 μg/mg	20 (0.5) μg/mg

[a] Composition of samples. Binaca (Reckitt and Colman, Spain): dodecyldimethyl (2-phenoxyethyl) ammonium bromide, 0.1%; sodium monofluorophosphate, 0.8%; sodium benzosulphimide, 0.1%. Micralax (IBYS laboratory, Spain): sodium citrate, 90%; sorbic acid, 0.1%. Bacteriostatic shampoo: tego betain, 13%; triethanolamine, 3%; fluid bisulphur 4%; thioxolone, 0.5%. Antiscurf shampoo: Pyrithione Zinc, 2%; Tween 80, 2%; lanaethoxyl alcohol 5%. Antifungal suspension: ketoconazole, 2%; salicylic acid, 6%; triethanolamine, 3%.
[b] Average of three determinations.

racy, the sample pH should not vary by more than ±0.05 units from that of the standards (pH 2.4).

3. Results and discussion

3.1. Optimization of the reaction conditions

In order to obtain the best possible sensitivity and lowest detection limit in the determination of SDS, two objectives were considered in selecting the most appropriate reactant concentrations, namely: (a) the accelerating effect of the surfactant on the ferroin formation reaction should be maximal, and (b) the concentration above which micellar catalysis by SDS starts should be minimal. For these reasons two types of graphs were obtained for studying each variable potentially affecting the reaction, viz initial rate vs. concentration and initial rate vs. SDS concentration. Because of the rapidity of this reaction, use of the stopped-flow technique was mandatory in order to determine its initial rate. All concentrations given in the graphs are initial concentrations in the syringes (twice the actual concentrations in the reaction mixture at time zero after mixing).

The presence of anionic micelles of SDS allowed ferroin to be formed in more acidic media. Thus, from Fig. 1A it follows that the complex was formed at about pH 1.4 and 2 in the presence (curve 2) and absence (curve 1), respectively, of the anionic micellar system. The influence of pH values ca. 2.6 on the ferroin formation reaction could not be determined because the reaction rate was too high to be monitored with the stopped-flow module used [6]. The maximum signal for a given SDS concentration was achieved at ca. pH 2.4, as shown in Fig. 1, curve 3, which was obtained by subtracting the experimental values from curve 1 and 2. The pH also influenced the concentration above which SDS exhibited micellar catalysis, as can be inferred from the intercept of the calibration graphs obtained at pH 2.4 (Fig. 1B, curve 2) and 2.2 (Fig. 1B, curve 1). The sensitivity, defined as the slope of these graphs, was not altered by this variable.

Fig. 2A shows the influence of 1,10-phenanthroline concentration on the rate of formation of ferroin. At high enough ligand concentrations (ca. 0.96×10^{-3} M), the rate of reaction in the aqueous (curve 1) and micellar (curve 2) medium coincided. This fact seemly indicates that the micellar catalysis of SDS on this reaction could be essentially arisen from concentration of the reactants at the micellar surface. Maximal acceleration by the surfactant was obtained at a 1,10-phenanthroline concentration of ca. 0.4×10^{-3} M (Fig. 2A, curve 3). On the other hand the ligand concentration had no influence on the SDS concentration above which the surfactant exhibited micellar catalysis, even though it considerably altered the sensitivity of the determination, since the intercept of the calibration graphs at two ligand concentrations did not change (Fig. 2B, curves 1 and 2). This fact means that the cmc of SDS

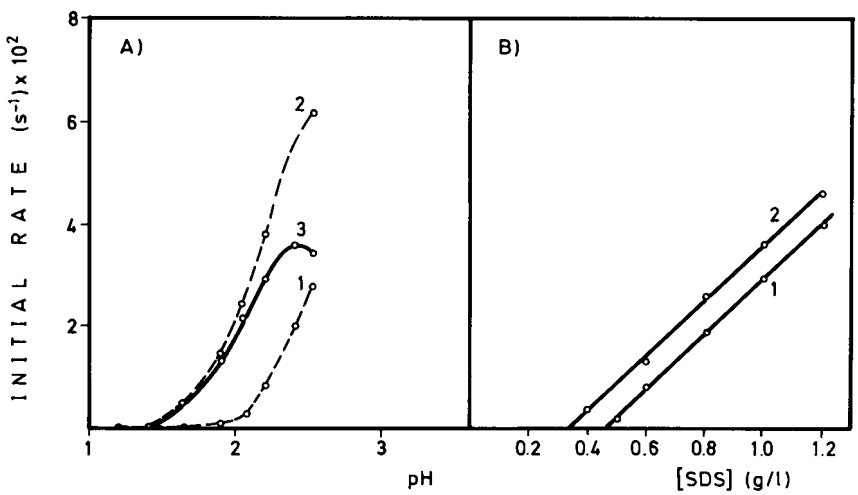

Fig. 1. (A) Influence of pH on the rate of the uncatalysed (curve 1), SDS-catalysed + uncatalysed (curve 2) and SDS-catalysed (curve 3) reaction between iron(II) and 1,10-phenanthroline. [SDS] = 1.0 g/l. (B) Calibration graphs for the determination of SDS at pH 2.2 (curve 1) and 2.4 (curve 2). Experimental conditions: Temperature = 60°C, [1,10-phenanthroline] = 4.0×10^{-4} M, [Fe(II)] = 4.0×10^{-5} M.

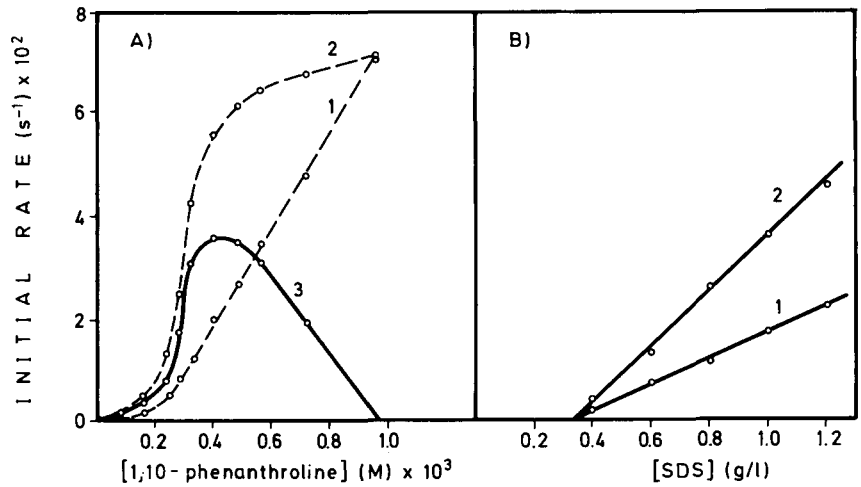

Fig. 2. (A) Influence of the 1,10-phenanthroline concentration on the rate of the uncatalysed (curve 1), SDS-catalysed + uncatalysed (curve 2) and SDS-catalysed (curve 3) reaction between iron(II) and 1,10-phenanthroline. [SDS] = 1.0 g/l. (B) Calibration graphs for the determination of SDS at a 2.8×10^{-4} M (curve 1) and 4×10^{-4} M (curve 2) 1,10-phenanthroline concentration. Experimental conditions: Temperature = 60°C, pH 2.4, [Fe(II)] = 4.0×10^{-5} M.

did not appreciable modify in the presence of 1,10-phenanthroline.

The dependence of the rate of formation of ferroin on the iron(II) concentration was similar for both the uncatalysed (Fig. 3A, curve 1) and SDS-catalysed (Fig. 3A, curve 3) reaction. An iron(II) concentration of 1×10^{-4} M was chosen as optimal for the determination of SDS. This ion had no influence on the SDS concentration above which the surfactant exhibited micellar catalysis (Fig. 3B), therefore the presence of iron(II) did not change the cmc of SDS.

The temperature, the effect of which was studied between 20 and 70°C, affected the reaction in the aqueous (Fig. 4A, curve 1) and the SDS micellar (Fig. 4A, curve 3) medium in a different way. The dependence of the initial rate on the temperature for the SDS-catalysed reaction was related to the effect of this parameter on the cmc of the surfactants. As is well known [10],

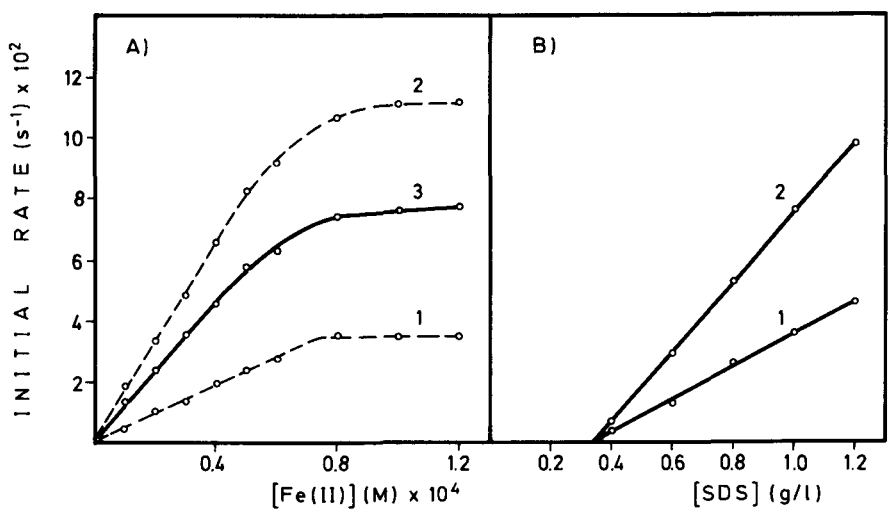

Fig. 3. (A) Influence of the iron(II) concentration on the rate of the uncatalysed (curve 1), SDS-catalysed + uncatalysed (curve 2) and SDS-catalysed (curve 3) reaction between iron(II) and 1,10-phenanthroline. [SDS] = 1.0 g/l. (B) Calibration graphs for the determination of SDS at a 4.0×10^{-5} M (curve 1) and 1×10^{-4} M (curve 2) iron(II) concentration. Experimental conditions: Temperature = 60°C, pH 2.4, [1,10-phenanthroline] = 4×10^{-4} M.

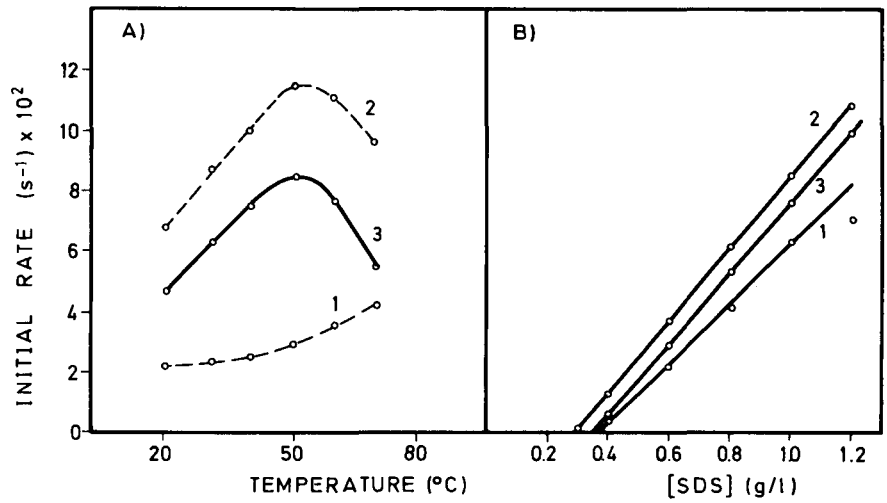

Fig. 4. (A) Influence of temperature on the rate of the uncatalysed (curve 1), SDS-catalysed + uncatalysed (curve 2) and SDS-catalysed (curve 3) reaction between iron(II) and 1,10-phenanthroline. [SDS] = 600 μg/ml. (B) Calibration graphs for the determination of SDS at 30°C (curve 1), 50°C (curve 2) and 60°C (curve 3). Experimental conditions: pH 2.4, [Fe(II)] = 1.0×10^{-4} M, [1,10-phenanthroline] = 4.0×10^{-4} M.

the cmc of a surfactant decreases with temperature to a minimum value and then increases with further increases in temperature. A temperature rise decreases hydration of hydrophilic groups, which favours micellization. However, temperature rise also disrupt the structured water surrounding hydrophobic groups, which hinders micellization. Therefore the relative magnitude of these two opposing effects determines whether the cmc increases or decreases over a particular temperature range. From the results shown in Fig. 4A (curve 3), the cmc for SDS should reach a minimum at about 50°C, as reflected in initial rate vs. SDS concentration plots obtained at three different temperatures, namely 30°C (Fig. 4B, 1), 50°C (Fig. 4B, 2) and 60°C (Fig. 4B, 3). A temperature of 50°C was chosen as optimal for the determination of SDS.

The influence of the presence of the electrolyte sodium chloride on the rate of the studied reactions is

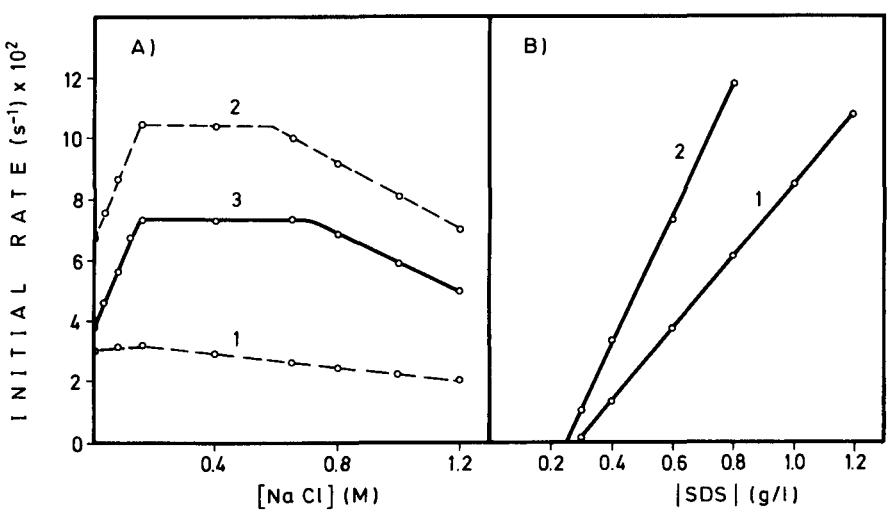

Fig. 5. (A) Influence of the sodium chloride concentration on the rate of the uncatalysed (curve 1), SDS-catalysed + uncatalysed (curve 2) and SDS-catalysed (curve 3) reaction between iron(II) and 1,10-phenanthroline. [SDS] = 0.6 g/l. (B) Calibration graphs for the determination of SDS in the absence (curve 1) and presence (curve 2) of 0.4 M sodium chloride. Experimental conditions: Temperature = 50°C, pH 2.4, [Fe(II)] = 1.0×10^{-4} M, [1,10-phenanthroline] = 4.0×10^{-4} M.

shown in Fig. 5A. This electrolyte gradually (though slightly), decreased the rate of formation of ferroin in the aqueous medium (curve 1) at concentrations above ca. 0.25 M. The rate of SDS-catalysed reaction (curve 3) exhibited a significantly different behaviour at NaCl concentrations below ca. 0.2 M, which could be related to the "electrolyte effect" on micellization. As is well known [10], the presence of electrolytes in aqueous solutions decreases the cmc, the effect being more pronounced with ionic than for zwitterionic and non-ionic surfactants. The depression of the cmc of ionic surfactants is mainly due to the decrease in the thickness of the ionic atmosphere surrounding the ionic head groups in the presence of the additional electrolyte and the consequently decreased electrical repulsion between them in the micelles. This is reflected in Fig. 5B, the presence of the electrolyte (curve 2) decreased the cmc of SDS relative to water (curve 1). However, since the sensitivity also increased as a result, the initial rate was irreproducible owing to the rapidity of the reaction. Therefore, since no substantially decreased detection limit for the surfactant was obtained in the presence of sodium chloride, the electrolyte was not added to the reaction medium.

In order to effectively reduce the SDS concentration above which the surfactant exhibited micellar catalysis, we studied the effect of the formation of mixed micelles. Mixed micelles of Triton X-100 and SDS were selected for this purpose. Single micelles of Triton X-100 (the cmc for which under our reaction conditions was found to be 1.2×10^{-4} M) exerted no micellar catalysis on the ferroin complex-formation reaction (Fig. 6A, curve 1). Addition of Triton X-100 to solutions containing SDS substantially increased the rate of formation (Fig. 6A, curve 3) and, more important, dramatically decreased the SDS concentration above which SDS exhibited micellar catalysis [compare the calibration curves in Fig. 6B for SDS in the absence (curve 1) and presence (curve 2) of 2.08×10^{-3} M Triton X-100]. Thus, the use of mixed micelles of SDS–Triton X-100 shifts the calibration curve for SDS to a zero intercept. The cmc for SDS obtained under our reaction conditions (1.73×10^{-4} M) was only slightly higher than that obtained for the SDS–Triton X-100 mixed micelles (9×10^{-5} M for an SDS mole fraction of 0.4).

From these results it follows that the catalytic action of SDS single micelles on the formation of ferroin complex is not altered by the formation of SDS–Triton X-100 micelles, as can be inferred from the parallel lines 1 and 2 in Fig. 6B. Therefore, the mixed micelles exert their catalytic effect through the SDS monomers in them. Addition of increasing concentrations of Triton X-100 to a reaction medium containing a fixed concentration of SDS (Fig. 6A, curves 2 and 3) caused SDS single micelles to be replaced with SDS–Triton

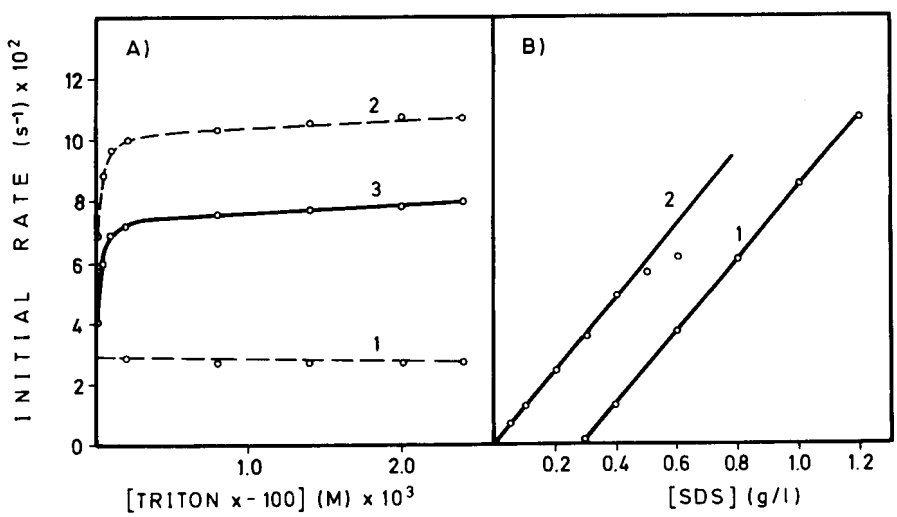

Fig. 6. (A) Influence of the Triton X-100 concentration on the rate of the uncatalysed (curve 1), SDS-catalysed + uncatalysed (curve 2) and SDS-catalysed (curve 3) reaction between iron(II) and 1,10-phenanthroline. [SDS] = 0.6 g/l. (B) Calibration graphs for the determination of SDS in the absence (curve 1) and presence (curve 2) of 2.08×10^{-3} M Triton X-100. Experimental conditions: Temperature = 50°C, pH 2.4, [Fe(II)] = 1.0×10^{-4} M, [1,10-phenanthroline] = 4.0×10^{-4} M.

X-100 mixed micelles and the catalytically effective micellar concentration to be increased since the mixed micelles consisted of a given number of monomers. An apparent increase in the initial rate with increase in the Triton X-100 concentration was thus observed, even though this surfactant had no catalytic effect on the reaction.

The detection limit for the determination of the SDS surfactant concentration was given by the minimum number of monomers needed for mixed micelles to have a catalytic effect, and the maximum concentration of this surfactant that can be determined was given by that at which reactant incorporation into micelles was maximal.

3.2. Features of the analytical method

Fig. 7 shows typical kinetic curves obtained for the reaction in an aqueous (curve 1) and an SDS–Triton X-100 micellar (curve 2) medium by using the stopped-flow technique. A calibration graph for SDS was run under the above optimal conditions. The determination of this ion was feasible over the range 50–400 μg/ml. The standard error of the estimate was 8.4×10^{-4} s^{-1} and the correlation coefficient 0.999 ($n=7$). The sensitivity was $(1.66\pm0.02)\times10^{-4}$ s^{-1} μg^{-1} ml. The detection limit (3σ) was 15 μg/ml.

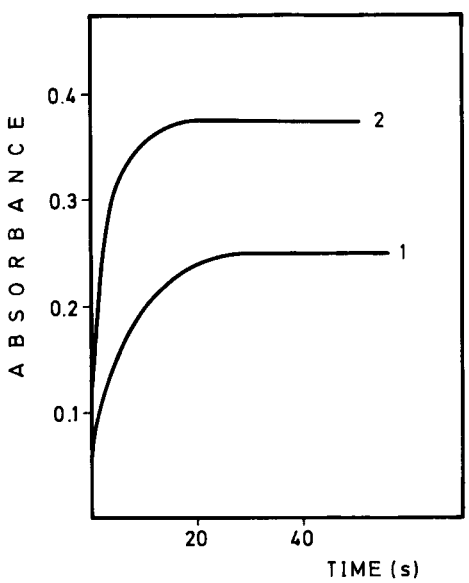

Fig. 7. Kinetic curves for the (1) Fe(II)–1,10-phenanthroline and (2) Fe(II)–1,10-phenanthroline–SDS system in the presence of 2.08×10^{-3} M Triton X-100.

Finally the precision, expressed as the relative standard deviation, was 3% and 3.3% for 200 μg/ml and 50 μg/ml, respectively ($n=11$).

The selectivity of the proposed method was assessed by evaluating the effect of anionic and non-ionic surfactants of variable structure. The anionic surfactants tested included sulphates [sodium 3,9-diethyl-6-tridecyl sulphate (Tergitol 7), sodium octylsulphate and sodium decylsulphate], sulphonates [sodium dodecylbenzene sulphonate (SDBS)] and sulfosuccinates [sodium bis(2-ethylhexyl) sulphosuccinate (Aerosol OT)]. The non-ionic surfactants tested were Triton X-100 and Brij 35. Their effect on the ferroin complex formation reaction in an aqueous medium and in SDS-catalysed and SDS–Triton X-100-catalysed micellar media was investigated in order to compare the selectivity in the absence and presence of single and mixed micelles. The surfactans were tested at concentrations below and above their cmc.

Micellar catalysis in the aqueous medium was only exerted by surfactants structurally similar to SDS (octylsulphate and decylsulphate). On the other hand, non-ionic surfactants and Tergitol 7 had no effect on the formation of ferroin. The influence of Aerosol OT and SDBS could not be determined at concentrations above their cmc as they precipitated in the reaction medium.

The determination of SDS based on the formation of single micelles of this surfactant was markedly influenced by the presence of other non-ionic and anionic surfactants structurally different from SDS. In fact, they increased the reaction rate at concentrations one or two orders of magnitude lower than their cmc, thus suggesting the potential formation of mixed micelles with SDS in the reaction medium. Maximum acceleration was obtained at an interferent concentration of ca. 10^{-3} M , the maximum rate enhancement ranging from ca. 60–80% of the rate obtained with SDS alone. It should be noted that octylsulphate and decylsulphate did not affect the micellar catalysis of SDS at concentrations below and above their cmc.

The use of SDS–Triton X-100 mixed micelles was found to substantially enhance the selectivity for the determination of SDS; none of the surfactants tested altered the reaction rate, at concentrations slightly above their cmc. This is quite significant because the preferential formation of mixed micelles of SDS with Triton X-100 introduces a high degree of selectivity in

the determination of this surfactant, in addition to increased sensitivity, relative to single SDS micelles.

3.3. Analysis of pharmaceutical preparation

The proposed method was applied to the determination of SDS in pharmaceuticals. Table 1 gives the results obtained for commercially available and magistral formulations. As can be seen, all were consistent with the nominal contents.

4. Conclusions

Micellar aggregate properties can be useful tools for the determination of surfactans in some instances. Using micellar catalysis offers some advantages over monomer properties, as in the proposed method for the determination of SDS, which features greater experimental simplicity and requires none of the organic solvents typically used in most spectrophotometric methods for the determination of ionic surfactants. One major additional advantage derived from the relationship between the reactant solubility and the surfactant structure is the increased selectivity obtained for some surfactants. Thus, micellar catalysis in the ferroin complex reaction is only exerted by linear alkyl sulfate surfactants. On the other hand, the formation of mixed micelles results in additional selectivity when preferentially formed by the surfactant of interest.

The main disadvantage of using micellar catalysis against monomer properties, arises from the need to get the cmc in the reaction medium, which usually results in higher detection limits than those provided by methods based on monomer properties. This precludes use in environmental applications, which typically involve the determination of surfactant concentrations at the nanogram-per-millilitre level, even though the proposed method is clearly advantageous for the analysis of manufactured products where the detection limit afforded by the micellar catalysis is more than adequate. The use of mixed micelles considerably decreases the surfactant concentration that can be determined and provides an excellent means for exploring the potential of micellar properties in the determination of surfactants. Research under way in our laboratory seems to demonstrate that surfactants can be determined at the nanogram-per-millilitre level by measuring the cmc of anionic-nonionic mixed micelles as a function of the molar fraction of their constituents.

Acknowledgements

The authors gratefully acknowledge financial support from the CICyT (Project No. PB91-0840).

References

[1] D.C. Cullum and P. Platt, in M.R. Porter (Eds.), Recent Developments in the Analysis of Surfactants, Elsevier Applied Science, London, 1992, pp. 5–74.
[2] R.A. Hearmon, Anal. Proc., 22 (1985) 147.
[3] APHA-AWWA-WPCF, Standard Methods for Examination of Water and Wastewater, American Public Health Association, Washington, DC, 1980, pp. 530.
[4] D. Sicilia, S. Rubio and D. Pérez-Bendito, Anal. Chem., 64 (1992) 1490.
[5] D.N. Rubingh, in K.L. Mittal (Ed.), Solution Chemistry of Surfactants, Vol 1, Plenum Press, New York, 1978, pp. 337–354.
[6] D. Pérez-Bendito and S. Rubio, Trends Anal. Chem., 12 (1993) 9.
[7] D. Sicilia, S. Rubio and D. Pérez-Bendito, Talanta, 38 (1991) 1147.
[8] A. Loriguillo, M. Silva and D. Pérez-Bendito, Anal. Chim. Acta, 199 (1987) 29.
[9] P. Mukerjee and K.J. Hysels, Critical Micelle Concentrations of Aqueous Surfactant Systems, NSRDS-NBS 36, U.S. Department of Commerce, Washington, DC, 1971.
[10] M.J. Rosen, Surfactants and Interfacial Phenomena, Wiley, New York, 1978, pp. 83–122.

ELSEVIER

Analytica Chimica Acta 298 (1994) 415–421

ANALYTICA CHIMICA ACTA

Direct injection of urine and determination of acetaminophen by micellar liquid chromatography with a wall-jet cell/carbon fibre microelectrode

Wenfeng Peng, Tao Li, Huimei Li, Erkang Wang *

Laboratory of Electroanalytical Chemistry, Changchun Institute of Applied Chemistry, Chinese Academy of Sciences, Changchun 130022, China

Received 17 January 1994; revised manuscript received 26 June 1994

Abstract

A wall-jet cell/carbon fibre microelectrode detector was designed and used for the micellar liquid chromatographic assay of acetaminophen. The separations were carried out in an analytical column packed with C_{18} stationary phase and the mobile phase was 0.05 mol l^{-1} sodium dodecyl sulfate (SDS) containing 3% (v/v) n-propanol at pH 7.15. It is demonstrated that the oxidation current of acetaminophen can be enhanced by SDS micelles. The linear response range for acetaminophen was from 0.02 to 70 μg ml^{-1}, with a detection limit of 0.02 μg ml^{-1} (signal-to-noise ratio = 2). Three urine samples were injected directly without time-consuming protein precipitation, and were analysed with a good recovery.

Keywords: Liquid chromatography; Acetaminophen; Micellar LC; Urine

1. Introduction

Molecules that possess both hydrophilic and hydrophobic groups may associate in solution to form dynamic aggregates commonly called micelles, provided that the concentration of these molecules is increased above a characteristic value known as the critical micelle concentration (CMC). The use of micelles as mobile phases in liquid chromatography was first introduced by Armstrong and Henry [1]. They showed that micelles can provide a hydrophobic site for interaction with the solute in the mobile phase and can be used in place of organic modifiers such as methanol and acetonitrile. Since that time, several investigators have used micellar mobile phases to illustrate certain important advantages of these systems over traditional aqueous–organic mobile phases. For instance, micellar liquid chromatography (MLC) has unique and modifiable selectivity and it can simultaneously separate ionic and non-ionic components [2]; micelles are themselves an inexpensive substitute for organic mobile phases both at purchase and at disposal and they are less toxic and flammable than most organic media; in practical applications, the solute and associated matrix components can be solubilized preferentially into or onto a micelle assembly, allowing direct injection of biological samples without previous sample extraction [3,4]. In addition, micelles offer the possibility of enhanced

* Corresponding author.

SSDI 0003-2670(94)00284-3

detection in separation, they can enhance fluorescence and can afford stabilized room-temperature fluorescence, and even micelle-enhanced chemiluminescence is a possibility [5–7]. To date, detection techniques used in MLC have mainly been UV and UV–visible spectrophotometry [3,8] and spectrofluorimetry. The combination of MLC with amperometric detection was studied about 10 years ago by Khaledi et al. [9]. More recently, Qu et al. [4] used a glassy carbon electrode in the MLC determination of dopamine with high sensitivity.

Microelectrodes have found increasing applications in continuous-flow analysis. Their advantages include high current density, substantially reduced flow noise [10], negligible *iR* drop and capacitive charging current [11,12]. Of different kinds of microelectrodes, carbon fibre microelectrodes have gained considerable popularity. In addition to high sensitivity, this kind of electrode has a very small geometrical size and is flexible in construction in any flow streams. For example, Chi et al. [13] and Wang et al. [14] fixed carbon fibres in polyethylene flow tubing, Jorgenson and co-workers [15–17] and Baur and Wightman [18] constructed on-column fibre detectors for open-tubular LC and Wang and Li [19] described an on-valve detector using a carbon fibre electrode for speedy flow-injection analysis. However, these microelectrodes are not easy to mount and special facilities such as precision positioners and microscopes for construction are required. Moreover, the carbon fibres are likely to break when they are manipulated improperly or used in vigorous flows.

In this paper, a novel wall-jet cell/carbon fibre microelectrode detector is presented. This device is highly sensitive, robust and convenient in construction, and it has been applied in the MLC determination of acetaminophen, an important analgesic drug. The sensitivity is higher than that of traditional reversed-phase LC – electrochemical detection with glassy carbon electrodes [20,21], a modified electrode [22] or a bipotentiostated dual-electrode detection scheme [23]. More importantly, the proposed method permits the direct injection of biological fluids without complicated sample pretreated procedures.

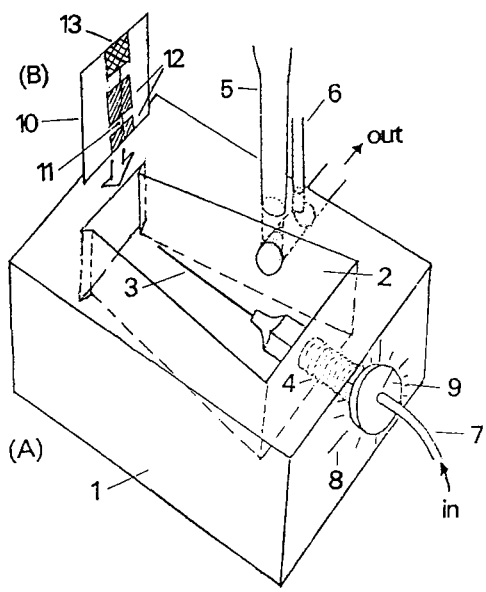

Fig. 1. Schematic diagram of the wall-jet cell (A) carbon fibre microelectrode detector (B) 1 = PMA base; 2 = cell; 3 = stainless-steel needle; 4 = PMA screw; 5 = SCE; 6 = auxiliary electrode; 7 = polyethylene tube; 8 = scale marks; 9 = screw handle with a radial pointer; 10 = polyester sheet; 11 = carbon fibre microelectrode; 12 = epoxy resin; 13 = silver paint.

2. Experimental

2.1. Apparatus

The chromatographic separations were carried out with a Model 510 pump (Waters), a Rheodyne U6K injection valve with a sample loop of 10 μl and a Nucleosil C_{18} (5-μm particle size) separation column (250 × 4 mm i.d.). In order to minimize dissolution of the analytical column packing, a precolumn (50 × 4.6 mm i.d.) packed with silica gel (15–25 μm) was placed between the pump and the injection valve to saturate the mobile phase with silica.

Electrochemical measurements were carried out using a CMBP-1 bipotentiostat (Jiangsu Electroanalytical Instrument Factory) fitted with a Model 902-PA picoamperometer (Ninde Analytical Instrument Factory). A three-electrode configuration with a carbon fibre working electrode, a saturated calomel reference electrode (SCE) and a platinum auxiliary electrode was used throughout. Voltammograms and

chromatograms were recorded with a Type 3033 recorder (Yokogawa Hokushin Electric) and a Type 056 recorder (Hitachi), respectively.

The chromatographic experiments were carried out at room temperature (24–26°C).

2.2. Flow cell construction

As illustrated in Fig. 1, the flow-through detector was a large-volume (ca. 5 cm^3) wall-jet cell in a polymethacrylate (PMA) base. A needle tip served as the fluid jet; it was fitted with a PMA screw by means of which the jet–electrode distance could be adjusted. The microelectrode device was inserted into a slit cut in the back of the cell and the height of the electrode device was adjusted so that the electrode exposed was at the same level as the jet. The reference electrode and auxiliary electrodes were arranged at the outlet of the cell. To avoid leakage of solution from the cell, vacuum silicone grease was applied to the fittings.

The microelectrode device was similar to that of dual-cylinder electrodes reported previously [24]. It was prepared by fixing a 14.5-μm diameter carbon fibre (Kureha Chemical) on polyester sheet with semi-cured epoxy resin (AD-U; Dongfeng Chemical Plant). The distance between the two pieces of epoxy resin was ca. 0.5–1 mm and this length of fibre was exposed to sample solutions. Silver paint (DH-1; Scientific Instruments) was used to make electrical contact.

The flow cell and the picoamperometer were arranged inside a grounded Faraday cage to ensure a low external noise level.

2.3. Reagents and mobile phase

Acetaminophen (Harbin Medical), sodium dodecyl sulfate (SDS) (Beijing Branch of Chinese Medical) and other chemicals were of analytical-reagent grade. All solutions were prepared using doubly distilled water. The chromatographic mobile phase was a 0.05 mol l^{-1} SDS solution (pH 7.15) with a buffer composition of 0.02 mol l^{-1} Na_2HPO_4, 3% (v/v) n-propanol and 1×10^{-3} mol l^{-1} disodium ethylenediaminetetraacetiate (EDTA). Prior to use, the mobile phase was filtered through a Type FH filter membrane with a 0.5-μm pore size (Millipore) followed by sonication for 15 min for degassing.

2.4. Procedures

Electrode pretreatment

Original carbon fibres were thoroughly washed in sequentially with isopropyl alcohol, acetone and 1 mol l^{-1} sulfuric acid. Electrochemical preconditioning was performed in 0.5 mol l^{-1} Na_2HPO_4 buffer by scanning the potential from -2.0 to $+2.0$ V with respect to SCE at 100 mV s^{-1} for 5 min.

Standard solutions

A stock standard solution was prepared by dissolving 13 mg of acetaminophen in 0.02 mol l^{-1} Na_2HPO_4 buffer solution in a 250-ml volumetric flask; the solution was stored at 4°C in the dark. An aliquot was diluted to the appropriate concentrations with mobile phase just before analysis.

Sample preparation

Three urine samples taken from a subject at different times after the last of six 4-hourly 450-mg acetaminophen doses were immediately filtered through a G-4 glass filter (pore size 2–5 μm), the samples were diluted tenfold with the mobile phase and were kept at 4°C in the dark. The concentrations

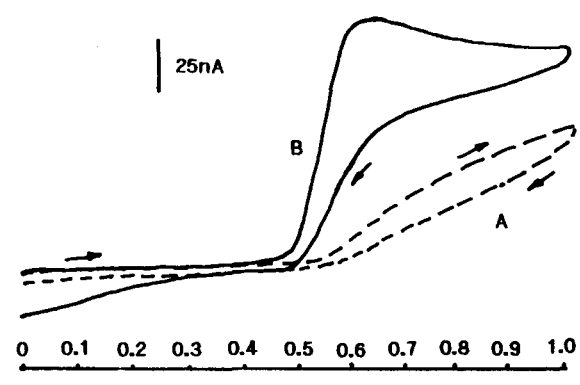

Fig. 2. Cyclic voltammograms of 3.44×10^{-4} mol l^{-1} acetaminophen (in 0.02 mol l^{-1} KH_2PO_4 buffer, pH 7.15) at a carbon fibre microelectrode (A) before and (B) after electrochemical treatment. Scan rate, 50 mV s^{-1}.

of acetaminophen in urine samples were determined from a calibration graph.

3. Results and discussion

3.1. Electrochemistry of acetaminophen

It has been reported that pretreatment of carbon fibre electrodes has a marked effect on their response to many species [25], and is required in order to observe reproducible and reliable electrochemical behaviour. The voltammetric behaviour of acetaminophen at a carbon fibre microelectrode is illustrated in Fig. 2; the voltammogram obtained with an untreated carbon fibre electrode is fairly drawn-out. After electrochemical pretreatment, acetaminophen shows a well-defined sigmoigal *i–E* curve, the half-wave potential was shifted from +0.78 to +0.54 V vs. SCE and the current was greatly increased in height (at +0.65 V vs. SCE, the current amplitude was increased by a factor of 8). The pronounced peak characteristics of the oxidation wave suggests a two-dimensional diffusion profile at the cylindrical electrode surface.

With the pretreated working electrode, the influence of three surfactants above the CMC on the voltammograms of acetaminophen was tested; typical voltammograms are shown in Fig. 3. The surfactants studied were SDS, cetyltrimethylammonium bromide (CTAB) and Triton X-100, which represent anionic, cationic and non-ionic surfactants, respectively. It can be seen that the presence of the surfactants gives rise to radically different responses. Triton X-100, a polyoxyethylene alcohol, gives a voltammogram not usually seen in electrochemistry, and it is drawn-out to some extent with CTAB, there is an apparent current loss compared with surfactant-free analyte solution. In contrast, SDS micelles cause an increase in the current amplitude, the half-wave potential shifts by 50 mV in the negative direction and the current measured at +0.65 V vs. SCE was increased by 55%. Generally, there is a higher local viscosity in micellar solutions and the low rate of molecular diffusion towards the electrode is most likely to cause a lower current, as has been demonstrated by Qu et al. [4] for the dopamine–SDS system. The adsorption of surfactants on electrodes

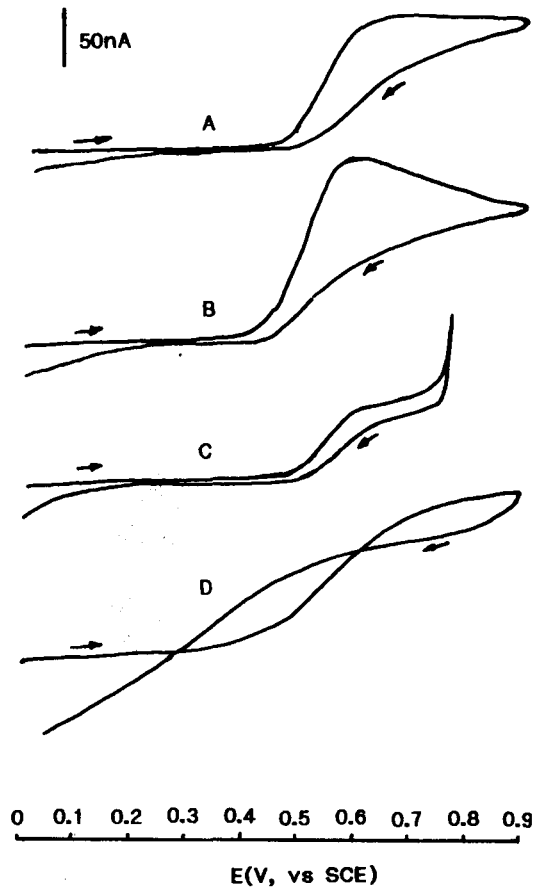

Fig. 3. Cyclic voltammograms of 3.44×10^{-4} mol l^{-1} acetaminophen (in 0.02 mol l^{-1} KH_2PO_4 buffer, pH 7.15) at a pretreated carbon fibre microelectrode (A) and in the presence of (B) 0.05 mol l^{-1} SDS (C) 0.05 mol l^{-1} CTAB and (D) 5% (v/v) Triton X-100. Scan rate, 50 mV s^{-1}.

has proved to have a profound influence on electron transfer rates and reaction rates for fluids organized by surfactants [5,6]. There is still a poor understanding of the effects of surfactants on the double-layer structure and on the kinetics and thermodynamics of the electron transfer process. However, two fundamental processes must be taken into account, solubilization of the analyte by the micelles and interaction of the surfactants with the electrode surface. SDS molecules can aggregate dynamically on the electrode surface, forming a hydrodynamic absorbed film, and this heterogeneous micro-environment can accelerate or inhibit the electron transfer rate of the

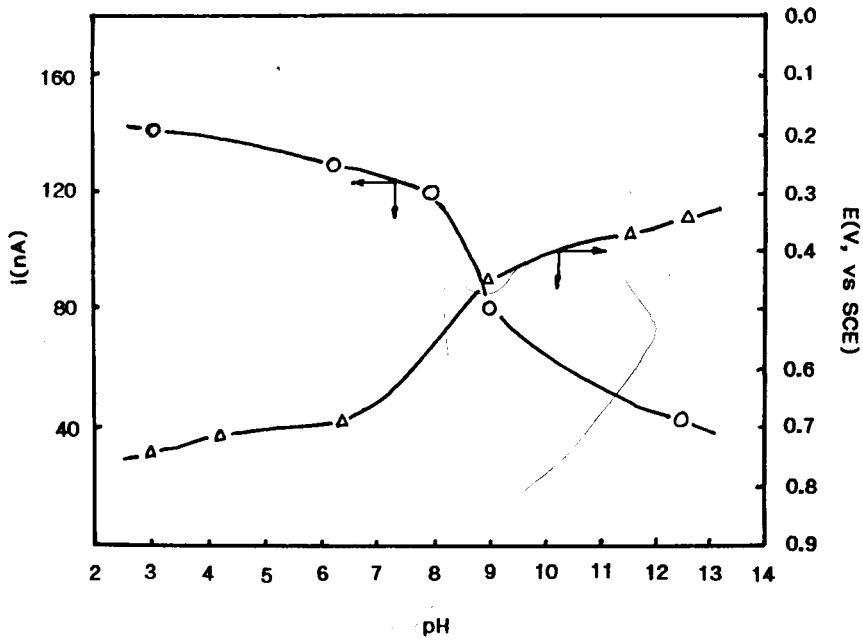

Fig. 4. Dependence of oxidation current and half-wave potential of acetaminophen on pH. Conditions as in Fig. 3B.

electroactive species, hence resulting in current enhancement or depression.

The effect of pH on the voltammetric response of acetaminophen in SDS micellar solutions is shown in Fig. 4. When the pH increased from 3.0 to 12.5, the half-wave potential shifted from +0.75 to +0.35 V vs. SCE, and in step with this change the oxidation current decreased. As a higher current and lower potential are desirable for amperometric monitoring in flow systems (a low detection potential results in higher selectivity), pH 7.15 buffered by 0.02 mol l^{-1} Na_2HPO_4 was chosen.

3.2. Hydrodynamic behaviour

The carbon fibre electrode device illustrated in Fig. 1 works on the principle of the wall-jet cell [26]: since the microelectrode is fixed on a polyester sheet, the solution from the jet impinges perpendicularly on the microelectrode and spreads radially over the surface of the sheet. As a consequence, only fresh species from the bulk solution reach the electrode, whereas species from the bulk solution are excluded. With 0.05 mol l^{-1} SDS at pH 7.15 as the mobile phase, hydrodynamic experiments were performed without installation of a separation column. As illustrated in Fig. 5, the *i–E* curve of acetaminophen is similar to that obtained from static electrolyte solution. There is clearly a plateau after +0.62 V vs. SCE, so +0.65 V vs. SCE was chosen as the operating potential.

The influence of flow-rate (V) in the range 0.4–1.4 ml min^{-1} was studied and was shown to obey

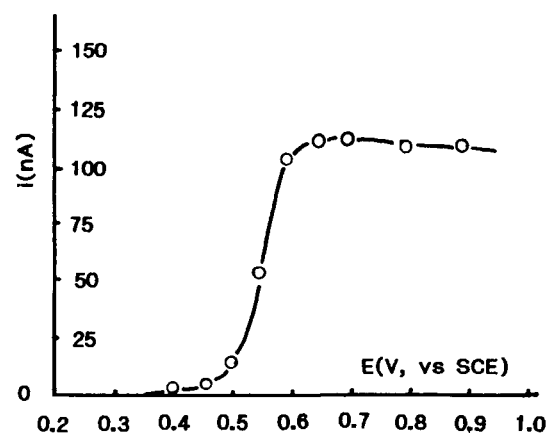

Fig. 5. Hydrodynamic voltammogram of 3.44×10^{-4} mol l^{-1} acetaminophen. Mobile phase, 0.05 mol l^{-1} SDS solution containing 0.02 mol l^{-1} Na_2HPO_4; flow-rate, 1.0 ml min^{-1}.

the relationship $\log I = 0.41 \log V + K$, where K is a constant involving all the other items. The slope of 0.41 is much smaller than the 0.75 [27] for conventional electrodes, showing that the flow-rate dependence of the current is substantially reduced. This is a special advantage as a major source of noise in flow systems arises from flow fluctuations [10]. Hence a lower detection limit is obtained. The dependence of peak current on the nozzle–electrode separation was tested at a flow-rate of 1.0 ml min^{-1}. It was found that in the region of 2–9 mm the distance between the jet nozzle and electrode hardly affects the current amplitude and in subsequent experiments a ca. 5 mm separation was used.

The flow-injection response was highly reproducible. For 20 replicate injections of 10 μg ml^{-1}, the relative standard deviation of the peak currents was 3.1%, showing that the performance of the pretreated carbon fibre electrode was very stable.

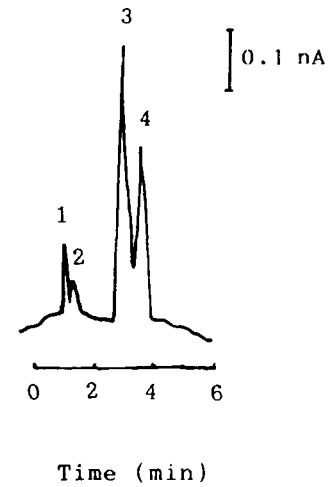

Fig. 6. Chromatogram of 0.08 μg ml^{-1} (1) ascorbic acid (2) uric acid, (3) acetaminophen and (4) 4-aminophenol. Mobile phase, 0.05 mol l^{-1} SDS solution containing 0.02 mol l^{-1} Na_2HPO_4, 3% (v/v) n-propanol and 1×10^{-3} mol l^{-1} EDTA; detection potential, +0.65 V vs. SCE; flow-rate, 1.0 ml min^{-1}.

3.3. MLC detection

For the purpose of detecting acetaminophen in urine, it is necessary to separate it from ascorbic acid, uric acid and 4-aminophenol. In order to ensure a high separation efficiency, the mobile phase was modified with a small amount (3%, v/v) of n-propanol; 1×10^{-3} mol l^{-1} EDTA was also added to the mobile phase to reduce the noise that may be caused by the presence of the trace metal impurities. Fig. 6 was obtained using this mobile phase under the above-selected detection conditions. It can be seen that the chromatographic peak of acetaminophen is well resolved from those of uric acid, ascorbic acid and 4-aminophenol, the retention times for the four compounds being 2.30, 1.30, 1.05 and 3.24 min, respectively. The peak of acetaminophen was found to be directly proportional to its concentration from 70 μg ml^{-1} down to 0.02 μg ml^{-1}, the regression equation being i (nA) = 0.02 + 0.31 C (μmol/ml) with a correlation coefficient of 0.997 ($n = 12$); the detection limit was 0.02 μg ml^{-1} at a signal-to-noise ratio of 2.

As indicated above, a significant application of MLC is the ability to inject serum or urine samples directly on to a reversed-phase column without the need for a tedious protein precipitation and without pressure build-up problems, probably because the proteins can be solubilized into or on to the micellar aggregates and the protein–micelle aggregates are so large that they are excluded from the pores of the stationary phase support eluted with the void volume. Three urine samples taken from a healthy subject who has orally taken acetaminophen tablets were directly injected and chromatographed; these samples were simply filtered to remove deposits.

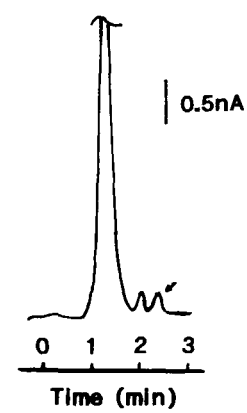

Fig. 7. Chromatogram of a diluted (1+9) urine sample from a subject 2 h after the last of six 4-hourly 450-mg acetaminophen doses. Conditions as in Fig. 6.

Table 1
Results for the determination of acetaminophen in urine samples

Amount added (ng)	Amount found (ng) [a]		
	Sample 1	Sample 2	Sample 3
5	8.6	12.0	13.5
10	14.0	16.5	18.2
15	18.7	22.0	23.4
20	23.6	26.5	27.8
30	32.4	35.8	38.0
50	54.4	56.0	58.0
150	153.2	156.3	158.0
500	504.1	506.4	507.1
1500	1503.6	1506.2	1508.0
3000	3003.2	3006.4	3008.0
Blank	3.8	6.7	8.2
Average recovery (%)	98.3	95.7	97.6

The samples were taken from a subject at different times (1–3 h) after the last of six 4-hourly 450-mg acetaminphen doses.
[a] Each value represents the mean of three measurements.

Results of the analysis are represented in Table 1. The concentrations of acetaminophen in the urine samples were found to be 0.38, 0.67 and 0.82 $\mu g\ ml^{-1}$ and the overall recovery was satisfactory.

4. Conclusions

SDS micelles have been demonstrated to be able to enhance the electrochemical oxidation of acetaminophen. To our knowledge, enhanced amperometric detection in MLC has not previously reported. With SDS micellar solution as the mobile phase, a novel flow-through cell was constructed for the amperometric detection of acetaminophen, the use of an electrochemically pretreated carbon fibre microelectrode resulted in high sensitivity and the detection limit obtained was better than those reported hitherto. The method allows the direct injection of biological samples, which eliminates prior sample pretreatment procedures and significantly shortens the analysis time. In addition, the minimal sample handling required reduces sources of error and possible losses of analyte. The method proposed is sensitive, rapid, simple and economical.

Acknowledgement

This work was supported by the National Natural Science Foundation of China.

References

[1] D.W. Armstrong and S.J. Henry, J. Liq. Chromatogr., 3 (1980) 657.
[2] C.M. Kirkman, C. Zu-Ben, P.C. Uden, W.J. Stratton and D.E. Henderson, J. Chromatogr., 317 (1984) 569.
[3] F.J. DeLuccia, M. Arunyanart and L.J. Cline Love, Anal. Chem. 57 (1985) 1564.
[4] Y. Qu, P. Hu and P. Zhu, J. Liq. Chromatogr., 14 (1991) 2755.
[5] I.I. Hewala, Anal. Lett., 27 (1994) 561.
[6] S.A. Myers, R.A. Mackay and A. Brajter-Toth, Anal. Chem. 65 (1993) 3447.
[7] W.L. Hinze and D.W. Armstrong, ACS Symposium Series, No. 342, American Chemical Society, Washington, DC, 1987.
[8] I. Carretero, M. Morell and J.J. Laserna, J. Liq. Chromatogr., 16 (1993) 1767.
[9] M.G. Khaledi and J.G. Dorsey, Anal. Chem., 57 (1985) 2190.
[10] L.J.M. Magee, Jr., and J. Osteryoung, Anal. Chem., 62 (1990) 2625.
[11] D.L. Luscombe and A.M. Bond, Talanta, 38 (1991) 65.
[12] R.J. Tait, A.M. Bond, B.C. Finnin and B.L. Reed, Collect. Czech. Chem. Commun., 56 (1991) 192.
[13] H. Chi, Y. Wang, T. Zhou and C. Jin, Anal. Chim. Acta, 235 (1990) 273.
[14] H. Ji, J. He, S. Dong and E. Wang, J. Electroanal. Chem., 290 (1990) 93.
[15] J.G. White and J.W. Jorgenson, Anal. Chem., 58 (1986) 2992.
[16] J.G. White, R.L. St. Clair and J.W. Jorgenson, Anal. Chem., 58 (1986) 293.
[17] M.D. Oates and J.W. Jorgenson, Anal. Chem., 61 (1989) 432.
[18] J.E. Baur and R.M. Wightman, J. Chromatogr. 482 (1989) 65.
[19] J. Wang and R. Li, Anal. Chem., 62 (1990) 2414.
[20] K.S. Pang and A.M. Taburet, J.A. Hinson, J.R. Gillette, J. Chromatogr., 174 (1979) 165.
[21] J.W. Munson, R. Weierstall and H.B. Kostenbauder, J. Chromatogr., 145 (1978) 328.
[22] J. Wang and T. Golden, Anal. Chim. Acta, 217 (1989) 343.
[23] J. Zhou and E. Wang, Anal. Chim. Acta, 236 (1990) 293.
[24] W. Peng, P. Li and X. Zhou, J. Electroanal. Chem., 347 (1993) 1.
[25] T.E. Edmonds, Analytica Chimica Acta, 171 (1985) 1.
[26] F. Fleet and C.J. Little, J. Chromatogr. Sci., 12 (1974) 747.
[27] J. Mada and H. Matsuda, J. Electroanal. Chem., 44 (1973)

ELSEVIER

Analytica Chimica Acta 298 (1994) 423–430

ANALYTICA CHIMICA ACTA

Influence of alcoholic modifiers on the selectivity of the separation of a group of polycyclic aromatic hydrocarbons by micellar liquid chromatography

M.A. Rodríguez Delgado, M.J. Sánchez, V. González, F. García Montelongo *

Department of Analytical Chemistry, Food Science and Toxicology, University of La Laguna, 38071 La Laguna, Spain

Received 7 March 1994; revised manuscript received 27 June 1994

Abstract

The role of micelles and alcohols as the modifiers of the aqueous mobile phase in reversed-phase liquid chromatography in controlling retention and selectivity of polyaromatic hydrocarbons (PAHs) is studied. Elution strength increases with an increase in the alcohol or micelle concentration, and enhancement of separation selectivity with elution strength was observed. Increasing micelle concentration has an opposite effect, when compared to increasing alcohol modifier concentration, on the separation selectivity, showing that for this group of PAHs the separation selectivity is better with mobile phases of medium concentration of micelles and moderately high alcohol percentages. The selectivity enhancement can be explained in terms of the competing equilibria in micellar liquid chromatography.

Keywords: Liquid chromatography; Alcohols; Micelles; PAHs

1. Introduction

Micellar liquid chromatography (MLC) has experienced a solid growth period since its first reported use by Armstrong and Henry [1]. The popularity of this mode of separation has increased because of several unique advantages such as the simultaneous separation of ionic and non-ionic compounds, the ability of micellar aggregates to dissolve sample protein and other compounds and consequently direct sample injection of biological material into the column, shorter equilibration times for gradient elution, gradient compatibility with electrochemical detectors, enhanced luminescence detection, etc. [2–7].

Low chromatographic efficiency is the most important disadvantage of MLC. Poor wetting of the stationary phase [8] and restricted mass transfer [9] are the reasons for this decrease in efficiency. The addition of small amounts of alcohols to MLC systems has been shown to improve column efficiencies significantly, especially when measured with hydrophobic analytes such as benzene. These alcohols are normally of short-chain (methanol, propanol or butanol) and the range of concentration must not be very high, because it might reduce the role of micelles and bring the system closer to a hydroorganic system. The most common reasoning is that the addition of the alcohols reduces the loading of the surfactant in the stationary phase and that this leads to improvements in the mass transfer and wetting of the stationary phase [8,10–12]. Furthermore, the effect of alcohols on selectivity in MLC has been stud-

* Corresponding author.

SSDI 0003-2670(94)00287-8

ied by a few workers, and Khaledi and co-workers [15–19] have reported their effect on the retention and selectivity for alkylbenzenes, amino acids, peptides, phenols and benzoic acids concluding that the selectivity is influenced by the competing partitioning equilibria and the characteristics of micelles.

In this paper, we report the results of the effect of adding alcohols to micellar eluents on the selectivity of a series of PAHs of environmental concern and the effect of the nature of the surfactant as well as the role of the type and concentration of the alcohol additive used in the mobile phase on solvent strength and selectivity in MLC, with the aim of developing a separation method giving good resolution between consecutive peaks with a not too long elution time.

2. Experimental

2.1. Apparatus

All measurements were made with a Waters 600 Multisolvent Delivery System equipped with an U6K sample injector, a Waters Lambda-Max 481 LC variable wavelength spectrophotometric detector operating at 254 nm, and a Baseline 810 Chromatography Workstation. The analytical column was a Waters Nova-Pack C_{18}, 150 × 3.9 mm i.d., 4-μm particle diameter. A silica precolumn was employed to saturate the mobile phase with silicate to protect the analytical column and to avoid hydrolysis of the bonded stationary phase. The analytical column and the mobile phase reservoir were water-jacketed and temperature-controlled with a circulating bath.

2.2. Reagents

The surfactants, sodium dodecylsulfate (SDS) and cetyltrimethylammonium bromide (CTAB), were of electrophoresis grade obtained from Aldrich and used as received. Methanol (MeOH), ethanol, 2-propanol (PrOH) and *n*-butanol (BuOH) were Merck, pro analysi products. Naphthalene (1), acenaphthylene (2), fluorene (3), anthracene (4), phenanthrene (5), 9-methylanthracene (6), fluoranthene (7), pyrene (8), chrysene (9), benzo[*a*]anthracene (10), benzo[*b*]-fluoranthene (11), benzo[*a*]pyrene (12), benzo[*e*]-pyrene (13), perylene (14), dibenz[*ac*]anthracene (15) and benzo[*ghi*]perylene (16) were Aldrich products. Numbers identify the compound in tables and figures.

2.3. Procedure

The appropriate weight of SDS or CTAB was dissolved in Milli-Q (Millipore) water containing the desired alcohol content, and the solution filtered through a 0.45-μm nylon membrane filter (Whatman). The mobile phase was degassed under vacuum in an ultrasonic bath prior to use. Stock solutions of PAHs were prepared in ethanol, and diluted with the same solvent when necessary.

The void volume of the system was measured by multiple injections of water or sodium nitrate solution and found to be 0.81 ml, and was used for all k' calculations. The k' values were measured at 60 ± 1°C for SDS at 40 ± 1°C for CTAB, injections of 20 μl were made.

Chromatograms shown were obtained with a test solution: naphthalene (0.256 μg ml^{-1}), acenaphthylene (0.308 μg ml^{-1}), fluorene (0.332 μg ml^{-1}), anthracene (0.356 μg ml^{-1}), 9-methylanthracene (0.384 μg ml^{-1}), pyrene (0.405 μg ml^{-1}), chrysene (0.454 μg ml^{-1}), benzo[*a*]anthracene (0.455 μg ml^{-1}), perylene (0.252 μg ml^{-1}), dibenz[*ac*]-anthracene (0.139 μg ml^{-1}).

3. Results and discussion

The addition of an alcohol to micellar mobile phases significantly alters the equilibrium of the solute away from the micelle toward the bulk aqueous phase, which becomes more non polar [20,21]. In this investigation we concentrate on two parameters which cause a large change in retention and selectivity and which are easy to vary: the concentration of the surfactant, SDS or CTAB, and the concentration and type of the alcohol modifier.

The study of the chromatographic behaviour of homologous series provides information of great utility for a better characterization of the effects of the mobile and stationary phases on retention and selectivity in MLC. Therefore we have selected a group of PAHs of environmental concern, which not only have some density of negative charge, a characteristic of the aromatic

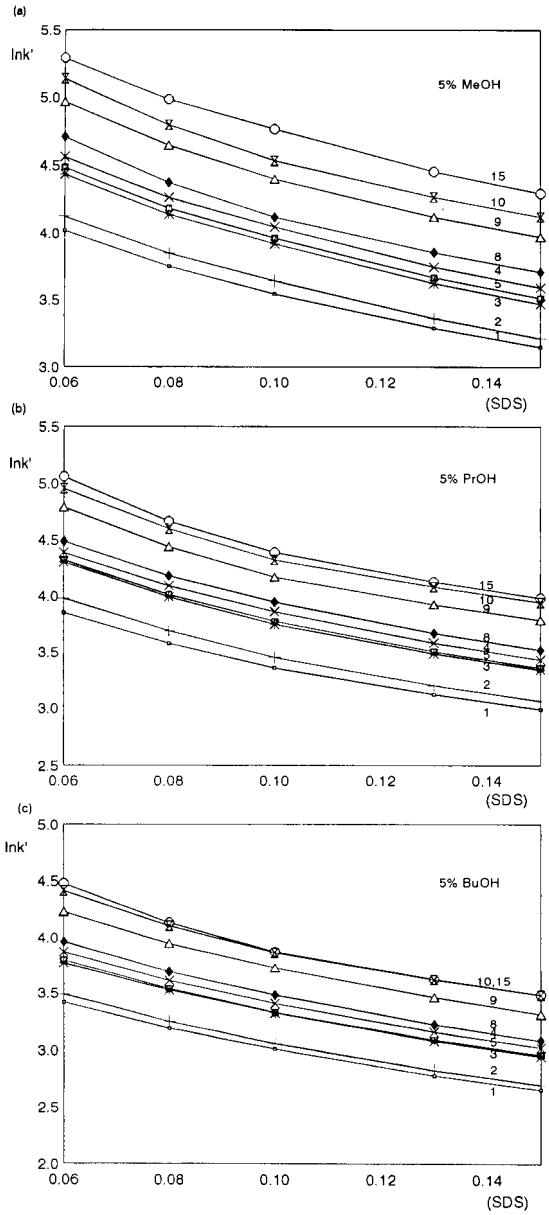

Fig. 1. Variation of the retention of PAHs as a function of the concentration of surfactant (SDS) in the hybrid micellar mobile phase: (a) methanol, (b) 2-propanol and (c) butanol.

ring electron delocalization, but also a wide range of hydrophobicity.

Figs. 1 and 2 illustrate the variation of retention of different PAHs for the same percentage of different alcohols in the two surfactant systems. As expected [13,14] retention diminishes as surfactant concentration increases, and there is a net difference in selectivity values not only between surfactants, selectivity decreases on increasing the surfactant chainlength, but also when the alcoholic modifier changes.

In a micellar system retention and selectivity are controlled by the three characteristic partition equilibria namely the distribution of the solute between the micelle and the bulk water, between the stationary phase and the micelle, and between the stationary phase

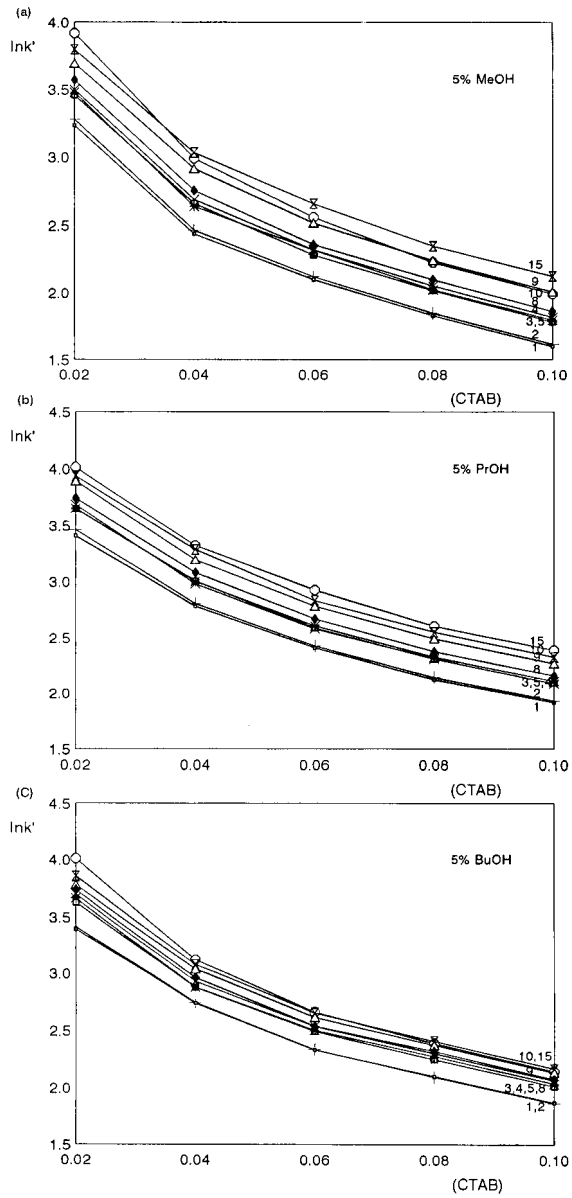

Fig. 2. Variation of the retention of PAHs as a function of the concentration of surfactant in the hybrid micellar mobile phase: (a) methanol, (b) 2-propanol and (c) butanol.

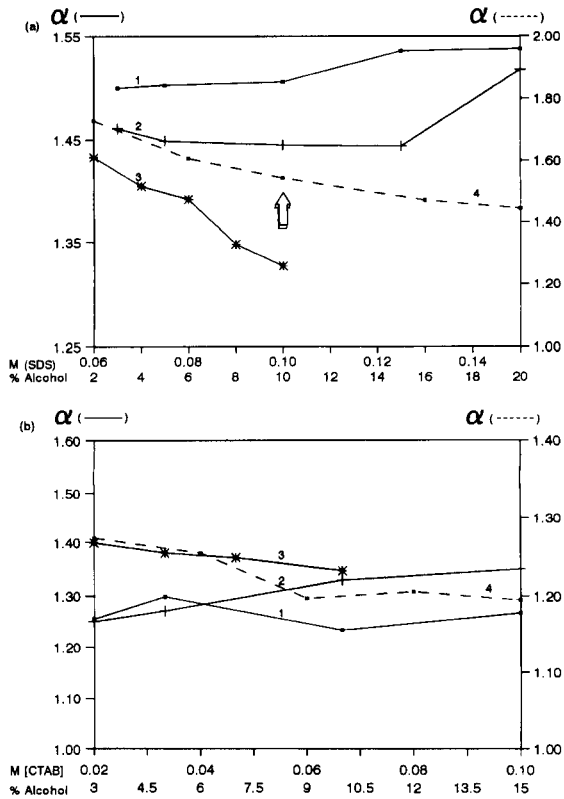

Fig. 3. Variation of benzene ring selectivity, $\alpha_1 = k'_{\text{phenanthrene}}/k'_{\text{naphthalene}}$ with percentage of modifier, (1) MeOH, (2) PrOH, (3) BuOH and (4) concentration of surfactant: (a) SDS, (b) CTAB.

and water. Thus, on modifying the micelles through mixed micelle formation, which changes the critical micelle concentration, and consequently the stationary phase, the selectivity of compounds separation is modified, Figs. 1 and 2. We must keep in mind that variations in selectivity include different types of interactions (electrostatic, hydrophobic, etc.) that are possible between the solute and the mobile phase, the micelle and the stationary phase and the type of solute-micelle interaction, which depends upon the characteristics of both solute and surfactant.

Fig. 3a and b shows for SDS and CTAB how selectivity diminishes as surfactant concentration increases, at a constant concentration of, i.e., PrOH, while increasing methanol and propanol modifier percentage increase the selectivity of the separation, at a constant concentration of the surfactant used. These changes are higher for SDS than for CTAB. That is to say modifying micelle concentration has an opposite effect on selectivity as compared to changes in modifier concentration. This effect has already been observed by Kord and Khaledi [18] who suggested that the effect of these two parameters on the selectivity of a group of amino acids, peptides and substituted benzenes could be quite different, even opposite. However, for the most hydrophobic BuOH selectivity diminishes rapidly especially with SDS mobile phase. Thus the chromatographic selectivity of BuOH is different from that of PrOH or MeOH, that is to say hydrophobicity of both PAHs and the organic solvent are important factors in controlling their interaction with the micelle. Thus is the best separation could be obtained using a moderately high concentration of SDS, between 0.08 and 0.15 M, and $\geq 15\%$ methanol or 2-propanol as the modifier. However, as the elution time using SDS–MeOH–H_2O mobile phases takes a longer time, see below, a 0.15 M SDS–PrOH–H_2O was tested, and the results in Fig. 4 indicate that a 0.15 M SDS–15% PrOH–H_2O will give an acceptable separation.

These conclusions were checked and Fig. 5 shows how in the absence of a modifier (Fig. 5a) there exist strong overlaps and co-elution of peaks, especially with the most hydrophobic PAHs. Separation can be improved introducing another variable in optimization strategy, namely the type of modifier. Thus when using 15% methanol (Fig. 5b) a better peak resolution is obtained and even the later ones appear as well defined peaks. With the same percentage of 2-propanol (Fig. 5c) a similar resolution is obtained while the analysis time is reduced by 50%. Notwithstanding, in the presence of 7% butanol (10% maximum solubility) (Fig. 5d) resolution is lost.

However, Fig. 5c shows that using 0.15 M SDS with 15% 2-propanol as mobile phase does not resolve all

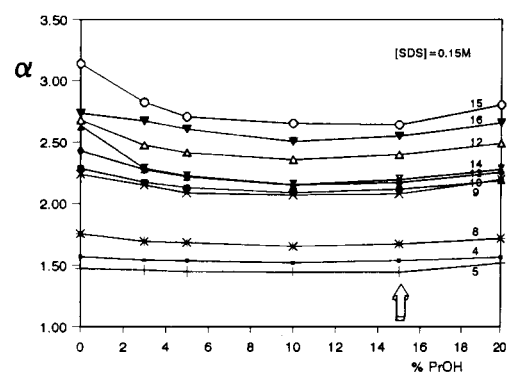

Fig. 4. Benzene ring selectivity, $\alpha_{n(\text{benzene ring})} = k'_{(\text{PAH})}/k'_{\text{naphthalene}}$ at 0.15 M SDS with increasing percentage of 2-propanol.

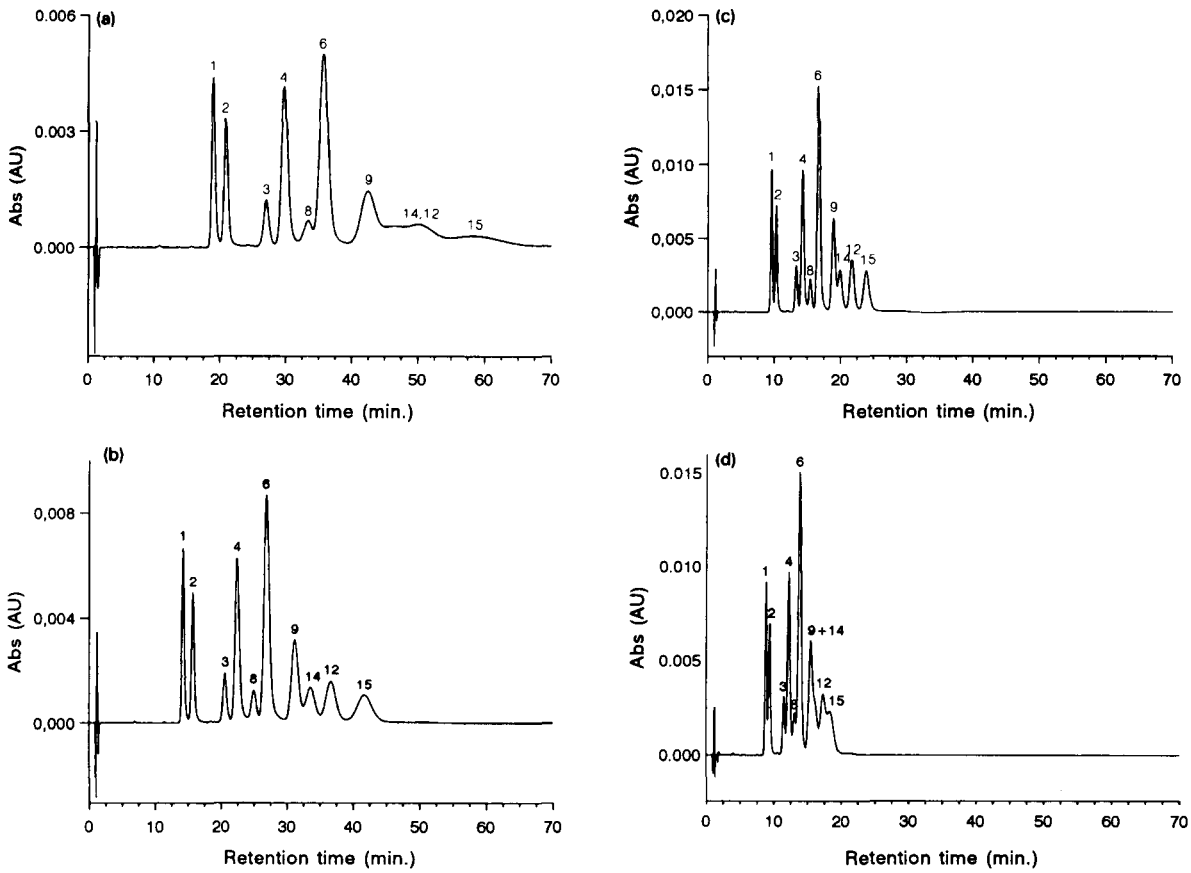

Fig. 5. Chromatograms of a mixture of ten PAHs eluted with: (a) purely micellar phase 0.15 M SDS, (b) 0.15 M SDS and 15% methanol, (c) 0.15 M SDS and 15% 2-propanol and (d) 0.15 M SDS and 7% butanol.

the peaks and one can see that apart from the pair 9–14 other peaks are not resolved up to the baseline. Thus, taking into account the results in Fig. 3a, a somewhat less concentrated SDS solution, namely 0.10 M was tested and Fig. 6 shows that a better resolution is obtained even for peaks 9–14.

Since the organic modifier does not decrease the equilibria equally for all the solutes tested [21,22], the modifier changes the selectivity of the mobile phase. The alcohol in the micellar mobile phase reduces the amount of sorbed surfactant on the stationary phase, and it will solvate the hydrocarbonaceous bonded phase. Taking into account that BuOH has a higher solvating power than PrOH and MeOH, it will modify more strongly the three characteristic equilibria of the micellar phases, and this effect will be most relevant for the most hydrophobic compounds, which on being transferred from the mobile phase to the stationary phase will undergo a smaller change in their environment and will be transferred faster to a more apolar medium, as demonstrated by their shorter retention times.

Although a widely accepted technique to characterize LC solvents is Snyder's selectivity triangle [23], where the solvents grouped in the same area of the triangle should have a similar chromatographic selectivity at equal solvent strength, this classification is no longer valid in MLC with hybrid mobile phases as can be deduced from the selectivity changes already mentioned. These changes are not found with the hydroorganic mobile phases where no modification occurs on using alcohols as modifiers as they belong to the same group II of Snyder's triangle.

Another important effect to be considered is that of surfactant and modifier on solvent strength. It has been established that with hybrid mobile phases the relation

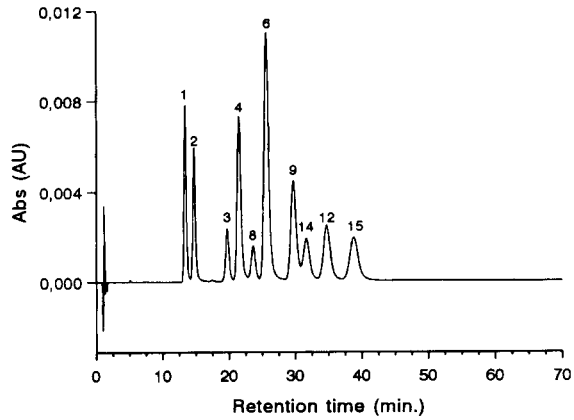

Fig. 6. Chromatogram of a mixture of ten PAHs eluted with a hybrid mobile phase of 0.10 M SDS and 15% 2-propanol.

between retention and volume fraction of organic solvent can be expressed as

$$\ln k' = -S_{hyb}\Phi + \ln k_o$$

where S_{hyb} is the solvent strength parameter in hybrid systems, Φ is the volume fraction of the organic solvent and $ln\ k_o$ is the retention in a purely aqueous micellar eluent. This equation is valid for a small range of concentrations, 3–15%, of 2-propanol [19].

In Table 1, the S_{hyb} values calculated for the PAHs are listed for MeOH, PrOH and BuOH as the modifiers with SDS and CTAB micelles. As shown, the values can be ranked as $S_{BuOH} > S_{PrOH} > S_{MeOH}$, which is similar to conventional hydroalcoholic systems as BuOH is the strongest solvent and MeOH the weakest. The larger S_{hyb} for BuOH (3–5 times) corroborates that this solvent interacts more strongly with micelles and consequently can solvate more effectively, thus it can compete better with micelles for interaction with solutes. With PrOH and MeOH interaction with greater hydrophobic solutes is lower and higher with less hydrophobic ones.

When solutes are ranked according to their S_{hyb} values, one can point to the different impact of micelles of SDS and CTAB on the ranking of the alcohols. Unlike in conventional hydroorganic systems, where the same ranking exists as the solvents belong to the same selectivity group of the Snyder triangle, in MLC variations are very different depending on the alcohol modifier, which can be explained as these solvents interact differently with micelles.

Another important aspect is the fact that S_{hyb} values for a hydroorganic mobile phase change significantly with solute size in a homologous series. However, there are no great variations in solvent S_{hyb} when using micellar mobile phases, see Table 1, which means that solute

Table 1
Absolute value of the slope for the 16 PAHs, calculated by linear regression of the retention data, ln k', vs. the percentage of the organic modifiers in the hybrid eluents water–alcohol–0.15 M SDS and water–alcohol–0.02 M CTAB micelles [a]

Component	SDS			CTAB		
	MeOH	PrOH	BuOH	MeOH	PrOH	BuOH
Dibenz[*ac*]anthracene	2.7	2.7	8.3	1.9	2.5	8.8
Benzo[*ghi*]perylene	2.7	2.9	7.9	1.3	2.2	8.0
Fluoranthene	2.4	3.1	7.9	1.3	1.9	9.1
Chrysene	2.3	3.1	8.1	1.7	2.1	7.2
Benzo[*a*]anthracene	2.3	2.9	8.2	1.4	1.9	7.4
Benzo[*e*]pyrene	2.1	2.8	7.6	1.4	2.6	6.4
Perylene	2.1	2.9	8.1	1.6	2.7	6.7
Benzo[*a*]pyrene	2.0	3.0	8.7	1.5	2.2	6.7
Pyrene	2.0	3.2	8.0	1.4	2.5	7.9
9-Methylanthracene	1.9	3.0	7.3	1.4	2.6	8.7
Benzo[*b*]fluoranthene	1.9	2.9	7.9	2.0	2.4	6.9
Phenanthrene	1.8	3.0	8.3	1.2	3.2	9.2
Anthracene	1.8	3.2	8.0	1.2	3.1	9.6
Naphthalene	1.8	3.3	7.3	1.4	4.1	6.9
Acenaphthylene	1.7	3.2	7.5	1.5	4.2	6.3
Fluorene	1.6	2.9	8.0	1.4	3.2	10.2

[a] Methanol (MeOH), 2-propanol (PrOH) and butanol (BuOH).

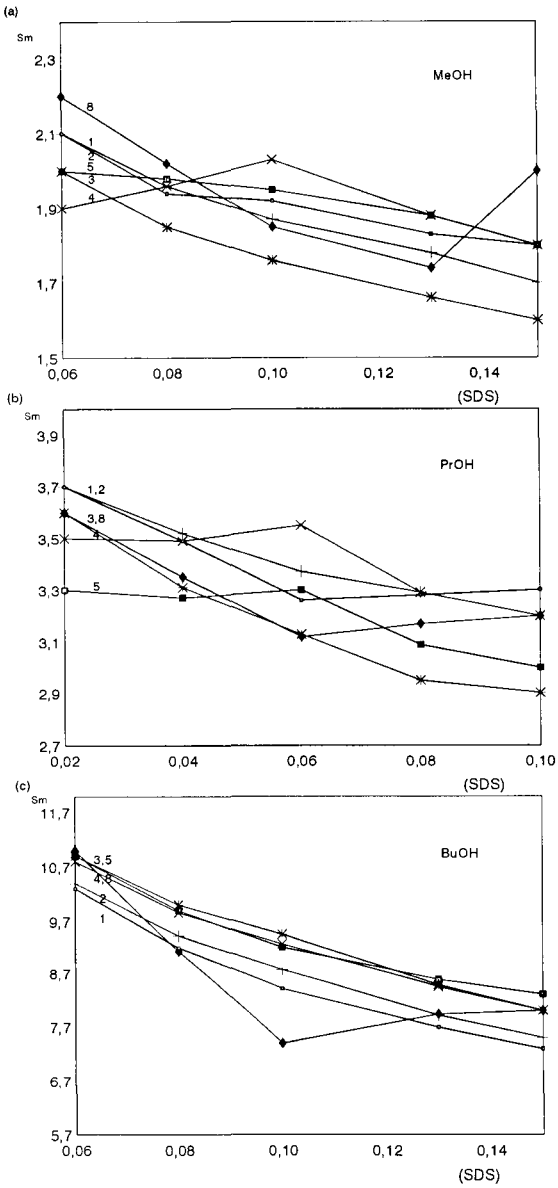

Fig. 7. Variation of S_{hyb} value for some PAHs with micelle concentration: (a) methanol, (b) 2-propanol and (c) butanol.

size is less important compared with the solvating effect of the alcohol modifier.

The values of S_{hyb} for the PAHs decrease with increasing micelle concentration (Fig. 7), this diminution being greater when BuOH is the modifier. Taking into account that the degree of reduction in S_{hyb} is a function of the solute–micelle interactions, it can be concluded that when using modified mobile phases there are no high interaction differences between PrOH and MeOH but interactions are lower with BuOH because of the competition between this alcohol and the micelles for a solute. In other words, molecules such as naphthalene, acenaphthylene, fluorene or anthracene are far less affected by the addition of modifiers, as these relatively less hydrophobic molecules strongly interact with micelles and are less accessible to polar solvents such as methanol. Solute interaction with micelles diminishes with less polar alcohols such as PrOH, and this effect is more relevant for more hydrophobic molecules which have large water–micelle partition coefficients, and was lowest for the less polar BuOH.

4. Conclusion

The results obtained show that solute–mobile phase interactions play an important role in controlling retention and selectivity of PAHs in MLC with hybrid mobile phases, as demonstrated by the great variation in selectivity caused by the use of alcohols as modifiers of the mobile phase, which are greater with longer chain alcohols. Thus, in the separation process it is necessary to take into consideration not only the concentration and charge of the surfactant but also the concentration of alcohol. Both, the increase in micelle concentration and the increase in the alcohol modifier, will influence different solutes in different ways. Thus the simultaneous study of both factors is of special importance for the separation process as the selectivity can be changed drastically by changing the alcohol added to the mobile phase.

For the PAHs studied the use of SDS gives a better separation selectivity than CTAB, and the selectivity diminishes as surfactant concentration increases, but the selectivity increases as the alcohol modifier concentration increases. The optimum selectivity is obtained with relatively high percentages of 2-propanol ($\approx 15\%$) and intermedium concentrations of surfactant (≈ 0.1 M) with the final objective of not increasing the time of analysis.

Acknowledgements

The authors gratefully acknowledge the financial support of this work by grant PB88-0427 from CICYT (Spain).

References

[1] D.W. Armstrong and S. Henry, J. Liq. Chromatogr., 3 (1980) 657.
[2] D.W. Armstrong, Sep. Purif. Methods, 14 (1985) 213.
[3] W.L. Hinze, in W.L. Hinze and D.W. Armstrong (Eds.), Ordered Media in Chemical Separation, ACS Symposium Series 342, American Chemical Society, Washington, DC, 1987.
[4] M.G. Khaledi, Biochromatography, 3 (1988) 20.
[5] M.G. Khaledi, Trends Anal. Chem., 7 (1988) 293.
[6] J.G. Dorsey, Adv. Chromatogr., 27 (1987) 167.
[7] L.J. Cline Love, J.G. Habarta and J.G. Dorsey, Anal. Chem., 56 (1984) 1132A.
[8] J.G. Dorsey, M.T. De Echegaray and J.S. Landy, Anal. Chem., 55 (1983) 924.
[9] P. Yarmchuk, R. Weinberger, R.F. Hirsch and L.J. Cline Love, J. Chromatogr., 47 (1984) 283.
[10] J.S. Landy and J.G. Dorsey, Anal. Chim. Acta, 178 (1985) 179.
[11] M.F. Borgerding, R.L. Williams, W.L. Hinze and F.H. Quina, J. Liq. Chromatogr., 12 (1989) 1367.
[12] F. Borgerding, W.L. Hinze, L.D. Stafford, G.W. Fulp and W.C. Hamlin, Anal. Chem., 61 (1989) 1353.
[13] P. Yarmchuk, R. Weinberger, R.F. Hirsch and L.J. Cline Love, Anal. Chem., 54 (1984) 2233.
[14] D.W. Armstrong and G.Y. Stine, Anal. Chem., 55 (1983) 2317.
[15] M.G. Khaledi, Anal. Chem., 60 (1988) 876.
[16] M.G. Khaledi, J.K. Strasters, A.H. Rodgers and E.D. Breyer., Anal. Chem., 62 (1990) 130
[17] J.K. Strasters, E.D. Breyer, A.H. Rodgers and M.G. Khaledi, J. Chromatogr., 511 (1990) 17.
[18] A.S. Kord and M.G. Khaledi, Anal. Chem., 64 (1992) 1894.
[19] A.S. Kord and M.G. Khaledi, J. Chromatogr., 631 (1993) 125.
[20] F.P. Tomasella, J. Fett and L.J. Cline Love, Anal. Chem., 63 (1991) 474.
[21] M.A. Rodríguez, M.J. Sánchez, V. González and F.G. Montelongo, Chromatographia, 38 (1994) 342
[22] G.L. McIntire, D.M. Chappardi, R.L. Casselberr and H.N. Blount, J. Phys. Chem., 86 (1982) 2632.
[23] L.R. Snyder and J.J. Kirkland, Introduction to Modern Liquid Chromatography, Wiley, New York, 2nd edn., 1979, p. 260.

ELSEVIER

Analytica Chimica Acta 298 (1994) 431–438

ANALYTICA CHIMICA ACTA

Chemiluminescence determination of catecholamines in human blood plasma and urine using 1,2-diphenylethylenediamine as pre-column derivatization reagent in liquid chromatography

Gamal H. Ragab, Hitoshi Nohta, Masaaki Kai, Yosuke Ohkura *

Faculty of Pharmaceutical Sciences, Kyushu University 62, Maidashi, Higashi-ku, Fukuoka 812, Japan

Received 3 December 1993; revised manuscript received 7 June 1994

Abstract

A chemiluminescence detection of the fluorescent derivatives of catecholamines (norepinephrine, epinephrine and dopamine) and isoproterenol as an internal standard is described for the highly sensitive liquid chromatographic determination of these compounds. The amines were converted by reaction with 1,2-diphenylethylenediamine into the corresponding fluorescent derivatives, which were separated on a reversed-phase column (TSK gel ODS-120T) with isocratic elution. The derivatives in the column eluate were detected by the post-column chemiluminescence reaction system using bis[4-nitro-2-(3,6,9-trioxadecyloxycarbonyl)phenyl] oxalate and hydrogen peroxide. The method allowed the determination of catecholamines in 50 μl of human blood plasma and 10 μl of 20 times diluted urine. The detection limits for the amines were 150–450 amol per 100-μl injection volume at a signal-to-noise ratio of 3.

Keywords: Chemiluminescence; Liquid chromatography; Catecholamines; Peroxyoxalates; Plasma; Urine

1. Introduction

Catecholamines (CAs) [epinephrine (E), norepinephrine (NE) and dopamine (DA)] play important roles as neurotransmitters and/or hormones in mammals. The measurement of their levels in blood plasma and urine is informative in diagnoses of many diseases [1,2]. However, their measurement is very difficult and needs a great deal of precautions because plasma CAs are present at extremely low concentrations, and thus a highly sensitive assay is required.

Several methods have been reported for the determination of CAs in biological samples, such as radioenzymatic method [3] and liquid chromatography (LC) with electrochemical [4–10] or fluorimetric [11–17] detection. For the sensitive detection of CAs in LC, chemiluminescence (CL) detection methods based on the peroxyoxalate reaction have been studied [18,19], in which CAs were converted into dansyl [18] or fluorescamine [19] derivatives, followed by LC with CL detection. These methods, however, lack both specificity and sensitivity for the determination of CAs at the femto- or subfemtomole level in complex biological samples. Recently, an LC with peroxyoxalate CL detection for plasma CAs, using ethylenediamine for the post-column derivatization of CAs was reported [20]. The method permitted the determination of CAs in 200 μl human plasma.

We have developed a sensitive and selective fluorescence derivatization of CAs with 1,2-diphenylethyle-

* Corresponding author.

SSDI 0003-2670(94)00293-2

nediamine (DPE) in pre-column derivatization LC [22], which permitted the determination of CAs in 500 μl human plasma [14]. The present study aimed to further increase greatly the sensitivity of the LC method by introducing a peroxyoxalate CL reaction after LC separation of the DPE derivatives of CAs and isoproterenol (IP) used as an internal standard, to allow reduction of the sample volume. The CL reaction conditions were investigated manually (static system) and then applied to the on-line CL detection system. The post-column CL reaction, LC separation and sample clean-up were optimized for the determination of CAs in human plasma and urine.

2. Materials and methods

2.1. Reagents and solutions

NE hydrogen tartrate and DA hydrochloride were purchased from Wako Pure Chemicals (Osaka), E hydrogen tartrate from Sigma (St. Louis, MO, USA) and IP hydrochloride from Nacalai Tesque (Kyoto). DPE was synthesized as recommended by Irving and Parkin [21] and purified as described previously [15]. Water was purified with a Milli-Q II system (Nihon Millipore, Tokyo). DPE solution (0.1 M, pH 6.5) was prepared by dissolving 212 mg of DPE in approximately 8 ml of 0.1 M hydrochloric acid, adjusting the pH with 0.1 M hydrochloric acid to pH 6.5 and diluting with water to 10 ml.

Bis[4-nitro-2-(3,6,9-trioxadecyloxycarbonyl)phenyl] oxalate (TDPO) from Wako Pure Chemicals was dissolved in ethyl acetate (0.3 mM). Hydrogen peroxide solution (31%, Mitsubishi Gas Kagaku Co., Tokyo) was diluted with a mixture of acetonitrile and ethyl acetate (1:9, v/v) to the appropriate concentrations. Imidazole (reagent grade, Wako Pure Chemicals) was recrystallised twice from benzene. The pHs of the imidazole buffers (60 mM) were adjusted with 2 M nitric acid. Lithium phosphate buffer (0.2 M, pH 5.8) was prepared as described previously [14].

Stock solutions (10 mM) of NE, E, DA and IP were prepared in 0.1 M hydrochloric acid, and stored at −20°C. The solutions were diluted with water to the desired concentrations before use.

Toyopak IC-SP S cartridge (strong cation exchanger, sulphopropyl resin, 0.15 ml, Na^+ form, particle size 19–40 μm; Tosoh, Tokyo) was washed successively with 2 ml of ethanol (twice), 5 ml of water (twice) and 1 ml of 0.2 M lithium phosphate buffer (pH 5.8) (three times) prior to use. The cartridges were regenerated as previously described [14]. Heparinized human blood (0.5 ml) was brought into a cooled polyethylene tube containing 5 mg of reduced glutathione and centrifuged at 1000 *g* at 4°C for 15 min. The resulting plasma was stored at −70°C until use. Occasional human urine was diluted 20 times with water before derivatization.

2.2. Fluorescence derivatization of standard CAs

To 10 μl of an aqueous solution of CAs and IP, 1.0 ml of a mixture of acetonitrile and 0.5 M potassium chloride (3:2, v/v), 10 μl of 75 mM potassium ferricyanide(III) and 100 μl of 0.1 M DPE were added successively. The mixture was incubated at 37°C for 40 min. A portion of the mixture was used for static CL reaction or LC.

2.3. Static CL reaction and CL measurement

To 10 μl of the DPE reaction mixture of E, 40 μl of 60 mM imidazole buffer (pH 6.0) and 50 μl of a mixture of methanol and acetonitrile (1:5, v/v) were added (the mixture corresponded to the DPE derivatives of E in the LC eluate). The CL intensity was measured after the addition of 100 μl of a mixture of 0.6 mM TDPO and 0.3 M hydrogen peroxide (1:1, v/v). The CL reaction was carried out at room temperature (20–25°C) in a 75 × 12 mm glass tube. The measurement of the intensity was performed with a photon-counting luminometer, Lumat LB9501 (Berthold Co., Wildbad, Germany); its operation and data processing were controlled by a PC 9801 ES2 personal computer (NEC Corp., Tokyo) using a luminescence program, LB 9501/9801 Ver. 1.41 (Japan Berthold Co., Tokyo). The CL intensity represents maximum photon count in each measurement.

2.4. Clean-up procedures for plasma and urine samples and fluorescence derivatization

Plasma sample. To 50 μl of plasma were added 10 μl of 2.5 pmol ml^{-1} IP (internal standard) and 0.5 ml of 0.2 M lithium phosphate buffer (pH 5.8). The mix-

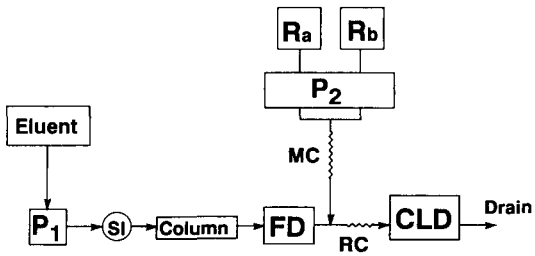

Fig. 1. Block diagram of the LC system with CL detection. P_1, LC pump; SI, sample injection valve; FD, fluorescence detector; Ra, hydrogen peroxide solution; Rb, TDPO solution; P_2, reagent-delivery pump; MC, mixing coil; RC, reaction coil; CLD, CL detector.

ture was poured into a Toyopak IC-SP S cartridge. The cartridge was washed successively with 5 ml of water (twice) and 1 ml of aqueous acetonitrile (60%, v/v). The adsorbed amines were eluted with 500 μl of 0.6 M potassium chloride–acetonitrile (2:3, v/v). To the eluate, 10 μl of potassium ferricyanide(III) (0.6 mM) and 100 μl of the DPE solution were added. The mixture was allowed to stand at 37°C for 40 min. Aliquots (100 μl) of the mixture were injected into the chromatograph. The amounts of CAs were calculated based on the internal standard method.

Urine sample. To 1–100 μl urine sample, an equal volume of 1.0 nmol ml^{-1} IP solution was added, and the mixture was diluted 10 times with water (20 times diluted urine sample). To 10 μl of the diluted urine sample was added 0.5 ml of lithium phosphate buffer (0.2 M, pH 5.8). The mixture was treated in the same way as the plasma sample except that the adsorbed amines in the cartridge were eluted with 1.0 ml of 0.6 M potassium chloride–acetonitrile (2:3, v/v).

2.5. LC system and its operating conditions

A block diagram of the LC system is illustrated in Fig. 1. A Shimadzu LC-6A liquid chromatograph was used, equipped with a Rheodyne 7125 syringe-loading sample injector valve (100-μl loop) and a TSK gel ODS-120T column (particle size 5 μm, 250×4.6 mm I.D.; Tosoh). The column temperature was ambient (20–25°C). The mobile phase was a mixture of acetonitrile, methanol and 60 mM imidazole buffer (pH 5.5) (8:1:8, v/v/v) and the flow-rate was 0.8 ml min^{-1}. A Hitachi F1000 fluorescence spectrofluorimeter fitted with a 12-μl flow-cell, which was installed in the system to compare the sensitivity and selectivity of the CL detection with those of the fluorescence detection, was operated at an excitation wavelength of 350 nm and an emission wavelength of 480 nm.

In the post-column CL reaction system, 0.3 mM TDPO and 0.2 M hydrogen peroxide were delivered at a flow-rate of 0.48 ml min^{-1}, each by a dual head pump, SSP PM-2M 1024 (Sanuki Kogyo Co., Tokyo). Both reagent solutions were mixed through a stainless-steel coil (5 m×0.5 mm I.D.), then the stream was introduced into the column eluate stream and mixed through a stainless-steel coil (1.6 m×0.25 mm I.D.). The generated CL was monitored with a Luminomonitor-I Model AC-2220 (ATTO Co., Tokyo).

3. Results and discussion

3.1. Static CL reaction

In order to establish the optimum conditions for the CL detection of the DPE derivatives, the parameters affecting the reaction were first investigated in a static system using the fluorescence derivatization reaction mixture of E. Four different peroxyoxalates (TDPO, bis[2-(3,6-dioxaoctyloxycarbonyl)-4-nitrophenyl] oxalate (DOPO), bis(2,4,6-trichlorophenyl) oxalate (TCPO) and bis(2,4-dinitrophenyl) oxalate (DNPO) were examined as their 2.0 mM solutions for the CL activity at pH 4–9 in imidazole buffer (60 mM) (Fig. 2). Of the peroxyoxalates, TDPO gave the highest CL intensity at pH 6.0. The CL intensity was increased

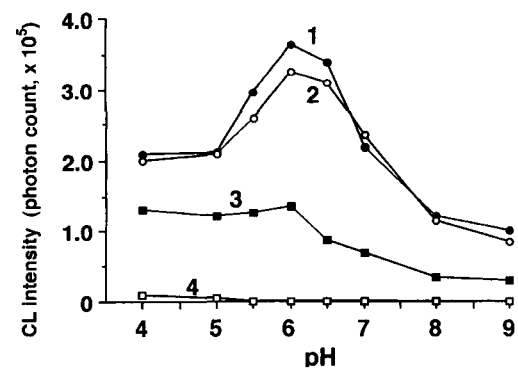

Fig. 2. Effects of peroxyoxalates and pH on the CL intensity. A portion (10 μl) of 1.0 nmol ml^{-1} E was treated with DPE under the conditions of the fluorescence derivatization, and 10 μl of the reaction mixture (8.9 pmol ml^{-1} E) were subjected to the static CL reactions with various 2.0 mM peroxyoxalates at different pHs of 60 mM imidazole buffer. Curves: 1 = TDPO; 2 = DOPO; 3 = TCPO; 4 = DNPO.

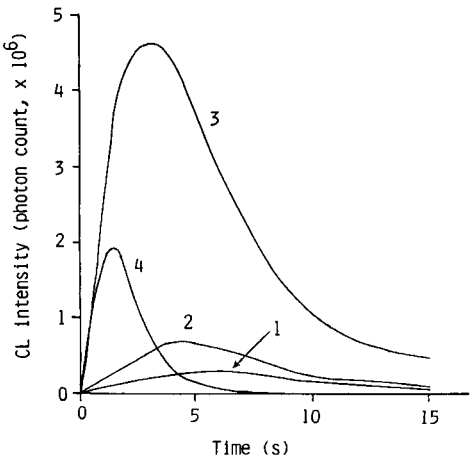

Fig. 3. Time-course of the CL intensity at different pHs of 60 mM imidazole buffer. A portion (10 μl) of 1.0 nmol ml^{-1} E was treated in the same manner as for Fig. 2 and the reaction mixture (8.9 pmol ml^{-1} for E) was used for the static CL reaction with TDPO at various pHs of the buffer. Curves (pH): 1 = 4.0; 2 = 5.0; 3 = 6.0; 4 = 7.0.

with increasing TDPO concentration in a range 0.1–3 mM, although the background also resulted in higher levels; 0.6 mM TDPO was selected as optimum for the maximum CL intensity.

The catalytic effect of various organic bases (18 species; heterocyclic amines, aromatic amines, alkylamines and quaternary ammonium salts) at different pHs (20–100 mM) on the CL reaction was investigated. Of the bases tested, imidazole was the best catalyst for the CL reaction, in the same way as for the CL detection of dipyridamole in LC [23]. The CL intensities obtained with the other bases were lower than 6% of that obtained with imidazole. The imidazole concentration affected the CL intensity, increasing the imidazole concentration (30–70 mM) resulted in an increase in the CL intensities of both the tested solution and reagent blank; 60 mM was selected as optimum. The pH of the imidazole buffer had a great influence on the time-course of the CL generation (Fig. 3); pH 6.0 was optimum for the CL reaction.

The effect of hydrogen peroxide concentration on the CL intensity showed that the intensity increased with increasing hydrogen peroxide concentration (0.1–0.6 M); 0.3 M was optimum.

Ethyl acetate at higher concentrations (23.5–47.5%, v/v) in the reaction mixture resulted in an increase in the CL intensity. Thus, ethyl acetate was used as a solvent for TDPO. However, the commercially available hydrogen peroxide solution is immiscible with

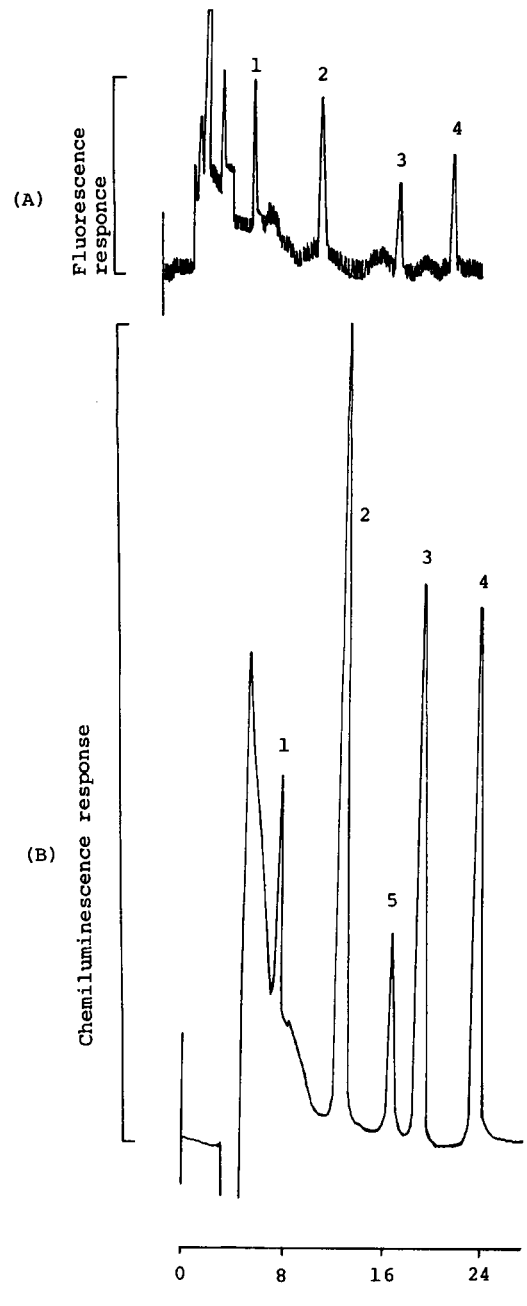

Fig. 4. Chromatograms of the DPE derivatives of CAs and IP (8.9 fmol each per 100-μl injection volume) obtained by (A) fluorescence and (B) CL detection. A portion (100 μl) of the fluorescence derivatization mixture of CAs and IP was injected into the chromatograph. Peaks: 1 = NE; 2 = E; 3 = DA; 4 = IP; 5 and others = reagent blank.

ethyl acetate, and thus the solution was diluted with a mixture of acetonitrile and ethyl acetate (1:9, v/v) to prepare 0.3 M hydrogen peroxide. Ethyl acetate concentration in the CL reaction mixture was 47.5% (v/v).

3.2. LC separation and on-line CL reaction

The fluorescent derivatives of NE, E, DA and IP in the reaction mixture were separated on a reversed-phase column (TSK gel ODS-120T) with isocratic elution (Fig. 4). After the fluorescence detection (Fig. 4A), the column eluate was mixed with TDPO and hydrogen peroxide solutions for the CL detection (Fig. 4B). The mobile phase consisted of a mixture of 60 mM imidazole buffer (pH 5.5), methanol and acetonitrile (8:1:8, v/v/v). In spite of the negative effect of methanol on the CL reaction [24], it was necessary for the efficient separation of the fluorescent derivatives; in its absence, the peak for DA (Fig. 4B, peak 3) and one of the peaks of the reagent blank (Fig. 4B, peak 5) overlapped although the peak heights of CAs and IP were approximately 1.2 times greater than those in the presence of methanol.

In the LC system, imidazole buffer was used to obtain a high sensitivity in the detection of the DPE derivatives of CAs and IP. The optimum pH of the imidazole buffer was 5.5, which was slightly different from that in the static reaction system (Fig. 2). Higher CL intensities of the fluorescent derivatives were attained with higher concentrations of the imidazole buffer pH 5.5 (Fig. 5A). However, the base-line and its noise levels due to the background were also increased, and thus 60 mM was selected because at this concentration the highest signal-to-noise ratios for the peaks of CAs and IP were attained. The optimum concentrations of TDPO and hydrogen peroxide were 0.3 mM and 0.2 M, respectively (Fig. 5B and C).

The length of the CL reaction coil (0.25 mm I.D.) affected the CL production in the range 0.2–3.0 m; the most intense CL response was achieved at a length of 1.6 m for which the passing time was approximately 3 s.

3.3. LC determination

The calibration graphs obtained by plotting the CL peak heights for NE, E, DA and IP against their concentrations were all linear (1–100 fmol each per 100-μl injection volume) and passed through the origin. The correlation coefficient for each straight line was in the range 0.985–0.999. The detection limits for NE, E,

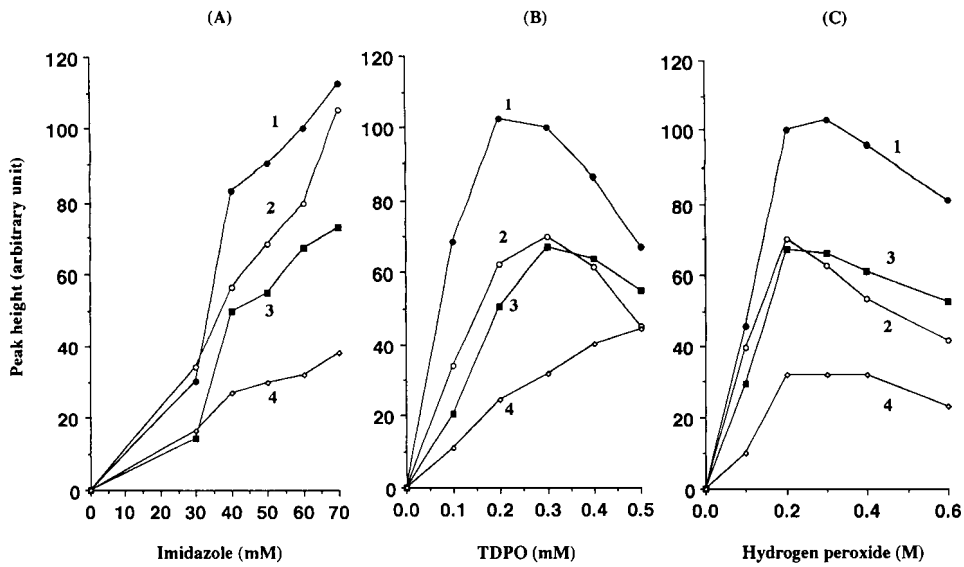

Fig. 5. Effects of the concentration of (A) imidazole, (B) TDPO and (C) hydrogen peroxide on the CL peak heights of the DPE derivatives of CAs and IP. The fluorescence derivatization mixture of CAs and IP was treated in the same manner as for Fig. 4, but various concentrations of imidazole buffer (pH 5.5), TDPO or hydrogen peroxide were subjected to the CL reaction in the LC system. Curves: 1 = E; 2 = DA; 3 = IP; 4 = NE.

DA and IP were 450, 150, 190 and 200 amol, respectively, at a signal-to-noise ratio of 3.

The within-day reproducibility of the CL detection was established by repeated measurements ($n = 10$) of a standard CAs solution (10 pmol ml^{-1} each). The relative standard deviations were 5.0, 2.3, 2.3 and 3.5% for NE, E, DA and IP, respectively.

3.4. Determination of plasma and urinary catecholamines

Typical chromatograms obtained with plasma and urine samples are shown in Fig. 6A and B, respectively. The DPE derivatives of the amines can be separated within 24 min and the reagent blank peaks were completely separated from those of CAs and IP. The peaks for CAs were identified as follows: (1) comparison of the retention times with those of the standards; (2) co-chromatography with the standards; (3) the peaks disappeared when DPE solution was omitted in the derivatization procedure.

3.5. Sample clean-up

Proteins, reducing compounds (e.g. thiol compounds, ascorbic acid, etc.) and other catechol com-

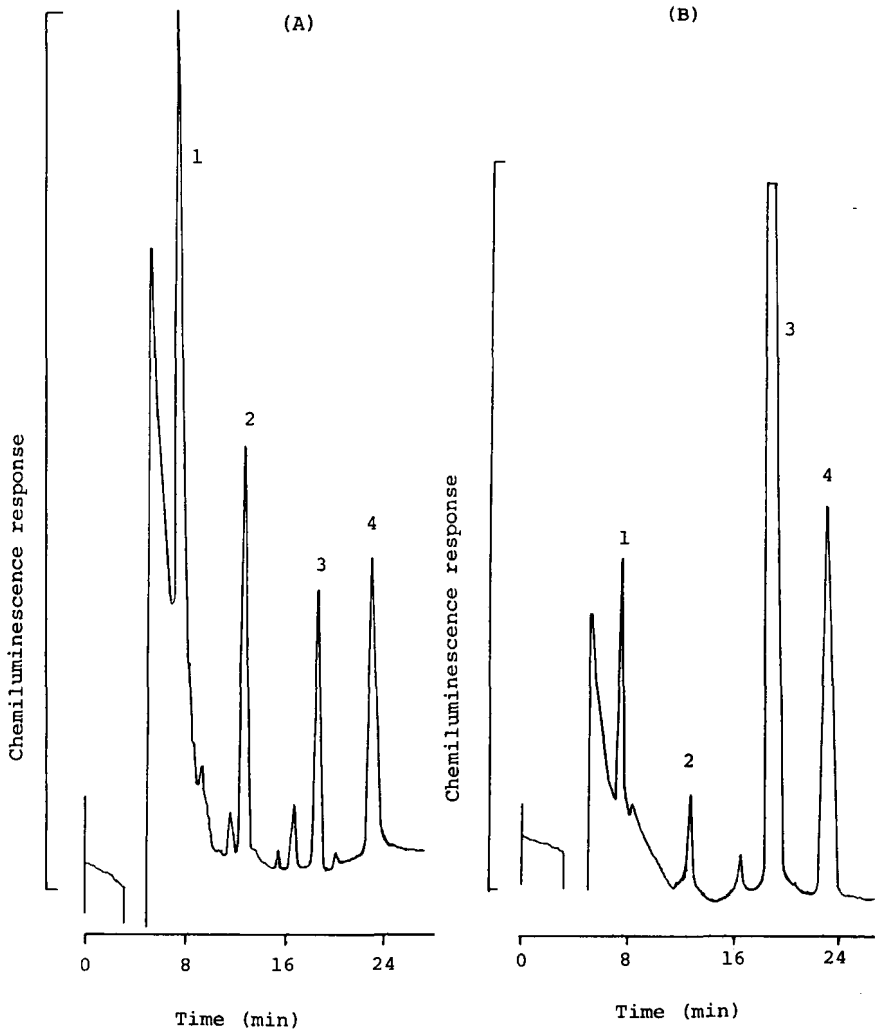

Fig. 6. Chromatograms obtained with (A) normal human plasma and (B) urine. Peaks; 1 = NE, 2 = E, 3 = DA and 4 = IP. Concentrations (for plasma CAs, pmol ml^{-1}): NE = 2.3, E = 0.46 and DA = 0.39; (for urinary CAs, nmol ml^{-1}): NE = 0.68, E = 0.08 and DA = 1.6, others = reagent blank.

pounds (e.g. L-DOPA, 3,4-dihydroxyphenylethyleneglycol and 3,4-dihydroxyphenylacetic acid) may interfere with the determination of CAs if they are present in plasma and urine samples in high concentrations [14,22]. For the removal of these compounds, solid phase extraction on a cartridge of strong cation exchanger (Toyopak IC-SP S) gave very satisfactory results as shown in the chromatograms obtained with normal plasma and urine (Fig. 6A and B). The recoveries [mean ± standard deviation (S.D.), $n=5$] of standard CAs (100 fmol each) added to 50 μl of human plasma were 98 ± 2% and those added to 10 μl of the diluted urine in amount of 250 fmol each were 100 ± 2%. In a previous study [14], the laboratory-made Toyopak SP cartridge (resin 0.1 ml) was used for the clean up of CAs in 500 μl of human plasma and the recoveries for CAs were approximately 85%. The improvement of the recovery in the present method is probably due to the use of small volumes of the samples and larger volumes of the ion-exchange resin and the elution mixture.

For urinary CAs, a direct derivatization of CAs in 20 times diluted samples was tried according to the previous fluorimetric LC method where 10 μl of urine sample were used [22]. However, DPE derivatives of unknown substances interfered with the determination of NE and E in the present LC system.

Linear relationships were obtained between the ratios of the peak heights of CAs to that of IP and the amounts of CAs in the range 10–200 fmol each in 50 μl human plasma. The correlation coefficients for the straight lines were: 0.949 for NE, 0.999 for E and 1.000 for DA. The detection limits for NE, E and DA in plasma were 27, 9 and 12 fmol ml^{-1} (450, 150 and 220 amol per 100 μl injection volume of the reaction mixture) at a signal-to-noise ratio of 3, which corresponds to 0.45–1.35 fmol per 50 μl human plasma and 0.5 μl of urine.

The precision of the method was established by repeated determinations ($n=6$) using normal human plasma and urine. The coefficients of variation for NE, E and DA were 2.5, 3,0 and 4.8% and 3.5, 3 and 2%, for plasma (2.2, 0.44 and 0.39 pmol ml^{-1}) and urine (0.6, 0.12 and 1.8 nmol ml^{-1}), respectively.

The concentration values of CAs in plasma samples from healthy volunteers (mean ± S.D., $n=6$) were 2.15 ± 0.22, 0.41 ± 0.12 and 0.38 ± 0.1 pmol ml^{-1} plasma for NE, E and DA, respectively. The results are in good agreement with the previously published data [14,20]. The concentrations in urine samples from male volunteers (mean ± S.D., $n=6$) were 0.55 ± 0.28, 0.09 ± 0.03 and 1.67 ± 0.41 nmol ml^{-1} for NE, E and DA, respectively. These values coincided well with the published data [14,15].

4. Conclusion

The sensitivity of the present CL detection was approximately 20 times higher than that of the fluorescence detection using the DPE derivatives [14] and approximately 4, 40 and 100 times higher than those of the CL detections using ethylenediamine [20], dansyl [18] and fluorescamine [19] derivatives, respectively. The considerable increase in the sensitivity for the present CL detection of CAs makes it possible to determine CAs in 50 μl of human plasma. Therefore, the present method should be useful not only for biomedical investigations of CAs, but also for the practical applications in diagnosis and the follow-up of many diseases.

References

[1] B. Kågedal and D.S. Goldstein, J. Chromatogr., 429 (1988) 190.
[2] T.R. Kosten, J.W. Mason, E.L. Giller, R.B. Ostroff and L. Harness, Psychoneuroendocrinology, 12 (1987) 13.
[3] K. Engelman, B. Portnoy and W.A. Lovenburg, Am. J. Med. Sci., 255 (1968) 259.
[4] H. Hallman, L.D. Farnebo, B. Hmberger and G. Jonson, Life Sci., 23 (1978) 1049.
[5] I.N. Mefford, M.M. Word, L. Milles, B. Taylor, M.A. Chesney, D.L. Keegan and J.D. Barchas, Life Sci., 28 (1981) 447.
[6] D.S. Goldstein, G.Z. Feuerstein, I.J. Kopin and H.R. Keiser, Clin. Chim. Acta, 117 (1981) 113.
[7] K.F. Frayn and P.F. Maycock, Clin. Chem., 29 (1983) 1426.
[8] B.L. Lee, K.S. Chia and C.N. Ong, J. Chromatogr., 494 (1989) 303.
[9] R.T. Peaston, J. Chromatogr., 424 (1988) 263.
[10] M.K. Adarsh, K. Mohendra, B.F. Jesus, A.M. Thomas and E. Carl, J. Liq. Chromatogr., 14 (1991) 3547.
[11] K. Imai, M. Tsukamoto and Z. Tamura, J. Chromatogr., 137 (1977) 357.
[12] L.D. Mell, A.R. Dasler and A.B. Gustafson, J. Liq. Chromatogr., 1 (1978) 261.
[13] A. Yamatodani and H. Wada, Clin. Chem., 27 (1981) 1983.
[14] A. Mitsui, H. Nohta and Y. Ohkura, J. Chromatogr., 344 (1985) 61.

[15] H. Nohta, A. Mitsui and Y. Ohkura, J Chromatogr., 380 (1986) 229.
[16] M. Hamaji and T. Seki, J. Chromatogr., 163 (1979) 329.
[17] F. Boomsma, G. Alberts, F.A.J. Van der Hoorn and A.J. Man, J. Chromatogr., 574 (1992) 109.
[18] G. Mellbin, J. Liq. Chromatogr., 6 (1983) 1603.
[19] S. Kobayashi, J. Sekino, K. Honda and K. Imai, Anal. Biochem., 112 (1981) 99.
[20] S. Higashidate and K. Imai, Analyst, 117 (1992) 1863.
[21] M.N. Irving and R.M. Parkin, J. Inorg. Nucl. Chem., 27 (1965) 270.
[22] H. Nohta, A. Mitsui and Y. Ohkura, Anal. Chim. Acta, 165 (1984) 171.
[23] K. Imai, A. Nishitani, Y. Tsukamoto, W.H, Wang, S. Kanda, K. Hayakawa and M. Miyazaki, J. Biomed. Chromatogr., 4 (1990) 100.
[24] S. Kobayashi and K. Imai, Anal. Chem., 52 (1980) 424.

ELSEVIER

Analytica Chimica Acta 298 (1994) 439–442

ANALYTICA CHIMICA ACTA

Author Index

PUBLICATION SCHEDULE FOR 1995

	O'94	N'94	D'94	J	F	M	A	M	J	J	A	S
Anal. Chim. Acta	296/2 296/3 297/1–2	297/3 298/1 298/2	298/3 299/1 299/2	299/3 300/1–3 301/1–3	302/1 302/2–3 303/3							
Vib. Spec.		8/1		8/2		8/3		9/1		9/2		9/3

INFORMATION FOR AUTHORS

Detailed "Instructions to Authors" for *Analytica Chimica Acta* was published in Volume 289, No. 3, pp. 381–384. Free reprints of the "Instructions to Authors" of *Analytica Chimica Acta* and *Vibrational Spectroscopy* are available from the Editors or from: Elsevier Science B.V., P.O. Box 330, 1000 AH Amsterdam, The Netherlands. Telefax: (+31-20) 4852 459.

Manuscripts. The language of the journal is English. English linguistic improvement is provided as part of the normal editorial processing. Authors should submit three copies of the manuscript in clear double-spaced typing on one side of the paper only. *Vibrational Spectroscopy* also accepts papers in English only.

Rapid publication letters. *Letters* are short papers that describe innovative research. Criteria for letters are novelty, quality, significance, urgency and brevity. Submission data: max. of 2 printed pages (incl. Figs., Tables, Abstr., Refs.); short abstract (e.g., 3 lines); *no* proofs will be sent to the authors; submission on floppy disc; *no* revision will be possible.

Abstract. All papers, reviews and letters begin with an Abstract (50–250 words) which should comprise a factual account of the contents of the paper, with emphasis on new information.

Figures. Figures should be suitable for direct reproduction and as rich in contrast as possible. One original (or sharp glossy print) and two photostat (or other) copies are required. Attention should be given to line thickness, lettering (which should be kept to a minimum) and spacing on axes of graphs, to ensure suitability for reduction in size on printing. Axes of a graph should be clearly labelled, along the axes, outside the graph itself.

All figures should be numbered with Arabic numerals, and require descriptive legends which should be typed on a separate sheet of paper. Simple straight-line graphs are not acceptable, because they can readily be described in the text by means of an equation or a sentence. Claims of linearity should be supported by regression data that include slope, intercept, standard deviations of the slope and intercept, standard error and the number of data points; correlation coefficients are optional.

Photographs should be glossy prints and be as rich in contrast as possible; colour photographs cannot be accepted. Line diagrams are generally preferred to photographs of equipment. Computer outputs for reproduction as figures must be good quality on blank paper, and should preferably be submitted as glossy prints.

Nomenclature, abbreviations and symbols. In general, the recommendations of IUPAC should be followed, and attention should be given to the recommendations of the Analytical Chemistry Division in the journal *Pure and Applied Chemistry* (see also *IUPAC Compendium of Analytical Nomenclature, Definitive Rules*, 1987).

References. The references should be collected at the end of the paper, numbered in the order of their appearance in the text (*not* alphabetically) and typed on a separate sheet.

Reprints. Fifty reprints will be supplied free of charge. Additional reprints (minimum 100) can be ordered. An order form containing price quotations will be sent to the authors together with the proofs of their article.

Papers dealing with vibrational spectroscopy should be sent to: Dr J.G. Grasselli, 150 Greentree Road, Chagrin Falls, OH 44022, U.S.A. Telefax: (+1-216) 2473360 (Americas, Canada, Australia and New Zealand) or Dr J.H. van der Maas, Department of Analytical Molecular Spectrometry, Faculty of Chemistry, University of Utrecht, P.O. Box 80083, 3508 TB Utrecht, The Netherlands. Telefax: (+31-30) 518219 (all other countries).

0003-2670/94/$07.00

Time-of-Flight Mass Spectrometry and its Applications

Edited by **E.W. Schlag**, Institut für Physicalische und Theoretische Chemie, Universität München, Germany

Previously published as a special issue of the journal
International Journal of Mass Spectrometry and Ion Processes, Volume 131 (1994)

The present set of contributions attempts to give a survey of current applications from many of the active groups in the field. A variety of new applications are considered which are no doubt just the beginning of large new areas of application.

Contents: Laser assisted reflectron time-of-flight mass spectrometry (B.A. Mamyrin). How to specify the ion optical system of a time-of-flight mass spectrometer (T. Bergmann, T.P. Martin). The application of ion optics in time-of-flight mass spectrometry (D. Ioanoviciu). Design considerations in energy resolved time-of-flight mass spectrometry (A.E. Giannakopulos *et al.*). Laser ion sources for time-of-flight mass spectrometry (U. Boesl *et al.*). Photoemission electron impact ionization in time-of-flight mass spectrometry: an examination of experimental consequences (S.M. Colby, J.P. Reilly). High-resolution mass spectrometry in a linear time-of-flight mass spectrometer (J.M. Grundwürmer *et al.*). The design and performance of an ion trap storage-reflectron time-of-flight mass spectrometer (B.M. Chien *et al.*). Pulse amplitude analysis: a new dimension in single ion time-of-flight mass spectrometry (P.V. Bondarenko *et al.*). Mass analyzed threshold ionization: structural information for a mass spectrum and mass information for ionic spectroscopy (P.M. Johnson, L. Zhu). Decay energetics of molecular clusters studied by multiphoton mass spectrometry and pulsed field threshold ionization (H.J. Neusser, H. Krause). Using reflectron time-of-flight mass spectrometer techniques to investigate cluster dynamics and bonding (S. Wei, A.W. Castleman, Jr.). The one dimensional photofragment translational spectroscopic technique: intramolecular clocking of energy redistribution for molecules falling apart (H.J. Hwang *et al.*). Quantitative determination of kinetic energy releases from metastable decomposition of sputtered organic ions using a time-of-flight mass spectrometer with a single-stage ion mirror (D.F. Barofsky *et al.*). Kinetic energy analysis in time-of-flight mass spectrometry: application of time of flight methods to clusters and pyrolysis studies in supersonic expansions (J.S. Riley, T. Baer). Photodissociation of magnesium ion-molecule complexes in a refectron time-of-flight mass spectrometer (C.S. Yeh *et al.*. Resonance-enhanced two-photon ionization time-of-flight spectroscopy of cold perfluorinated polyethers and their external and internal van der Waals dimers (D.S. Anex *et al.*). Time-of-flight mass spectrometry of DNA laser-ablated from frozen aqueous solutions: applications to the Human Genome Project (P. Williams). Factors affecting the resolution in matrix-assisted laser desorption-ionization mass spectrometry (A. Ingendoh *et al.*). Sequencing of peptides in time-of-flight spectrometer: evaluation of post-source decay following matrix-assisted laser desorption-ionization (MALDI) (P. Kaufmann *et al.*). Energy-isochronous time-of-flight analyzers (H. Wollnik). Author index. Subject index.

©1994 422 pages Paperback
Price: Dfl. 215.00 (US$122.75)
ISBN 0-444-81875-8

ELSEVIER
An imprint of Elsevier Science

ORDER INFORMATION
ELSEVIER SCIENCE B.V.
P.O. Box 330
1000 AH Amsterdam
The Netherlands
Fax: +31 (20) 5862 845
For USA and Canada
P.O. Box 945
Madison Square Station
New York, NY 10159-0945
Fax: +1 (212) 633 3680

US$ prices are valid only for the USA & Canada and are subject to exchange rate fluctuations; in all other countries the Dutch guilder price (Dfl.) is definitive. Customers in the European Union should add the appropriate VAT rate applicable in their country to the price(s). Books are sent postfree if prepaid.